Forelimb Muscle and Muscle Attachment Morphology

by

Karyne Rabey

A thesis submitted in conformity with the requirements
for the degree of Doctor of Philosophy

Graduate Department of Anthropology
University of Toronto

Forelimb Muscle and Muscle Attachment Morphology

Karyne Rabey
Doctor of Philosophy
Graduate Program of Anthropology
University of Toronto
2014

Abstract

The ability to make behavioural inferences from skeletal remains is critical to understanding the lifestyles and activities of past human populations and extinct animals. Muscle attachment site (enthesis) morphology has long been assumed to reflect muscle strength and activity during life, but little evidence exists to directly link activity patterns with muscle development and the morphology of their attachments to the skeleton. This research used a primate sample (*Pongo pygmaeus abelii*, *Macaca fuscata*, and *Macaca sylvanus*) and an experimental mouse model (*Mus musculus,* CD-1 wild-type female outbred) to test how locomotor and postural behaviours influence the development of the forelimb muscles, bone growth rate, bone remodelling, cross-sectional geometry, and the gross morphology of their humeral attachment sites.

A total of twenty-two muscles attaching to the humerus from the three species of primates were analysed. No consistent patterns between muscle architecture and entheseal morphology were found, although considering the underlying cortical bone of an attachment site seemed more informative of the associated muscle. Results demonstrate how variable muscle and bone can be even when considering factors such as age, sex, species, body mass, and locomotion.

Over an eleven-week period, data was collected on the activity levels in one control group and two experimental activity groups (running, climbing) of female mice. The three muscles attaching to the deltoid crest (spinodeltoideus, acromiodeltoideus and superficial pectoralis) were examined. Results show that both activity type and level increased bone growth rates, remodelling and muscle architecture, including differences in potential muscular excursion (fibre length) and potential force production (physiological cross-sectional area). However, despite significant influences on muscle and bone development, activity had no observable effect on enthesis size or morphology. The results of this study suggest that the gross morphology of entheses is less reliable than the internal bone structure for making inferences about an individual's past behaviour. Further knowledge of the functional significance and development of entheseal morphology is needed if one is to accurately reconstruct behaviour based solely on skeletal and fossil remains.

Acknowledgements

The preparation and completion of this thesis would not have been possible without the support, encouragement, and help of the institutions, funding agencies, and people surrounding me. My professional and intellectual development during the Ph.D. program has been greatly affected by my advisor David Begun. His encouragements and inputs have contributed greatly to the completion of my dissertation. David allowed me to grow academically and helped me become a strong independent thinker. He showed me how to increase my circle of knowledge and has directed me on the road ahead. Thank you for all the time you have given me during this journey.

I am also very grateful for my core committee members: Drs. Susan Pfeiffer and Shawn Lehman. Both have made my tenure as a graduate student so much easier. I would not be where I am today if I was not encouraged by such strong researchers. Each time I needed help or advice, they were there and ready to give me their undivided attention. I am very grateful for all the comments, critiques, reflections, and discussions we have shared. I am also thankful for the comments and support provided by Dr. Genevieve Dewar, as well as my external committee member Dr. Jay Stock. Thank you for taking the time to read this very long dissertation and providing me with future guidance. To the entire faculty and staff at the University of Toronto whom have been outstanding when it comes to support, I would like to express my gratitude and I would like to particularly mention Natalia Krencil, Sophia Cottrell, and Drs. Mary Silcox, Sherry Fukuzawa, Michael Schillaci, Edward Swenson, and Ted Banning for their help, comments, access to material, and push along the way during my stay in Toronto.

I cannot express how grateful I am to have met my mentor Tracy Kivell. She helped me with my journey and keeps being extremely helpful no matter where she is in the world. She never

hesitates to answer all of my questions and always goes out of her way to make sure I am happy with my decisions. Tracy, you have been an amazing mentor and friend and I am so happy to have you in my life both personally and academically. I am so thankful for my first mentor, Dr. Michelle Drapeau. I learned so much under her supervision during my early graduate career, and I owe my passion for this project to her. You are the one who pushed me to excel in this subject and I would not be here today if it was not for our many discussions we have had throughout my graduate years. Finally, I am so grateful to my current mentor Dr. Daniel Schmitt for giving me my last push to finish this thesis and for the continued time and wisdom you are providing me. I would also like to thank the Duke Animal Locomotion Lab (Sara Doyle, Anne-Claire Fabre, Michael Granatosky, Roxy Larsen, Charlotte Miller, and Angel Zeininger) for helping me survive the last part of the dissertation. You are the ones that gave me the encouragement to finally finish this adventure!

To the "U of T anthro gang" who have provided me with a community where I could have tremendous support, laughs and gin; I thank you. For her incomparable dedication of time to me, I would like to thank my best friend, roommate, and colleague Amber MacKenzie. For their friendship and help I thank Laura Eastham (Mentee), Laura Adlam, Catherine Merritt, Jarred Heinrich, Mark Dolynskyj (Team Fun!), Emily Holland, Sarah Ranlett, Steven Dorland, Leila Watamaniuk, Stephanie Calce, Renee Willmon, Andrew Riddle, Shelbie McCormick, Joel Cahn, Abigail Ross, Keriann McGoogan, Danielle MacDonald, Lesley Harrington, Jaime Ginter, Bess Doyle, Isabelle Guimont, Emma Yasui and everyone else who I have met (especially my "mentees") and who had to put up with me during my stay at U of T.

I am indebted to Drs. David Green, Shannon McFarlin, and Brian Richmond for kindly providing the mouse sample, along with their guidance and expertise for the hard tissue analyses. For their mentorship, friendship, and collaboration I am tremendously grateful. I am also very thankful to Drs. Bernard Wood and Chet Sherwood for their support and guidance during my stay in Washington DC. I was very lucky to have met a wonderful group of graduate students, postdocs, and researchers at GW who have given me their support, time, and extremely fond memories. I thank all of the "CASHP" gang I have met, especially Amy Bauernfeind, Cheryl Stimpson, Janine Chalk, Erin Marie Williams, Kevin Hatala, and Andrew Du. You are amazing and made my stay in the U.S. so much fun.

The data presented in Chapters 5 and 6 would not be possible without the help, time, and collections given to me by many individuals and institutions. Thanks are due to Dr. Timothy Bromage for taking time to explain many of the microscopic concepts that I used to analyse the mouse sample. Also, I would like to thank Drs. Andrea Taylor and Mark Teaford who have opened their home and lab for me while my many visits to Duke University for sarcomere analysis. Andrea has been endlessly helping me with my thesis throughout the years, and I look forward to more collaboration with her. Thanks are due to Stephanie Holowka who volunteered her time at the Hospital for Sick Children to CT scan the primate sample. Despite her busy schedule, Stephanie always found extra time to have me come in with all of the bones and always had a big smile and great stories to share. A special thank you goes to the museums and their collection managers who granted me access to their skeletal remains and kindly coordinated my visits: Eileen Westwig (American Museum of Natural History), Linda Gordon (National Museum of Natural History), Judy Chupasko (Museum Comparative Zoology), and Susan Woodward (Royal Ontario Museum). I would also like to express my gratitude to Rob Javonillo

and Judy Chupasko for opening their homes during my data collection in Washington and in Boston respectively. I am greatly in debt to Graham Crawshaw and Dyann Powley from the Toronto Zoo for donating to the lab their primates. They were always open to have me come work in their facilities, and have helped me immensely with all of the details that come with the research of primate tissue. Finally, I would like to thank all the members of the Archaeology Centre at the University of Toronto, the Hard Tissue Research Laboratory at the George Washington University, and the Soft Tissue Laboratory at Duke University for graciously providing access to their labs and equipments. The analyses of this dissertation would not have been possible without your help, time, and dedication.

A huge thank you also goes to all my family Lise Lafontaine, Robert Rabey, Alan Rabey, Marika Leclerc, Olivia Rabey, Jocelyne Lortie, Gaëtane Cerantola, Aldo Cerantola, Maxime Cerantola, William Rabey, Linda Rabey; you have shown so much support through the good and the tougher periods of this journey and never let me believe that I would be anything else but a success in your eyes. I am very grateful to be so well surrounded. I cannot forget all those friends who have contributed to keeping me sane all throughout my graduate career; Erin Boyd, Donna Locke, Darren Kelly, Robert Vandeloo, Wayne Adlam, Makar Yeliseykin, Claudiane Beaudoin, Sabrina Gloux, Stéphane Lepage, Marie-Christine Berthiaume, Marie-Eve Lamarre, Brigitte Lapointe, Alison Kooistra, Anna-Maria Lacriola, Bryn Letham, Dominique Côté, Glen Norton, Janie Smith, Julienne Lima, Kari Hanson, Lia Casaca, Yanick Perron, and the THE500 crew. I would not be where I am today if it was not for everyone who have surrounded me in Montréal, Toronto, Washington, and Rudabánya.

Last but certainly not least; this research would not have been possible without the financial assistance of several funding sources. Both the Department of Anthropology and School of Graduate Studies at the University of Toronto have provided me with resources in order to collect my data, and present my findings at conferences. Finally, General Motor's Women in Science Award along with the Wenner-Gren Dissertation Fieldwork Grant helped fund the bulk of my dissertation research.

Table of Contents

List of Tables

Table

List of Figures

Figure

List of Appendices

Chapter 1

1. Introduction

"There is a perfectly understandable drive to make the most of what little evidence survives in the skeleton and this sometimes has the effect of overwhelming critical faculties" (Waldron, 1994:98).

***

Providing information on habitual activities of past populations from skeletal and fossil material is crucial to studies in biological anthropology. When faced with a scarcity of anatomical information due to the loss of soft tissue, researchers assume a functional relationship between bone morphology and the missing musculature. Muscle attachment sites, also known as entheses, frequently exhibit morphological variation within (e.g., differences in size, more or less rugose surface area) and between (e.g., presence or absence of a scar, difference in location) species, and are assumed to reflect differences in behaviour. Specifically, musculoskeletal research implies a causal relationship between enthesis expression and the amount of time and intensity of stress placed by the muscle or tendon on a bone over a lifetime (Hawkey and Merbs, 1995; Hawkey, 1998; Wilczak, 1998a, b; Knüsel, 2000; Eshed et al., 2004; Wang et al., 2004; Weiss, 2003, 2004, 2007, 2010; Molnar, 2006, 2010; Marzke et al., 2007; Havelková et al., 2011). In bioarchaeology, this assumption of change in response to activity-related stress has led to a series of studies such as activity-induced pathology (habitual and specific activities) (Hawkey and Merbs, 1995; Hawkey, 1998; Weiss, 2007; Molnar, 2006; Niinimäki and Sotos, 2013), tool use (Eshed et al., 2004), and evidence of occupation (Stock and Pfeiffer, 2001; Molnar, 2006; Cardoso and Henderson, 2010). Others have used muscle attachment sites to study intra and inter population variation, such as subsistence strategy differences (Hawkey, 1998), cultural changes

(Weiss, 2007; Molnar, 2011), sexual differences in labour (Churchill and Morris, 1998; Villotte et al., 2010b, Weiss, 2010; Havelková et al., 2011; Niinimäki, 2011; Henderson et al., 2013a), social stratification (Havelková et al., 2011, 2013), and disabilities (Hawkey, 1998; Villotte, 2006, Villotte et al., 2010a; Molnar et al., 2011). In fields as diverse as human and dinosaur palaeontology, muscle attachment sites have been used to analyse locomotion (e.g., evolution of bipedalism) (Davis, 1964; McGowan, 1979; Eliot and Jungers, 2000; Wang et al., 2004; Zumwalt, 2005, 2006), tool use (e.g., handedness) (Marzke et al. 2007; Drapeau 2008), as well as habitual and specific activities (Davis, 1964; McGowan, 1979; Eliot and Jungers, 2000; Wang et al., 2004; Zumwalt, 2005, 2006; Marzke et al. 2007; Drapeau 2008). Recently, other studies have focused on developing new methods to interpret muscle attachment sites (Wilczak 1998a, b; Mariotti et al., 2004, 2007; Zumwalt, 2005, 2006; Villotte, 2006; Havelková et al., 2013; Henderson et al. 2013b; Nolte and Wilczak, 2013), while others have attempted to develop new definitions for better interpretations of entheses (Villotte, 2006; Cardoso and Henderson, 2010; Villotte et al., 2010a; Jurmain et al., 2012; Villotte and Knüsel, 2013).

Despite the attention paid to enthesis morphology as a window into past behaviour, little is understood about the relationship between the gross appearance of the bony features and the structure and function of the associated attaching soft-tissues. Efforts to reconstruct soft-tissues rely on the presence or absence of muscle scars and their approximate positioning, and assume that all muscle attachments leave readily interpretable scars on the bony surface. To date, empirical studies have produced conflicting results, making it difficult to draw direct links between the developmental bone loading patterns, muscle size, muscle force, and enthesis morphology (Davis, 1964; McGowan, 1979; Zumwalt, 2005, 2006; Marzke and Shrewbury, 2006; Schoenau and Fricke, 2008; Cardoso and Henderson, 2010; Schmitt et al., 2010; Meyer et

al., 2011; Jurmain et al., 2012). Moreover, a number of studies have been unable to detect the most basic relationship, that being the one between a muscle and the presence of its attachment (Bryant and Seymour, 1990; Eliot and Jungers, 2000; Marzke and Shrewsbury, 2006; Marzke et al., 2007). Because many muscle attachments to bone do not leave readily interpretable scars in extant vertebrates, the use of entheses as surrogates of muscle strength becomes impossible at times. This further hinders the ability to test the proposed functional significance of entheses, and thus the ability to draw reliable conclusions about past human and nonhuman behaviours is limited.

1.1 Objectives

Muscular anatomy is highly plastic during an individual's lifetime (Close, 1972; Salmons and Henriksson, 1981; Asfour et al., 1984; Ishihara et al., 1998; Allen et al., 2001; Caiozzo, 2002; Lieber, 2002; Hansen et al., 2003; Botticelli and Reggiani, 2006; Marini and Veicsteinas, 2010; Harber et al., 2012) particularly if there is a change in the exercise regime. Likewise, physical activity is believed to influence morphology of bones, particularly during growth (see Currey 2002; Parfitt, 2004; Pearson and Lieberman, 2004; Robling et al., 2006 for a review). However, the relationship between fibre architectural parameters of muscle (fibre length and orientation, physiological cross-sectional area) and the morphology of associated muscle attachment sites is poorly understood. Thus, the aim of this dissertation was to determine how normal variation (non-pathological) in muscular activity influenced the size, shape, and growth of entheses. Prior research seeking to reconstruct muscle anatomy and function has been based on the assumption that an increase in the size or shape of an entheseal surface is evidence of increased muscle activity as a result of continued muscle use in habitual daily behaviours (Hawkey and Merbs, 1995; Churchill and Morris, 1998; Hawkey, 1998; Wilczak, 1998a, b; Knüsel, 2000; Eshed et al.,

2004; Wang et al., 2004; Weiss, 2003, 2004, 2007, 2010; Molnar, 2006, 2010; Marzke et al., 2007; Havelková et al., 2011). However, this assumption has not been adequately tested, and more questions relating to the morphology of healthy (normal) variation of entheses have been raised.

This thesis considered the anatomy and architecture of muscles attaching to the humerus. The humerus was chosen for this study because it comprises all types of attachment sites, including fibrocartilaginous (e.g., insertion of teres minor) and fibrous (e.g., insertion of deltoideus) entheses (see Chapter 3 for definitions). This helped explore the above assumption further. The humerus is also a bone that is often available in the fossil record with relatively complete muscle attachments (Rose, 1989; Pilbeam et al., 1990; Gebo, 1993; Rose, 1994; Larson, 1995; Aiello and Dean, 2002; Madar et al., 2002; Wang et al., 2004; Kunimatsu et al., 2007) and used frequently in bioarchaeology to discuss activity in past populations (Pfeiffer and Zehr, 1996; Wilczak, 1998a, b; Eshed et al., 2004; Mariotti et al., 2007; Shaw and Stock, 2009b; Cardoso and Henderson, 2010; Villotte et al., 2010a, b; Havelková et al., 2013; Henderson et al., 2013a, b).

This dissertation first explored entheseal variation within a primate sample. Locomotion and animal posture highly influence the anatomy of a muscle due to the high frequency and high loads involved. The general role of the forelimb in primates is to provide the mobility necessary to reach the irregular supports of an arboreal substrate. Among higher primates, grasping hands have evolved into manipulatory organs, emphasizing the need for mobility at the shoulder and relative stability at the elbow (Miller, 1932; Rose, 1988, 1993; Fleagle, 1999; Ankel-Simons, 2000; Aiello and Dean, 2002; Kurtzer et al., 2006). Adaptations for enhanced mobility generally result in reduced stability of the joint. However, no primate except human has the forelimb

completely freed from support and locomotor roles. Thus, the morphology of the forelimb is always a compromise between the conflicting functional demands for mobility in order to reach and grasp arboreal supports and to allow effective use of the hand as a manipulatory organ, versus the need for sufficient stability to support the weight of the body and to withstand the disruptive forces generated during locomotion (Larson, 1993). The primates used in this study included *Pongo pygmaeus abelii* (2 males, 1 female), *Macaca fuscata* (1 female), and *Macaca sylvanus* (1 female). These primates were chosen due to their differences in locomotor and postural behaviours. Orangutans use wide ranges of motion during their main locomotor behaviours, which is described as suspensory locomotion, slow quadrumanous climbing, quadrupedal walking on ground, and bipedal standing, while macaque locomotion is generally described as being quadrupedal walking and running (arboreal and terrestrial), very little leaping, and occasional hanging during feeding (Ashton and Oxnard, 1962a, b; Oxnard, 1963; Tuttle, 1986; Galdikas, 1988; Hunt et al., 1996; Rowe, 1996; Fleagle, 1999; Chatani, 2003; Ankel-Simons, 2007). Locomotor and postural behaviour differences, as well as varying body masses in these primates, allowed muscular and entheseal morphologies to be compared, and tested how these morphologies varied with known behaviour.

This project also explored the entheseal morphology within a mouse (*Mus musculus*) experimental model. Thirty wild-type female outbred (CD-1) separated into one control and two experimental groups (running and climbing) were used for this study. The mice consisted of two age groups at the beginning of the experiment (25 and 46 days old). The muscles attaching to the left deltoid crest (spinodeltoideus, acromiodeltoideus, superficial pectoralis) were analysed. Experimental models allow for the control of settings such as age, weight, growth, and activity to be accurately recorded, which is ideal for studying how entheses may change in response to these

factors. Mice were also ideal for this study due to their small body size and rapid development (Carlson et al., 2008). This mouse experimental model may raise questions concerning the effects of scale when comparing the bone biology of mice to that of larger primates. Outside of a small number of extant strepsirrhines and fossil taxa, primates are larger, in most cases, many times larger, than mice. At their small size, geometric similarity predicts that mouse skeletons would be relatively strong (Biewener, 1990). However, mice experience strain magnitudes comparable to those of larger vertebrates during locomotion (Lee et al., 2002). The broad similarity in peak strain and bone safety factor in mammals across a large size range (Rubin & Lanyon, 1982) is likely due to the strong relationship between body mass and limb posture (Biewener, 1990); in other words, larger mammals maintain comparable strain levels by adopting less flexed limb postures. Therefore, mouse skeletons experience similar stress and strain regimes to those of large mammals. Mice demonstrate similar biological mechanisms present in human skeletal tissue and allow for skeletal and muscular exploration via dissections (Schlecht 2012a, b). The well-documented response of bone tissue to elevated loading environments has made mice and other small mammals important animal models for understanding general mammalian bone biology, including bone biomechanics relevant to human health (Kimes et al., 1981; Robling et al., 2006; Byron et al., 2010; Burr & Allen, 2013).

This dissertation represents a study incorporating aspects of both macro- and micro-structural features of muscle and bone in relation to daily activities. It combines soft- and hard-tissue data to explore the question of how activity influences the development of enthesis morphology to contribute to a more comprehensive interpretation of muscle function, animal posture, locomotion, and activity patterns. A better understanding of the relationship between activity, muscle, and bone is crucial for the interpretation of skeletal and fossil samples.

1.2 Organization of this thesis

Chapter 2 of this dissertation provides a general review of muscle anatomy and function. It looks at the structural composition of a skeletal muscle, followed by a brief description of muscle fibre architecture. Details on structures of the forelimb muscles in relation to locomotion are then discussed and the chapter ends with hypotheses to be tested for the soft-tissue variables.

Chapter 3 gives an overview in bone biology with a focus on the morphology and classification of entheses. It includes some details on bone cross-sectional geometry and bone microstructure. This chapter focuses particularly on details reflecting the influence of daily locomotor activities and the development of muscle-bone interface found on the humerus. It also provides the hypotheses to be tested for the bony variables.

Chapter 4 describes the samples and the selection criteria of the specimens used for this dissertation. The specimen preparation methodology is described, including dissection and skeletonization protocols, as well as the embedding and histological preparations. Finally, description of measurements, imaging methods, and an overview of the statistical analyses performed are presented.

Chapter 5 and 6, present the results found from both samples of the dissertation. Chapter 5 provides hard- and soft-tissue observations of the humerus reported for the primate sample. Results are presented in three main sections corresponding to the research objectives outlined: forelimb internal muscle structure and function (and by extension, behaviour), humerus entheseal

surface morphology (assume to reflect behaviour), and biomechanical shape (bone strength) of the humerus.

Chapter 6 provides hard- and soft-tissue analyses of the left humerus for the mouse sample. For this chapter, results are presented in four main sections: muscle anatomy and function of the forelimb muscles attaching to the deltoid crest, deltoid entheseal surface anatomy, cross-sectional bone geometry analyses at the crest, and bone histology (variation and growth).

Finally, Chapter 7 summarizes the main results of this dissertation and their significance. This is followed by a discussion of the broader implications of this research for the study of muscle attachments in bioarchaeological and fossil samples, and the avenues for future investigations.

Chapter 2

2. Muscle anatomy and function

Skeletal muscle is a highly organized, complex, and dynamic tissue that responds to the mechanical forces placed upon it (Close, 1972; Caiozzo, 2002; Lieber 2002; Botticelli and Reggiani, 2006). It provides maintenance of body posture against force by distributing loads and absorbing shocks (Lorenz and Campello, 2001). Skeletal muscles are composed mainly of contractile material, and enable the bones to move at the joints. These contractile properties can strongly influence normal muscle function, and therefore muscle force transmission, maintenance, and repair (Gillies and Lieber, 2011). The following chapter will review the structural composition and physiology of skeletal muscles from the micro to macroscopic levels. It will then discuss the architectural variables that influence muscle power, followed by a brief discussion in muscle functional specialization for different positional and locomotor behaviours. The chapter concludes with hypotheses to be tested.

2.1 Muscle structural biology

The structural unit of the skeletal muscle is the fibre, a long and cylindrical cell with hundreds of nuclei, which is enclosed in connective tissue called endomysium (Lorenz and Campello, 2001; Lieber, 2002). Endomysium provides strength and support to the muscle, and contains capillaries, lymphs, and terminal nerves. A muscle fibre can range in diameter from 10 to 100 microns (μm) (Close, 1972; Lorenz and Campello, 2001; Lieber, 2002), and may run the entire length of a muscle, or may only be a few centimetres long. A wide variation in fibre lengths exists among muscles in an individual and within homologous muscles across animal taxa

(Anapol and Jungers, 1986; Antón, 1994, 1999, 2000; Anapol and Barry, 1996; Gibbs et al., 2002; Lieber, 2002; Anapol and Gray, 2003; Taylor and Vinyard, 2004; Organ, 2007, 2009; Taylor et al., 2009). The variation in diameter and length found in muscle fibres influences the potential power of the whole muscle (e.g., potential strength, excursion, and contractile velocity) (Lieber 2002, Williams et al., 2008).

A fibrous membrane, the perimysium, surrounds a bundle of fibres, called fascicles (Figure 2.1). Many fascicles are then also bound together by an overcoat of dense connective tissue, called epimysium covering the entire muscle, which is visible during gross dissections. The epimysium blends into a strong cordlike tendon (or into a sheet-like aponeurosis for fibrous attachments [see Chapter 3]) to attach muscle directly to bone and/or cartilage (Lieber, 2002). Tendons are mostly tough collagenic parallel fibres, with no contractile properties, but able to withstand high unidirectional (tensile) force. Thus, tendons allow muscle bellies to be at an optimal distance from the joint on which they act without requiring an extended length of muscle between the origin and insertion (Lorenz and Campello, 2001).

Because tendons have no contractile properties, those properties are limited to the muscle fibres. Each fibre is made of numerous myofibrils surrounded by sarcoplasmic retinaculum. Myofibrils are arranged in parallel and approximately 1 μm in diameter (Close, 1972; Lorenz and Campello, 2001; Lieber, 2002; Gillies and Lieber, 2011) and are composed of many sarcomeres (muscle segment) arranged in a series end-to-end. Sarcomeres are the functional unit of muscle contraction and are approximately 2 μm long (see section 2.2). Whole adult muscles cannot grow by adding muscle fibres to fascicles, except during injury repair where new muscle fibres can build from muscle fibre stem cells assembled around each myofibril (Lieber, 2002). Muscle

growth can instead occur by one of two mechanisms (Goldspink, 1968; Williams and Goldspink, 1971, 1973, 1976, 1978; Antón, 1994; Lieber, 2002; Organ, 2007; Marini and Veicsteinas, 2010): 1) myofibrils can add sarcomeres at the tendon sites, thereby increasing length (which increases contraction velocity and excursion), or 2) muscle fibres can hypertrophy, increasing fibre diameter, which increases force production. These mechanisms are crucial to differentiate specialization of a muscle for postural and locomotor behaviours, and therefore important for the goals of this project.

Power production also depends on the metabolic properties of the muscle fibre. Fibres have been histologically and histochemically distinguished into types based on the metabolic pathways by which they produce adenosine triphosphate (ATP), as well as the speed with which they contract (Lorenz and Campello, 2001, 1989; Lieber, 2002). In general, these types can be classified as 1) Type I fibres (slow-twitch oxidative [SO]), and 2) Type II fibres (Type IIA; fast-twitch oxidative-glycolytic [FOG] and Type IIB; fast-twitch glycolytic [FG]) (see Lieber, 2002 for review). Muscles are composed of a mixture of these fibre types, and therefore the relative proportion of fibre types within a given muscle depends on the function of the muscle itself. Type I fibres are usually found in higher proportions in postural muscles (e.g., pectoral muscles) than in phasic muscles (e.g., deltoid). This means that postural muscles can maintain repetitive contractions for longer periods of time before becoming fatigued. Phasic muscles, with higher concentrations of Type II fibres, are better suited for movement but are more easily fatigued (Anapol and Junger, 1986; Jouffroy and Médina, 1996; Jouffroy et al., 1998; Lorenz and Campello, 2001; Lieber 2002; Higham and Biewener, 2011). Just as important as fibre type composition is the organization of the fibres within the entire muscle. This muscle fibre

architecture will determine the force and velocity with which a muscle can contract (see section 2.3).

2.2 Sarcomeres and the mechanics of muscle contractions

As mentioned above, the functional units of skeletal muscles are the sarcomeres. The number of sarcomeres within a myofibril is variable and related to muscle function (Hill, 1953; Hegarty and Hooper, 1971; Goldspink, 1968; Williams and Goldspink, 1973, 1976, 1978; Lieber et al., 1994; Goulding et al., 1997; Burkholder and Lieber, 2001; Lieber, 2002; Langenderfer et al., 2004). Sarcomeres are composed of two sets of contractile filaments, called myofilaments, which differ in their relative thickness. The thicker set contains the protein myosin, while the thinner set of myofilaments contains the protein actin (which also includes contractile regulatoratory proteins named tropmyosin and troponin). The myosin and actin filaments overlap to produce muscle contractions and give the skeletal muscle its striated appearance. Finally, sarcomeres also include an elastic filament, which is primarily composed of the protein titin and plays an important role in passive muscle tension (Gans, 1982; Lorenz and Campello, 2001, 1989; Lieber, 2002).

Under a polarized light microscope, regions of a sarcomere have different appearances (Lorenz and Campello, 2001, 1989; Lieber, 2002; Felder et al., 2005) (Figure 2.2). Regions containing thick myosin filaments are called A-band and are anisotropic (appear light) under polarized light. Regions with thin actin filaments are named I-band and are isotropic (appear dark) under polarized light. The thin actin filaments are found at the ends of the sarcomere and are anchored in a region called the Z-band. The Z-band links the thin filaments to the adjacent sarcomeres. From the Z-band, the actin filaments (I-band) extend toward the centre where they overlap with the myosin filaments (A-band). In the centre of the A-band is a light region called the H-zone,

which contains only thick filaments. In the middle of the H-zone, is a line called the M-line, where thick filaments are linked to the adjacent thick myosin. Z-bands are connected to M-lines by titin molecules that parallel the myosin filaments (Lorenz and Campello, 2001, 1989; Lieber, 2002). Therefore, to measure the length of a sarcomere is to measure the distance from one Z-band to the next.

To have a better comprehension of how a whole muscle contracts, contractions at the sarcomere level must first be described. In its simplest terms, muscle contraction occurs when myosin filaments slide past actin filaments (Gans, 1982; Gans and de Vree, 1987; Lorenz and Campello, 2001, 1989; Lieber, 2002; Moore and Agur, 2007). Thus, the filaments themselves do not contract; they remain the same length. In order for the myosin filaments to slide past actin filaments, cyclic movements of myosin cross-bridges (i.e. myosin heads) are achieved along the actin filaments within the A-band. These cross-bridges rotate around a fixed position on the myosin surface while sliding the actin filament toward the centre of the sarcomere. Therefore, the Z-bands move closer together. The movements of the filaments through one cross-bridge are very minimal, which means that each individual cross-bridge must separate from its receptor site to reattach to another further down the line of action. Finally, this process is repeated a number of times (see Lorenz and Campello, 2001, 1989; Lieber, 2002 for review).

2.2.1 Muscle contraction: energy supply and innervation

ATP is present only in small amounts within a muscle (enough for about ten rapid contractions). Creatine phosphate (organic phosphate molecule) is present in greater amounts, and its phosphate group is transferred to adenosine diphosphate (ADP) as supplies of ATP become exhausted. The oxidation of carbohydrates, stored in the muscle (glycogen), replenishes the

creatine phosphate supplies within the muscle. Between 0.5 - 2% of the wet weight of a muscle is stored in glycogen (Aiello and Dean, 2002; Lieber, 2002).

Muscle contraction is initiated when a nerve impulse arrives at a neuromuscular junction also called motor end plate. The impulse spreads and extends over the surface of the muscle fibres as an electric depolarization. The muscle-cell membrane (sarcolemma) covering each fibre connects with the deeper parts of the muscle by transverse tubules (T-system) that run across the muscle cells near the Z-lines. The sarcoplasmic retinaculum that surrounds each muscle fibre contains calcium ions. Each wave of depolarization spreads through the T-system and causes an increase in the permeability of the membrane of the sarcoplasmic retinaculum to calcium ions. The calcium ions are then released and interact with the myofilaments altering their configurations and permitting interaction between myosin and actin molecules (Lorenz and Campello, 2001; Aiello and Dean, 2002; Lieber, 2002).

The number of nerve fibres that innervate a muscle is smaller than the number of muscle fibres. Within a muscle, nerve fibres branch and innervate several muscle fibres. This motor unit varies in size depending on the muscle function (see below). The excitatory impulses of the motor units can be recorded as an electromyogram (EMG), which is the recording of the extracellular potential of the muscle. In a fully relaxed muscle no change in potential is recorded, but with an increasing force of contraction, action potentials or impulses show up on the EMG. This method is greatly used to explore the mechanism of muscle contraction potential in different muscles as well as different species (Tuttle and Basmajian, 1978a, b; Jungers and Stern, 1980; Susman and Stern, 1980; Susman et al., 1982; Tuttle et al., 1983; Larson and Stern, 1986, 1989, 1991, 1992, 2006, 2007; Whitehead and Larson, 1994; Larson, 1995; Demes et al., 1998; Jouffroy et al.,

1998; Larson et al., 2000, 2001; Stern and Larson, 2001; Aiello and Dean, 2002; Lieber, 2002; Diederichsen et al., 2007; Moore and Agur, 2007).

2.2.2 Launch of a muscle contraction and force

Muscle contraction begins when calcium ions and ATP are available to the contractile elements (Gordon et al., 1966; Huxley, 1972; Lorenz and Campello, 2001, 1989; Lieber, 2002). When a muscle is relaxed, the tropomyosin and troponin proteins (found with the thin actin filaments) completely cover the myosin cross-bridge receptor sites. In the presence of calcium released by a nervous stimulation from the sarcoplasmic reticulum, the tropomyosin and troponin shift, which allows the myosin cross-bridge to bind to the actin filament. In order for the filaments to move (continuation of the contraction), ATP is required to break down the cross-bridges (Gordon et al., 1966; Huxley, 1972; Lorenz and Campello, 2001, 1989; Lieber, 2002). The potential of cross-bridges that form depends on the overlap between the filaments. The greater the number of cross-bridges, the greater the potential movement and muscle force production (Hill, 1953; Gordon et al., 1966; Huxley, 1972; Gans, 1982; Gans and de Vree, 1987; Lorenz and Campello, 2001, 1989; Lieber, 2002; Moore and Agur, 2007).

Whole muscle contractions can be classified on whether or not they are producing movement at a joint (Gans, 1982; Gans and de Vree, 1987; Lorenz and Campello, 2001, 1989; Lieber, 2002; Moore and Agur, 2007). A contraction that does not produce joint movement, when no mechanical work is performed, is called isometric. Muscle length remains the same and no movement occurs, but muscle tension is increased above tonic levels in response to a load placed by an externally applied force. Thus, isometric contraction maintains joint posture in response to external loads (e.g., deltoid holding the arm in abduction). A contraction that produces

movement, when mechanical work is performed, is called isotonic. Muscle changes in length (increases/eccentric contraction or decreases/concentric contraction) in response to an externally applied force, while muscle tension remains relatively constant. These contractions rarely occur in isolation (Gans, 1982; Gans and de Vree, 1987; Lorenz and Campello, 2001, 1989; Lieber, 2002; Moore and Agur, 2007).

The amount of pulling force (tension) a muscle can exert during isometric contraction varies with the muscle length at which the contraction started. Maximal isometric tetanic tension is produced when an individual sarcomere is at its resting length (Gordon et al., 1966). At this length, the myosin and actin completely overlap and the number of cross-bridges formed is maximized. When the myofibril lengthens beyond resting point, the overlap and cross-bridges between filaments decreases up to no overlapping filaments, which result in a loss of isometric tension. When the myofibril shortens below resting length, isometric tension (i.e. muscle force output) also decreases. The decrease in muscle tension is either due to overlapping adjacent actin filaments and therefore interference of the cross-bridge formation, or due to the interference with the Z-band (Gordon et al., 1966; Huxley, 1972).

Striated muscle produces active force by the sliding of actin and myosin filaments past each other in an energy-consuming mechanism (Huxley, 1972). When relaxed muscle fibres are stretched beyond a certain degree, they develop a passive tension (demonstrated to be borne mostly by myofibril). Single titin molecules span the distance from the Z-disk to the M-line covering an entire half-sarcomere (titin acts as a blueprint for sarcomeric assembly). The same relationship is seen in whole muscles (Figure 2.3) with the exception of the presence of passive tension generated by titin molecules, associated tendons, apeunoroses, and intrinsic connective

tissues (e.g., epimysium) (Lorenz and Campello, 2001). For isotonic contractions (eccentric or concentric), the relationship can be examined between force and contraction velocity (Figure 2.3). Velocity of concentric contraction exponentially decreases as force (e.g., load) increases. When the external force on a muscle is equal to the maximum tetanic tension in a muscle, the velocity of contraction equals zero, and the muscle contracts isometrically (Figure 2.4) (Lorenz and Campello, 2001). These parameters can be estimated by examining the fibre architecture of whole muscles.

2.3 Muscle fibre architecture

The arrangement of internal muscle structures influences the force production of a muscle (Gans, 1982; Gans, 1988; Lieber and Brown, 1992; Lieber, 2002; Williams et al., 2008; Lieber and Ward, 2011). The relationship between force and these fibre architectural features is important for understanding how the muscle functions along with the skeleton. Fibre architecture of homologous muscles can vary widely among taxa, and these differences are often due to specialized postural, locomotor, and feeding behaviours (Gans, 1982; Anapol and Jungers, 1986; Zajac, 1992; Anapol and Barry, 1996; Antón, 1994, 1999, 2000; van Eijden et al., 1997; Anapol and Gray, 2003; Taylor and Vinyard, 2004; Carlson, 2006; Payne et al., 2006a; Smith et al., 2006; Oishi et al., 2008, 2009; Organ et al., 2009; Taylor et al., 2009; Higham and Biewener, 2011). Some muscles have fibres that are arranged in parallel relative to the force-generating axis of the muscles (parallel-fibred muscle), while others have fibres that insert at an angle relative to the force-generating axis (pennate-fibred muscle). The number of fibres can vary from one to several hundreds, according to the size and function of the muscle. Where precision movements are needed, the motor unit, which is the motor neuron and muscle fibre, can contain only a few muscle fibres (e.g., hand muscles), while large motor units (one neuron supplying hundreds of

muscle fibres) are found in large muscles (e.g., shoulder and arm muscles) (Lieber 2002, Moore and Agur, 2007).

To better understand muscle function, one must consider a simplistic model where fibres of a given muscle are equal in length and parallel to the muscle belly. Sarcomeres line up in series of overlapping actin and myosin filaments. The distance per unit of time through which a muscle fibre shortens is a function of its absolute length. Therefore, the number of sarcomeres in a series determines muscle fibre length, and is proportional to a muscle's maximum excursion and velocity of contraction (Gans, 1982; Gans, 1988; Lieber and Brown, 1992; Lieber, 2002; Williams et al., 2008; Lieber and Ward, 2011). Long parallel fibres shorten the most, giving a wide range of movement at a joint (excursion) and speed of contraction, but with less power (e.g., parallel-fibred muscles) (Figure 2.5). Muscle power increases with the total number of sarcomeres. Pennation allows for packing of shorter, muscle fibres into a given space and potentially a smaller area of attachment to the bone. As a result, short and wide pennate muscles have the most fibre bundles that shorten less but are more powerful (e.g., pennated-fibred muscles). Physiological cross-sectional area (PCSA) represents the sum of the cross-sectional areas of all muscle fibres within a given muscle, and is an important proxy for potential maximum force generating output of a muscle (Gans, 1982; Anapol and Jungers, 1986; Hurov, 1986; Gans and De Vree, 1987; Antón, 1994; Lemelin, 1995; Anapol and Barry, 1997; Lieber, 2002; Medler, 2002; Anapol and Gray, 2003; Organ, 2007; Williams et al., 2008; Taylor et al., 2009).

The external work performed by a muscle is the product of force it generates and the distance that its free attachment moves (Figure 2.5). The external work is also related to the length of the

muscle fibres since most muscle can contract to about one-third of their resting state. Two muscles of the same cross-sectional area will have the same potential force of contraction but if one is twice as long, it will be able to contract further and thus perform more external work. However, the external work performed by a pennate muscle cannot be greater than that of a parallel fibred muscle despite its increase in force, because the distance moved at its insertion is greatly reduced (Gans, 1982; Anapol and Jungers, 1986; Hurov, 1986; Gans and De Vree, 1987; Antón, 1994; Lemelin, 1995; Anapol and Barry, 1997; Aiello and Dean, 2002; Lieber, 2002; Medler, 2002; Anapol and Gray, 2003; Organ, 2007; Williams et al., 2008; Taylor et al., 2009).

The relative contribution of tendons to the overall musculo-tendon length can indicate whether a muscle is architecturally designed for isotonic (higher energy cost) or isometric (lower energy cost) contraction. As mentioned previously, since tendons are non-contractile tissues, measuring the relative proportion of contractile (fibre) and non-contractile (tendon) tissues within a muscle may indicate how energetically cost-efficient a muscle is (Elliot, 1965; Elliot and Crawford, 1965; Zajac, 1992; Biewener, 1998; Alexander, 2002; Roberts, 2002; Suzuki et al., 2002, 2003; Anapol and Gray, 2003; Hansen et al., 2003; Michilsens et al., 2009). Therefore, differences in internal muscle structures can affect functional variables such as the potential maximum tetanic tension generated by a muscle, potential maximum excursion (range of motion) and contraction velocity of a muscle, the active energetic cost of muscle function, and whether a muscle is better suited for isotonic or isometric contraction.

2.4 Forelimb myology and hypotheses to be tested

The relationship between muscles and bones is ontogenetically and mechanically related. Muscles are the active partners, while bones are the passive support structure on which the

muscles and their tendons exert forces (i.e. pulling and stretching forces) (Aiello and Dean, 2002; Lieber, 2002; Ankel-Simons, 2007). Thus, the morphology of the postcranial skeleton is adapted to a variety of locomotor and postural activities. Anatomical variation of the forelimb muscles in mammals have been investigated using animal experimental models (Anderson et al., 1993; Carry et al., 1993; Edman, 2005; Montgomery et al., 2005; Hamrick et al., 2006a, b, 2010; Green, 2010; Green et al., 2011, 2012), radiography and telemetered electromyography (EMG) (Tuttle and Basmajian, 1978a, b; Jungers and Stern, 1980; Susman and Stern, 1980; Susman et al., 1982; Tuttle et al., 1983; Larson and Stern, 1986, 1989, 1991, 1992, 2006, 2007; Whitehead and Larson, 1994; Larson, 1995; Demes et al., 1998; Jouffroy et al., 1998; Larson et al., 2000, 2001; Stern and Larson, 2001; Diederichsen et al., 2007), video photography, computerized support, theoretical and biomechanical models (Amis and Dowson, 1979; Amis et al., 1979; An et al., 1981; Reid et al., 1989; Jouffroy et al., 1998; Biewener, 2000; Cheng and Scott, 2000; Davidson and Buford, 2006; Isler et al., 2006; Langenderfer et al., 2006; Oizumi et al., 2006; Abdulaliyev et al., 2007; Holzbaur et al., 2007a, b), and of course through gross dissections (Ashton and Oxnard 1962a, b, 1963; Oxnard, 1963, 1967; Gibbs et al., 2002; Anapol and Gray, 2003; Diogo et al., 2009; Michilsens et al., 2009). Researchers usually focus on single muscles (e.g., triceps brachii) or a group of muscles (e.g., abductors of the arm) with the purpose to find the full range of variation that exists and to determine the principal function of the muscle. The results of these studies in muscular activity show both inter- and intra-specific diversity; such factors as age, sex, behavioural lateralization, locomotor and postural behaviour, as well as body weight must be considered when analysing internal muscular structures.

Researchers have also shown that muscular anatomy is highly plastic during an individual's lifetime (Close, 1972; Kiliaridis, 1989; Kelly, 1996; Asfour et al., 1984; Caiozzo, 2002; Lieber,

2002; Hansen et al., 2003; Botticelli and Reggiani, 2006; Atzeva et al., 2007; Marini and Veicsteinas, 2010) particularly if there is a change in the exercise regime. All of the internal muscle structures discussed above can change with a given stimulus, ranging from a modification in contractile activity (e.g., inactivity, endurance, exercise denervation, electrical stimulation), modification of imposed load (resistance exercise, unloading, microgravity), and other environmental factors such as heat, hypoxia, nutrient availability, growth factors, and inflammation mediators (Marini and Veicsteinas, 2010). Increased use of a muscle can alter fibre architecture, fibre type distribution, tendon length, and capillary density (Laros et al., 1971; Lieber, 2002; Zumwalt, 2005, 2006; Green, 2010; Marini and Veicsteinas, 2010; Green at al., 2012). Skeletal muscle responds to the amount and type of activity that is imposed upon it. Different training protocols can induce different results in the recruitment of muscle fibres. Exercise can be distinguished between endurance and strengthening. The type of exercise refers to the amount of exercise (e.g., minutes per day × days per week × total weeks), and makes reference to exercise intensity (e.g., percent of maximum voluntary contraction in an isometric exercise). Therefore, when evaluating changes in muscle properties possibly due to exercise, many factors have to be included (e.g., type of muscle, type of exercise, amount of exercise). On the other hand, skeletal muscle can also respond to decreased use. Lack of muscular stimulation can be characterized by muscle fibre atrophy, decreased muscle force generating capacity, and a slow-to-fast muscle fibre type conversion if the disuse is extreme enough (Dysart et al., 1989; Lieber, 2002; Hamrick et al., 2006a). Essentially, this relationship represents a reversal of the increased use response, which is often seen in older individuals. Considering the high plasticity of the muscles in adult individuals, researchers further emphasize the variability of muscle morphology and the importance of fully understanding muscle anatomy, physiology, and function

in order to identify morphological features useful in the functional interpretation of skeletal and fossil material.

2.4.1 Hypotheses to be tested

It has been argued theoretically (e.g., Gans, 1982; Biewener and Gills, 1999; Lieber, 2002; Williams et al., 2008) and demonstrated empirically (e.g., Taylor et al., 2009) that a muscle cannot be simultaneously optimized for maximum force generation (high PCSA) and excursion/contraction velocity (long fibre length) (Figure 2.5). This architectural trade-off is expected among the different primate species (*Pongo pygmaeus abelii*, *Macaca fuscata*, and *Macaca sylvanus*), and the different mouse groups (*Mus musculus*) used for this project. As mentioned above, fibre architecture of homologous muscles can vary widely among taxa, and these differences are often due to specialized postural, locomotor, and feeding behaviours (Gans, 1982; Anapol and Jungers, 1986; Zajac, 1992; Anapol and Barry, 1996; Antón, 1994, 1999, 2000; van Eijden et al., 1997; Anapol and Gray, 2003; Taylor and Vinyard, 2004; Carlson, 2006; Payne et al., 2006a; Smith et al., 2006; Oishi et al., 2008, 2009; Organ et al., 2009; Taylor et al., 2009; Higham and Biewener, 2011). Physical activity will also affect aspects of internal muscular structure. An increase in muscle size is often associated with exercise (Gans, 1982; Anapol and Jungers, 1986; Hurov, 1986; Gans and De Vree, 1987; Antón, 1994; Kelley, 1996; Wang and Kernell, 2001; Lieber, 2002; Anapol and Gray, 2003; Hansen et al., 2003; Zumwalt 2005, 2006; Smith et al., 2006; Green, 2010, 2012). Therefore, it is expected that the internal fibre architecture of the forelimb muscles in the primates and mice studied will vary in relation to their different locomotor and postural behaviours as well as the amount of activity performed by each animal.

In association with locomotor patterns, other factors such as age, sex, and body mass may alter the internal muscle structures. For example, females tend to have smaller muscles than males. This difference is mainly due to physiological reasons; males in general have larger muscles than do females associated with body size, locomotion and/or activity patterns (Hawkey and Merbs, 1995; Hawkey 1998; Wilczak 1998a, b; Knüsel, 2000; Eshed et al., 2004; Weiss, 2003, 2004, 2007, 2010; Molnar, 2006, 2010; Jurmain et al., 2012; Nolte and Wilczak, 2013).

The following hypotheses with associated null hypothesis related to differences in muscle fibre architecture of the forelimb will be tested for all animals:

H1 = Different locomotor patterns in the animals studied will result in corresponding changes in muscle architecture of the forelimb muscles.

H1.1 (tested on the mouse sample only) = Increased activity in the animals studied will result in the development of forelimb muscles with greater maximum force-generating potential output.

H1.2 = Differences in sex and age of the animals studied will result in corresponding changes in the internal muscle structures of the forelimb muscles. Males and adults will develop muscles with greater maximum force-generating potential output.

H0 = There is no difference in the muscle anatomy of the forelimb muscles attaching to the humerus in the animals studied.

2.4.2 Primate forelimb muscles

As seen in Chapter 1, the morphology of the forelimb in primates is always a compromise between the conflicting functional demands for mobility in order to reach and grasp arboreal supports and to allow effective use of the hand as a manipulatory organ, versus the need for sufficient stability to support the weight of the body and to withstand the disruptive forces generated during locomotion (Larson, 1993). Orangutans are found in rain forests and are the largest primate that is almost completely arboreal (Tuttle, 1986; Galdikas, 1988). Orangutans do not brachiate while moving in their arboreal habitat due to their large size. Their main form of locomotion in the trees is quadrumanus climbing used to achieve maximal weight distribution across as many supports as possible. While terrestrial, the orangutans use the sides of their hands and feet as the main body support during "fist walking" quadrupedalism. They can also do some bipedal standing (Ashton and Oxnard, 1962a, b; Oxnard, 1963; Tuttle, 1986; Galdikas, 1988; Hunt et al., 1996; Rowe, 1996; Fleagle, 1999; Ankel-Simons, 2007). Theoretically, these locomotor behaviours should involve larger propulsive and arm-raising muscles, larger elbow flexors, and more developed wrist flexors. More specifically, previous studies have characterized forelimb musculature of suspensory/arboreal primates (e.g., orangutan, chimpanzees, gibbons) with: large digital flexors, strong elbow and wrist flexors, large supinator, latissimus dorsi and teres major muscles (Ashton and Oxnard, 1962a, b; Oxnard, 1963; Tuttle, 1972; Jungers and Stern, 1980; Fleagle, 1999; Thorpe et al., 1999; D'Août et al., 2004; Carlso, 2006; Thorpe and Crompton, 2006; Oishi et al., 2008, 2009; Michilsens et al., 2009). Based on these past studies, it is expected that the orangutans will have highly pennated, shorter fibres, but larger physiological cross-sectional areas of the elbow and wrist flexors in order to generate more potential force output. These (especially the wrist flexors) should be coupled with long tendons (isometric contraction and therefore maximal force production). Shoulder muscles, because they need to

have a wide range of motion, are expected have long and parallel (smaller PCSA) muscle fibres. The males in this sample are also predicted to have greater body size, and therefore larger and more pennated muscles than the females.

The genus *Macaca* lives in various environments with diverse ecological conditions, and each species is adapted to its own environment. Japanese macaques (*Macaca fuscata*) live in mainly temperate deciduous or evergreen broadleaf forests, which can be covered in snow during parts of the year. In general, Japanese macaques are semiterrestrial, and mainly walk and run quadrupedally with some occasional leaping (Chatani, 2003). Barbary macaques (*Macaca sylvanus*) live mainly in high altitude mountains, cliffs, and gorges surrounded by temperate forests. They also experience cold temperatures. Their arboreality shifts with the seasons. They are more terrestrial in the summers and more arboreal in the winters. Barbary macaques quadrupedally walk and run, leap, and can hang from cliffs (Ashton and Oxnard, 1962a, b; Oxnard, 1963; Hunt et al., 1996; Rowe, 1996; Fleagle, 1999; Chatani, 2003; Ankel-Simons, 2007). These two species of macaques were studied because they were found in the same enclosures at the zoo, and were able to adapt to the same environment. It is expected that their smaller body size and different locomotor and postural patterns from orangutans will be reflected in their internal muscle structures of the forelimbs. Theoretically, these locomotor behaviours should involve more developed propulsive muscles, and larger elbow and wrist extensors. Indeed, previous studies have characterized forelimb musculature of quadrupedal primates with: strong shoulder protractors, large and strong elbow and wrist extensors (Ashton and Oxnard, 1962a, b; Oxnard, 1963; Kimura and Takai, 1970; Cheng and Scott, 2000; Larson and Stern, 2007). Based on this, it is expected that the macaques will have highly pennated, shorter fibres, with larger physiological cross-sectional areas of the elbow and wrist extensors in order to

generate more potential force output (opposite from the suspensory orangutan). Once again, these should be coupled with long tendons (isometric contraction and therefore maximal force production). Contrary to the orangutans, the shoulder muscles, particularly the protractors, are expected to have highly pennated, shorter fibres, with large PCSAs.

2.4.3 Mouse forelimb muscles

Advances in medical science often come from information gained through the use of mouse models. Although comparative anatomy of muscle is less common, recent comparative muscle studies have identified notable differences between humans and other animals (e.g., Diogo et al., 2009) and emphasize the need to have a firm understanding of the unique features of an animal model and how those features can relate to humans. Differences in gait are usually related to many of these unique features seen in mammalian models (Cavagna et al., 1977; Alexander, 2002; Mathewson et al., 2012). Mice (*Mus musculus*) are small, terrestrial, quadrupedal animals that can run walk, jump, climb, and swim. The forelimb muscles of a quadrupedal animal should therefore be specialized in weight bearing, since they are critical in stabilization and force production during gait (Clarke and Still, 1999; Green, 2010; Green et al., 2011, 2012). Mathewson and colleagues (2012) found that mice were characterized with large, force producing forelimb flexors, and greater excursion forelimb extensors. They did not however look at any of the muscles studied in this research. The spinodeltoideus muscle inserts on the entire lateral surface of the deltoid crest, while the acromiodeltoideus muscle and the superficial pectoralis muscle share the medial surface of the prominent ridge (see Figure 4.6 for illustration). The spinodeltoideus and the acromiodeltoideus represent the fibres of the deltoid that attach to the scapular spine and acromion in primates. Their insertion is combined as one on the deltoid tuberosity in primates, while it is separated on either side of the deltoid crest in mice. The

superficial pectoralis is equivalent to the pectoralis major in primates, although its attachment is inferior to the acromiodeltoideus muscle in the mouse. These three muscles that attach to the deltoid crest are the principal protractors (superficial pectoralis and acromiodeltoideus) and retractors (spinodeltoideus) of the humerus, which help the animal propel itself forward, maintain its balance, and resist gravitational forces. These muscles help maintain glenohumeral joint flexion when standing, walking, and running. They are essential to the habitual gaits experienced by all three groups of mice (running, climbing, control – see Chapter 4 for details). It is expected that the acromiodeltoideus and superficial pectoralis muscles will be larger and stronger (high PCSA and muscle mass for the limb protractors) with more pennated fibres, compared to the spinodeltoideus muscle (represented by longer, less pennated and smaller in size for the limb retractor).

Exercise regime (running, climbing) is expected to have a greater influence on muscular morphology than in the control mice. Both of the experimental groups should have more powerful muscles than the control mice. More specifically, it is predicted that the higher intensity exercise (running) will result in the development of muscles with greater maximum force-generating potential output (increased muscle mass and physiological cross-sectional areas, with shorter and more pennated fibres). Conversely, the muscles of the intermediate intensity exercise (climbing) are expected to be capable of producing more excursion and higher contraction velocities than the other mice, since muscles are generally structured to maximize either potential force production or contraction velocity. No difference is expected between the age groups because they will both be of adult body size and passed sexual maturity by the end of the experiment (Kilborn et al., 2002). Neither group will have reached an age associated with muscle deterioration. Therefore the total external power of the muscles should be the same.

Figure 2.1 Schematic structural organization of a muscle tissue from sarcomere to whole muscle (modified from Lorenz and Campello, 2001).

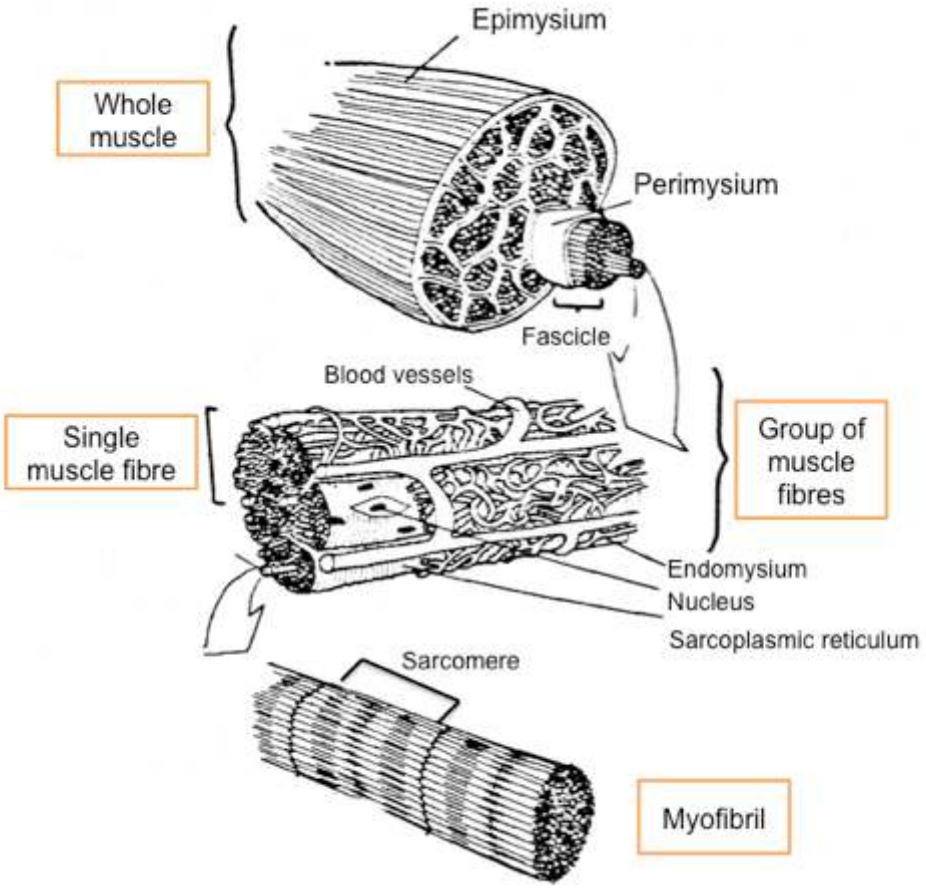

Figure 2.2 Schematic structural characteristics of a sarcomere and the overlapping arrangement of thick (myosin) and thin (actin) filaments. Within the actin filaments are the regulatory proteins tropomyosin and troponin (modified form Lieber, 2002).

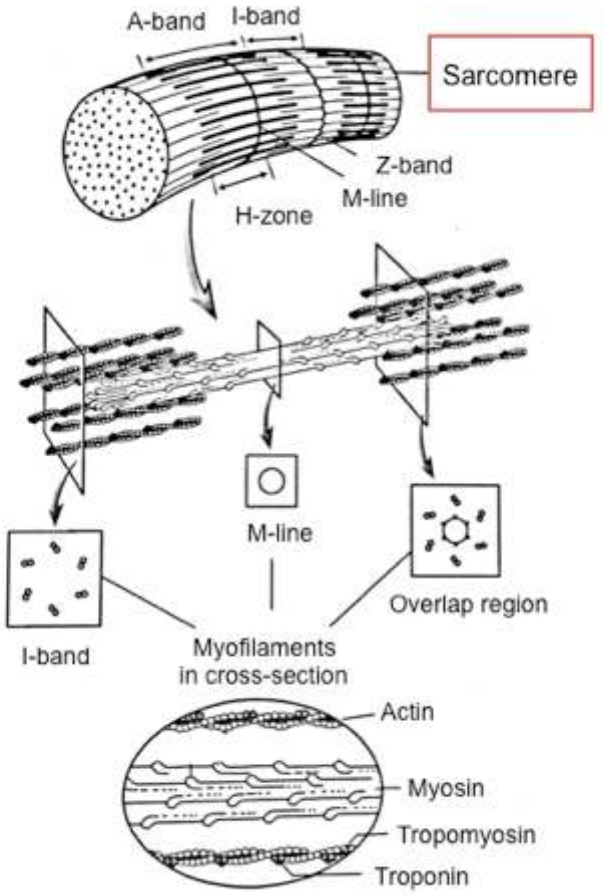

Figure 2.3 Length-tension curves: A) Sarcomere length-tension curve (modified from Lieber, 2002). Curve line represents passive muscle tension generated by connective tissues (e.g., endomysium, sarcoplasmic reticulum). B) Whole muscle length-tension curve during isometric contraction. Active muscle tension is generated by the contractile elements of the muscle tissue, while passive tension is generated by non-contractile elements. Optimal muscle tension is generated when the muscle is at resting length (modified from Lorenz and Campello, 2001).

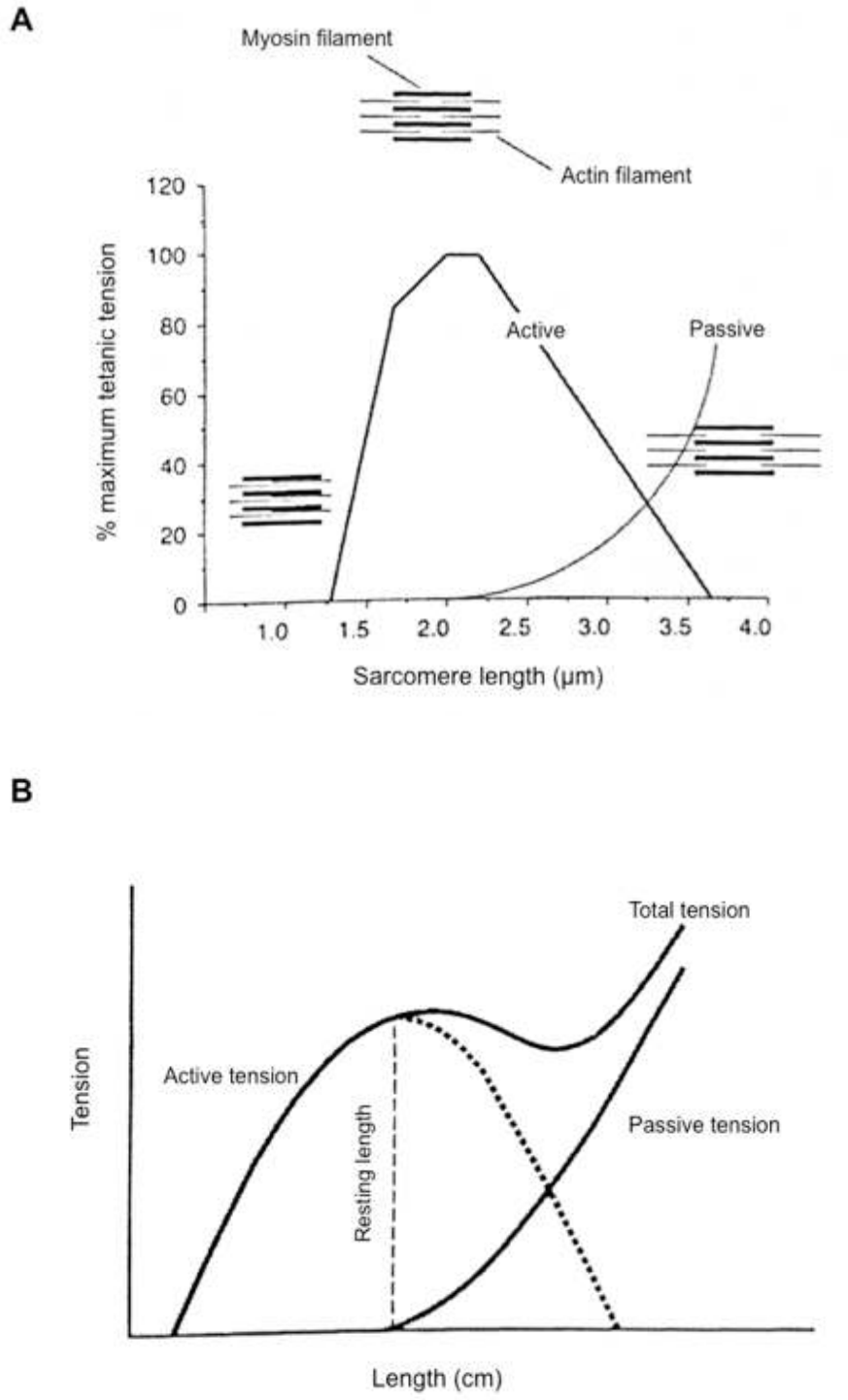

Figure 2.4 Load-velocity curve generated by plotting the velocity of the muscle lever arm against the external load. When the external load imposed on the muscle is negligible, the muscle contracts concentrically with maximal speed. With the increasing loads the muscle shortens more slowly. When the external load is equal to the maximum force that the muscle can exert (red start), the muscle fails to shorten (has zero velocity) and contracts isometrically. When the load is increased further, the muscle lengthens eccentrically. This lengthening is more rapid with greater loads (modified from Loranz and Campello, 2001).

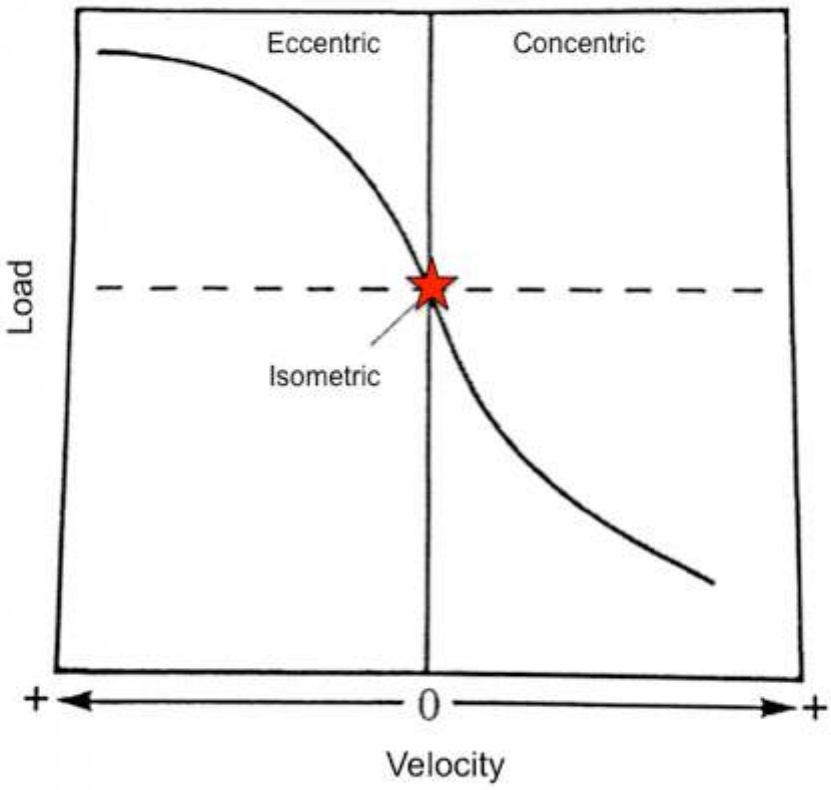

Figure 2.5 Schematic representation of the architectural trade-off between potential muscle force generating output (physiological cross-sectional area [PCSA]) and potential muscle excursion or contraction velocity (muscle fibre length [L_f]). The blue arrows show how a muscle is likely to increase in power (orange circle) with increased fibre length or physiological cross-sectional area (modified from Williams et al., 2008).

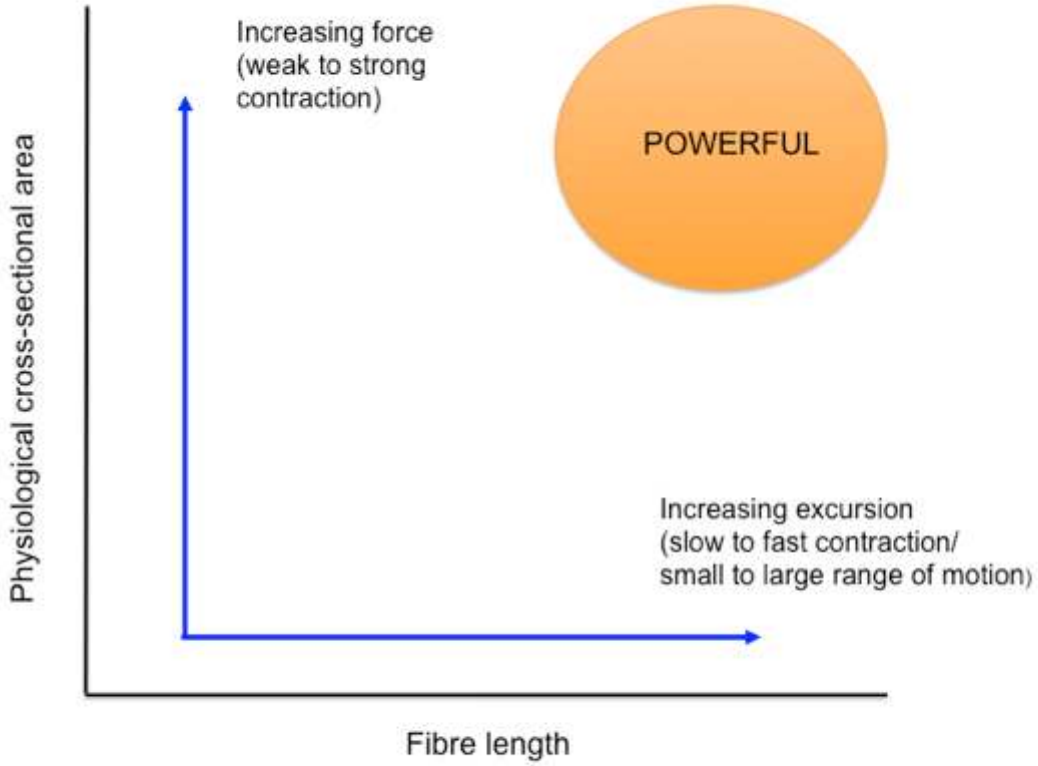

Chapter 3

3. Bone anatomy and function

Bone, like muscle, is a specialized and dynamic tissue that performs metabolic and mechanical functions. The functions of bone include maintaining mineral homeostasis, production of blood cells, protection of internal viscera, providing antigravity support, providing rigid kinematic links and muscle attachment sites, as well as facilitating muscle action and body movement (Martin et al., 1998; Frankel and Nordin, 2001; Currey, 2002; Huiskes and van Rietbergen, 2005). Bone is a highly vascularized tissue, with great self-repair capacities, meaning that it can alter its physical properties and configuration in response to changes in mechanical demands (Frankel and Nordin, 2001). Given this plasticity, bone is an invaluable tool for the study of evolution and behaviour. This chapter focuses on details reflecting the influence of daily locomotor activities on the development of muscle-bone interface found on the humerus. It provides a background in bone biology with a focus on the morphology and classification of entheses. Details on bone geometry and microstructure are also discussed as possible tools to analyse muscle attachment sites. Hypotheses to be tested are also outlined.

3.1 Bone structure and function

Bone exhibits considerable variation in its macroscopic as well as microscopic organization, which is a reflection of ontogenetic, local (functional), environmental, and phylogenetic factors (Enlow, 1963; Ricqles, 1993; Martin et al., 1998; Castanet et al., 2001). Bone tissue is a specialized connective tissue that is composed of water, cells, and an extracellular matrix (ECM) produced by those cells. The ECM of bone consists mainly of Type I collagen fibres,

proteoglycan ground substance (decorin and biglycan), and a small amount of non-collagenous proteins (Martin et al., 1998; Carter and Beaupré, 2001; Frankel and Nordin, 2001; Currey, 2002; Huiskes and van Rietbergen, 2005). The collagen provides flexibility and tensile strength to bone structure, and determines its structural organization (Martin et al., 1998; Burr, 2002). However, what distinguishes bone from other connective tissue is its high inorganic material content. Mineral salts such as phosphate and calcium are organized in small synthetic crystals of hydroxyapatite and can contain small amounts of carbonate, fluoride, and citrate (Martin et al., 1998; Frankel and Nordin, 2001). The mineral crystals add rigidity and compressive strength to the bone (Martin et al., 1998; Carter and Beaupré, 2001; Frankel and Nordin, 2001; Burr, 2002; Currey, 2002; Huiskes and van Rietbergen, 2005).

3.1.1 Bone cells

Four types of cells are responsible for the formation, maintenance, and resorption of bone tissues: osteoblasts, osteocytes, bone lining cells, and osteoclasts. Osteoblasts, osteocytes, and bone lining cells represent stages in maturation from a mesenchymal origin, while osteoclasts are derived from the monocyte-macrophage cell line. The differentiation and activities of these cells are regulated by a number of different hormones, transcription factors, and growth factors (Martin et al., 1998; Goldman, 2001; McFarlin, 2006; Maggiano, 2012; Stout and Crowder, 2012).

Osteoblasts (bone forming cells) are distinct cuboid shaped cells located near bone surfaces (periosteum [outside surface], endosteum [inside surface], marrow stroma [inside bone]) separated by an osteoid seam, which is a thin layer representing the lag time between osteoid formation and mineralization. They are responsible for the formation of bone, specifically the

non-mineralized osteoid substance and the non-collagenous proteins. Osteoblasts secrete proteins and regulate mineralization as well as osteoclast differentiation (Martin et al., 1998; Martin, 2000). Once an osteoid matrix becomes mineralized, the osteoblasts become embedded within that matrix and differentiate into osteocytes (Figure 3.1). These stellate-shaped cells are usually enclosed within spaces, called lacunae, and maintain connections with adjacent osteocytes (and cells at the bone surface) through small canals called canaliculi. Osteocytes participate in the passage of minerals in and out of the bone, and are thought to be key in the sensing and responding to mechanical strain (Martin et al., 1998; Martin, 2000). Meanwhile, osteoblasts that remain on the surface once bone is formed differentiate into bone lining cells. These flattened shaped cells form a barrier between the bone fluid compartment and interstitial fluids, and communicate with osteocytes and adjacent bone lining cell. They are capable of becoming active osteoblasts and they participate in the initiation of bone resorption during the process of remodelling (by undergoing changes in their disposition on the bone surface to provide access to osteoclasts) (Parfitt, 1994, Martin et al., 1998). Finally, osteoclasts (bone resorbing cells) are large multinucleated cells with irregular (ruffled) borders, usually found in contact with the bone surface within spaces called Howship's lacunae, which are formed through their own resorptive activity. Osteoclasts secrete hydrogen ions into the spaces, which lower the pH and create a conductive microenvironment to break bone mineral down. They also secrete proteolytic enzymes, which digest organic components of the matrix (Martin et al., 1998; Burr, 2002).

3.1.2 Bone tissue types

The components that make up the bony matrix and the cells involved in its development, maintenance, and resorption, are similar in all bone tissues. However, the proportions and organization of the components, the density and organization of the cells, and the degree of

vascularity differs between tissue types. Macroscopically, bone can be divided into two types: cortical (compact) and trabecular (cancellous) (Figure 3.1). Both of these types of bones can be found in most mammals, including primates and mice (Enlow, 1957; Francillon-Vieillot, 1990). Cortical bone forms the dense outer shell (cortex) of irregular and flat bones, the ends of bones, and the majority of long bone diaphyses. Trabecular bone is porous and marrow filled and forms the majority of irregular shaped bones, flat bones, and epiphyses (Martin et al., 1998; Carter and Beaupré, 2001; Frankel and Nordin, 2001; Burr, 2002; Currey, 2002; Huiskes and van Rietbergen, 2005). Microscopically, compact and cancellous bones differ in their vascularity, organization, collagen fibres and mineral crystals, and their cellular components. These variations can be attributed to differential rates of osteogenesis and in origin of development (periosteal or endosteal origin). The diversity and distribution of tissue types in vertebrates is a reflection of variability in life history, development patterns, phylogeny, and mechanical needs (Enlow and Brown, 1956, 1957, 1958; Enlow, 1962; Currey, 1984; Francillon-Vieillot et al., 1990; Bromage, 1991; de Ricqlès et al., 1991; Mulhern and Ubelaker, 2012). Below is a brief description of the more commonly recognized tissue types.

Three fundamental patterns are recognized based on the organization of the collagen fibres (from randomly organized to highly-ordered arrangement) and vascular density: woven, parallel fibred, and lamellar. Woven bone (fibrous) is rapidly formed and is found in the foetal skeleton, regions of the young postnatal skeleton, and areas of callus formation. It is loosely packed with collagen fibres running in all directions, and is highly vascularized. Osteoblasts and osteocytes are randomly distributed and more numerous compared to other tissue types (Enlow, 1963; Francillon-Vieillot et al., 1990; de Ricqlès et al., 1991). Parallel fibred bone is characterized by closely packed fibres having a single orientation and running parallel to one another (Francillon-

Vieillot et al., 1990; de Ricqlès et al., 1991). It is intermediate in organization, vascularization, and distribution of osteoblasts and osteocytes. Finally, the highly organized lamellar bone is comprised of layers of bone called lamellae where the osteoblasts tend to follow a linear course. Osteocytes are less distributed and the layered appearance seems to be a result of regular change in the orientation of the collagen fibres (Francillon-Vieillot et al., 1990; de Ricqlès et al., 1991; Currey, 2002). It is important to note that since collagen fibre is organized along a continuum, there are many other tissue types that can be grouped into those broader categories (e.g., lamellar-zonal bone, fibro-lamellar bone) (Enlow, 1963; Francillon-Vieillot et al., 1990; de Ricqlès et al., 1991; McFarlin, 2006; Goldman et al., 2009).

3.1.3 Primary and secondary origin of bone

Bone can be classified as being either primary (modeling) or secondary (remodelling) in origin (Enlow, 1963; Castanet et al., 1993; Francillon-Vieillot et al., 1990; Martin et al., 1998; Currey, 2002; McFarlin, 2006; Stout and Crowder, 2012). Primary bone tissues are deposited during growth at the periosteal or endosteal surface, where bone tissue did not previously exist. Vascular canals in primary tissues are embedded within the forming front of growing bones. Primary osteons can also be found in this tissue. Primary osteons are vascular canals that are surrounded by at least one layer of bone tissue concentrically deposited around the canal. Their formation does not involve resorption of older bone tissues and, unlike secondary osteons (see below) they are not delimited from adjacent bone tissue by the presence of a cement line (Enlow and Brown, 1956; Francillon-Vieillot et al., 1990).

Primary bone formation takes place via two mechanisms: 1) endochondral ossification (deposition occurs within a cartilaginous model), and 2) intramembranous ossification

(deposition takes place directly within condensations of mesenchyme without a cartilage intermediate) (e.g., Scheuer and Black, 2000). Cartilage is an avascular connective tissue with unmineralized ECM. It is therefore capable of undergoing interstitial (i.e. cell proliferation and matrix production within the cartilage) and appositional (i.e. cell proliferation and addition of new matrix at its surface) growth. Interstitial and appositional growth of hyaline cartilage at the epiphyseal plate provides a linear growth of long bones. Linear bone growth stops when chondrocytes at the epiphyseal plate(s) stop proliferating. Chondrocyte proliferation slows and eventually ceases during puberty under the influence of systemic hormones, mainly oestrogen (Schoenau and Frost, 2002; Fricke and Schoenau, 2007; Plochocki, 2009). Long bone epiphyseal union occurs at varying time across skeletal sites. The distal humerus is among the first to fuse and the proximal humerus usually among the last to fuse in primates and in mice (Scheuer and Black, 2000; Kilborn et al., 2002; McFarlin 2006). Then as a mineralized tissue, bone is only capable of appositional growth. Bone therefore grows in linear and cross-sectional dimensions, and must be continuously re-shaped or remodelled (Enlow 1962, 1976).

Secondary bone tissues are formed at the endosteal, periosteal, and intracortical surfaces of the bone. Secondary bone is deposited following resorption of an existing bone through the sequential action of osteoclasts and osteoblasts (Enlow, 1963; Francillon-Vieillot et al., 1990; Frost, 1990; Martin et al., 1998; Currey, 2002; Huiskes and van Rietbergen, 2005; Stout and Crowder, 2012). Two types of remodelling can occur: growth and secondary. Growth remodelling results in sequential relocation of bone regions into new locations during growth, serving either to maintain or to make local adjustments in bone shape. Secondary remodelling occurs at a reduced rate following skeletal maturity (Martin et al., 1998). Three successive stages of activity are recognized (also called the basic multicellular unit [BMU]): 1) activation in

response to hormonal or mechanical stimulus, 2) resorption of bone by osteoclasts, and 3) formation of new bone at the same bone site by recently differentiated osteoblasts (Frost, 1990). If remodelling occurs at the intracortical surface, the resulting structure is a secondary osteon (Haversian system), which is delimited from the surrounding tissue by a cement (reversal/resting) line (Parfitt, 1994; Martin et al., 1998; Currey, 2002) (Figure 3.1). The canal left in the centre for the passage of blood vessels and nerves (Haversian canal) provides nourishment for the adjacent osteocytes and bone lining cells. It is also the passageway for exchange of minerals between the skeleton and the bloodstream (Parfitt, 1994; Martin et al., 1998).

Presence of primary and secondary origin of bone can help determine the age of an individual (e.g., number of secondary osteons can be used to estimate age at death) (Enlow, 1976; Aiello and Dean, 2002; Pfeiffer et al., 2006; van Oers et al., 2008), but the type of tissues seen in most mammals show highly diverse conditions in their bones. Therefore, mammals grow and resorb their bones differently. Large primates with greater longevity, like apes and humans, have dense Haversian bone tissue (especially in older individuals) in most parts of the cortex. Small primates and rodents may show simplified primary bone patterns in the cortex and some moderate Haversian substitution and remodelling will be most active in the cancellous regions (Enlow, 1957; Francillon-Vieillot, 1990)

3.2 Mechanical properties of bone

The mechanical behaviour of bone or the behaviour under the influence of forces and moments, is affected by its mechanical properties, its geometric characteristics, the loading mode applied, direction of loading, rate of loading, and frequency of loading (Frankel and Nordin, 2001;

Currey, 2002; Huiskes and van Rietbergen, 2005). Functionally, the most important mechanical properties of bone are its strength and its rigidity. Loading causes a deformation, or a change in dimensions to a structure (bone), temporarily or permanently. When a load (stress) of known direction and magnitude is imposed on the structure, the deformation of that structure (strain) can be measured and plotted on a deformation curve (Figure 3.2). The initial portion of the curve (elastic region) indicates the loads under which bone will return to its original shape after the load is removed. Elasticity is often recorded in terms of Young's modulus, where a low value indicates an elastic material. The amount of load a bone can sustain without permanent deformation is called the stiffness (rigidity) of the bone. Stiffness is measured as the linear slope of the graph, where stiffer structures will have higher linear slopes. As loading continues past the elastic region, the outermost fibres in the bone begin to yield, and deformation becomes permanent. The second region of the graph is called the plastic region. The endpoint of the plastic region is the ultimate failure point: the point at which the bone fractures. The magnitude of the load at the failure point is referred to as the strength of the bone. Therefore, stronger bones fail at greater loads (Martin et al., 1998; Turner, 1998; Frankel and Nordin, 2001; Currey, 2002; Martin, 2007).

Three basic types of mechanical load can be experienced during a bone's lifespan: compression, tension, and shear (Figure 3.3). Compression occurs when equal and opposite loads are applied to the surface of bone, and the two loads are directed toward one another, such as loads at both ends of long bones. Under compressive loading, bone shortens and widens. Conversely, tension causes bone to lengthen and narrow, as the forces are applied to the surface of the long bone and directed outward from one another. Bone can also undergo shear loading, when opposing loads are applied perpendicular to the long axis of the bone, and when the bone is loaded in torsion

(twisting). Unlike compression and tension, deformation by shear forces occurs at an angle to the long axis of the bone (Martin et al., 1998; Frankel and Nordin, 2001; Currey, 2002). It is rare that bone experiences one of the three basic types of loading in isolation. Under normal loading, bone is exposed to a combination of these forces, such as in bending and torsion. In bending loads, the forces are applied to a bone such that the bone bends about an axis. Bending causes the bone to compress on one side of the neutral axis, which compresses the bone on one side and tenses the bone on the other side of the neutral axis (Figure 3.4). Torsional loading combines compression and tension and a significant amount of shearing (Martin et al., 1998; Frankel and Nordin, 2001; Currey, 2002).

The mechanical demands on the skeleton require that bone be sufficiently strong and stiff to resist permanent deformation while minimizing the risk of fractures (Frankel and Nordin, 2001). There is a long and well-documented history of researches looking at the correlation between bone shape and mechanical loading history (Lieberman and Crompton, 1998; Martin et al., 1998; Burr et al., 2002; Lieberman et al, 2004; Hamrick et al., 2006b, Fricke and Schoenau, 2007; Turner, 2007; Plochocki et al, 2008; Plochocki, 2009; Shaw and Stock, 2009a, b; Green, 2010; Elkasrawy and Hamrick, 2010; Ozcivici et al., 2010; Green at al., 2012). In general, the findings show that bone responds to its mechanical environment by adapting strength and rigidity properties. Animal models subjected to increased activity, such as mice, rats, pigs and sheeps, have shown increased bone mass and/or cortical dimensions compared to controls (e.g., Woo et al., 1981; Robling et al., 2002). Others have shown a decrease in bone mass and/or strength with decreased activity (e.g. Jaworski et al., 1980). However other researchers showed that the amount and location of mechanically induced changes can be affected by a number of factors other than mechanical, such as genetic and ontogenetic (e.g., Pearson and Lieberman, 2004;

Montgomery et al., 2005; Plochocki, 2009). For example, hormones such as oestrogen and parathyroid hormones may influence the osteogenic response of bone to mechanical loading (Fricke and Schoenau, 2007; Plochocki, 2009; Ozcivici et al., 2010). Aside from their direct influence on bone cell activity, hormones may also indirectly act to promote bone growth via their effects on growth in body size and muscles mass (thereby increase mechanical loads), which themselves are thought to be important determinant of diaphyseal geometry (see below). Hormones levels also change throughout development and their effect may also vary with age. Although numerous investigations have demonstrated that bone responds to its mechanical environment, to date our understanding of how bone specifically responds and adapts to its mechanical environment on a physiological level is limited (Robling et al., 2006; Ozcivici et al., 2010 ; Burr and Allen, 2013).

Adjustments of bone to mechanical loading are accomplished by growth remodelling at the periosteal and endosteal surfaces to maintain peak bone strain within acceptable limits. Regulation of bone resorption in response to mechanical stimuli is not entirely understood, although osteoblast-lineage cells are known to play an important role (Martin et al., 1998; Burr and Allen, 2013). The process is thought to be homeostatically regulated with osteocytic mechanosensors detecting strain levels within bone (Martin et al., 1998; Fricke and Schoenau, 2006; Hedgecok et al., 2007; Burr and Allen, 2013). An increase in strain within the bone results in bone deposition, reducing strain levels back to peak bone strain within acceptable limits. A decrease in strain results in bone resorption, which also restores the bone to optimum strain levels. It has been recently suggested that osteocytic mechanosensors do not directly respond to mechanical strain, but instead respond to elevated hydrostatic pressure in the bone marrow that results from mechanical loading (Robling et al., 2006; Gurkan and Akkus, 2008; Puetzer et al.

2013). Studies have observed the release of messengers (e.g., prostaglandins, nitric oxide, other signalling molecules) by osteocytes in response to mechanical stimulus, although the exact stimulus (or stimuli) is unknown (Robling et al., 2006; Gurkan and Akkus, 2008). Despite the lack of understanding of how the mechanosensors actually function, it is recognized that they function to adapt bone to its mechanical environment.

To summarize, normal bone architecture development and maintenance, including the size and shape of whole bones, is strongly influenced by functional demands, such as posture, locomotion, protection, and homeostasis. The following sections review muscle attachment sites and bone cross-sectional geometric properties as sources of information of functional history.

3.3 Muscle attachment sites

Muscle attachment sites have been described as the "Holy Grail" of bioarchaeology due to their potential ability to help us understand locomotor behaviour, daily lives, and perhaps even how and who performed past tasks (Jurmain et al., 2012). Muscle attachment sites are (often) distinct skeletal indicators that occur where a muscle, tendon, ligament, or capsule inserts onto the periosteum and/or the outer layer of bone, then into the underlying bony cortex (e.g., Benjamin et al., 2002; Jurmain et al., 2012). There are three main reasons why entheses are of interest to biological anthropologists: 1) the areas of attachments are (usually) easily visible on dry bones and fossils, making them easy to study and compare between populations and species, 2) entheses exhibit a number of morphological variations (e.g., more or less pronounced changes such as irregularity and porosity), so changes can be scored or measured, and 3) attachment sites are regularly under heavy strain during physical activity, and changes can (hypothetically) be used to reconstruct past physical activities (Dutour, 1986; Hawkey and Merbs, 1995, 1998;

Wilczak, 1998a, b; Bejamin et al., 2004; Hieronymus, 2006; Jurmain and Villotte, 2010; Jurmain et al., 2012).

3.3.1 Nomenclature of muscle attachment sites

Historically, some studies in palaeontology and archaeology used muscle attachment sites to describe locomotion and change in behaviour, but it was not until the 1980s that the concept of attachment sites started to be commonly used to reconstruct behavioural patterns over the course of a lifetime (e.g., Dutour, 1986; Kennedy, 1989). Since then, a considerable body of literature has been published using these to reconstruct activity patterns in osteological and fossil samples.

Muscle attachment sites have been given many different names such as: musculoskeletal stress markers (MSM), enthesopathies, enthesiopathies, enthesophytes, and entheseal changes (EC). Enthesopathies, enthesiopathies, and enthesophytes are terms found mainly in the clinical literature and are often described as hypertrophy of bone or pitting/furrowing at the insertion site associated with age or trauma (Villotte 2006, Jurmain et al., 2012; Villotte and Knüsel, 2013). After Hawkey and Merbs' (1995) publication, the terminology "MSM" gained wide acceptance. Musculoskeletal stress markers (also called occupational markers) have been used to tell or support a story about skeletal remains since MSM predispose a relationship between the attachment sites and activity related stress (Jurmain et al., 2012). Jurmain and colleagues (2010, 2012) have questioned the direct implication of the causal relationship between enthesis expression and the amount of time and intensity of stress placed by the muscle or tendon on a bone and suggested to change the terminology from MSM to entheseal changes. EC simply describes the changes seen in muscle attachment sites and avoids explicitly specifying the aetiology of these changes. With a new name comes new definitions; according to Jurmain and

colleagues (Jurmain and Villotte, 2010; Jurmain et al., 2012) entheseal changes can take two forms: 1) new bone formation, or 2) bone destruction (which can vary in size, shape, and distribution). Therefore, the most currently used terminologies are: entheses (designating the areas where muscle, tendon, capsule, or ligament attaches to bone), enthesopathy (indicating pathological changes of this structure), and entheseal changes (designating all alterations of entheses seen in skeletal material). For the purpose of this dissertation, *muscle attachments sites, entheses,* and *muscle-bone interface* will be used to describe the area where a muscle, tendon, and/or ligament attaches, and *entheseal change* will only be used if a change from normal variation is observed.

3.3.2 Entheseal overview

Entheses are grouped into two main categories based on their cartilaginous tissue type and anatomical location, although a spectrum of morphologies is observed between these two categories that is understood to represent different mechanical loading conditions (Cardoso and Henderson, 2010). Fibrocartilaginous (FC) attachments are primarily located close to the ends of long bones and on short bones, and are characterized by a limited attachment area. They are the most commonly studied and leave small, well-defined bony scars (Bennett et al., 1993; Benjamin et al., 1986, 2002; Hurov, 1986; Wilczak, 1998a, b; Zumwalt 2005, 2006; Cardoso and Henderson, 2010; Jurmain et al., 2012; Villotte and Knüsel, 2013). FC attachments are characterized histologically by four zones: 1) tendon or ligament, 2) uncalcified fibrocartilage, 3) calcified fibrocartilage, and 4) subchondral bone (Figure 3.5). The function of the attachment zones is not well understood, but is suspected to be a gradual transmission of the tensile force between soft-tissue and bone (Nawata et al., 2002). The layers of unmineralized and mineralized fibrocartilage (layers 2 and 3) are separated by a “tidemark” (a relatively rectilinear calcification

front) through which collagen fibres cross but not the blood vessels (Cooper and Misol, 1970; Benjamin et al., 1986, 2002; Benjamin and Ralph, 1998). At the periphery of the attachment, the collagen fibres merge into the periosteum and blood vessels may be present (Dörfl, 1969; Benjamin et al., 1986). The tidemark is also the point where soft-tissue is removed during maceration, and the calcified zone is usually preserved in skeletal remains. Due to the rectilinear shape of the tidemark, a healthy FC enthesis should appear as a well circumscribed, smooth, and without vascular foramina surface (Benjamin et al., 2002; Jurmain et al., 2012; Villotte and Knüsel, 2013).

Fibrous attachments are mainly found on the shaft of long bones where there is a large surface for the muscles to attach. In contrast to fibrocartilaginous attachments, anatomical and pathological descriptions for fibrous attachments are rare. The usually large muscles attach directly to the bone or via periosteum and are anchored by Sharpey's fibres – extrinsic coarse collagen fibres that are continuous with the connective tissue of muscles and anchor them to bone (Figure 3.5) (Hoyte and Enlow, 1966; Hems and Tillmann, 2000; Benjamin et al., 2002; Hieronymous, 2006). Blood vessels from the soft-tissue can then anastomose with those of the bone (Dörfl, 1969). Due to the highly vascularized attachment, and the physiological transition from periosteal to bony attachment, fibrous attachments are difficult to distinguish on skeletal remains. Benjamin and colleagues (2002) note that relatively little attention is paid to fibrous attachments in any field, even though they are associated with the largest and most powerful muscles.

Many attachments, such as the masticatory muscles, are classified as "mixed" (Hems & Tillmann, 2000; Hieronymous, 2006; Cardoso and Henderson, 2010; Villotte and Knüsel, 2013).

For example, the attachment of the masseter muscle on the mandible is partly periosteal, osseous, and fibrocartilaginous (Hems and Tillmann, 2000). Fibrocartilage may also exist in a small quantity at the fibrous enthesis, particularly on the metaphysis of long bones (e.g., insertion of the pectoralis major muscle). There can also be morphological diversity within a species for the same attachment (e.g., insertion of the iliopsoas muscle). Recognizing that different interface structures exist between the soft and hard components of the enthesis is important in entheseal research.

3.3.3 Entheseal development

Although little information is available about the development of attachment sites, the two categories of entheses seem to also develop differently. Early in life, tendons and ligaments attach to perichondrium (dense irregular connective tissue which surround the cartilage of developing bone – once vascularized, perichondrium becomes periosteum) and follow epiphyseal cartilage. During growth, entheses seem to act as growth plates (Hurov, 1986; Shaw et al., 2008). Cartilage is resorbed at the inner side and produced at the outer side, possibly by metaplasia (change from one tissue type to another). The classic appearance of a fibrocartilaginous enthesis (with the four histological zones) appears when growth slows or stops (Nawata et al., 2002). For example, the boundary between uncalcified and calcified fibrocartilage is not distinguishable until growth slows. Therefore, this progressive organization during development could explain the lack of clearly distinguishable FC entheseal areas in young skeletons (Huroz, 1986; Nawata et al., 2002; Shaw et al., 2008). The development of fibrocartilaginous attachment sites is not described in humans and therefore these observations come from animal models. It is not known whether all FC entheses are modified by muscle contractions in a similar fashion and at the same rate. All previous palaeoanthropological and

bioarchaeological studies assume that all species (e.g., apes and humans) modify their entheses in a similar fashion and at the same rate. If one species has a quicker morphological transformation of its entheses in response to similar stimuli than a second species, the first is likely to present wider variation of morphologies, while the latter will be much more homogeneous (Drapeau, 2008). This obviously causes major problems when comparing species.

During adulthood, the degenerative process related to age and mechanical demands affects both the tendon and the fibrocartilaginous enthesis (Benjamin et al., 2007). Deterioration in the physical properties of the tendon (tendinous resistance decreases, tendon is less vascularized and hydrated, amounts of collagen and glycoproteins decrease) can aid mechanically induced changes in the entheses (Villotte, 2006). With age, FC entheses undergo a degenerative process: 1) microtears and microdamage of one of the four histological zones, 2) formation of enthesophytes (bony spurs) caused by the healing process after microtears, 3) disturbance of collagen fibres and organization of cell columns, 4) calcific deposits, 5) increase thickness of calcified fibrocartilage layer, 6) vascularization of the calcified and uncalcified fibrocartilage layers, and 7) erosion of the surface and bone resorption beneath the enthesis (Benjamin et al., 2007). Excessive mechanical stress (e.g., frequency, speed, and/or intensity) can cause micro-damage that can disturb the tissue structure of the FC enthesis. In young adults, these mechanical stresses seem to be the main factor in the occurrence of an activity-related entheseal change (Villotte, 2006). In older individuals, the gradual depletion of tendon vascularity close to the attachment favours the chances of lesion. Overuse (e.g., sports) changes are similar to degenerative ones in older individuals (van der Meulen et al., 2000; Benjamin et al., 2004, 2007).

Growth of fibrous attachments is also only described in animal models, and the relationship between muscle activity, muscle properties, and the morphology of the developing attachment sites is debated (Hoyte and Enlow, 1966; Laros et al., 1971; Dörfl, 1980a, b; Hurov 1986; Dysart et al., 1989; Doschak and Zernicke 2005; Montgomery et al., 2005; Zumwalt. 2005). During growth, muscles and tendons attach primarily to the periosteum. Only after longitudinal bone growth is completed, do the muscles appear to pass through the periosteum and attach firmly to the underlying bone (Wilczak, 1998a, b; Zumwalt, 2005, 2006 but see Hoyte and Enlow, 1966; McFarlin et al., 2008 for evidence to the contrary). This mechanism seems to allow the attachment of soft-tissues to properly migrate across the bone surface during growth, such that they maintain a constant position relative to the growth plate and adjacent joints (Hoyte and Enlow, 1966). Both osteoclastic and osteoblastic activity is present and seems to be related to the migration of the attachments of soft-tissues during the growth in length of the long bones (Chen et al., 2007). What roles the muscles have to make the migration and normally formed bone possible are unknown. It is thought however, that the morphology of juvenile muscle attachment sites tends not to fully reflect the size or activity of the attaching muscle and that only after growth has ceased do the attachments take permanent root in bone and may then leave observable marks (Hurov, 1986; Wilczak, 1998a, b; Zumwalt, 2005, 2006).

Despite the fact that definition of healthy fibrocartilaginous entheses can be applied to some attachments (see above), it seems that fibrous attachments do not even have a definition of what a normal site looks like. Very few clinical studies have been undertaken to determine what could cause entheseal changes at fibrous entheses. Benjamin and colleagues (2002) document that the periosteum layer can often disappear with age and leave the soft-tissue attaching to bone without a mediating layer. It has been hypothesized that the physiological transition from the periosteal

to a bony attachment in early adulthood may explain the high frequency of skeletal changes and irregularities seen in young/middle-aged adults (Villotte, 2008). Later in adulthood, a second process related to cellular degeneration could explain major EC (e.g., bony ridges). Genetic factors, body mass, and diseases have also been hypothesized to play an important role in EC at fibrous entheses (Weiss 2003, Villotte, 2008; Villotte et al., 2010b). More research of fibrous attachments is needed to see how vulnerable these entheses are to overuse (Benjamin et al., 2002). The overall observation that muscle attachment sites develop with age suggests that entheses may develop due to habitual, low intensity contractions. The morphological change is therefore thought to be additive, with more marked attachments with time. Theoretically, an increase in habitual use of a muscle should result in a faster rate of bone deposition. This again assumes that all entheses are modified in a similar fashion and at a similar rate.

3.3.4 Methodology considerations in entheseal research

Many muscle-bone interface studies seek to estimate muscle use based on differences in the bony surface morphology at the attachment since the mechanical stress (e.g., muscle force) experienced by a surface area (e.g., enthesis) has been thought to be proportional to the force applied in each unit area of that surface (Biewener, 1992). Therefore, hypertrophy of bony attachments for larger and/or more active muscles is a theoretically advantageous mechanism to reduce stress or maintain acceptable stress magnitudes. When entheses are subjected to the force of a contracting muscle, blood flow to periosteal bone increases, which can stimulate bone growth and increase the size of the attachment site to strengthen it (Hawkey and Merbs, 1995, 1998). With those mechanical changes in mind, many different methodologies were developed to document activity via muscle attachment sites.

The method most widely used to study entheses is a visual reference system first proposed by Hawkey and Merbs (1995). The visual reference system comprised of three scoring variables: 1) robusticity: rugged ridges or crests at the muscle attachment site associated with habitual use, 2) stress: micro-trauma expressed as pitting or furrows into the cortical matrix (can resemble a localized lytic lesion but is not disease related), 3) ossification: result of sudden macro-trauma, causing an exostosis (formation of new bone) to form at the site. Each variable is evaluated on a three points scale: faint, moderate, or severe (stress considered to be a continuation of the robusticity category continuum). Therefore, more "obvious" attachment sites with high scores are assumed to have a relative increase in muscle size and use. There are however, many disadvantages to this categorical data analysis of muscle attachment sites, such as: 1) this method was develop to mainly describe FC attachment sites despite the fact that it is used to also score fibrous entheses, 2) the development and subsequent description of the ordinal category criteria themselves have flaws, 3) the reduction of a great range of variability in entheseal morphology into a few ordinal categories is problematic, and 4) scoring of the prominence of muscle attachments may be influenced by the robustness or gracility of the underlying bone (Wilczak 1998a, b; Niinimäki, 2011; Davis et al., 2013). Davis and colleagues (2013) tested the role of inter-observer error for this method and found that the rates of reproducibility were slightly higher than what would be predicted by chance alone. They found that the entheses with the lowest levels of reproducibility were predictably those sites that generally had the most complicated and variable morphology (versus those characterized with a broad area of attachment without well defined borders or else a dense smooth attachment site such as fibrous attachments). Therefore, important variation is ignored when using this method and the fibrous attachments are always scoring very low due to their usually smooth cortical morphology.

Quantitative methods of measurement for entheses have also been proposed (Wilckzak, 1998a, b; Molnar, 2006; Zumwalt, 2005, 2006; Nolte and Wilczak, 2013). To measure the attachment, the area covered by the tendinous attachment and the areas immediately adjacent to this attachment that show formation of new bone on the smooth cortical surface are usually included. These methods allow better documentation of the fibrous muscle attachment sites. Although these methods eliminate some of the pitfalls of using ordinal scoring systems on categorical data, there are still many limitations. A relatively high percentage of measurement error is found using quantitative methods (since it is very difficult to distinguish where a fibrous attachment begins and ends) and the rugosity of the attachment site is often not considered (Zumwalt, 2005; Jurmain et al., 2012).

Recently, other studies have focused on developing new methods to interpret EC modifying the original method used by Hawkey and Merbs (Wilczak 1998a, b; Mariotti et al., 2004, 2007; Zumwalt, 2005, 2006; Villotte, 2006; Havelková et al., 2013; Henderson et al. 2013b; Nolte and Wilczak, 2013), while others have attempted to develop new definitions for better interpretations of entheses (Villotte, 2006; Cardoso and Henderson, 2010; Villotte et al., 2010a; Jurmain et al., 2012; Villotte and Knüsel, 2013). The major issue of these new definitions and methods is how to categorize "normal" variation. For example, Jurmain and Villotte (2010) have suggested that a certain range of robust attachments be called enthesopathies even though normal morphology is at times encompassed by the term. In general, all of these methods have similar limitations. The perception of an attachment site itself (i.e. being faint or well-developed) can be biased if the observer does not control for normal variations between populations or the relative robusticity of the underlying bone (Robb, 1998; Weiss, 2003; Zumwalt, 2005, 2006). Further challenges include methodological consistency across studies in defining the boundaries of attachment

areas, and determining which aspects of the muscle attachment site are the most meaningful for the interpretation (Wilczak, 1998a, b).

The relationship between behaviour and entheseal change may not be as straightforward as posited by these previous methodologies, and this limits the ability to interpret muscle function from attachment site morphology (Hoyte and Enlow, 1966; Eliot and Jungers, 2000; Marzke and Shrewsbury, 2006; Schoenau and Frike, 2008; Cardoso and Henderson, 2010; Jurmain et al., 2012). These prior studies revealed the complexity of influences on muscle attachment site morphology, but none have directly tested the interaction effects between activity, muscle mass and/or architecture, and attachment site morphology. There are a number of factors besides muscle size and activity that may contribute to the development of attachment sites. Bone does not respond to all stimuli, and when it does, similar or disparate conditions may lead to different bony responses (Turner, 1998, 2000; Burr et al., 2002; Currey, 2002; Robling, 2009). Finally, the extent of sex, age, hormone level, and genetics on entheseal response to muscular activity is highly debated (Montgomery et al., 2005; Zumwalt 2005, 2006; Hamrick et al., 2006; Ravosa et al., 2008; Plochocki, 2009; Ozcivici et al., 2010; Jurmain et al., 2012).

3.4 Hypotheses to be tested

Muscle attachment sites have been hypothesized to be the result of an accumulation of stresses experienced by an individual, and therefore by extension, activity has been correlated to the hypertrophy at muscle insertions. Thus, the aim is to determine how normal variation in muscular activity influences the size and shape of the humeral muscle attachment sites. As seen in Chapter 2, it is expected that the animals will exhibit different muscle attachment sites due to their differential posture and locomotion.

The following hypotheses with associated null hypothesis related to differences in humeral attachment sites will be tested:

H2 = Different locomotor patterns in the animals studied will result in corresponding changes in entheseal morphology of the humerus.

H2.1 (tested in the mouse sample only) **=** Increased activity in the animals studied will result in higher rates of bone growth and hypertrophied entheses with altered shape. Increased activity will also result in a humerus that is stronger and more rigid in bending, torsion, and axial compression/tension.

H2.2 = Differences in sex and age in the animals studied will result in corresponding changes in muscle attachment sites of the forelimbs. Males and adults will have hypertrophied entheses with altered shape, but younger individuals will exhibit stronger bones.

Ultimately this dissertation is testing the following hypothesis:

H3 = Larger and stronger muscles in the animals studied will result in stronger bones with higher rates of bone growth and hypertrophied entheses with altered shape.

H0 = There is no relationship between the internal structure of the forelimb muscles in the animals studied and their corresponding entheseal morphology.

It is predicted that the larger and stronger muscles will be associated with more hypertrophied attachments sites. Sexual differences are also expected. Males are predicted to have more hypertrophied entheses. Oestrogens have an inhibitory effect on periosteal appostition and endocortical resorption (Plochocki, 2009), which may also explain why females tend to have smaller attachment sites in general. Body mass should also have an effect on the humeral entheses. Larger body masses should be correlated with larger and more robust muscle attachment sites. Finally, the age of the primates in the sample should not be associated with any entheseal changes. All primates are considered relatively old since they all died of natural causes at the zoo. Therefore, all primates should have very well defined and robust attachment sites.

Physical activity is believed to influence the morphology of bones, particularly during growth. Given that muscle attachment sites seem to be developing in response to muscle use and size, they are often used as a surrogate of the strength of the muscles. However, it is unknown how growth and physical activity influences fibrous attachment sites. This study will test the effect of exercise to evaluate changes at the deltoid crest, a fibrous enthesis. It is therefore expected that exercise regime (running, climbing) will have a longer, wider, and more robust deltoid crest than in the control mice. Both of the experimental groups should have a hypertrophied enthesis. More specifically, it is predicted that the higher intensity exercise regime (running) will result in the greatest entheseal changes. Two age groups are studied in the mouse sample. Past research have stipulated that the morphology of juvenile muscle attachment sites tends not to fully reflect the size or activity of the attaching muscle (Hurov, 1986; Wilczak, 1998a, b; Zumwalt, 2005, 2006). Therefore, it is predicted that the younger mice will have smaller and less defined attachment sites compared to the older animals.

3.5 Bone cross-sectional geometry

Development of long bone structure is influenced by both systemic and local mechanical factors. The skeleton is thought to adapt to variable mechanical loadings associated with increases in body size and changes in positional behaviour by making appropriate adjustments in the quantity and distribution of bone. Bone structural properties and their relationship to skeletal function has been the focus of many studies, which have relied on the application of engineering "beam theory" to the analysis of long bone cross-sectional geometry (Huiskes, 1982; Ruff and Hayes, 1983; Hamrick et al., 2000; Ruff, 2000, 2002, 2003; Stock, 2002; Lieberman et al., 2004; O'Neill and Ruff, 2004; Pearson and Lieberman, 2004; Stock and Shaw, 2007; Goldman et al., 2009; Shaw and Stock, 2009a, b; Harrington, 2010; Shaw and Ryan, 2012). All of these studies looked at the robusticity of the bone; the strengthening or buttressing of skeletal element through the addition of bone tissue. Therefore, like musculoskeletal research, cross-sectional geometric analyses investigate the robustness, or the thickness of a bone at a particular location.

As mentioned above, one way to determine the strength and rigidity of a bone is by modeling the long bone as an engineering beam. Using beam theory is possible to estimate the resistance of a bone to axial compression and tension, bending and torsion, by considering the geometric distribution of bone tissue in a cross-section of a whole bone (Huiskes, 1982; Biewener, 1992; Ruff and Haynes, 1983). Therefore, several cross-sectional geometric properties characterize the amount and distribution of bone material around a given cross-section, and are thought to be proportional to the resistance of long bones to the stresses and strains produced by different kinds of loading. Although trabecular bone is also thought to be organized in response to mechanical demands, the scope of this research is limited to the study of humeral cortical robusticity.

Analysis of the diaphyseal cross-sectional geometry quantifies four types of properties: areas, second moments of areas, polar second moments of areas, and section moduli. Cortical area (CA) is a measure of the amount of bone in a cross-section and a proxy for resistance to pure axial compression and tension. A hollow beam subjected to pure bending will experience its maximum tensile strains in its outer convex surface and its maximum compressive strains on its outer concave surface (Figure 3.4). The central axis of the beam about which no deformation occurs is called the neutral axis. Tensile and compressive strains experienced by material within the bone are proportional to their distance from the neutral axis. If bone material is distributed economically and optimally, greater structural reinforcement is expected in the plane where maximal bending occurs (Biewener, 1992). Total area (TA) is also important to the extent that as the tissue furthest away from the neutral axis has the most effect on bending and torsional rigidity (Bertram and Swartz, 1991).

The most critical cross-sectional geometric property for estimating section strength or rigidity is second moment of area/inertia (*I*). It takes into account the amount of bone material and its distribution relative to the neutral axis. Bending strength in the antero-posterior plane about the medio-lateral axis is termed I_x, and bending in the medio-lateral plane about the antero-posterior plane is called I_y. The maximum and minimum second moments of area (I_{max} and I_{min}) represent the directions of greatest and least bending rigidity in the section. The angle theta (θ) specifies the orientation of the plane of the greatest bending rigidity and is measured counter-clockwise from the medio-lateral plane (Ruff and Haynes, 1983). The ratio I_{max}/I_{min} provides an index of circularity of the cross-section. A circular cross-section resists bending loads occurring in each and every plane, equally (Huiskes, 1982; Ruff and Haynes, 1983; Biewener, 1992).

Long bones are also subjected to torsional loads, in which shear strains are generated about the neutral axis. The polar moment of area (*J*) provides a measure of bone strength under torsional loading in cylindrical cross-sections. *J* provides a measure of average or overall bending strength and is calculated as the sum of any two perpendicular second moments (e.g., $I_x + I_y$). The magnitudes of bending strains are proportional to their distance from the neutral axis, and a more relevant estimate of strength is the section modulus (Z) (Ruff, 2002). Section modulus takes into account the perpendicular distance from the bone neutral axis to the outer perimeter, where the maximum bending strains are predicted to occur. Finally, the polar section modulus (Zp) is a measure of torsional strength and can be estimated by dividing polar moment of area (*J*) by the average radial distances in two orthogonal axes. Since it is based on *J*, the polar section modulus can also be interpreted as a summary of average bending strength (Ruff, 2002).

To summarize, bone strength, or rigidity, can be improved by making several adjustments in bone structural properties: 1) by increasing cortical area, thereby improving resistance to axial loads, and 2) by increasing subperiosteal dimensions (particularly in the axis subjected to the greatest bending strains), thereby increasing resistance to bending and torsional loads (Ruff and Haynes, 1983; Biewener, 1992). Although cross-sectional geometric analysis can be studied throughout the long bone diaphysis, most research concentrates only on certain areas of the bone (e.g., midshaft of the diaphysis) with little attention paid to muscle sites (Shaw and Stock, 2009a, b). This study seeks to evaluate the variation within an enthesis using diaphyseal cross-sectional geometry.

3.5.1 Limitations to cross-sectional geometric analyses

Cross-sectional geometric analyses are less applicable to the bone region having extensive amounts of cancellous bone, such as the ends of long bones or to cross-sections departing substantially from circularity (Ruff and Haynes, 1983; Biewener, 1992). These analyses are also limited in their assumption that the material properties of the structure are homogeneous and isotropic (Biewener, 1992). In fact, bone is both heterogeneous and anisotropic (Martin et al., 1998). It has also been shown that axes of greatest structural rigidity (I_{max}) do not always coincide with experimentally determined axes where the greatest bending loads occur (e.g., Demes et al., 1998; Lieberman et al., 2004). Despite these limitations, application of beam theory to the structural analysis of limb bones can provide a useful means of quantifying variation in cross-sectional shape, which may relate to the pattern of loads to which limb bones are subjected. The extent to which many of these factors influence estimates of bone strength derived from beam theory can be considered by combining cross-sectional geometric properties with microstructural and experimental data (McFarlin, 2006; McFarlin et al., 2008; Goldman et al., 2009). In this dissertation, cross-sectional geometric properties were compared to the microstructural data in the mouse experimental model.

3.5.2 Cross-sectional geometry in primates

Many researchers have examined structural properties of long bone diaphyses in an attempt to assess the influence of body size and skeletal function on diaphyseal geometry in primates (Burr et al., 1981; Burr et al., 1989; Delson et al., 2000; Ruff, 2002, 2003; McFarlin 2006; McFarlin et al., 2008). These studies have shown that species of macaques are reported to have lowest bending rigidity at midshaft, while orangutans exhibit greatest strength relative to humeral length

when compared to other primates. In general, the humerus of primates' show less variation in diaphyseal geometry among taxa characterized by different locomotor specializations than does the femur. Often no clear relationship between specific locomotor behaviour (e.g, arboreal) and diaphyseal shape is found (e.g., Carlson et al., 2006).

Influence of body mass: Cross-sectional geometric properties are predicted to scale with positive allometry to avoid failure with increased body size and mechanical loading (Biewener, 1991). The limb bones of mammals across a large size range are observed to scale close to geometric similarity (Bertram and Biewener, 1990), however the mechanism by which similar peak bone strains and safety factors are maintained are suggested to vary with increasing size (Biewener, 1991). Animals of medium size (0.1 – 300 kg) are predicted to reduce force exerted on the skeleton mainly by altering limb posture (e.g., using more extended limb postures), thereby increasing the mechanical advantage of limb musculature, and exhibiting only slight positive allometry. Anthropoid primates show similar general scaling as observed among medium-sized mammals, exhibiting isometry or slight positive allometry of geographic properties with body mass (Ruff, 2002).

Given differences in body mass and forelimb behaviour among the taxa studied here, it is expected that the humeri will reflect the elevated stress they habitually resist. Therefore, it is predicted that the species with forelimb suspensory behaviour will have relatively stronger and larger humeri, compared to the terrestrial species. Thus, the orangutan humerus is expected to be stronger (larger section moduli) and more rigid (larger second moments of area) in bending, torsion, and axial compression/tension (cortical area) than the macaques as a result of the increased stress and strain incurred during suspension. It is also predicted that the fibrous muscle

attachment sites will not change in shape along the location sequence (proximal, midpoint, and distal) since muscle fibres from fibrous attachments enter the periosteum potentially at the same angle throughout the insertion, no change is expected. This is predicted for all primate species in the study.

3.5.3 Cross-sectional geometry in mice

Mice are often used as animal models to investigate cross-sectional geometric variables of bone. At their small size, geometric similarity predicts that mouse skeletons would be relatively strong (Biewener, 1990). However, mice experience strain magnitudes comparable to those of larger vertebrates during locomotion (Lee et al., 2002). The broad similarity in peak strain and bone safety factor in mammals across a large size range (Rubin & Lanyon, 1982) is likely due to the strong relationship between body mass and limb posture (Biewener, 1990); in other words, larger mammals maintain comparable strain levels by adopting less flexed limb postures. Therefore, mouse skeletons experience similar stress and strain regimes to those of large mammals.

As mentioned above, some of these studies show that bone responds to its mechanical environment by adapting strength and rigidity properties. Therefore, animals exposed to increased activity should show increased bone mass and/or cortical dimensions compared to controls (e.g., Woo et al., 1981; Robling et al., 2002). Given differences in magnitude and frequency of exercise practiced by the mice studied for this project, it is expected that the humeri will reflect the elevated stress. It is predicted then that the experimental mice (runners and climbers) will have relatively stronger as well as larger humeri, than the control mice. Specifically, the humerus from the high intensity exercise group (runners) is expected to be stronger (larger section moduli) and more rigid (larger second moments of area) in bending,

torsion, and axial compression/tension (cortical area) than the other groups. It is also predicted that the younger individuals might exhibit stronger bones as well, since geometric properties seem to be more influential during growth. As predicted for the primate sample, it is expected that the fibrous muscle attachment site will not change in shape along the location sequence (proximal and distal deltoid crest).

3.5.4 Mouse cortical bone growth

Mechanical factors are important determinants of the manner in which the appropriate form of a given bone is acquired. Bone remodelling during growth may entail differential rates of bone deposition across different regions of the same bone, as well as local destruction of tissues deposited during earlier growth stages. These local variations in bone growth and remodelling processes are thought to produce changes in whole bone structure, which are mechanically appropriate (Enlow, 1962, 1963).

Growth remodelling involves temporally and spatially coordinated patterns of bone deposition and resorption at endosteal and periosteal surfaces. Cortical drift is accomplished by coordinated patterns of bone deposition and resorption on complementary endosteal and periosteal bone surfaces, resulting in the directional movement or “drift” of the bone cortex in morphological space. Bone is deposited on the surfaces facing towards the directions of drift, whole bone is removed from surfaces facing away from the direction of drift (Enlow, 1962, 1963). For example (Figure 3.6), cortical drift of a whole bone (cross-section) in an antero-medial direction is accomplished: 1) in the antero-medial cortex by bone deposition on the periosteal surface and bone resorption on the endosteal surface, and 2) in the postero-lateral cortex, by bone resorption on the periosteal surface and bone deposition on the endosteal surface. In the bone undergoing

cortical drift, depositional rates in the direction of drift may be substantially faster than in other regions of the cortex (Newell-Morris and Sirianni, 1982). Cortical drift is an important process involved in the development of long bone diaphyseal curvature.

Therefore, bone growth remodelling is one of the primary mechanism by which bones adapt to increase mechanical loading (although the responsiveness declines after skeletal maturity) (Martin et al., 1998; Pearson and Lieberman, 2004). Fluorescent vital labelling of bone in the mouse sample allowed this study to obtain quantitative measurements of bone depositional rates which can be related to bone microstructural organization and bone cross-sectional geometry (Newell-Morris and Sirianni, 1982; Castanet et al., 2004). Given differences in frequency and type of activity among mice studied here, it is expected that the bone growth in the exercise mice will reflect the elevated stress they habitually sustain. It is predicted that the experimental mice (runners and climbers) will have faster growing cortices, especially underlying the deltoid crest, compared to controls. This faster growing bone should also be characterized with more unorganized bone tissue (woven, parallel fibred) compared to more organized and slow forming tissue in the controls (e.g., lamellar). Specifically, the high intensity group (runners) are predicted to have faster growing deltoid crests compared to all other groups. The juvenile group should also exhibit more unorganized tissue with faster periosteal osteogenesis. On the other hand, the adult mice should have more organized tissue with the presence of more secondary bone remodelling (e.g., secondary osteons).

Figure 3.1 Schematic structural organization of a long bone (modified from Frankel and Nordin, 2001).

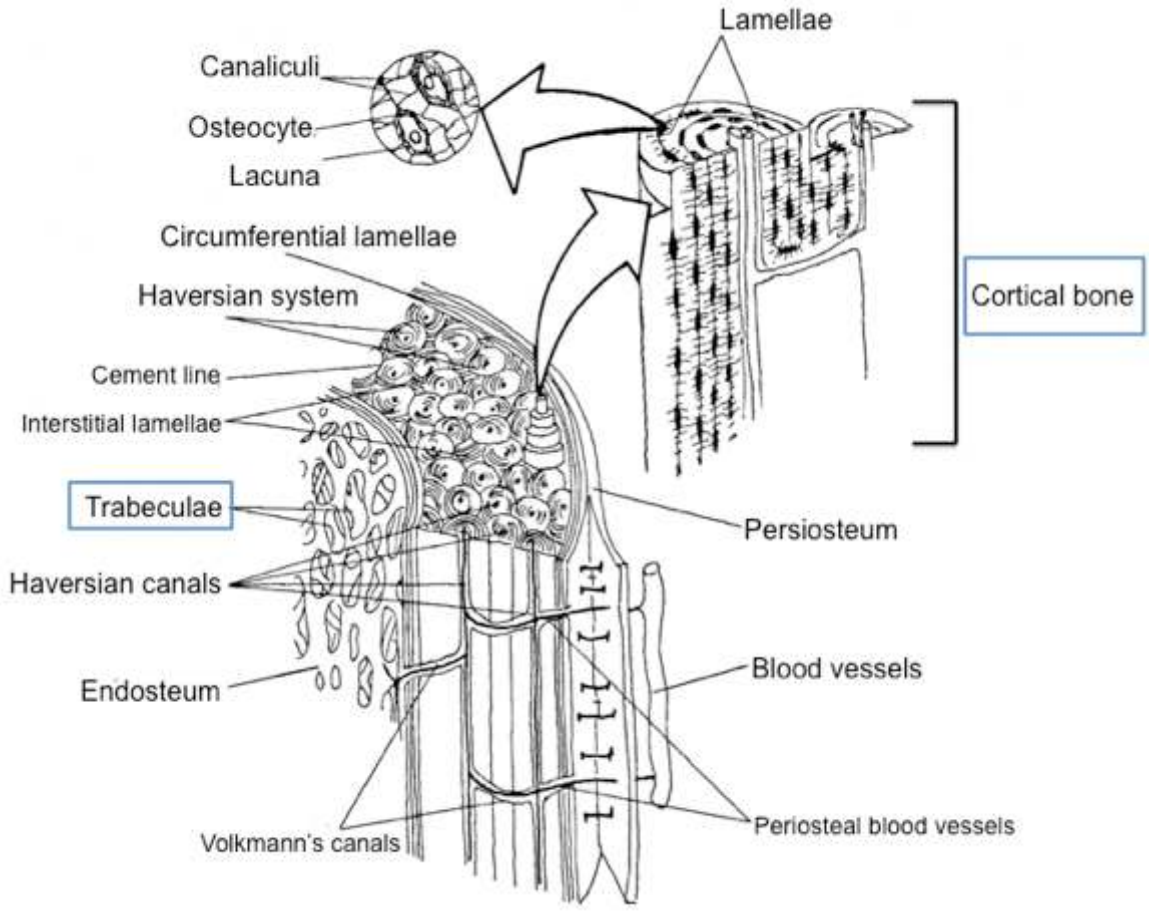

Figure 3.2 Load-deformation (stress-strain) curve for cortical bone. When a load (stress) is applied to the elastic region of the curve (up to yield point) and is then released, no permanent deformation is incurred. If loading continues into the plastic region of the curve (beyond the yield point) and then the load is released, the result is permanent deformation (up to ultimate failure point) (modified from Frankel and Nordin, 2001).

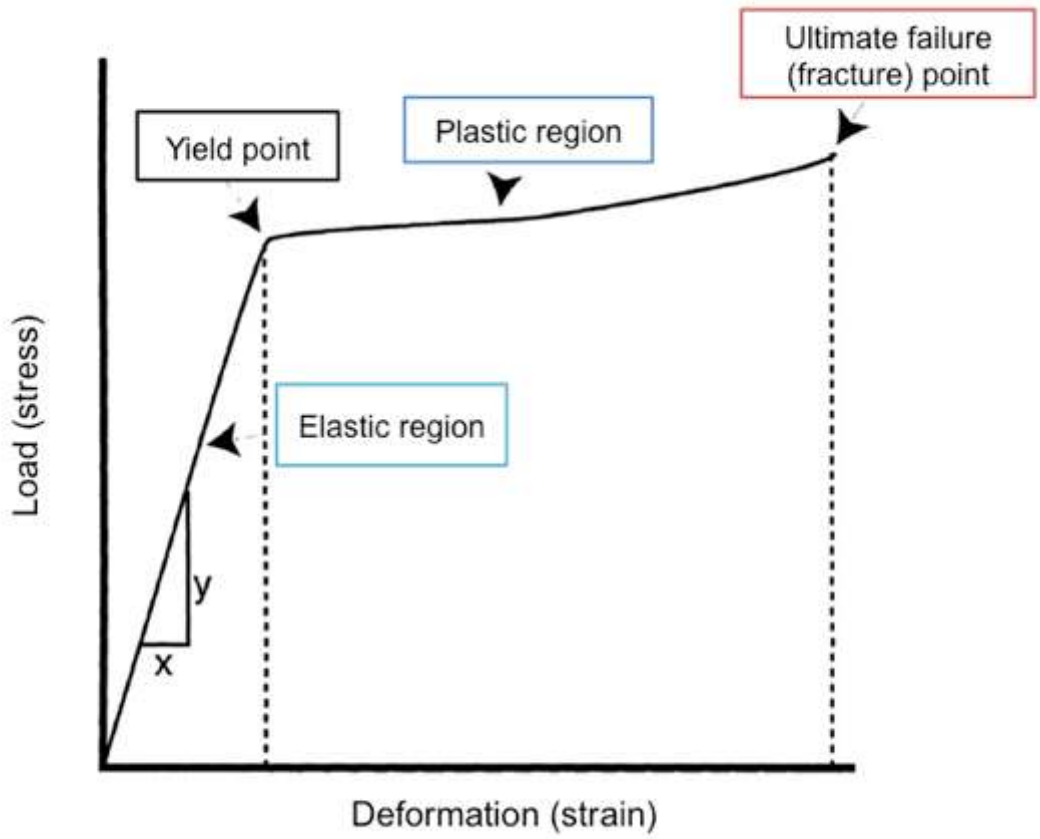

Figure 3.3 Schematic representations of various types of mechanical loading (modified from Frankel and Nordon, 2001).

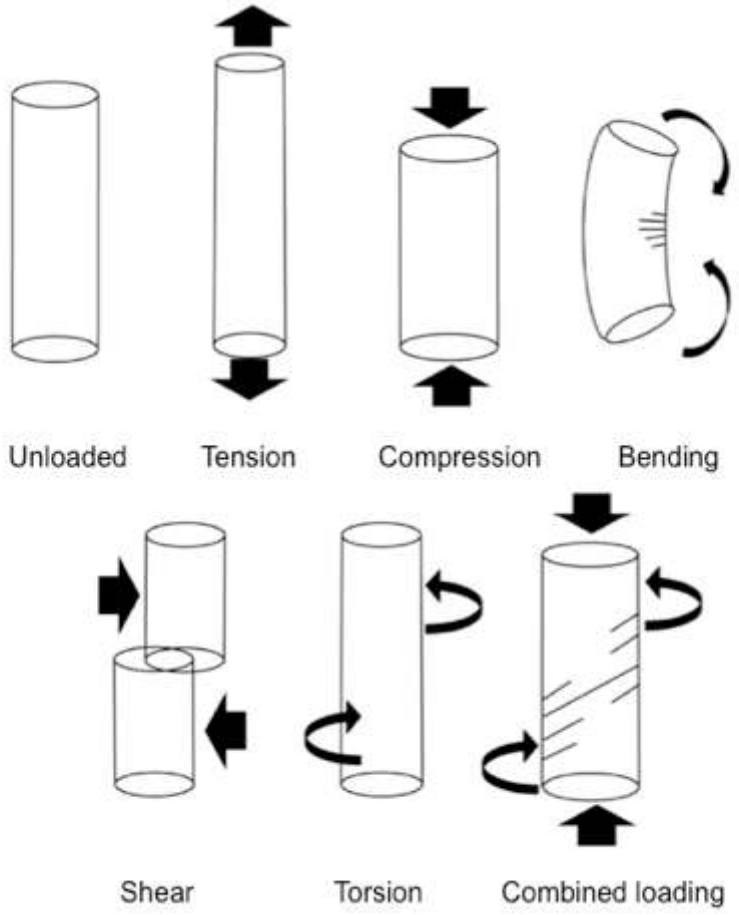

Figure 3.4 Schematic representation of a beam subjected to bending load. In a beam subjected to bending about the horizontal neutral axis, maximum tensile trains (pluses) will be experienced on its outer convex surface, and maximum compressive strains (minuses) will be experienced on its outer concave surface (modified from McFarlin, 2006).

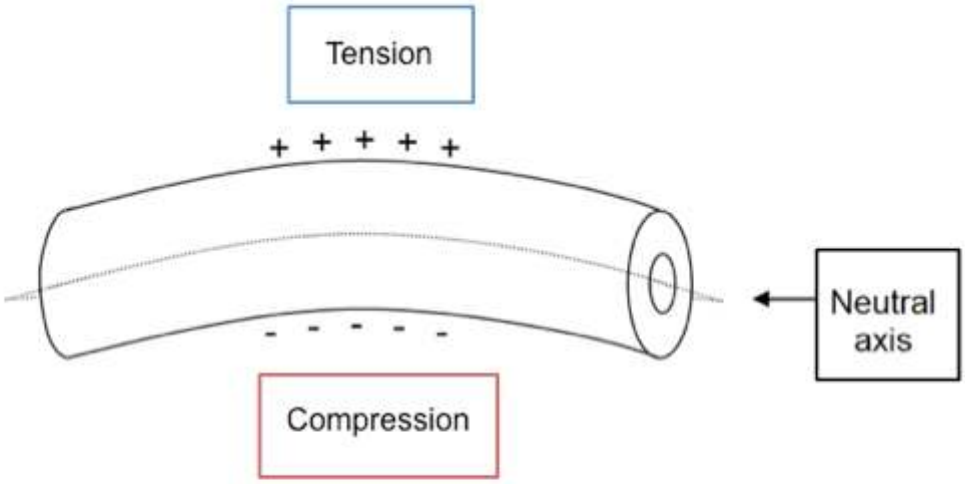

Figure 3.5 Representations of muscle attachment types. A) Section from a rat supraspinatus tendon to bone insertion (toluidine blue-stained) showing the functionally graded fibrocartilaginous transition (tendon, fibrocartilage, tidemark, mineralized fibrocartilage, and periosteal bone) (modified from Thomopoulos, 2008). B) Schematic representation of a fibrous enthesis (tendon fibres displacing the periosteum and continuing into periosteal bone, and C) schematic representation of a direct attachment (muscle fibres stop at periosteum, lacking Sharpey's fibres) (modified from Hieronymus, 2006).

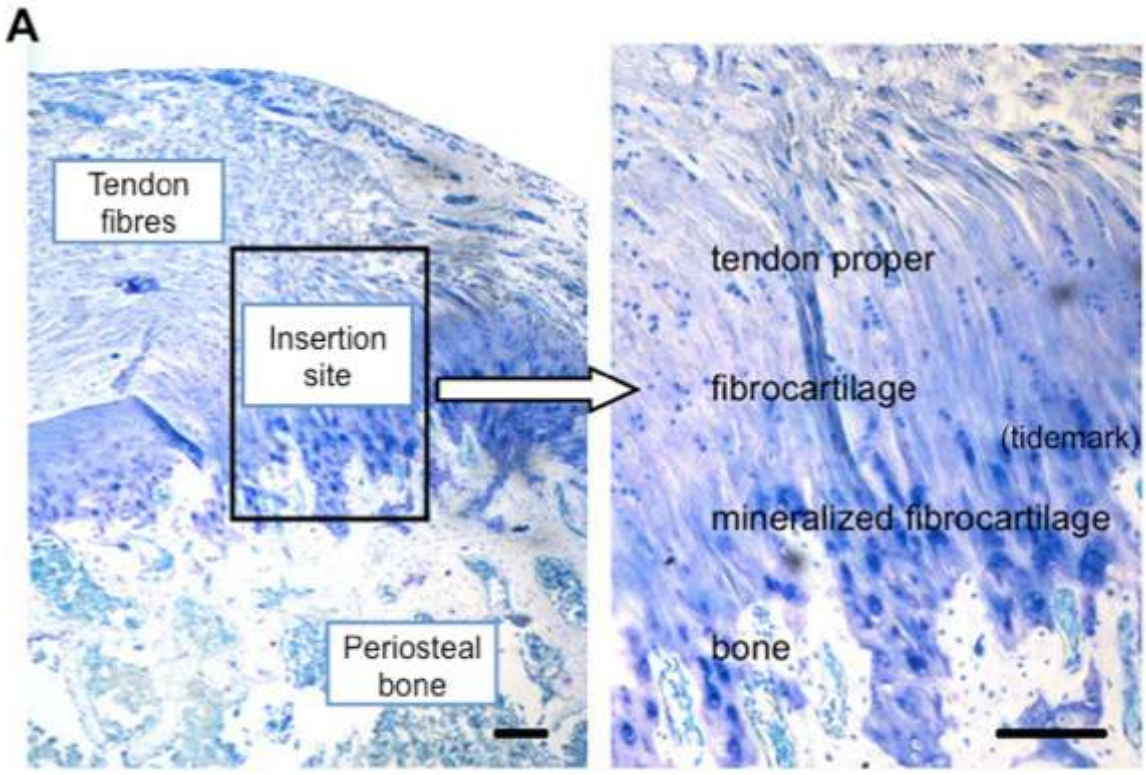

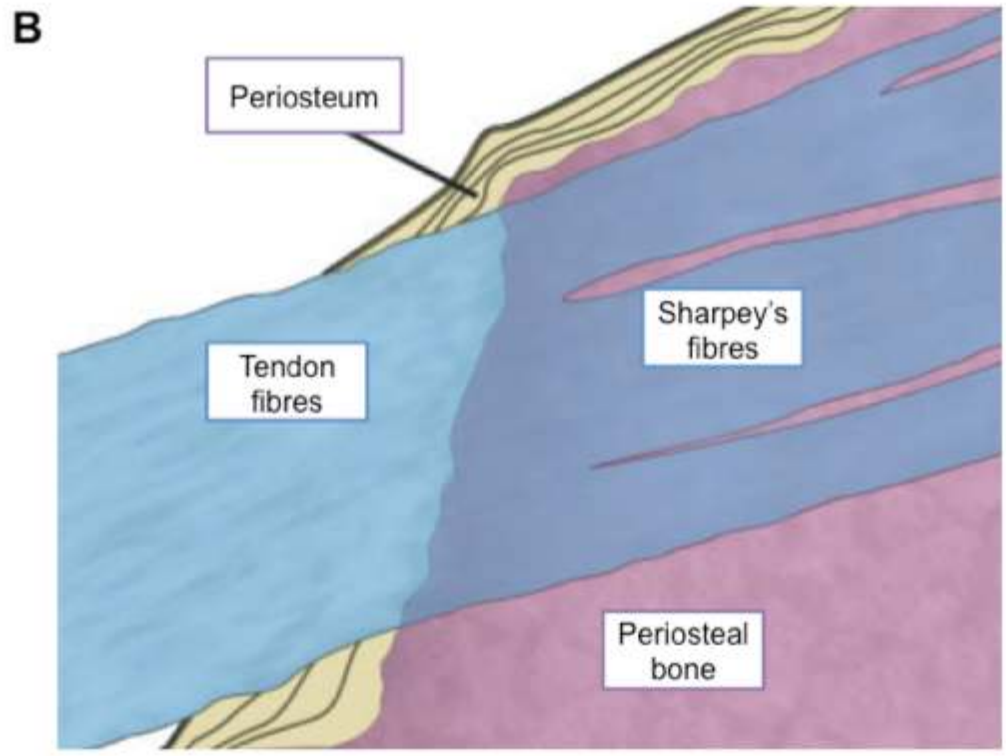
B
Periosteum
Tendon fibres
Sharpey's fibres
Periosteal bone

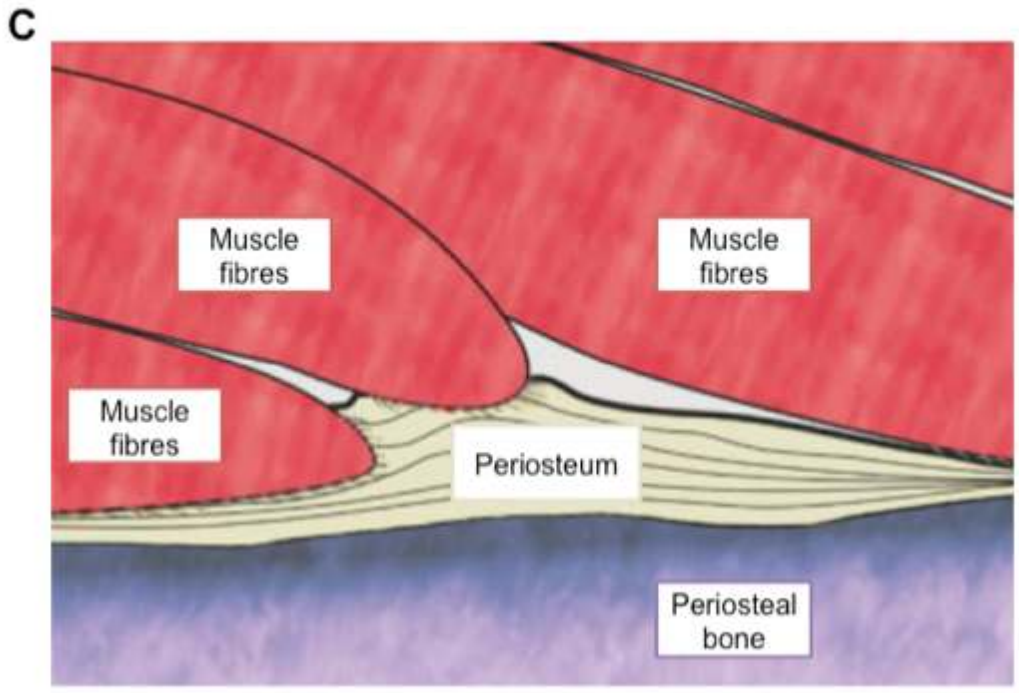
C
Muscle fibres
Muscle fibres
Muscle fibres
Periosteum
Periosteal bone

Figure 3.6 Schematic representation of cortical drift. Bone area is shaded grey, while previously resorbed bone regions are represented by hatched lines. Cortical drift in the direction indicated by the arrows and accomplished by a coordinated pattern of bone deposition (green pluses) and bone resorption (red minuses) (modified from Enlow, 1963).

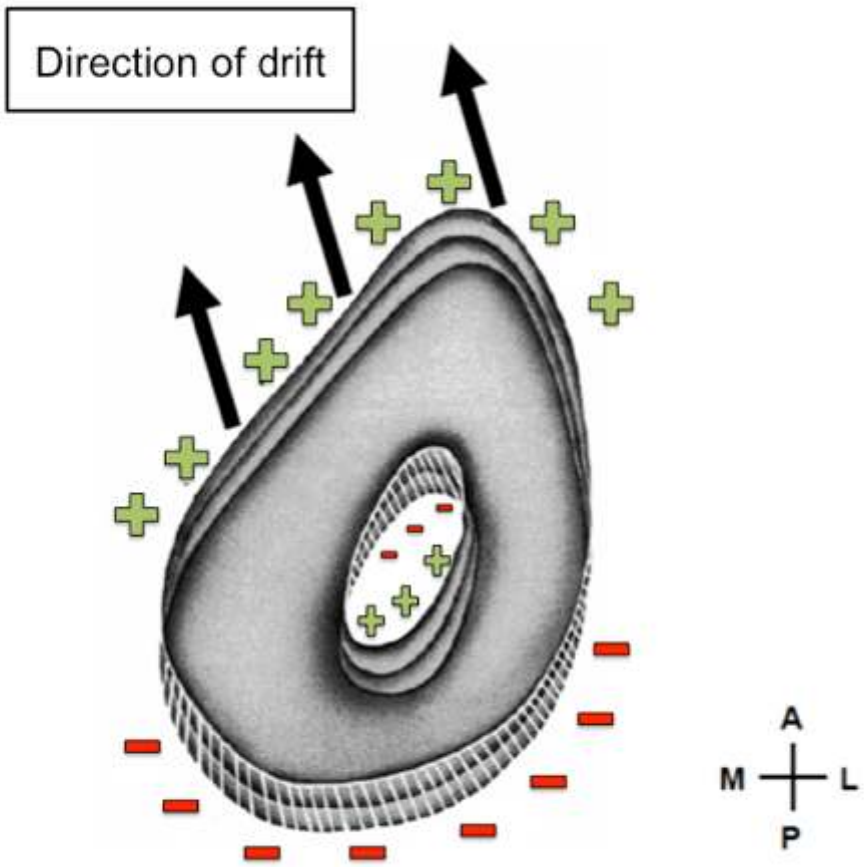

Chapter 4

4. Materials and methods

This chapter describes the sample and the selection criteria of the specimens used in the current study. The protocols for the primate sample are first explained, followed by the protocols for the mouse sample. The specimen preparation methodology is described, including dissection protocols, as well as the embedding and histological preparations. Finally, description of measurements, imaging methods, and an overview of the analyses performed are presented.

4.1 Primate

This research examines muscle architecture and their attachment sites in extant primate species to better reconstruct the locomotor and postural behaviour of past populations and extinct species. This requires an examination of primates that show diversity in their mode of locomotion. Both Old World monkeys and great apes are considered. The shoulder and elbow regions are of particular interest because of the potential insight they might provide in understanding the origin of erect posture and bipedalism. The humerus was therefore chosen to represent both these articulations as well as a variety of muscle form and functions that are critical to understanding the locomotor behaviour of primates.

4.1.1 Cadaver material

Primates can live a long time in captivity and cadaveric specimens are scarce. Deaths are unpredictable, and few animals are available for study outside zoological gardens, museums, or research centres. Many challenges come with primate soft tissue research, such as transportation

of these large animals, and finding facilities for the freezing, storing, and dissecting of these primates (Zilhman and McFarland, 2000). It becomes even more difficult to obtain primate specimens when destructive analyses of muscle and bone tissues are needed. Every primate cadaver is valuable, and although the sample size may be small, this research helps accumulate a database of soft- and hard-tissue variables for future projects examining variation between primates. All primate specimens for this research were obtained from the Toronto Zoo and eviscerated during post-mortem examination. The available cadavers determined the choice of primates in the sample. Cadavers were stored, dissected, and analysed in the Comparative Primate Dissection Laboratory at the University of Toronto.

Specimens were all adults based on patterns of tooth eruption and/or zoo records, and showed no sign of pathology (Table 4.1). Age is an important factor associated with attachment sites and only adult specimens are used to remove the potential confounding variable of growth. Since muscles attach primarily to the periosteum, and not the underlying bone, during growth, the morphology of juvenile muscle attachment sites is unlikely to reflect fully the size or activity of the attaching muscle, and are generally more difficult to define (Wilczak, 1998a, b; Zumwalt, 2005, 2006; Jurmain et al., 2012). Also, older individuals seem to have more pronounced muscle attachments than younger individuals. It is unclear if the defined markings are due to accumulation of micro-damage from muscular loads over time, or to metabolic and hormonal changes that comes with age (Jurmain et al., 2012). Overall, individuals seem to have greater markings because of their age even though these individuals' activity levels might have decreased during life due to advanced age (Zumwalt, 2005; Villotte et al., 2010a). Consequently, to reconstruct past lifestyles from muscle attachments, age differences must be taken into

account. Gravity and body size are other main forces that can influence bone morphology beside muscle force. The size of the primates was also considered.

Two female macaques, a Japanese macaque (*Macaca fuscata*) and a Barbary macaque (*Macaca sylvanus*), were obtained and stored in 10% buffered formalin several years ago. *Macaca fuscata* has a smaller body mass (female average: 8.03 kg) than *Macaca sylvanus* (female average: 11.0 kg) (Smith and Jungers, 1997). The Toronto Zoo no longer had records of these two individuals, but the zookeepers were able to give information on the captive environment of the animals. Both of these species were put in the same enclosure at the zoo, ate the same monkey chow, and were subject to the same daily stimuli. Their enclosure included access to fields, trees, and vertical rock substrates allowing the macaques to locomote the same ways as in the wild. Although macaques are often studied, very little is actually known about their muscle architectural structure. Therefore, this study can provide data that is currently unknown in macaques. The left forelimb was used to collect the data on muscle architecture and bony site of attachments. The female average body mass for each species was used to control for body size.

Three adult orangutans (*Pongo pygmaeus abelii*) of known age, sex, and body mass were also used in this study. As seen with the macaque species for this research, all orangutans from the Toronto Zoo were found in the same enclosure, had the same diet, and were subject to the same daily stimuli. The orangutans' enclosure included access to fields, trees, ropes, and vertical substrates allowing the apes to locomote the same ways as in the wild, but also including more time on vertical ground substrates. In the laboratory, the apes were stored in 10% buffered formalin before dissection except for one orangutan (P2). This male orangutan was dissected fresh since he was received while other dissections were underway in the laboratory. Once his

muscles were removed, they were then stored in 10% buffered formalin. The right forelimb of two individuals (P1 and P2) and the left forelimb of the other (P3) were dissected. Different sides of the forelimb were used due to better preservation conditions since some of the muscles had to be cut at the elbow to facilitate transportation from the zoo to the laboratory. Both sexes are represented in the apes specimens, therefore sex as a variable is taken into consideration. Males tend to have stronger muscle markings than females. This difference is mainly due to physiological reasons; males in general have larger muscles than do females associated with body size, locomotion and/or activity patterns (Hawkey and Merbs, 1995; Hawkey 1998; Wilczak 1998a, b; Knüsel, 2000; Eshed et al., 2004; Weiss, 2003, 2004, 2007, 2010; Molnar, 2006, 2010; Jurmain et al., 2012; Nolte and Wilczak, 2013). Body size was controlled using the final body mass provided by the zookeepers for the orangutans.

4.1.2 Gross dissections

Protocols for measurements and observations during the primate forelimb dissections are detailed below. Prior to dissections, primates were digitally photographed (Canon EOS Rebel XSi); measurements of the arm, forearm, and hand were taken with a measuring tape to the nearest 0.1 cm. Then, the skin and superficial fascia overlying the forelimb, chest, and back muscles were removed. A total of 28 muscles attaching to the humerus (Table 4.2) were identified following Swindler and Wood (1973), and Berringer et al. (1978); every dissecting stage was photographed and recorded. Before the removal of muscles, observations were made on size, position, and relationship of each muscle. One of the challenges of entheseal research (Wilczak, 1998a, b; Zumwalt, 2006; Notle and Wilczak, 2013) includes the need to define the boundaries of each surface area in a consistent manner. Careful attention of the muscle-bone

interface was given to each origin and insertion before and after the removal of the muscles to visually document attachment contours and reduce error (Figure 4.1).

Each muscle of the forelimb was systematically removed using methods seen in previous dissections (Schultz, 1942; Schultz, 1962; Tuttle, 1969; Gans, 1982; Carlson, 1983; Gans and de Vree, 1987; Antón, 1994; Lemelin, 1995; Smith and Jungers, 1997; Ogihara et al., 2005; Carlson, 2006; Payne et al., 2006a, b; Tubbs et al., 2006; Schmidt and Schilling, 2007; Oishi et al, 2008, 2009; Michilsens et al., 2009, 2010). After harvesting, muscles were cleaned of fat and excessive connective tissue. All muscles were then submerged in 10% buffered formalin for at least one week before any measurements were taken to ensure complete fixation. This complete fixation also ensures the density value used for muscle architectural variables to be constant (Ward and Lieber, 2005). After fixation was assured, full muscle-tendon unit (MTU = muscle fasciculus [L_f] + tendon length [TL]) was measured (from origin to insertion). Then, belly muscle length (L_b) was measured as the length between proximal ends of the most proximal and distal ends of the fibres of the muscles. The remaining length measurements for each muscle were taken using protocols previously outlined (Anapol and Jungers, 1986; Anapol and Barry, 1996; Anapol and Gray, 2003; Taylor and Vinyard, 2004; Taylor et al., 2009). First, muscles were pinned to a styrofoam block and sectioned longitudinally along the line of action, and five other sampling sites located approximately 1-3 cm apart were selected making sure to include various levels from superficial to deep within the belly of the muscle. Overall six neighbouring fasciculi were examined and measured (Figure 4.2) for:

1) The length of muscle fasciculus (L_f) between proximal and distal myotendinous junctions, or fleshy attachment(s) to bone

2) The perpendicular distance (a) from the proximal myotendinous junction to the tendon of distal attachment
3) The length of tendon (T_p) from the proximal attachment of the whole muscle to the proximal myotendinous junction
4) The length of the tendon (T_d) from the distal myotendinous junction to the distal attachment of the whole muscle. The sum of T_p and T_d is the total tendon length (TL).

All lengths were measured using digital callipers (Mitutoyo, Japan) to the nearest 0.01 mm. The muscles were then blotted dry, trimmed of excess tendon, and weighted using an electronic scale (Sartorius, Canada) to the nearest 0.1g. The angle of pennation (θ) was calculated as the arcsin of a/L_f.

Measurements of fibres and pennation angles are ideally taken at resting length; force is at maximum potential at this length (see Chapter 2). This ideal length can only be accomplished if the specimens are embalmed in typical postural position seen in observations of living animals just before locomotor progression (Anapol and Gray, 2003). Since cadavers are embalmed without regard of limb positions, and usually in a more flexed position, the lengths of the whole muscles are either greater or less than resting length. All variables that involve fibre length are thus altered. To address this problem, sarcomere length was measured to normalize muscle fibre length (Felder et al., 2005) using protocols from Taylor et al. (2009). Muscles were chemically digested in 30% nitric acid (HNO_3) diluted in saline; digestion time varied from 30 minutes to 4 hours depending on the size of the muscle, and tissue preservation. The tissues were then placed in 1 × PBS (phosphate buffered saline) to stop the chemical digestion. Small fibre bundles from all regions of the muscles were dissected using a Nikon SMZ1000 stereomicroscope (10X magnification), and careful attention was paid to remove entire fibre bundles from tendon to

tendon (or fleshy attachment(s) to bone). At this time, L_f could be taken a second time to test for error with previous method mentioned above. Six to ten fibre bundles per muscle were isolated, mounted on glass slides, and cover slipped with Permount (Fisher Scientific, New Jersey) mounting medium. Permount is a synthetic resin dissolved in toluene, which serves as a permanent adhesive for cementing cover glass to microscope slides. The slides were air dried over night. Laser diffraction was used to measure sarcomere length (Lieber et al., 1994). Laser diffraction works by having the light pass through the muscle-banding pattern formed by the arrangements of A-bands and I-bands within the sarcomere. The laser light diffracts through the I-bands within the sarcomere. Two to three sarcomere length measurements per fibre bundle were obtained. If that was impossible due to tissue preservation or mounting problems, three measurements on three separate fibre bundles of the same muscle region were taken and averaged. To normalize fibre length, the following equation was used:

$$(N)L_f = L_f * SL_s / L_s$$

where $(N)L_f$ is the normalized fibre length, L_f (cm) is the measured fibre length, SL_s is the standard sarcomere length (μm), and L_s the measured sarcomere length (μm) (Taylor et al., 2009). Standard sarcomere length used for the primate sample was 2.41 μm, which was calculated to be the optimal sarcomere length (length at which the maximum tetanic tension is generated) in macaque limb muscles (Walker and Schrodt, 1974).

4.1.3 Soft-tissue variables

Fibre architecture provides measurable features from which physiologic characteristics of whole muscles can be estimated to interpret muscle function (Close, 1972; Grand, 1977; Amis et al., 1979a, b; An et al., 1981; Gans and Gaunt, 1991; Zihlman, 1992; Jouffroy and Médina, 1996; Lieber and Fridén, 2000; Youlatos, 2000; Schoenau et al., 2002; Ogihara et al. 2005; Payne et

al., 2006a; Smith et al., 2006; Carlson. 2006; Oishi et al., 2008, 2009; Michilsens et al., 2009; Lieber and Ward, 2011). From the above measurements, the following variables were computed:

1) Mean fibre length (L_f) and pennation angle (θ) for each muscle

2) Physiological cross-sectional area (PCSA) to estimate potential force output of each muscle using the formula:

$$\text{PCSA } (cm^2) = \frac{(\text{muscle mass } (g) * \cos \theta)}{L_f \text{ (cm)} * 1.0564 \text{ } (g/cm^3)}$$

where 1.0564 is the specific density of muscle (Mendez and Keys, 1960; Murphy and Beardsley, 1974)

3) Muscle mass/predicted effective maximal tetanic tension (M/P_0) to compare the priority of force production (as a function of the number of fibres in parallel) versus contraction velocity (as a function of fibre elongation) using the following equation:

$$M/P_0 = \text{muscle mass } (g) / 22.5 \text{ N } cm^{-2} * \text{PCSA } (cm^2)$$

where 22.5 N cm^{-2} is the specific tension of muscle (Powell et al., 1984).

4) Estimated maximum excursion of the distal tendon of attachment (h) which considers fibre length (L_f) and pennation angle (θ) to estimate the excursion of a muscle during contraction:

$$h = L_f * ((\cos \theta) - (\sqrt{} \cos \theta^2 + n^2 - 1))$$

where n is the coefficient of contraction or fibre length after contraction/resting fibre length (adapted from Benninghoff and Rollhaüser, 1952). Here n = 0.767 for pennate fibres (Gans and Brock, 1965; Mulh 1982; Anapol and Gray, 2003; Taylor and Vinyard, 2004; Taylor et al., 2009). To adjust for size, h is divided by overall muscle length (L_b): (h/L_b).

5) Estimated energy cost of applying force to a substrate, and the extent a muscle might be used isometrically versus isotonically:

$$\text{TL:MTU} = \text{Total tendon length (TL)} / \text{Muscle-tendon unit (MTU)}$$

6) Priority index for force (*I*) to calculate the force production of a muscle at the expense of excursion:

$$I = \text{PCSA} / \text{V}^{2/3}$$

where V is the muscle weight (Woittiez et al., 1986; Weijs et al., 1987; van Eijden et al., 1997). Muscles of equal volumes but with shorter more pennated fibres enhance force at the expense of excursion. On the other hand, muscles with long and parallel fibres will increase excursion.

4.1.4 Hard-tissue variables

Once all the muscles of the forelimb were removed, the bones were skeletonized using a 1% Terg-A-Zyme solution diluted in distilled water. Terg-A-Zyme (Alconox, New York) is an active enzyme detergent powder that gently breaks down soft tissue without harming the bone (Green, 2010; Green et al., 2012). The solution was placed in front of a window in order for the detergent to react with ultraviolet rays (UV) and was changed every 24 hours until the bones were clean, which depending on size was from 14 to 20 changes. Once the bones were clean, maximum length of the humerus was measured to quantify body size, and to locate positions along the diaphysis where cross-sectional measurements would be taken. Each bone was digitally photographed. Osteological measurements could be taken using previous dissecting notes, measurements, and photographs as a guide to determine the location and defining contours of the enthesis. Proximal, distal, and midpoints (Stern, 1971), as well as maximum length, width, and two-dimensional surface area were measured for each muscle attachment sites on the humerus (Figure 4.3) with Image J version 1.44 (Rasban, 1997-2007).

Reconstruction of forelimb muscle mechanical loading was then examined using cross-sectional properties. Long bone robusticity can be quantified by applying an engineering principle called

"beam theory", to estimate the mechanical performance of a bone diaphysis (e.g., cortical thickness) under various loadings. Using this approach, biomechanical properties and behavioural differences can be compared between groups. Although cross-sections of the diaphysis can be reconstructed at any position along the diaphysis, previous studies (Ruff and Haynes, 1983; Pfeiffer et al., 1996; Pfeiffer and Zehr, 1996; Demes et al., 1998; Feik et al., 2000; Hamrick et al., 2000, 2002; Ruff, 2000; Schoenau et al, 2000; Stock and Pfeiffer, 2001; Stock, 2002; Liberman et al., 2004; O'Neil and Ruff, 2004; Pearson and Lieberman, 2004; McFarlin, 2006; Pfeiffer et al, 2006; Rauch et al., 2007; Stock and Shaw, 2007; Turner, 2007; McFarlin et al., 2008; Goldman et al., 2009; Harrington, 2010; Shaw and Stock, 2011; Skedros, 2012; Shaw and Ryan, 2012) concentrate only on certain areas of the bone (e.g., midsaft) with little attention being paid to muscles (Shaw and Stock, 2009a, b). The aim of this study was to analyse the interaction of the muscle and bone systems, and since some of the largest voluntary loads on bone come from the pull of muscles (Schoenau et al., 2000), cross-sectional variables can be used to observe potential change in cortical thickness throughout the attachment. The humeri of the primates were scanned using computed tomography (CT) at the Hospital for Sick Children in Toronto (Discovery CT750HD). Prior to scanning, bones were set up in standardized orientations (trochlea and capitulum of the humerus facing up), and cross-sectional locations were determined based on lengths taken during the soft- and hard-tissue measurements (Figure 4.3). From these CT scans, the proximal and distal edge as well as the midpoint of each muscle attachment was selected to analyse cross-sectional geometry (Figure 4.4). Only muscles that attach to the diaphysis of the humerus were analysed due to the limitations of using cross-sectional geometric analyses at the epiphyses of bones (Huiskes, 1982; Ruff and Haynes, 1983; Biewener, 1992). Since all of these cross-sections were found at different locations throughout the bone within specimens, the midshaft of the humerus was also analysed in order to have a

standard cross-section throughout the sample. From the CT images, calculations of diaphyseal geometric properties and measurements of bone rigidity (total subperiosteal [TA], cortical [CA], and medullary [MA] areas; second moment of area, maximum and minimum second moment of area, second moment of area [I_x and I_y axis], maximum and minimum second moment of area [I_{max} and I_{min}], polar second moment of area [J], theta [θ]; section modulus [Z]) provided estimates of the mechanical performance of the bone diaphysis (Table 4.3 and Figure 4.4). CT images were imported into Image J (Rasban, 1997-2007) to be analysed using Moment Macro Analysis for reconstruction of mechanical loading. Images were imported unaltered, but at times removal of trabecular bone was necessary using the drawing tool in the Image J software.

4.1.5 Data analysis and error studies

Before testing any hypotheses, each primate variable was tested for normal distribution using Shapiro-Wilk test for normality (Sokal and Rohlf, 2012). Given the small sample size and because some of the variables were not normally distributed (Tables 4.4 – 4.7), nonparametric statistical tests were used when applicable to explore the assumption that muscle use influences attachment morphology. To allow for comparisons between individuals and species, the data were normalized assuming geometric similarity (Thorpe et al., 1999; Payne et al., 2006; Zumwalt, 2006; Michilsens et al., 2009). Masses (M_b) were scaled to body mass, lengths to $(M_b)^{1/3}$, and areas to $(M_b)^{2/3}$. *M. fuscata* was scaled to 8.03 kg and *M. sylvanus* was scaled to 11 kg. The fibrous attachment sites were also adjusted for cortical bone area (CA) to examine if differences could be found in relation to the amount of bone that is found under the entheses. Only muscles that were harvested in all primates were compared to each other and muscles were also grouped in functional categories (Table 4.8).

To test if different locomotor patterns in the primates studied resulted in corresponding changes in muscle architecture of the forelimb muscle (H1) or in changes in entheseal morphology (H2), qualitative tables and plots of the soft-and hard-tissue variables provided a useful method of characterizing trends, which could be related to observations. Qualitative observations were also made to investigate the relationship between soft- and hard-tissue morphologies (H3). Qualitative observations had to be performed due to the small number of individuals of the sample, which inhibited correlation or regression testing. Therefore, qualitative observations were made to investigate differences between sex and species in relation to the internal muscle structures (H1.2) and muscle attachment site morphology (H2.2) parameters describing the soft- and hard-tissue variables of the sample.

A supplemental method used to test the different locomotor patterns in the primates studied with entheseal morphology (H2) included the distal-most point of attachment sites, which was calculated as a percentage of the total bone length (from the proximal end for the insertions and the distal end for the origins) to compare lever arms of each muscle. These measurements were normally distributed (Table 4.6) therefore a one sample two-tailed *t*-test was used to analyse the differences between *Pongo* and *Macaca*. The same tests were performed to compare the cross-sectional geometric variables.

Error studies compared two observation sessions for a sub-sample of randomly selected attachment sites (n = 10 entheses per primate). The observations were made approximately 6 months apart. Percent error was calculated as the difference between the first and second measurements. Intra-observer error could not be compared due to the destruction of the soft-tissues to measure sarcomere lengths. However, all soft-tissue measurements (e.g., muscle belly,

fibre length, tendon length, pennation angle) were taken five times and by at least two different individuals before any chemical digestion to assure the accuracy of the measurements. All statistical tests were performed using IBM SPSS Statistics version 20.0 for Mac.

4.2 Mouse

As seen with the primate sample, this research examined whether muscle use reflect the attaching bone morphology. While the primate sample looked at the bone and muscle relationship in a qualitative manner, the experimental mouse model section of the dissertation quantified the influence of activity patterns on the morphological development of muscles and the corresponding attachment. Entheseal research begins with the assumption that increased size of a muscle attachment is evidence of increased muscle activity as a result of continued use in habitual behaviours. Therefore, bigger and stronger muscles along with more activity should result in a bigger and more robust attachment site. This assumption was approached by examining the gross and microanatomy of the humerus in wild-type mice.

4.2.1 Sample

The George Washington University provided thirty (n = 30) of the ninety-nine female outbred wild-type mice (*Mus musculus*, CD-1, Charles River Laboratory derived, purchased from Harlan Laboratories, Indianapolis, IN, USA) used for Dr. David Green's dissertation (2010). All experimental procedures described were approved by the George Washington University Institutional Animal Care and Use Committee (IACUC #16-12,7). In Green's (2010) original experiment, ninety-nine mice were placed in cages housing seven to nine individuals. Mice were separated into one control and two experimental groups: (1) control mice (CON) housed in cages

with no exercise apparatus, (2) running wheel mice (WHL) housed in cages containing two activity wheels, and (3) climbing mice (CLB) housed in cages outfitted with one metre tall wire-mesh tower where water sources were positioned at the top. For the latter group, water sources were positioned approximately ten centimetres above the floor of the cage at the beginning of the experiment, and were raised 7-10 cm each day until the sources were one metre above the cage bedding (Figure 4.5). All mice were provided with food and water *ad libitum* (although CLB mice had to climb in order to drink). The experimental mice were free to use the exercise wheels and climb up the meshed cages at will. This allowed investigation of the influence of muscle activity within normal and non-pathological limits. This is important since experimental research on individuals who participate in strength training has shown that the biomechanical linkage between muscle and bone is influenced by confounding variables such as over training, which increases bone blood flow and changes in osteogenetic factors such as growth hormones (Montgomery et al., 2005, Zumwalt, 2005). To avoid these confounding variables, each mouse was left to exercise as much or as little as was comfortable. The amount of exercise from the running and climbing groups was recorded during the initial experiment (Green, 2010; Green et al., 2012). On average, the CLB group climbed approximately 140 metres a night representing about 70 trips up and down the meshed cages. This indicates that the mice regularly climbed regardless of whether or not they needed to drink. CLB mice were considered to be the intermediate intensity exercise group. The WHL mice did even more exercise, running approximately 1900 metres per night equivalent to about 40 minutes of running. WHL mice were considered to be the high intensity exercise group. These differences in the degree and type of activities (running/high intensity, climbing/intermediate intensity) were considered when analysing the muscle and bone data.

The experiment considered two age groups: (1) “juveniles” all of which were newly weaned and 25 days of age at the beginning of the experiment, and (2) “adults” all of which were 46 days of age at the outset. All animals were weighted twice throughout the duration of the experiment (at day 11 and day 26) and once more immediately following death. The experiment lasted a total of 78 days. Mice are usually considered skeletally and sexually matured shortly after being weaned since both males and females reach sexual maturity by 1-1.5 months (Kilborn et al., 2002) and are of adult body size by this time. However, it is worth noting that in mice, the growth plates of long bones do not fully fuse until five months of age (Kilborn et al., 2002). Despite being of adult body mass and sexually mature, the lack of growth plate closure may need to be addressed when analysing the entheseal morphology. For the current study, five “adult” mice and five “juvenile” mice of each activity group were randomly chosen to permit examination of the effects of activity and age at onset of the experiment on muscle architecture and attachment morphology in the sample (Table 4.9).

Finally, mice were given three subcutaneous injections containing fluorescent bone-labelling dyes at known intervals during the experiment: 1) Alizarin-red (25mg/kg) on day 2 of the experiment, 2) DCAF-green (15mg/kg) on day 15 (13 days interval), and 3) Xylenol-orange (80 mg/kg) on day 29 of the experiment (14 days interval) (van Galen et al., 2010). Fluorochromes bind to the mineralized front of newly deposited bone matrix, and stain the interface between osteoid (organic portion of the bone matrix that forms prior to maturation of bone tissue) and mineralized bone (Martin et al., 1998). These labels therefore represent known time points during the duration of the experiment, and allow for determination of rates of osteogenesis calculated as the distance between two adjacent labels divided by the time interval (Newell-Morris, 1982; Castanet et al., 2004; van Galen et al., 2010). The small body size and rapid

development of mice are also favourable when designing models of osteogenetic response to locomotor behaviours (Carlson et al., 2008).

4.2.2 Dissections and soft-tissue variables

To test the hypothesis that increased activity from different exercise patterns results in corresponding changes in muscle morphology, the muscles that attach to the deltoid crest (a fibrous enthesis) were examined. Protocols for measurements and observations during the micro-mammal dissections are detailed below. Prior to dissections, the female mice were digitally photographed using Infinity Capture Imaging software. Then, the skin and superficial fascia overlying the forelimb, chest, and back muscles were removed. The mouse deltoid crest presents as a prominent ridge protruding on the cranial side of the humerus (Greene, 1935; Chiasson, 1975; Wingerd, 1988) and is a clearly defined muscle insertion site for which surface anatomy and rates of osteogenesis in the underlying cross-section of bone can be documented. The spinodeltoideus muscle inserts on the entire lateral surface, while the acromiodeltoideus muscle and the superficial pectoralis muscle share the medial surface of the prominent ridge. The three muscles that attach to the deltoid crest are the principal protractors and retractors of the humerus, which help the animal propel itself forward, maintain its balance, and resist gravitational forces (e.g., maintain glenohumeral joint flexion when standing, walking, and running). They are essential to the habitual gaits experienced by all three groups of mice (Figure 4.6). The forelimb muscles were dissected under an Olympus S2X12 stereomicroscope and every dissecting stage was photographed and recorded. Before the removal of the muscles, the muscle belly length (L_b) and the pennation angle (θ) were measured using a reticle (accuracy, 0.01mm) on the dissecting scope (Mathewson et al., 2012). The spinodeltoideus, followed by the superficial pectoralis, and ending with the acromiodeltoideus were harvested, cleaned of excess fat and fascia, and

submerged in 10 % buffered formalin for at least 48 hours before any more measurements were taken; once again to ensure complete fixation and a constant specific muscle density (Ward and Lieber, 2005).

After fixation, muscle mass was taken to the nearest 0.001g using a Denver Instrument APX-200 analytical balance. Since these mice had been frozen and thawed for the previous experiment, the soft-tissues had most likely shrunk. In order to normalize the soft-tissue variables and assure proper muscle lengths, sarcomere length was also measured in the mice (Felder et al., 2005) using protocols from Taylor et al. (2009). Muscles were chemically digested for up to 6 hours in 30% nitric acid and then submerged in saline for 24 hours. Small fibre bundles were then manually dissected and isolated using a Nikon SMZ1000 stereomicroscope (10X magnification) and fibre length (L_f) was measured using a reticle (accuracy, 0.01mm). Six to ten fibre bundles per muscle were mounted on glass slides, and cover slipped with Permount mounting medium. The slides were air dried over night. Laser diffraction was used to measure in situ sarcomere length (Lieber et al., 1994). Two to three sarcomere length measurements per fibre bundle were obtained. Standard sarcomere length used for the mice sample was 2.4 μm, which was theoretically and experimentally determined to be the optimal sarcomere length (length at which the maximum tetanic tension is generated) in mice limb muscles (Hegarty and Hooper, 1971; Burkholder and Lieber, 2001; Edman, 2005; Gokhin et al., 2008). From the above measurements, fibre architecture variables were computed to interpret muscle function (see section 4.1.3 for descriptions): PCSA (mm^2:), M/P_0, and *I*.

4.2.3 Gross measurements of attachment sites

After dissections, the left forelimb of each mouse was prepared for measurement of the gross morphology of the deltoid crest. The limbs were skeletonized using 1% Terg-A-Zyme (Alconox, NY) solution diluted in distilled water, stored in a dark laboratory oven (Labline 3486M Imperial V) at 45°C with 24-hour changes over a period of one week. This prevented the bones from being exposed to UV rays, which would have faded the fluorescent labels. It also permitted the speeding up of the skeletonization process. Once the bones were cleaned, the humeri were digitally photographed using Infinity Capture program. Using Image J (Rasban, 1997-2007); 1) maximum length of the humerus, 2) maximum length and width of the deltoid crest on the lateral and medial side of the crest, 3) the area of both the lateral and medial side of the attachment, 4) the distal angle of the deltoid crest, and 5) crest thickness (measured at the histological section where growth measurements were taken) were all taken as seen in Figure 4.7.

4.2.4 Bone histology

Histological thin sections were prepared following the procedures in Goldman et al. (1998) with some modifications following McFarlin (2006) and Cho (2012) for better specimen embedding and mounting. After skeletonization, the humerus was cut transversely using an Isomet 1000 Buehler precision saw (Lake Bluff, Illinois), just distal to the deltoid crest to improve infiltration of the bone during embedding. The proximal end of the humerus was then dehydrated in a series of graded ethanol changes (50%, 75%, 95%, 100%) with frequent ultrasonication and vacuuming. Vacuuming allows for the solution to penetrate all vascular canals while an ultrasonic cleaner (Fisher Scientific FS20D, Pennsylvania) gently removes any debris from small spaces and the medullary cavity of the bone using sound waves. Clearing of the bone was done

using two changes of 100% Methyl Salicylate for 4 hours each. The process of dehydrating and clearing of bone took approximately five days. The bones were then embedded in Caroplastic (Carolina Biological Supply, North Carolina) polyester resin. Caroplastic is a clear polyester resin that will harden after a catalyst is added. It is a good medium to embed small bones, such as the humerus of mice. The bones were first put with un-catalyzed Caroplastic for 24 hours and vacuumed to make sure the monomer infiltrated all spaces. Finally, the bones were embedded in the Caroplastic with catalyst. The specimens were vacuumed until all bubbles were removed from the solution. The samples were finally placed in a laboratory oven set at 45°C for 48 hours, and then the embedded bones were left to cool down for another 24 hours. At this point, the bone blocks were broken out of their glass containers and ready for preparation of histological thin sections.

Two histological thin sections were prepared for analysis of bone growth rate (Figure 4.8). The first section was located at the distal margin of the deltoid crest. As the morphology and length of the deltoid crest (and hence, the diaphyseal location of this first section) varied among individuals, a second section was produced from a standardized diaphyseal level across the mouse sample. This second section was collected at 25% of maximum bone length (measured from the proximal epiphysis), which was still located within the deltoid crest. Each embedded block was ground on a series of carbomide emery papers (Buehler Ltd., Lake Bluff, Illinois) to 1200 grit. The blocks were ultrasonicated between each graded series and at the end to remove grit particles from the specimens. The prepared surface was then mounted to a plastic slide using superglue. A small weight was placed on the mounted blocks and it was left to dry overnight. After mounting, the block was then cut away from the slide on a Buehler Isomet slow-speed diamond blade saw, leaving behind a section of approximately 130 microns (μm) in thickness.

Mounted sections were then ground to a final thickness of 100 ± 5 μm, their imaging surface prepared to a surface topography of 1200 grit, and temporarily cover slipped for imaging. The remaining embedded bone block was re-sectioned for the second cut (25% inferior to the proximal epiphysis). The same protocol was applied for this standardized cross-section.

4.2.5 Histological imaging

Bone histomorphology can be viewed and measured using a transmitted light microscope. Since fluorescence decays over time, digital images of the bone cross-sections had to be captured to ensure accurate histomorphometric analyses. Digital montage images were collected of entire bone cross-sections on a Zeiss AxioImager microscope configured with an automated LUDL stage (0.1 μm accuracy in "X" and "Y"). Same field of view images were collected under 40X magnification in brightfield (BF), circularly polarized light (CPL), and fluorescence illumination for imaging of DCAF-green, Alizarin-red, and Xylenol-orange labels. Images were captured using a QImaging colour CCD camera (40X objective, 1 pixel = 1.346 μm) and an integrated MicroBrightField Stereo Investigator system with Virtual Slice, which automates the montaging of entire cross-sections. CPL images were used for the qualitative observations of the bone tissue found throughout the cross-sections. Endosteal and periosteal areas were collected on BF images. Fluorescent images were then imported to Adobe Photoshop CS3, and superimposed using the "Layers" function and their transparency adjusted to allow for visualization of relationships between fluorescent labels and bone features. The superimposed and flattened images were imported into Image J to calculate the rate of periosteal bone growth (Figure 4.9). Rates of osteogenesis were calculated as the distance between two fluorescent labels over the time elapsed (Newell-Morris, 1982; Castanet et al., 2004; Plochocki, 2009). Where all three fluorochromes were present, a total of two measurements could be taken at one location.

Maximum distance measurements were taken within each quadrant (anterior, posterior, medial, and lateral) across the cross-sections and at the deltoid crest. Finally, these measurements from both cross-sections were averaged to have an overall bone growth rate of the humeral shaft for each individual. In addition, the rate of osteogenesis for the bone region immediately underlying the deltoid crest was calculated from the cross-section at the distal margin of the deltoid crest. As data of bone growth and tissue variation were being collected, it became apparent that some of the cross-sections showed evidence of secondary remodelling activity (Figures 4.10 and 4.11). Modelling and remodelling of bone varies greatly among vertebrates. Cross-sections of long bones in rodents, especially rats and mice, are characterized as having circumferential lamellae containing few blood vessels and even fewer evidence of secondary osteons. In fact, tissue resorption seems to be disorganized and reconstruction into organized osteon bone seems to be mainly lacking (Enlow and Brown 1958; Enlow, 1963; Francillon-Vieillot et al., 1990; de Ricqlès et al., 1991). Osteon density was therefore added to the histological analysis to see if differences in bone remodelling were found between activity groups. To document osteon density, secondary osteons and drifting osteons (osteons with continuous resorption on one side and continuous formation on the other side [Robling and Stout, 1999]) were counted manually across the cross-sectional image (Figures 4.10 and 4.11).

Finally, images were converted to grey-scale images in Adobe Photoshop CS3 and imported into Image J to be analysed using Moment Macro Analysis for reconstruction of mechanical loading; measuring total area (TA), cortical area (CA), medullary area (MA), second moment of area (I_x and I_y axis), maximum and minimum second moment of area ($_{Imax}$ and I_{min}), polar second moment of area (J), theta (θ), and section modulus (Z) (Table 4.3 and Figure 4.4).

4.2.6 Data analysis and error studies

Before testing any hypotheses, each variable was tested for normal distribution using Shapiro-Wilk test for normality (Sokal and Rohlf, 2012). Not all of the variables were normally distributed (Tables 4.10 – 4.16) therefore to treat all of the variables the same and to be more conservative, non-parametric statistical tests were used to explore the assumption that muscle use influences attachment morphology. All variables are presented absolutely and relative to body mass (M_b), to evaluate if muscle mass or attachment size scaled differently with body size. For this, geometric scaling principles were used (Thorpe et al., 1999; Payne et al., 2006; Zumwalt, 2006; Michilsens et al., 2009), where muscle mass was divided by body mass (M_b), lengths were divided by $(M_b)^{1/3}$, and surface areas were divided by $(M_b)^{2/3}$.

First, to test if different locomotor patterns in the mice resulted in corresponding changes in muscle architecture (H1) and entheseal morphology (H2) all parameters describing the soft- and hard- tissue variables of the sample were contrasted between the activity groups using Kruskal-Wallis (for three or more independent samples) and Mann-Whitney (for two independent samples) tests. The hypotheses of increased activities (H1.1 and H2.1) as well as differences between age groups (H1.2 and H2.2.) could be tested using the same statistical tests. Wilcoxon's signed ranks test was used to test the hypothesis of bone growth differences with activity (H2.1) within histological cross-sections.

Then, to test for association between muscle architecture and variables describing enthesis size (H3), generalized linear mixed models (GLM) for multivariate variables were used, keeping in mind that not all the data were normally distributed. The muscle data were tested for relationships with their corresponding attaching bone morphology; relationships between the

spinodeltoideus muscle variables and the lateral maximum length, width, thickness, area, and angle of the deltoid crest were tested, while the relationships between the acromiodeltoideus and superficial pectoralis muscles and the medial maximum length, width, thickness, area, and angle of the deltoid crest were tested.

Due to multiple comparisons, the Dunn-Šidák correction test was used (Sokal and Rolhf, 2012) to reduce the probability of making a type 1 error. The Dunn-Šidák method is less conservative than the Bonferroni correction because it is derived by assuming that the individual tests are independent. The significant *P*-values considered are indicated below each table in Chapter 6 with the number of associated comparisons. All *P*-values are reported to highlight comparisons that were significant at the original $\alpha = 0.05$ level in addition to the adjusted alpha level, since the Dunn-Šidak method is considered to be an overly conservative test of significance.

Finally, error studies compared two observation sessions for a sub-sample of randomly selected attachment sites (n = 10 mice) and histological sections (n = 10 mice). The observations were made approximately 3 months apart. Percent error was calculated as the difference between the first and second measurements. Intra-observer error could once again not be compared due to the destruction of the soft-tissues to measure sarcomere lengths. However, all soft-tissue measurements (e.g., muscle belly, fibre length, pennation angle) were taken twice with two-week interval before any chemical digestion to assure the accuracy of the measurements. All statistical tests were performed using IBM SPSS Statistics version 20.0 for Mac.

Table 4.1 Primate specimen data used in this study.

	M1	M2	P1	P2	P3
Species	*Macaca fuscata*	*Macaca sylvanus*	*Pongo pygmaeus abelii*	*Pongo pygmaeus abelii*	*Pongo pygmaeus abelii*
Sex	Female	Female	Female	Male	Male
Age at death	Adult	Adult	41	32	49
Body mass (kg)	8.03*	11*	56.4**	140.0**	92.5**
Side used	Left	Left	Right	Right	Left
Humeral length (cm)	14.62	15.93	37.38	41.22	40.18
Forelimb length (cm)	42.1	46.4	102.9	119.8	121.1
Upper arm (cm)	15.8	19.6	39.6	49.1	42.6
Forearm (cm)	16.9	19.9	34.3	46.7	44.4
Hand (cm)	12.0	12.7	21.8	38.9	37.2

*Smith and Jungers (1997), **Toronto zookeepers

Table 4.2 Muscles, attachments, and actions of the forelimb in primates used for this research (modified from Swindler and Wood, 1973; Berringer et al., 1978; Aiello and Dean, 2002) Abbreviations used throughout this dissertation are provided. Attachments measured on the humerus are found in *italics*.

Muscles (Abbreviations)	Old World Monkey		Ape		Muscle actions
	Origin	**Insertion**	**Origin**	**Insertion**	
Latissimus dorsi (LD)	Spinous process of T6-T12, lumbar vertebrae via lumbar aponeurosis	*Floor of intertubercular groove of humerus*	Spinous process of T6-T12, lumbar and sacral vertebrae via lumbar aponeurosis, posterior iliac crest, caudal 3-4 ribs	*Floor of intertubercular groove of humerus*	Extends, adducts, medially rotates humerus, raises body toward arms during climbing
Pectoralis major/abdominalis (Pmaj/Pabd)	Pars major: Claviculomanubrial joint, lateral side of sternum Pars abdominalis: sheath of rectus abdominis lateral to the linea alba	*Pars major: Lateral lip of intertubercular groove of humerus* *Pars abdominalis: proximal ½ lateral lip of intertubercular groove of humerus via pectoral aponeurosis*	Pars thoracis: medial ½ anterior border of clavicle, lateral sternum to 7th rib Pars abdominalis: fascia over m. external oblique	*Lateral lip of intertubercular groove of humerus*	Adducts, flexes, medially rotates arm, protracts and retracts scapula, extends arm from flexed position
Deltoideus (D)	Entire anterior border of clavicle, caudal border of acromion, scapular spine	*Deltoid tuberosity of humerus*	Lateral 1/3 anterior border of clavicle, caudal border of acromion, scapular spine	*Deltoid tuberosity of humerus*	Flexes, medially rotates, abducts, extends, laterally rotates arm
Subscapularis (Sb)	Subscapular fossa of scapula	*Lesser tuberosity of humerus*	Subscapular fossa of scapula	*Lesser tuberosity of humerus*	Rotates medially humerus, provides stability to the shoulder joint during arm movement
Supraspinatus (Sp)	Supraspinous fossa of scapula	*Superior facet of greater tuberosity of humerus*	Supraspinous fossa of scapula	*Superior facet of greater tuberosity of humerus*	Abducts arm, provides stability to the shoulder joint during arm movement
Infraspinatus	Infraspinous fossa of	*Middle facet of greater*	Infraspinous fossa of	*Middle facet of greater*	Rotates laterally

(If)	scapula	*tuberosity*	scapula	*tuberosity*	humerus, provides stability to the shoulder joint during arm movement
Teres major (Tmaj)	Dorsal surface of inferior angle of scapula	*Medial lip of interubercular groove of humerus*	Dorsal surface of inferior angle of scapula	*Medial lip of interubercular groove of humerus*	Rotates medially, adducts, extends humerus
Teres minor (Tmin)	Glenoidal ½ axillary of scapula	*Lowest facet of the greater tuberosity of humerus*	Glenoidal ½ axillary of scapula	*Lowest facet of the greater tuberosity of humerus*	Rotates laterally humerus, provides stability to the shoulder joint during arm movement
Biceps brachii (BB)	Short head: coracoid process Long head: supraglenoid tuberosity of scapula	Radial tuberosity of radius	Short head: coracoid process Long head: supraglenoid tuberosity of scapula	Radial tuberosity of radius	Supinates forearm, flexes forearm when supinated, resists dislocation of shoulder, accessory flexor of arm
Coracobrachialis (Cb)	Coracoid process	*Profundus: surgical neck of humerus* *Medius: medial border of humeral shaft*	Coracoid process	*Medial border of humeral shaft*	Adducts, flexes humerus
Brachialis (B)	*Lower 2/3 anterior surface of humerus*	Coronoid process and tuberosity of ulna	*Lower 2/3 anterior surface of humerus*	Coronoid process and tuberosity of ulna	Flexes forearm
Triceps brachii (TB)	Long head: glenoidal ½ axillary border of scapula *Lateral head: upper posterior and lateral surface of humeral shaft to capsule of shoulder joint* *Medial head: entire posterior surface of humeral shaft*	Olecranon process of ulna	Long head: glenoidal ½ axillary border of scapula *Lateral head: proximal ½ posterior and lateral surface of humeral shaft* *Medial head: distal ¾ posterior surface of humeral shaft*	Olecranon process of ulna	Extends forearm, resists dislocation of humerus, adducts humerus
Dorsoepitrochlearis (De)	Tendon of latissimus dorsi	*By aponeurosis into medial and long head*	Tendon of latissimus dorsi	*By aponeurosis on medial epicondyle of*	Extends forearm

		of triceps brachii, fascial extension to medial epicondyle		*the humerus*	
Pronator teres (PT)	*Medial epicondylar ridge of the humerus*	Middle 1/3 of the lateral surface the radius	*Humeral head: medial epicondylar ridge of humerus* Ulnar head: medial side of coronoid process of ulna	Middle 1/3 of the lateral surface the radius	Pronates wrist
Flexor carpi radialis (FCR)	*Medial epicondyle of the humerus*	Bases of metacarpals 2 and 3	*Medial epicondyle of humerus, lateral border of radius*	Bases of metacarpals 2 and 3	Flexes, abducts the wrist
Palmaris longus (PL)	*Medial epicondyle of the humerus*	Palmar aponeurosis	*Medial epicondyle of the humerus*	Palmar aponeurosis	Flexes the wrist, resists shearing forces when gripping
Flexor carpi ulnaris (FCU)	*Humeral head: medial epicondyle of the humerus* Ulnar head: olecranon and dorsal border of ulna	Pisiform	*Humeral head: medial epicondyle of the humerus* Ulnar head: olecranon and dorsal border of ulna	Pisiform	Flexes, abducts the wrist
Flexor digitorum superficialis (FDS)	*Medial epicondyle of the humerus*	Volar surface of intermediate phalanges 2-5	*Humeral head: medial epicondyle of the humerus* Ulnar head: coronoid process Radial head: oblique line of radius	Volar surface of intermediate phalanges 2-5	Flexes wrist, metacarpophalangeal, and proximal interphalangeal joints of digits 2-5
Brachioradialis (Br)	*Proximal ½ lateral supracondylar ridge of humerus*	Lateral side of styloid process of the radius	*Lateral supracondylar ridge up to the deltoid tuberosity*	Lateral side of styloid process of the radius	Flexes forearm
Extensor carpi radialis longus (ECRL)	*Distal ½ lateral supracondylar ridge of humerus*	Dorsal surface of the base of metacarpal 2	*Distal ½ lateral supracondylar ridge of humerus*	Dorsal surface of the base of metacarpal 2	Extends, abducts the wrist
Extensor carpi radialis brevis	*Lateral epicondyle of the humerus*	Dorsal surface of the base of metacarpal 3	*Lateral epicondyle of the humerus*	Dorsal surface of the base of metacarpal 3	Extends, abducts the wrist

(ECRB)					
Extensor digitorum (ED)	*Lateral epicondyle of the humerus*	Sides of proximal phalanges, bases of intermediate phalanges of medial four digits	*Lateral epicondyle of the humerus*	Tendinous slips into dorsal surfaces of all three phalanges of medial four digits	Extends the wrist and medial four digits
Extensor digiti minimi (EDM)	*Lateral epicondyle of the humerus*	Ulnar side of dorsal surface of proximal phalanx 5	*Common extensor tendon*	Ulnar side of dorsal surface of proximal phalanx 5	Extends digit 5
Extensor carpi ulnaris (ECU)	*Lateral epicondyle of the humerus*	Dorsal surface of the base of metacarpal 5	*Lateral epicondyle of the humerus, posterior border of ulna*	Dorsal surface of the base of metacarpal 5	Extends, adducts the wrist
Anconeus (An)	*Postero-lateral surface of the elbow joint*	Posterior border of the ulna	*Lateral epicondyle of the humerus*	Lateral side of the olecranon and posterior border of ulna	Abducts ulna in pronation, extends elbow
Supinator (Sup)	*Lateral epicondyle of the humerus*, lateral border of the proximal ¼ of ulna	Lateral and volar surfaces of the proximal 1/3 of the radius	*Lateral epicondyle of the humerus*, lateral border of the proximal ¼ of ulna	Lateral and volar surfaces of the proximal 1/3 of the radius	Supinates the wrist

Table 4.3 Biomechanical variables measured using Moment Macro Analysis in Image J for both the primate and mouse sample (modified from Ruff and Hayes, 1983; Ruff, 2000; McFarlin, 2006; Harrington, 2009).

Cross-sectional property	Abbreviation/ Unit of measurement	Definition
Total area	TA (mm^2)	Area within subperiosteal surface (influences second moments of area)
Cortical area	CA (mm^2)	Axial strength (tensile and compressive)
Medullary area	MA (mm^2)	Area within medullary cavity (TA-MA)
Second moment of area about x-axis	Ix (mm^4)	Bending rigidity in A-P plane
Second moment of area about y-axis	Iy (mm^4)	Bending rigidity in M-L plane
Maximum second moment of area	Imax (mm^4)	Maximum bending rigidity
Minimum second moment of area	Imin (mm^4)	Minimum bending rigidity
Index of circularity	Imax/Imin	Bending rigidity
Polar second moment of area	*J* (mm^4)	Torsional strength and (twice) average bending rigidity (Ix + Iy)
Theta Angle between Ix and Imax	θ (degrees)	Orientation of plane of maximum bending strength
Section modulus about the x-axis	Zx (mm^3)	A-P bending strength
Section modulus about the y-axis	Zy (mm^3)	M-L bending strength
Polar section modulus	Zp (mm^3)	Torsional and (twice) average bending strength (*J*/mean of d_x and d_y)
Index of circularity (section modulus)	Zy/Zx	Summary estimate of average bending strength

Table 4.4 Results of Shapiro-Wilk test for normality in the primate sample for muscle fibre architecture measurements. If $P > 0.05$, the variable is normally distributed.

Muscle	M (g)	L_b (mm)	L_f (mm)	TL (mm)	MTU (mm)	PCSA (cm^2)
LD	**0.841**	**0.646**	**0.313**	**0.635**	**0.485**	**0.061**
D	**0.498**	**0.979**	**0.508**	0.033	**0.898**	**0.276**
Pmaj	-	-	-	-	-	-
Sb	**0.202**	**0.101**	**0.193**	**0.577**	**0.591**	**0.264**
Sp	**0.373**	**0.756**	**0.119**	0.05	**0.414**	**0.559**
If	**0.489**	**0.966**	**0.848**	**0.27**	**0.517**	**0.553**
Tmin	**0.988**	**0.268**	**0.184**	**0.947**	**0.445**	**0.986**
Tmaj	**0.564**	**0.68**	0.032	**0.254**	**0.815**	**0.634**
Cb	**0.383**	0.025	**0.152**	**0.124**	**0.2**	**0.198**
BB	**0.568**	**0.184**	**0.89**	0.025	0.049	0.045
TB	**0.552**	0.032	**0.727**	**0.072**	**0.193**	0.014
An	**0.315**	**0.113**	**0.174**	**0.271**	0.05	0.001
B	**0.321**	**0.477**	**0.898**	**0.666**	**0.209**	0.05
De	**0.997**	**0.448**	0.004	**0.867**	**0.354**	0.001
Br	**0.275**	**0.368**	**0.869**	**0.077**	0.05	0.011
Sup	**0.207**	**0.329**	0.45	**0.547**	**0.162**	0.022
PT	**0.218**	**0.206**	0.02	**0.386**	**0.164**	0.015
PL	**0.404**	**0.904**	**0.176**	**0.075**	0.035	0.012
FCR	**0.194**	0.05	**0.065**	0.03	0.01	0.011
FCU	**0.544**	**0.297**	**0.128**	**0.703**	**0.159**	0.017
FDS	**0.088**	**0.114**	0.026	0.04	0.015	0.028
ECRL	**0.567**	**0.366**	0.042	**0.402**	**0.126**	0.007
ECRB	**0.192**	**0.727**	**0.085**	**0.276**	0.033	0.016
ECU	**0.216**	**0.612**	**0.08**	**0.187**	**0.106**	0.01
ED	**0.251**	**0.412**	0.015	**0.282**	0.042	0.021
EDM	**0.214**	**0.686**	0.017	**0.502**	**0.092**	0.008

$P \leq 0.05$ = non-normal variable; **Bold** = normal variable

Table 4.5 Results of Shapiro-Wilk test for normality in the primate sample for body mass adjusted muscle fibre architecture measurements. If $P > 0.05$, the variable is normally distributed.

Muscle	M	L_b	L_f	TL/MTU	θ	PCSA	M/P_o	*I*	h
LD	**0.496**	**0.204**	**0.067**	**1.0**	**0.131**	**0.363**	**0.321**	**1.0**	0.00
D	**0.273**	**0.437**	**0.06**	**0.241**	**0.659**	**0.282**	**0.704**	**0.118**	**0.13**
Pmaj	-	-	-	-	-	-	-	-	-
Sb	0.033	**0.349**	**0.214**	**0.585**	**0.282**	**0.162**	**0.228**	0.021	**0.754**
Sp	**0.13**	**0.092**	**0.827**	**0.478**	0.002	0.146	**0.111**	**0.814**	**0.46**
If	0.046	**0.111**	**0.837**	**0.937**	**0.328**	**0.901**	**0.829**	**0.658**	**0.927**
Tmin	**0.097**	**0.342**	0.04	**0.794**	0.001	0.002	**0.177**	0.001	**0.437**
Tmaj	**0.216**	**0.424**	**0.912**	**0.603**	0.041	**0.262**	0.025	**0.787**	**0.502**
Cb	**0.183**	0.001	0.043	0.048	**0.099**	**0.402**	**0.155**	**0.147**	**0.68**
BB	**0.551**	**0.979**	**0.773**	**0.404**	0.05	**0.984**	**0.909**	**0.314**	0.003
TB	**0.091**	**0.417**	**0.857**	**0.23**	**0.454**	**0.519**	**0.685**	**0.928**	**0.082**
An	**0.65**	**0.881**	**0.977**	**0.952**	**0.33**	0.001	**0.115**	**0.195**	**0.195**
B	**0.272**	**0.428**	**0.72**	0.05	**0.173**	**0.657**	**0.903**	**0.543**	**0.332**
De	**0.416**	**0.918**	**0.988**	**0.467**	**0.124**	0.001	0.005	**0.683**	**0.241**
Br	**0.406**	**0.926**	**0.092**	**0.635**	**0.528**	**0.566**	**0.877**	**0.872**	**0.272**
Sup	**0.336**	**0.12**	**0.472**	**0.656**	**0.263**	**0.186**	**0.468**	**0.332**	0.05
PT	**0487**	**0.485**	**0.219**	**0.751**	0.013	**0.332**	0.027	**0.656**	**0.852**
PL	**0.939**	**0.102**	**0.801**	**0.382**	**0.839**	**0.492**	**0.201**	**0.222**	0.046
FCR	**0.35**	**0.417**	**1.0**	**0.325**	**0.338**	**0.754**	**0.067**	**0.146**	**0.272**
FCU	**0.576**	**0.441**	**0.53**	**0.636**	0.007	**0.94**	**0.14**	**0.747**	**0.858**
FDS	**0.214**	**0.311**	**0.515**	**0.076**	**0.097**	**0.251**	0.027	**0.685**	**0.325**
ECRL	**0.13**	**0.26**	**0.621**	**0.377**	**0.529**	**0.325**	0.042	**0.325**	**0.314**
ECRB	**0.116**	**0.243**	**0.182**	0.025	0.571	**0.272**	**0.1**	**0.967**	**0.177**
ECU	**0.352**	**0.073**	0.004	**0.745**	0.042	**0.98**	0.045	**0.685**	**0.171**
ED	**0.199**	**0.638**	**0.429**	0.001	**0.743**	0.048	0.016	**0.814**	**0.814**
EDM	**0.468**	**0.354**	**0.761**	**0.082**	0.029	0.046	0.018	0.006	**0.777**

$P \leq 0.05$ = non-normal variable; **Bold** = normal variable

Table 4.6 Results of Shapiro-Wilk test for normality in the primate sample for the muscle attachment sites measurements, including the distal position of attachment sites (length from the proximal end [insertions] or distal end [origins] of the humerus). If *P* > 0.05, the variable is normally distributed.

Muscle	Length	Width	Area	Distal position
LD	**0.497**	**0.497**	**0.149**	**0.498**
Pmaj	**0.546**	**0.113**	**0.698**	**0.395**
D	**0.7**	**0.519**	**0.367**	**0.655**
Sb	**0.171**	**0.971**	**0.117**	**0.108**
Sp	**0.113**	**0.3**	**0.181**	**0.094**
If	**0.397**	**0.322**	**0.497**	**0.916**
Tmaj	**0.458**	**0.323**	**0.114**	**0.744**
Tmin	**0.634**	**0.539**	**0.585**	**0.751**
Cbmed	**0.174**	**0.488**	**0.259**	**0.236**
Cbmin	**-**	**-**	**-**	-
B	**0.194**	**0.304**	0.039	**0.266**
TB(lat)	**0.287**	0.041	**0.239**	**0.788**
TB(med)	**0.108**	**0.355**	**0.457**	**0.461**
PT	**0.862**	**0.256**	0.044	**0.92**
CFO	**0.396**	**0.205**	**0.415**	**0.358**
Br	**0.322**	**0.251**	**0.075**	**0.326**
ECRL	**0.294**	**0.459**	**0.143**	**0.676**
CEO	**0.542**	**0.724**	**0.76**	**0.177**
An	**0.677**	**0.437**	**0.964**	**0.425**

$P \leq 0.05$ = non-normal variable; **Bold** = normal variable
CFO = Common flexor origin; CEO = Common extensor origin

Table 4.7 Results of Shapiro-Wilk test for normality in the primate sample for the body mass adjusted muscle attachment sites measurements. If *P* > 0.05, the variable is normally distributed.

Muscle	Length*	Width*	Area*	Length°	Width°	Area°
LD	**0.301**	**0.701**	**0.261**	**0.463**	0.00	**1.0**
Pmaj	**0.973**	**0.851**	**0.904**	**0.493**	**0.673**	**0.48**
D	**0.971**	**0.335**	**0.741**	**0.609**	0.049	**0.968**
Sb	**0.13**	**0.315**	**0.656**	**-**	**-**	**-**
Sp	0.018	**0.167**	**0.339**	**-**	**-**	**-**
If	**0.705**	**0.85**	**0.942**	**-**	**-**	**-**
Tmaj	**0.959**	**0.391**	0.023	**0.904**	**0.157**	**0.646**
Tmin	**0.282**	**0.519**	**0.707**	**-**	**-**	**-**
Cb	**0.397**	**0.164**	**0.626**	**0.143**	**0.129**	**0.307**
B	**0.686**	**0.456**	**0.485**	0.05	**0.454**	**0.09**
TB(lat)	**0.503**	**0.951**	**0.399**	**0.713**	**0.872**	**0.973**
TB(med)	**0.529**	**0.069**	**0.182**	**0.358**	**0.644**	**0.513**
PT	**0.478**	**0.124**	**0.077**	**-**	**-**	**-**
CFO	**0.103**	**0.993**	**0.708**	**-**	**-**	**-**
Br	**0.383**	0.035	**0.158**	**-**	**-**	**-**
ECRL	**0.412**	**0.425**	**0.374**	**-**	**-**	**-**
CEO	0.005	**0.412**	0.00	**-**	**-**	**-**
An	**0.092**	**0.522**	**0.131**	**-**	**-**	**-**

$P \leq 0.05$ = non-normal variable; **Bold =** normal variable
* Body mass adjusted variables; ° CA adjusted variables
CFO = Common flexor origin; CEO = Common extensor origin

Table 4.8 Functional categories of the primate muscles. For the shoulder joint: flexion/extension takes place in the sagittal plane, abduction/adduction in the frontal plane, and endorotation/exorotation in the transverse plane. For the elbow and wrist joints, movements follow classical convention; flexion/extension, and pronation/supination (modified from Thorpe et al., 1999, Michilsens et al., 2009).

Movement	Muscles
Shoulder flexion	D + BB + Cb + Pmaj
Shoulder extension	TB + Tmaj + LD +D
Shoulder abduction	D + Sp
Shoulder adduction	Cb + Tmaj +LD + Pmaj + TB
Shoulder endorotation	Sb + D + Tmaj + LD + Pmaj
Shoulder exorotation	If + Tmin + D
Elbow flexion	BB + B + Br +PT + FCR + PL + FDS + FCU
Elbow extension	TB + An + De
Elbow supination	BB + Sup + Br
Elbow pronation	PT + Br
Palmar flexion	FDS + FCU + FCR + PL
Dorsal flexion	ED + ECRL + ECRB + ECU + EDM + EDA
Ulnar deviation	ECU + FCU + EDM
Radial deviation	ECRL + ECRB + FCR

Table 4.9 Mouse specimen data used for this study; body mass (g) at death of the animals and maximum humeral length (mm) shown.

Specimen number	Activity group	Mass at death (g)	Humeral length (mm)
JV122	Control	32.034	12.926
JV126	Control	32.837	12.241
JV128	Control	36.269	12.742
JV142	Control	33.327	12.703
JV146	Control	35.638	12.724
AD213	Control	31.495	12.272
AD217	Control	31.271	12.054
AD231	Control	38.372	12.473
AD233	Control	34.362	12.282
AD235	Control	33.696	12.348
JV324	Activity-running	29.132	12.639
JV326	Activity-running	26.340	12.606
JV328	Activity-running	31.609	12.071
JV342	Activity-running	32.324	12.420
JV346	Activity-running	28.841	12.175
AD311	Activity-running	30.043	12.402
AD313	Activity-running	29.872	12.511
AD317	Activity-running	28.183	12.060
AD319	Activity-running	31.132	12.238
AD335	Activity-running	31.383	12.500
JV640	Activity-climbing	25.197	12.302
JV642	Activity-climbing	29.441	12.915
JV644	Activity-climbing	29.496	12.117
JV646	Activity-climbing	30.410	12.074
JV648	Activity-climbing	38.555	12.160
AD509	Activity-climbing	31.642	12.028
AD511	Activity-climbing	30.020	12.614
AD513	Activity-climbing	31.901	12.588
AD517	Activity-climbing	35.658	12.070
AD533	Activity-climbing	37.030	12.535

All specimens are female outbred wild-type mice. All humeral lengths are taken from the left side.
JV = juvenile group (age at start of experiment = 25 days; age at end of experiment = 108 days). AD = adult group (age at start of experiment = 46 days; age at end of experiment = 129 days). The running mice ran approximately 1900 m per night, and the climbing mice climbed approximately140 m per night.

Table 4.10 Results of Shapiro-Wilk test for normality in the mouse sample for body mass, acromiodeltoideus, spinodeltoideus, and superficial pectoralis muscle fibre architecture measurements. If $P > 0.05$, the variable is normally distributed.

Variable	Significance *P*
Body mass (g)	**0.567**
Acromiodeltoideus	
M (μg)	0.002
L_b (mm)	**0.593**
L_f (mm)	**0.522**
θ (°)	**0.308**
PCSA (mm^2)	**0.143**
M/P_o	**0.258**
I	**0.157**
Spinodeltoideus	
M (μg)	0.002
L_b (mm)	**0.281**
L_f (mm)	**0.099**
θ (°)	0.024
PCSA (mm^2)	0.002
M/P_o	**0.082**
I	0.038
Superficial pectoralis	
M (μg)	**0.118**
L_b (mm)	0.035
L_f (mm)	0.047
θ (°)	**0.1**
PCSA (mm^2)	0.05
M/P_o	0.042
I	**0.907**

$P \leq 0.05$ = non-normal variable; **Bold** = normal variable

Table 4.11 Results of Shapiro-Wilk test for normality in the mouse sample for body mass adjusted acromiodeltoideus, spinodeltoideus, and superficial pectoralis muscle fibre architecture measurements. Resulting numbers are dimensionless. If *P* > 0.05, the variable is normally distributed.

Variable	Significance *P*
Acromiodeltoideus	
M	0.019
L_b	**0.835**
L_f	**0.255**
PCSA	0.01
M/P_o	0.009
I	0.007
Spinodeltoideus	
M	**0.522**
L_b	**0.281**
L_f	0.017
PCSA	0.003
M/P_o	0.01
I	0.02
Superficial pectoralis	
M	**0.617**
L_b	**0.897**
L_f	**0.803**
PCSA	**0.091**
M/P_o	**0.815**
I	**0.133**

$P \leq 0.05$ = non-normal variable; **Bold** = normal variable

Table 4.12 Results of Shapiro-Wilk test for normality in the mouse sample for deltoid crest and humeral length measurements. If *P* > 0.05, the variable is normally distributed.

Variable	Significance *P*
Humerus length (mm)	**0.916**
Lateral	
Max length (mm)	**0.436**
Max width (mm)	0.005
Area (mm^2)	**0.403**
Medial	
Max length (mm)	**0.269**
Max width (mm)	**0.394**
Area (mm^2)	**0.795**
Thickness (mm)	**0.158**
Angle (º)	0.001

$P \leq 0.05$ = non-normal variable; **Bold** = normal variable

Table 4.13 Results of Shapiro-Wilk test for normality in the mouse sample for body mass adjusted deltoid crest and humeral length measurements. Resulting numbers are dimensionless. If *P* > 0.05, the variable is normally distributed.

Variable	Significance *P*
Humerus length (mm)	**0.43**
Lateral	
Max length (mm)	**0.42**
Max width (mm)	**0.14**
Area (mm^2)	**0.233**
Medial	
Max length (mm)	**0.435**
Max width (mm)	**0.272**
Area (mm^2)	0.046
Thickness (mm)	**0.195**

$P \leq 0.05$ = non-normal variable; **Bold** = normal variable

Table 4.14 Results of Shapiro-Wilk test for normality in the mouse sample for the biomechanical shape (bone strength) of the histological cut made at the 25% of maximum humeral length. If *P* > 0.05, the variable is normally distributed.

Variable	Significance *P*
TA (mm^2)	0.047
CA (mm^2)	**0.856**
MA (mm^2)	**0.719**
Ix (mm^4)	**0.488**
Iy (mm^4)	**0.601**
Imax (mm^4)	**0.39**
Imin (mm^4)	**0.301**
Imax/Imin	**0.246**
J (mm^4)	**0.875**
Theta (°)	**0.26**
Zx (mm^3)	**0.421**
Zy (mm^3)	**0.353**
Zp (mm^3)	**0.672**
Zy/Zx	**0.255**

$P \leq 0.05$ = non-normal variable; **Bold =** normal variable

Table 4.15 Results of Shapiro-Wilk test for normality in the mouse sample for the biomechanical shape (bone strength) of the histological cut made at the distal margin of the deltoid crest. If *P* > 0.05, the variable is normally distributed.

Variable	Significance *P*
TA (mm^2)	**0.227**
CA (mm^2)	**0.6**
MA (mm^2)	**0.874**
Ix (mm^4)	**0.166**
Iy (mm^4)	**0.551**
Imax (mm^4)	**0.112**
Imin (mm^4)	**0.471**
Imax/Imin	0.03
J (mm^4)	**0.132**
Theta (°)	**0.836**
Zx (mm^3)	**0.218**
Zy (mm^3)	**0.934**
Zp (mm^3)	**0.15**
Zy/Zx	0.035

$P \leq 0.05$ = non-normal variable; **Bold =** normal variable

Table 4.16 Results of Shapiro-Wilk test for normality in the mouse sample for rates of osteogenesis at each quadrant, the deltoid crest, and averaged across all quadrants within cross-sections (μm/day). If *P* > 0.05, the variable is normally distributed.

Variable	Significance *P*
Mean 25%-section	**0.197**
Mean crest-section	0.019
Total mean growth	**0.223**
Crest	**0.731**
Superior	**0.532**
Lateral	**0.320**
Inferior	**0.358**
Medial	**0.176**

$P \leq 0.05$ = non-normal variable; **Bold =** normal variable

Figure 4.1 Steps to define boundaries of each attachment site in the primate sample. Example from the right teres major muscle insertion from P2 (male orangutan). Careful attention of the muscle-bone interface was given to each origin and insertion before and after the removal of the muscles to visually document attachment contours and reduce error. Osteological measurements could be taken using previous dissecting notes, measurements, and photographs as a guide to determine the location and defining contours of the enthesis.

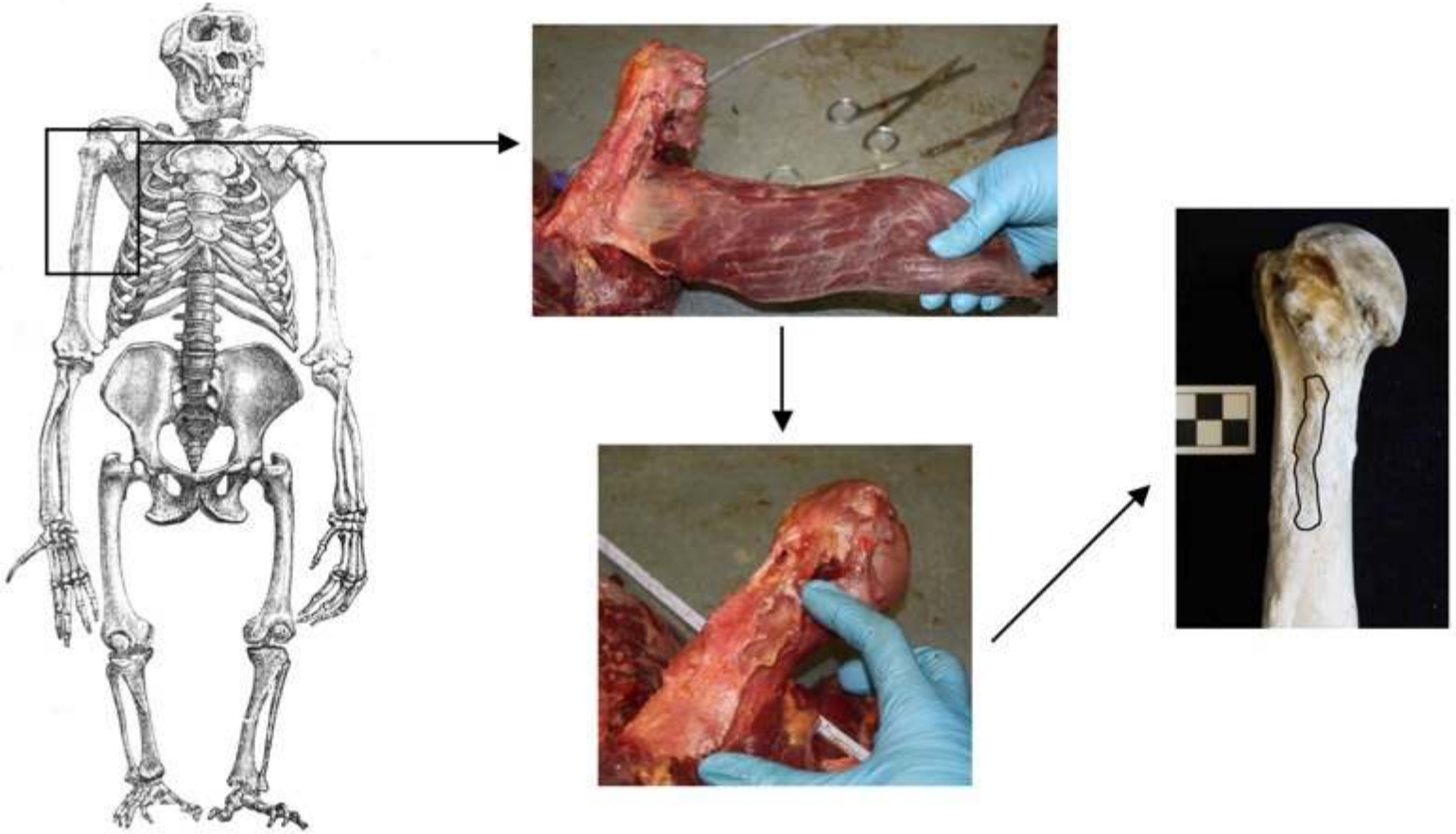

Figure 4.2 Architectural measurements from muscles. After removal, length of the muscle belly (L_b) (example from P2's infraspinatus muscle). Muscle was then sectioned longitudinally along the line of action. Overall six neighbouring fasciculi were examined. For each cut, 1) fibre length (L_f) was measured from the central tendon (dark star) to distal tendon (light star) of insertion, 2) the perpendicular distance (a) from the central to distal tendon used to calculate angle of pennation, 3) proximal tendon length (T_p) from the proximal bone attachment to proximal myotendinous junction, 4) distal tendon length (T_d) from the distal bone attachment to the distal myotendinous junction, used to calculate total tendon length (TL) (modified from Anapol and Barry, 1996).

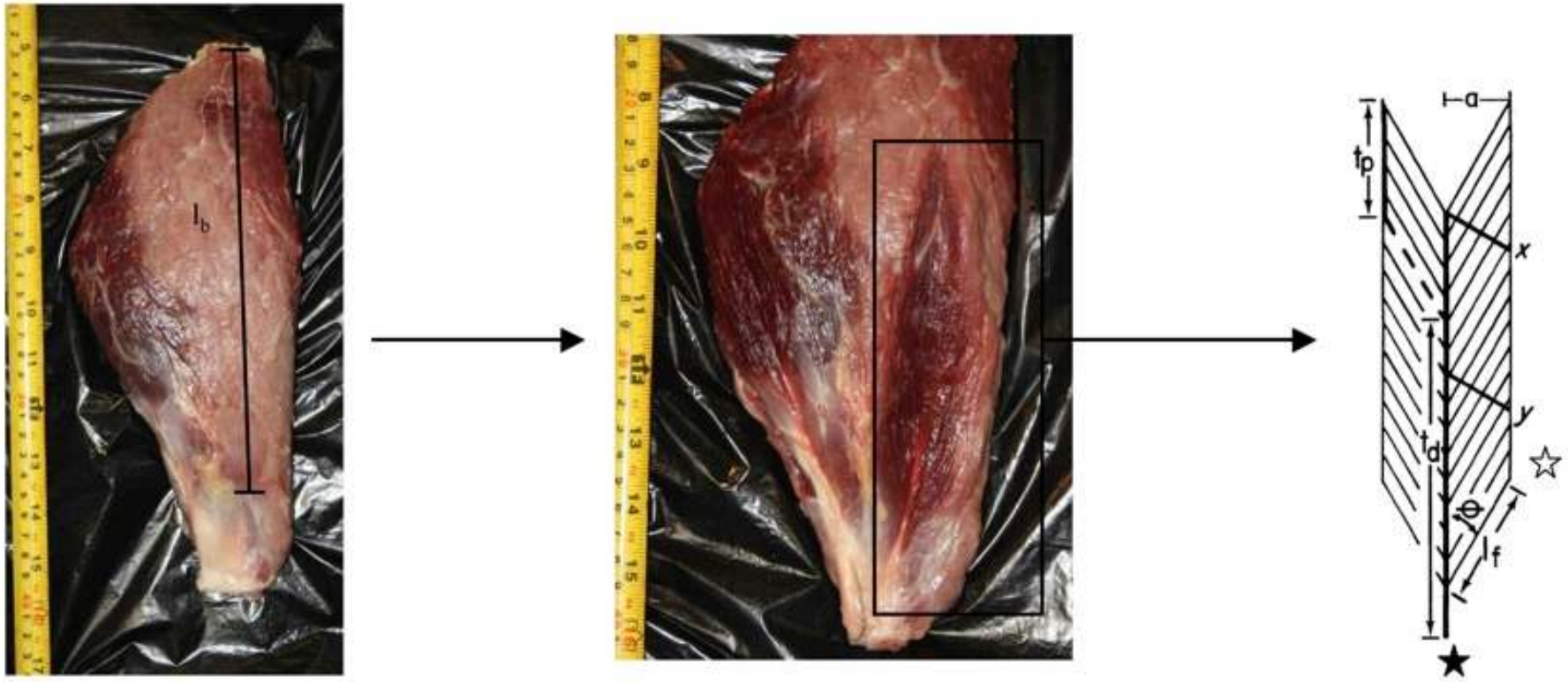

Figure 4.3 Measurements taken from the surfaces of the primate bones. A) Before removal of the muscle, the proximal (M_{prox}) and distal (M_{dist}) margins of the attaching muscle were measured (Stern, 1971). From these, the linear distance of attachment ($M_{spread} = M_{dist} - M_{prox}$) and the midpoint ($M_{mid} = M_{dist +} M_{prox} / 2$) were calculated. After skeletonization, the length of the humerus (L) was measured as the greatest distance between the top of the humeral head and the most distant point on the distal humerus parallel with the long axis of the bone. B) Maximum length and width (black arrows), and surface area (red contour) were measured for each muscle attachment sites on the humerus (example from P1's infraspinatus muscle insertion site).

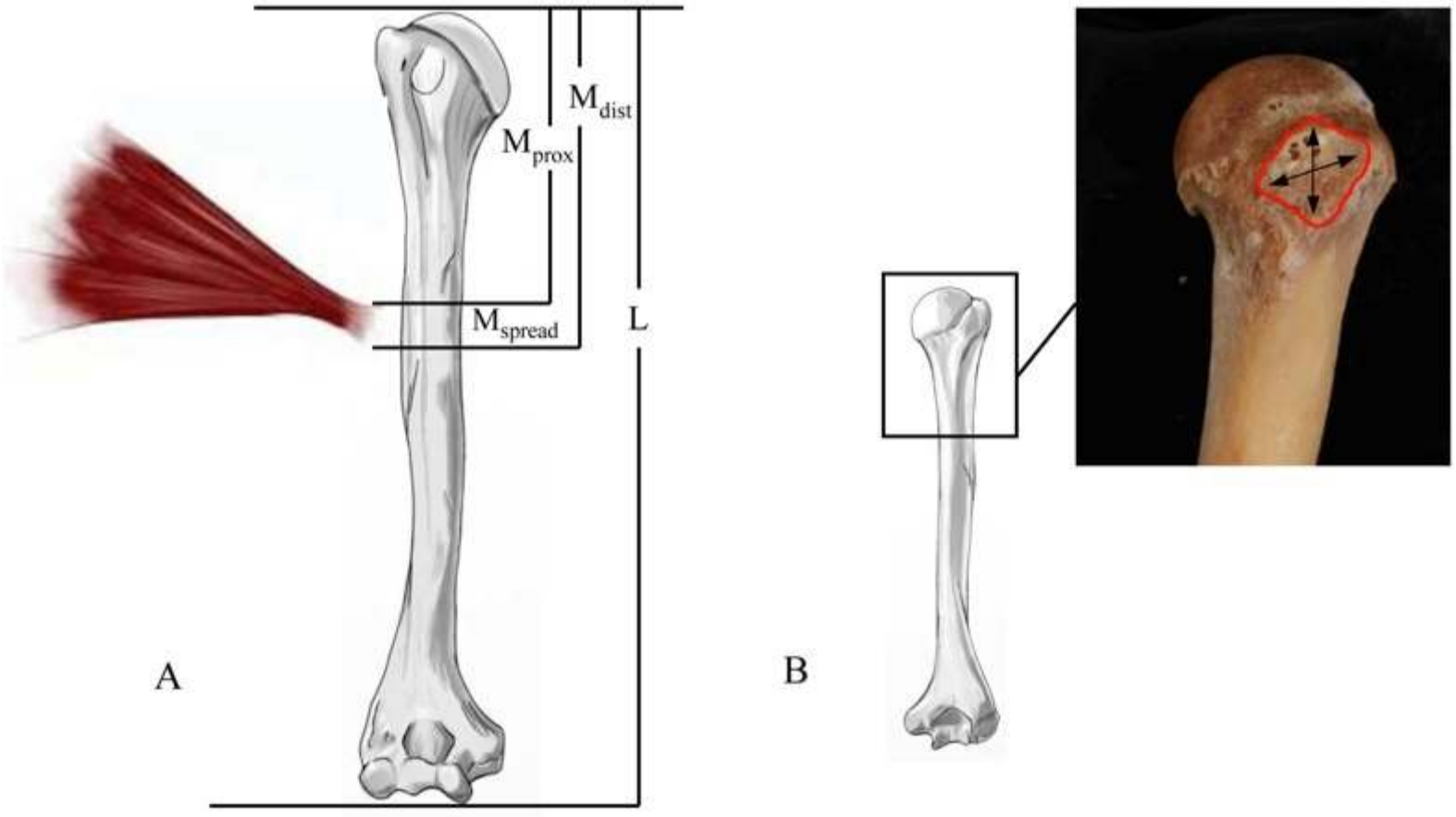

Figure 4.4 Example of image used for the calculations of diaphyseal geometric properties using Moment Macro Analysis in Image J for both the primate and mouse sample. Example shows a cross-section from the left humerus of a female wild-type mouse.

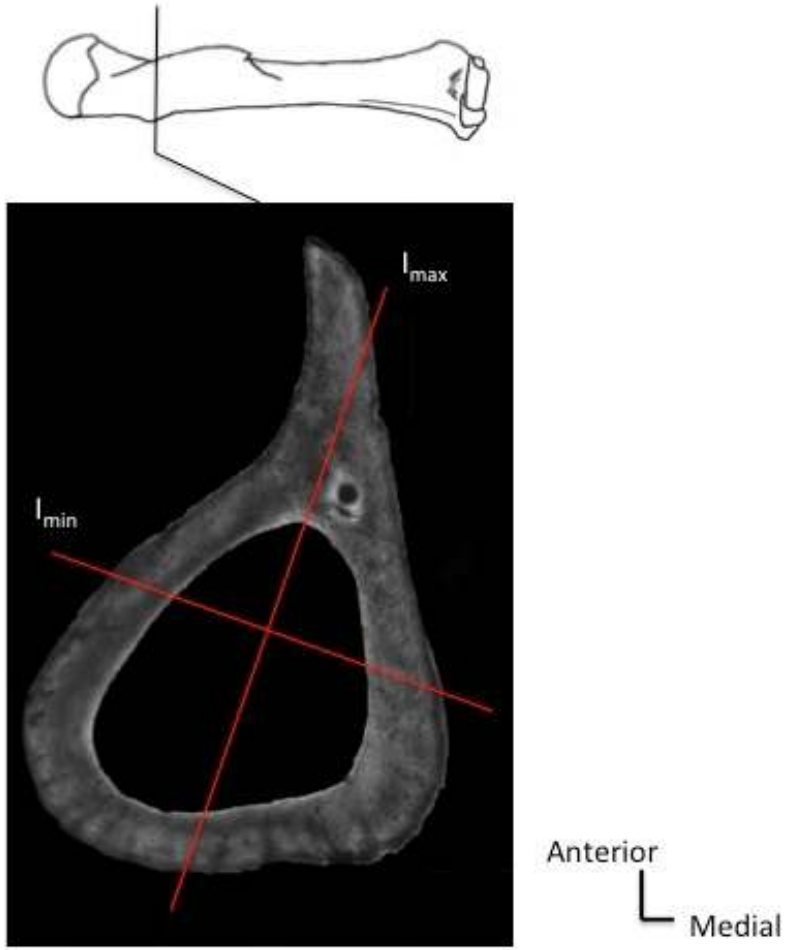

Figure 4.5 Mice experimental cages set up. The running mice ran approximately 1 900 m per night, and the climbing mice climbed (1 m meshed cage) approximately 140 m per night.

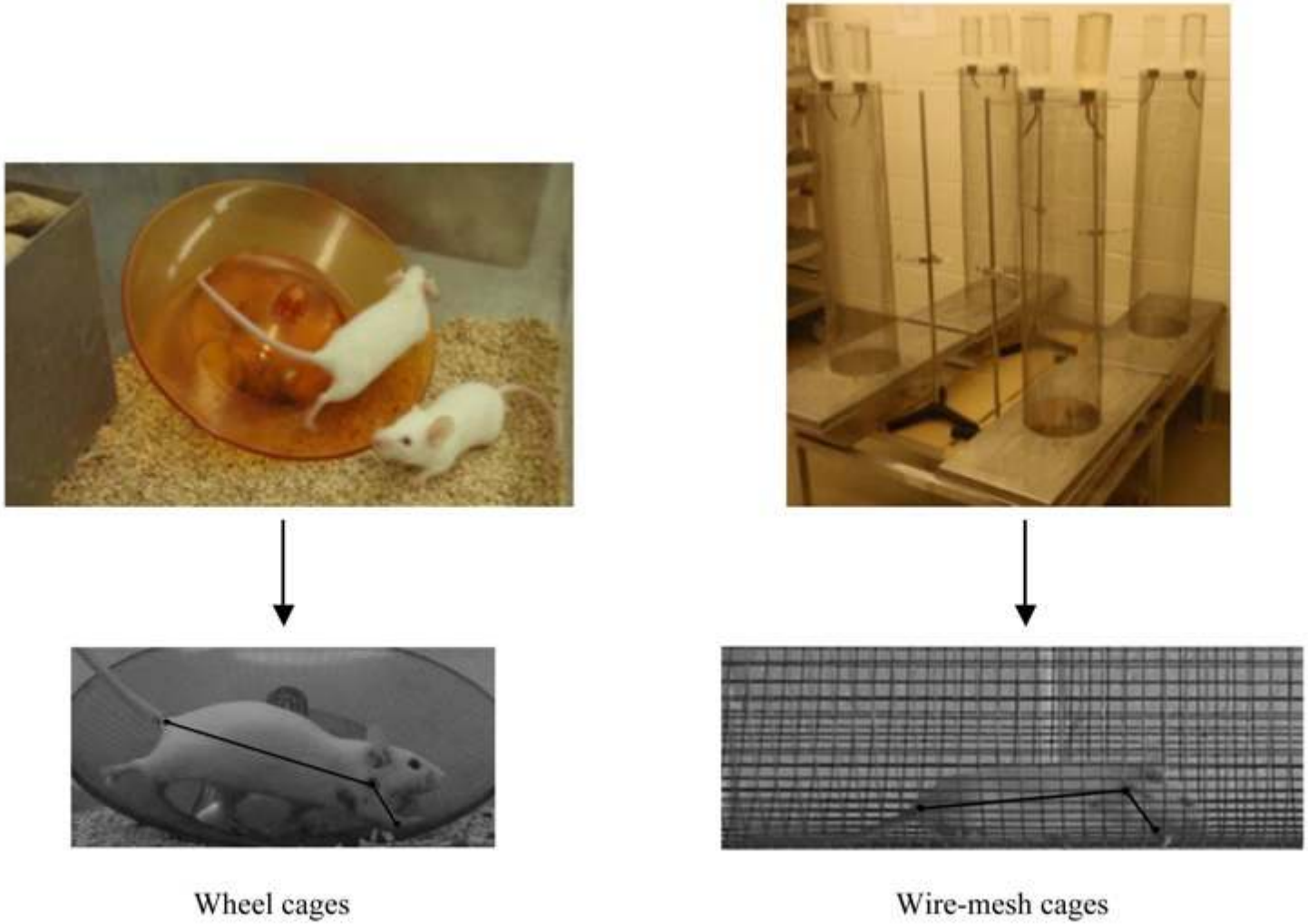

Figure 4.6 Schematic representations of the spinodeltoideus, acromiodeltoideus, and the superficial pectoralis muscles measured in the sample along with their attachment location on the deltoid crest of the humerus.

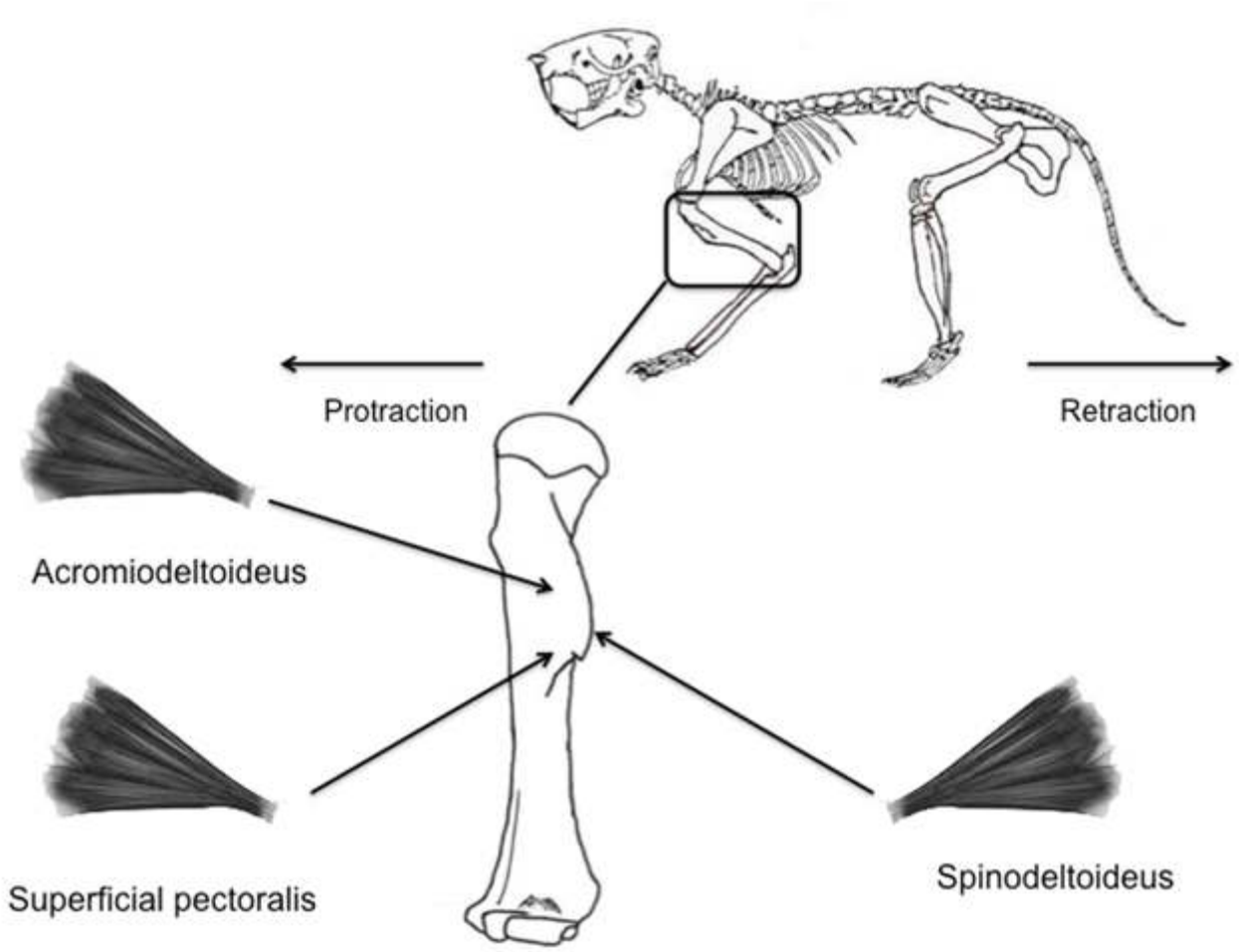

Figure 4.7 Bony measurements taken: A) maximum length of the humerus (L) was measured as the greatest distance between the top of the humeral head and the most distant point on the distal humerus parallel with the long axis of the bone; maximum length, width (white arrows), and area (black contours) of the deltoid crest, on the lateral (B) and medial side (C) of the crest; D) angle of the crest (θ) was measured at the distal edge of the prominent ridge; E) thickness of the crest measured in the distal margin of the crest cross-section.

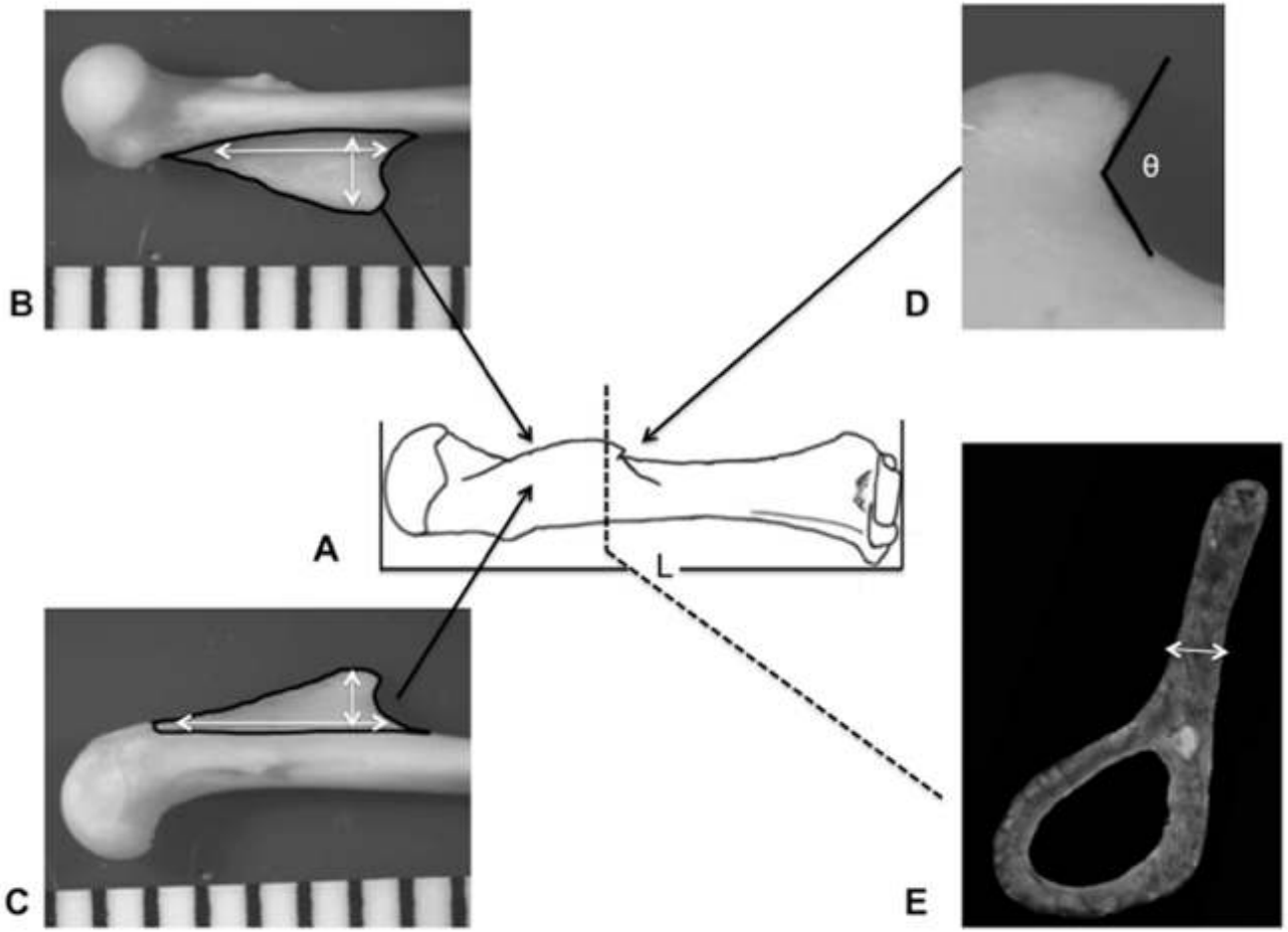

Figure 4.8 Two 100 μm thick cross-sections at the deltoid crest were prepared for histological analysis. The first was at the most distal edge of the deltoid crest to capture the insertion of the three muscles attaching. The second section was made to have a standardized cut in the mouse sample at the 25% of the maximum length of the humerus (taken from the proximal epiphysis).

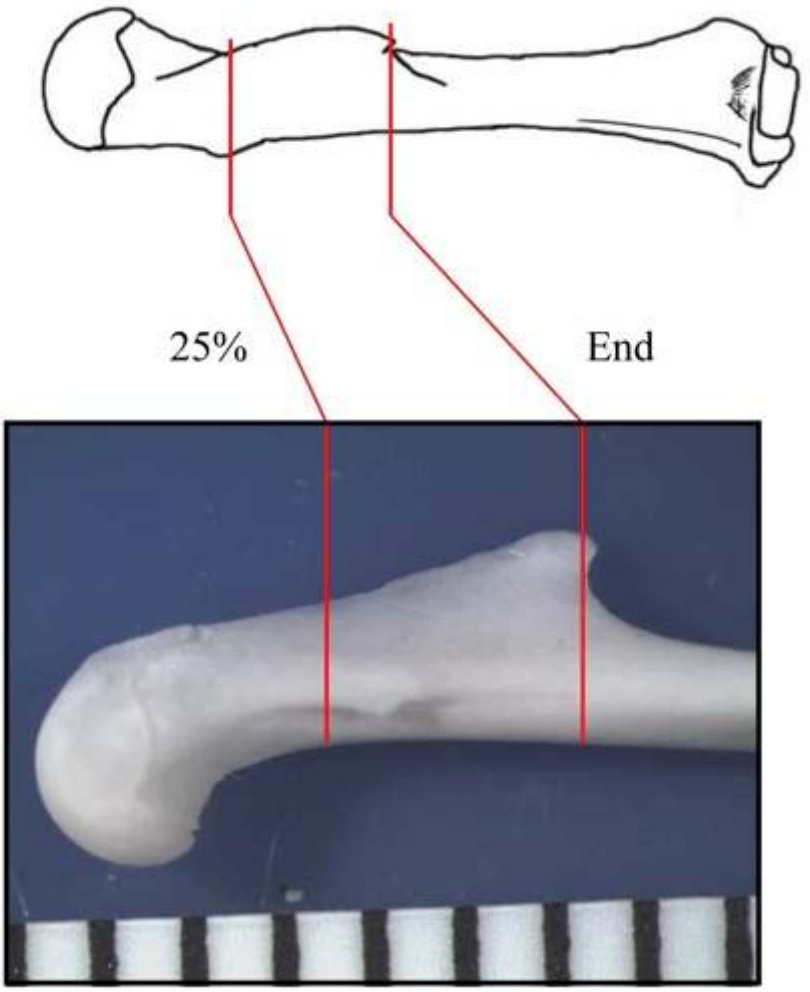

Figure 4.9 Representation of the superimposed microscopy images showing the fluorescent labeling used for bone growth rate calculations. The cross-section on the left is of the distal end of the deltoid crest (climbing mouse). The image on the right represents the measurements taken on the cranial quadrant of the cross section (white arrows). Measurements of distances between all pairs of consecutive labels were taken. Individual measurements were then averaged to derive a mean daily growth rate calculated for each individual. Black arrow (right) indicates the direction of periosteal bone growth.

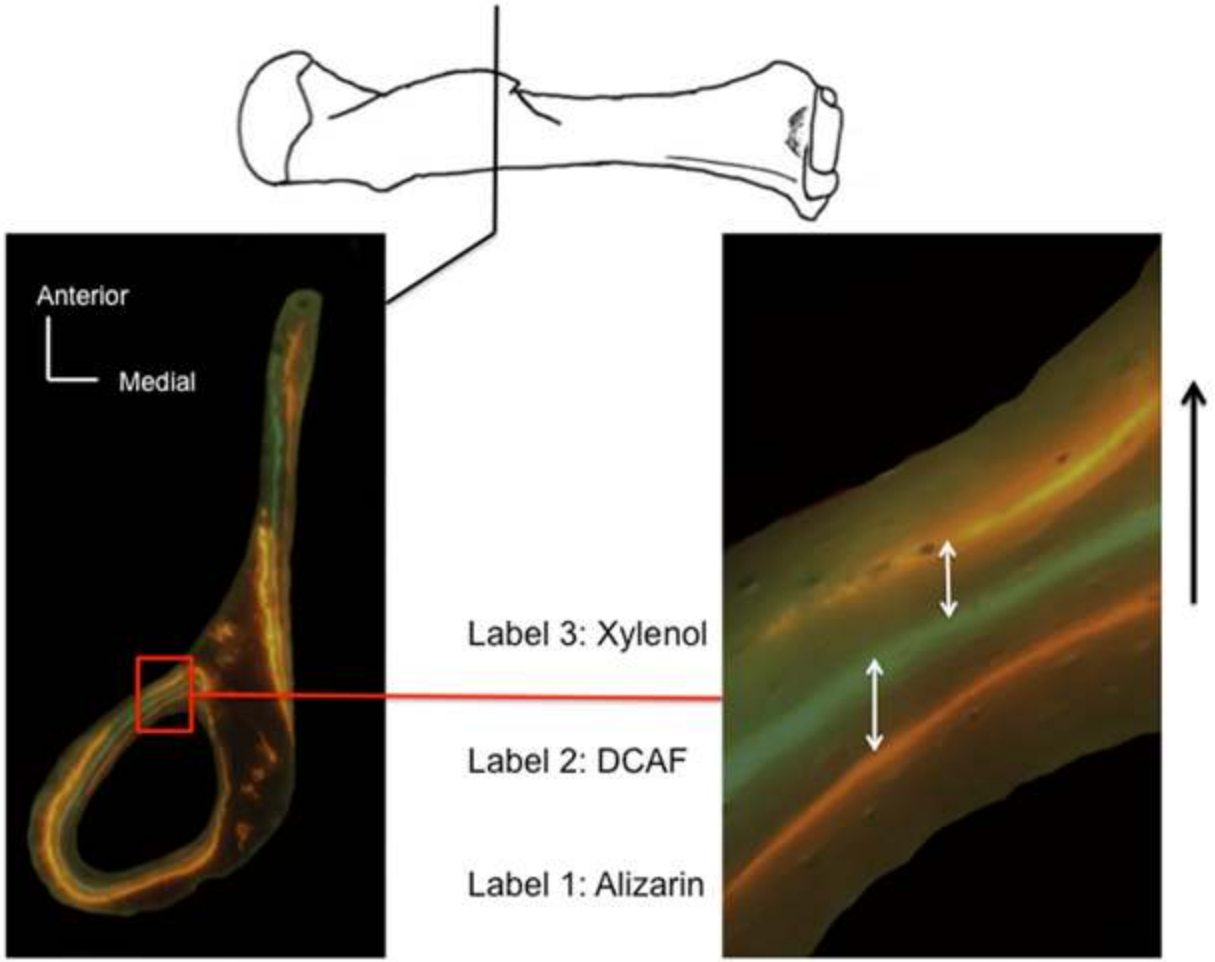

Figure 4.10 Example showing the presence of osteons observed in the mouse sample. The lower left corner shows a cross-section of the distal margin of the deltoid crest from an adult female climbing mouse. On the right, are images of an osteon in the same field of view under 40X magnification in brightfield (light microscopy), circularly polarized light (without filter), and fluorescence illumination (CPL with filter).

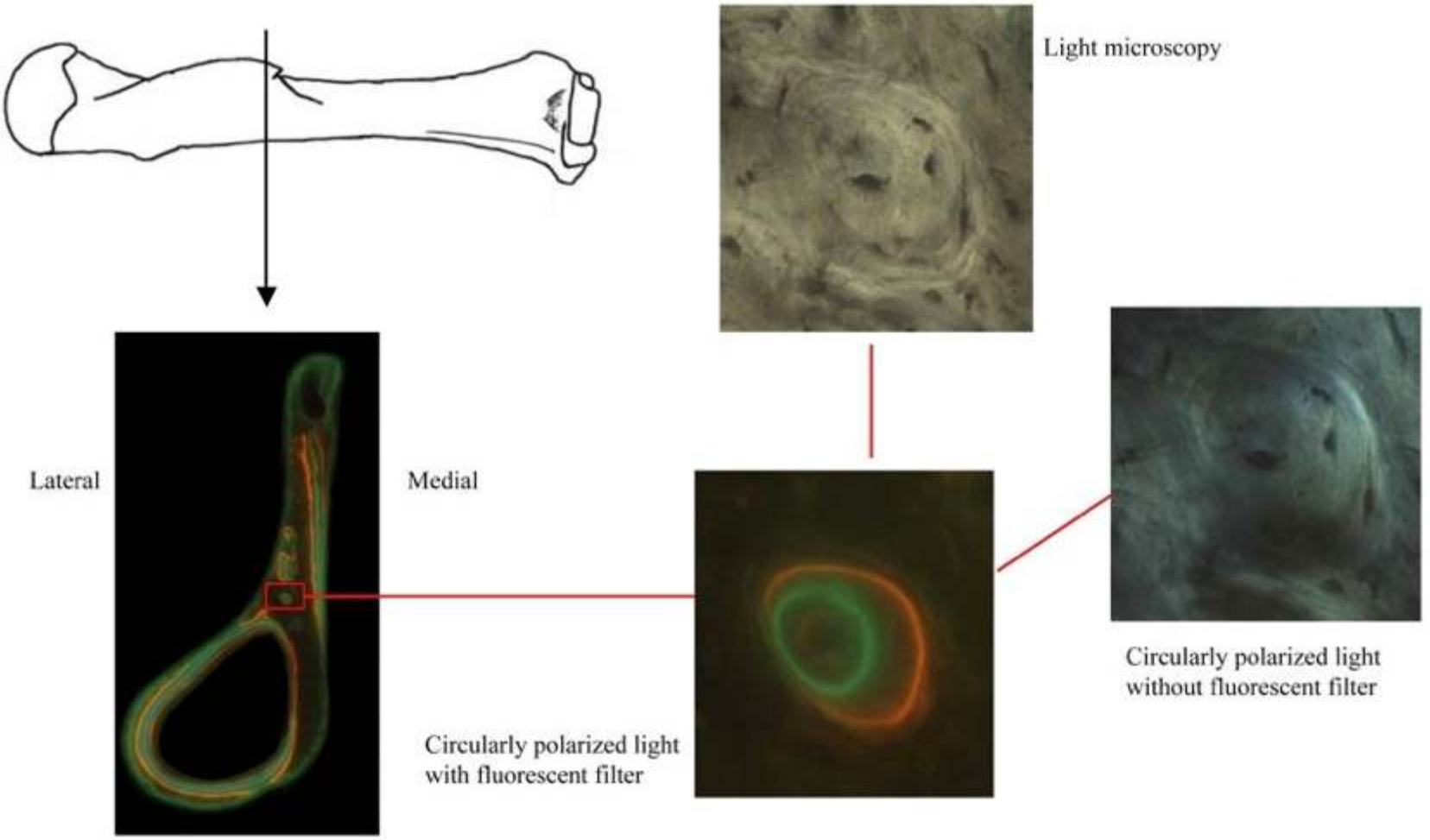

Figure 4.11 Example showing the presence of drifting osteons (Robling and Stout, 1999) observed in the mouse sample. The lower left corner shows a cross-section of the distal margin of the deltoid crest from an adult female climbing mouse. On the right, are images of an osteon in the same field of view under 40X magnification in brightfield (light microscopy), circularly polarized light (without filter), and fluorescence illumination (CPL with filter).

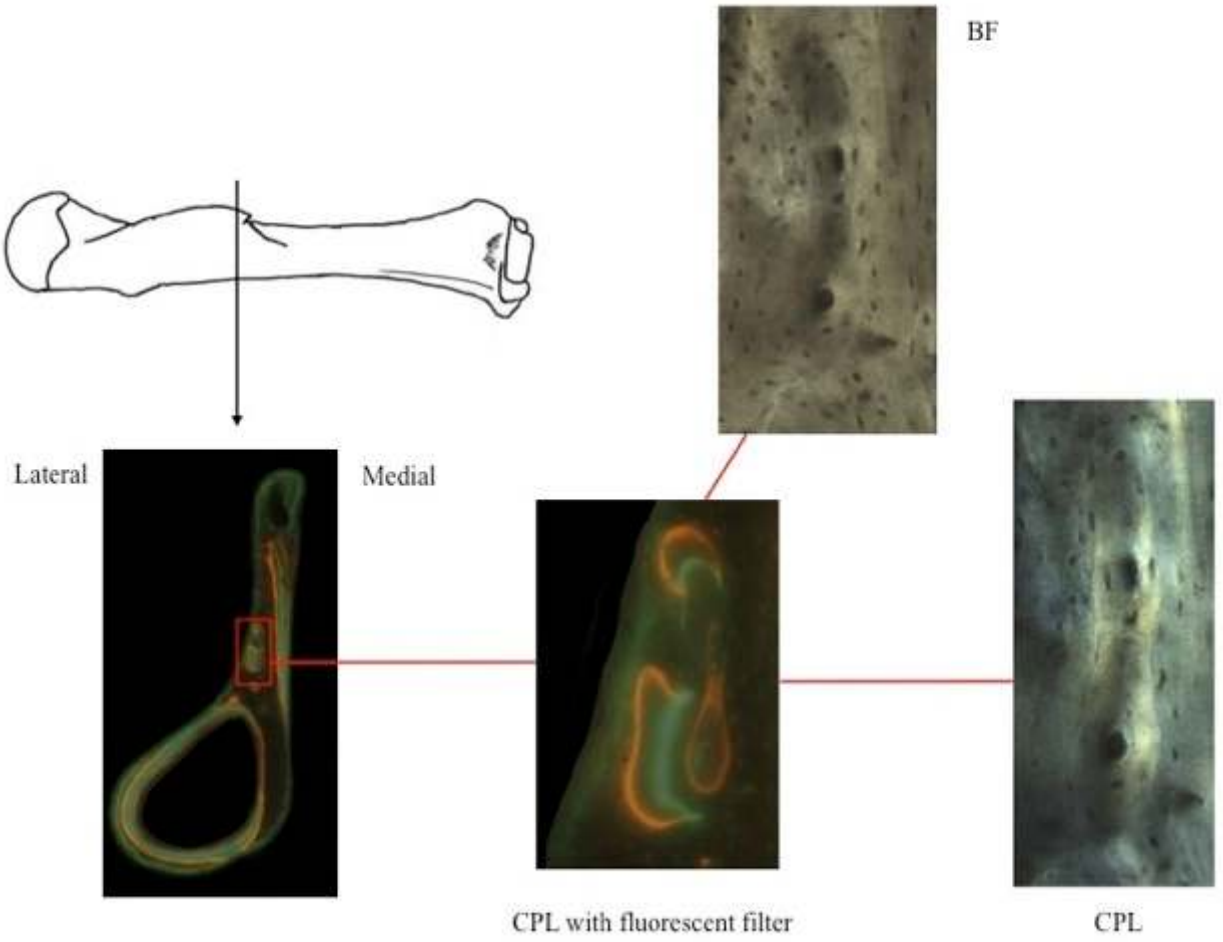

Chapter 5

5. Primate results

Hard- and soft-tissue analyses of the humerus are reported in this chapter for the primate sample. Results are presented in sections corresponding to the research questions and predictions outlined previously. Observations and results from the anatomy and function of the muscles attaching to the humerus are presented along with humeral entheseal surface anatomy analyses. Finally, biomechanical shape of the humerus, with emphasis on the muscle attachment areas, is explored. This chapter ends with a summary of the results found in the primate sample.

5.1 Overview of the primate data

In general, the forelimb musculature of the orangutans, the Barbary macaque, and the Japanese macaque had a similar organization as other primates. The following description will focus on irregularities from the description table in Chapter 4 and add details to the humeral attachment sites. First, all primates had some damage to their forelimb musculature; some caused by the zoo's autopsy or from transportation from the zoo to the laboratory at the University of Toronto. Therefore, when comparing muscle groups between individuals and species, only 22 of the 28 muscles could be used (Table 5.1). In the case of P2, many of his muscles were damaged at the back and at the elbow. P2 was such a large animal that most of his limbs were cut for transportation. Alhough the numbers reported for this specimen were as accurate as possible, some mass could be missing, especially for the large muscles crossing the elbow joint (e.g., brachialis, triceps and biceps brachii) and some of the back muscles attaching to the humerus (e.g., latissimus dorsi).

5.1.1 Overview of the dissections

This section describes the overall dissections of the primates and points out the differences that were found within the primates. Everything mentioned in this section came from the notes taken during the dissections of the primates. After skinning, the panniculus carnosus was the most superficial muscle of the back in both macaques and had to be removed to expose the latissimus dorsi (LD) and the trapezius (which were observed in all primates). Reflection of the trapezius muscles, revealed a tendinous sheet that covered the muscles attaching to the scapular spine (e.g., deltoideus [D] had a extensive attachment to the fascia also covering the infraspinatus [If] muscle, especially in the apes). Both the trapezius and LD shared an aponeurosis (lumbar) so careful attention had to be paid when separating the two muscles. In all primates, dorsoepitrochlearis (De) originated from the LD muscle. However in the orangutans De came from the LD muscle fibres, while in the monkeys De originated from the tendon of LD. Unlike other apes, such as *Pan*, LD from the orangutans did not attach to the inferior angle of the scapula. Reflection of LD and De revealed the origin of the long head of the triceps brachii (TB) and teres major (Tmaj). Tmaj and LD had a "sister relationship" (they were parallel and their fibres followed the same direction) sharing attachments to a tendinous sheath on the humerus; Tmaj was more fibrous at the attachment (especially in the orangutans) and located more medially, while LD was found to be completely fibrocartilaginous (FC) and inserting via a large tendon. This was also a location where the brachialis artery and the nerves innervating the posterior musculature of the arm and forearm passed by.

On the ventral surface, the pectoralis muscles were the first to be observed. In both monkeys pectoralis abdominalis (Pabd) was present. This muscle dove deep with the pectoralis minor (Pmin) where it shared a common attachment via the deep pectoral aponeurosis, which then

inserted at the shoulder capsule. M1 had her internal organs removed, and therefore her pectorals were cut and/or dried out from the autopsy. They were not included in the fibre architectural data. P1 had no attachment of the pectoralis major (Pmaj) muscle to the clavicle. Instead she had more of a monkey-like attachment to the sterno-clavicular joint area. Although P2 and P3 had a lengthy clavicular origin of Pmaj, this muscle could not be included in the analysis since it was too damaged. The deltoideus (D) muscle had to be reflected in order to reach Pmaj's humeral insertion (this was the case for all primates). By the fibrocartilaginous attachment of Pmaj on the humerus, in all primates the cephalic vein could be seen. In the monkeys, the attachment of Pmaj was higher up the diaphysis than the apes. This was mainly due to the higher insertion of the deltoid muscle in monkeys. Both macaques had small and flat deltoids but with clear three separate heads at the origin. The orangutans seemed to have larger and thicker deltoideus muscles but with one continuous origin. The insertion of the deltoid in the apes seemed low on the humerus compared to the monkeys (although the lack of a deltoid crest in apes might give the illusion that the muscle attaches lower; see section 5.2.2 for statistics). All primates had many blood vessels passing by the proximal end of the deltoideus insertion. All deltoideus muscles had direct and fleshy insertions on the humeral shaft. The origin of the brachialis (B) muscle surrounded the boundaries of the deltoideus insertion in the apes. Although a similar arrangement was found in the monkeys, brachialis clearly originated under the crest that is formed under the attachment of the deltoid muscle in the macaques. This clear border is harder to distinguish in the apes since no deltoid crest is present and both muscle attachments are fibrous.

In order to get to the muscles of the "rotator cuff", the rhomboids had to be reflected. The glenoid capsule also had to be removed to properly observe the muscles inserting around the humeral head. Although the orientation of the humeral head was not the same in monkeys and

apes, the rotator cuff muscles in all primates had tendon attachments (FC) to the metaphysis of the humerus and in relatively similar locations. Part of the subscapularis (Sb) muscle was attached to the capsule, while the remainder was found on the lesser tubercle extending inferiorly onto the humerus and inserting beside LD. When it came to their insertions, infraspinatus (If) had a "sister relationship" with teres minor (Tmin) (they were parallel and their fibres followed the same direction). Tmin inserted just below the anatomical neck (lowest facet on the medial side of the greater tubercle), while infraspinatus inserted on the greater tubercle superior to Tmin. Finally, the insertion of the supraspinatus (Sp) muscle was found superior to the greater tubercle (most superior facet). It should be noted that the greater tubercle is found higher than the humeral head in the macaques. Dissecting these rotator cuff muscles was useful to determine more accurately the location of their entheses, which covered more surface of the bone than just the facets around the tubercles.

Next, the muscles of the arm and forearm could be harvested. In the macaques, there is an extra muscle, the coracobrachialis mini (Cbm). Although it also originates on the coracoid process with the coracobrachialis medius (Cb) and the short head of the biceps brachii (BB), it is found deep to Cb (which is the equivalent of the coracobrachialis in the apes) and inserts just superior to it on the humeral shaft. Both Cb and Cbm had tendinous attachments on the humerus. In the orangutans, the coracobrachialis muscle (Cb) was found at a similar location on the humeral diaphysis, and inserted via a tendinous sheath. The biceps brachii (BB) was also removed and analysed despite not attaching to the humerus. It is a powerful flexor and supinator and may contribute to the shape of the underlying bone. The brachialis (B) muscle was found all around the delto-pectoral insertions and shared most of the humeral shaft with the medial head of the triceps brachii (TB) (i.e., where one ended the other one began). Both muscles had direct fleshy

origins on the diaphysis. In the monkeys, the origin of the brachialis seemed to cover more of the humeral shaft than the apes. Dorsoepitrochlearis (De) inserted perpendicular to the lateral head of TB by a tendinous sheath covering the medial epicondyle (medial and long head of TB insert on the ulna). In the monkeys, De was small and tendinous close to its insertion, while in the orangutans the muscle was still large before it became tendinous at the epicondyle. The ulnar nerve passed just below the attachment of the tendinous De in all primates. In the apes, brachioradialis (Br) muscle fibres originated not only on the supracondylar ridge (i.e., supinator crest), but some fibres were also shared with the long head of TB. Careful attention once again had to be paid when separating these two muscles. In all primates, Br originated on the upper surface of the "supinator crest" with part of the fibres inserting on the bony ridge.

Very little variation was found between the common flexors and extensors of the primates studied. Inferior and deep to Br was the extensor carpi radialis longus (ECRL), which originated from the majority of the supracondylar ridge and above the origin of the common extensors of the forearm. Its origin was also more fibrous than tendinous, which was unlike the other extensors. The remainder of the extensors (extensor carpi radialis brevis [ECRB], extensor carpi ulnaris [ECU], extensor digitorum [ED], and extensor digitorum mini [ECM] – found in that ascending order in their attachments) along with the supinator (Sup) muscle all attached to the end of the supracondylar ridge and the lateral epicondyle via a common sheath. The supinator was the most posterior muscle and had a second head that originated on the ulna. All of the "extensors" shared a common mixed origin enthesis, where both direct and tendinous attachments were found within the sheath. On the medial side, the flexors (flexor carpi radialis [FCR], flexor carpi ulnaris [FCU], and flexor digitorum superficialis [FDS]) along with the palmaris longus (PL) muscle and the pronator teres (PT) muscles also all shared a common

sheath attaching to the medial epicondyle. PL was present in all of the primates studied. In the apes, PT had two heads at its origin, one on the humerus and one on the ulna. The monkeys only had the humeral origin. FCU was the most posterior while PT was the most medial of the muscles and located low on the medial humerus. A small anconeus muscle was found in the primates going from the lateral epicondyle to the ulna, while the macaques had an extra small muscle that went from the medial epicondyle to the ulna called the epitrochleo-anconeus. Although these muscles were removed for analysis, much of their fibres were lacking, especially in the apes where the elbow was often cut. Both muscles had fibrous origins on the epicondyles.

5.1.2 Functional muscle groups

Body mass of the primates and forelimb muscle variables were grouped in functional categories and results are presented here (Figures 5.1 – 5.4). There was a wide range of body mass represented by the orangutans. P1 was a small female at 56.4 kg, and P3 was a larger male at 92.5 kg, but P2 was extremely large compared to the other two apes at 140 kg (see Table 4.1). The following data are all body mass adjusted analyses, and the absolute values for all muscle fibre architectural data can be found in Appendix A. Muscle mass of the forelimbs was first investigated at the shoulder, the elbow, and the wrist (Figure 5.1). Overall, the apes had greater forelimb muscle mass than both monkeys. Both male *Pongo* had the largest relative muscle masses, with P2 having the highest mass despite the damage to many of his muscles. The Japanese macaque (M1) had the lowest overall muscle mass.

Shoulder muscles

At the shoulder, the same trend as the overall muscle mass was observed (Figure 5.1), however the large male P2 had lower shoulder mass values, and was similar to the female's mass.

Although the Barbary macaque (M2) had similar masses for the extensor and abductor muscles to the apes, the general consensus showed that both monkeys had much lower muscle mass at the shoulder region, which is contrary to some of the predictions. It was predicted that the shoulder muscles of the monkeys, particularly the protractors would be larger than the apes, which was not the case in this sample. Although muscle mass is often used to represent the strength of a muscle, other muscle fibre architectural properties such as physiological cross-sectional area (PCSA), priority index of force (*I*), and the muscle-tendon unit (TL/MTU) might be more representative for maximum potential force of muscles (Figure 5.2) (Close, 1972; Grand, 1977; Gans and Gaunt, 1991; Zihlman, 1992; Jouffroy and Médina, 1996; Lieber and Fridén, 2000; Youlatos, 2000; Ogihara et al. 2005; Payne et al., 2006a; Smith et al., 2006; Carlson. 2006; Oishi et al., 2008, 2009; Michilsens et al., 2009; Mathewson et al., 2012). In general, the monkeys fell below the PCSA and *I* (considers how much a volume is due to shorter more pennate fibres) values of the orangutans, although *M. sylvanus* often fell close to the apes, especially for the abductors (D, Sp), adductors (Cb, Tmaj, TB) and exorotators (If, Tmin, D). However, when looking at the tendon characteristics (TL/MTU = estimated energy cost of applying force to a substrate) all primates had overlapping values, but *M. fuscata* had the highest tendon values in the shoulder extensors (TB, Tmaj, D), abductors, endorotators (Sb, D, Tmaj), and exorotators. In this region, the muscles in all primates seemed to be used mainly isometrically except for the shoulder abductors (more isotonic).

Since there is usually a trade-off between force and excursion, it is not surprising that an opposite pattern was observed in the belly length (L_b) and fibre length (L_f). Unlike what was predicted, however, the macaques had longer muscles (L_b and L_f), especially M1 (Figure 5.2). M/P_o (muscle mass/predicted effective maximum tetanic tension) considers how much muscle

mass is due to longer fibres, and hence dedication to excursion depicted by longer parallel fascicles (Powell et al., 1984; Taylor et al., 2009). So when muscle mass was considered with fibre length, the orangutans (especially P2) were found to have faster contracting muscles. On the other hand, h (estimated maximum excursion of the distal tendon) considers fibre length (L_f) and pennation angle (θ) to estimate the excursion of a muscle during contraction (Benninghoff and Rollhaüser, 1952), and monkeys could be considered to have the faster contracting muscles, especially for the shoulder flexors (D, BB, Cb) and endorotators. Overall, when the variables involved mass, the orangutans showed more powerful muscles, while for the variables considering length of muscle and tendon, the monkeys had the most powerful muscles. Both monkeys often grouped together, but *M. sylvanus* was often similar in shoulder muscle morphology to the apes.

Elbow and wrist muscles

It was predicted that the muscles that extend the elbow and wrist would be larger in the macaques with longer tendons, while the flexors would be more forceful in the orangutans. The two *Pongo* males had the greatest muscle mass for all muscles acting on the elbow and wrist (Figure 5.1). The female *Pongo* had overlapping muscles masses with the two monkeys. The Barbary macaque however did have high extensor (TB), palmar (FDS, FCU, FCR, PL), ulnar (ECU, FCU, EDM) and radial (ECRL, ECRB, FCR) muscle masses. Despite falling short to the large male orangutans, the monkeys did have large extensors and ulnar muscles.

Similarly, the two male orangutans had greater elbow and wrist muscle PCSA and *I* (Figures 5.3 and 5.4). However, the female orangutan did not have elbow and wrist muscles that had as much potential force as the male apes. In fact, P1 was often found between the two macaques in the

internal structures most likely to represent maximum force of a muscle. Surprisingly, the Barbary macaque (M2) had overall very large PCSA and index of force for all muscles in this region. Once again, the opposite pattern was seen with the variables, which considered the length of the muscle. Looking at the internal structures of the muscles (Figures 5.3 and 5.4), both macaques, but especially the Japanese macaque (M1), and the female ape had very long elbow and wrist muscles (L_b and L_f). As seen with the shoulder muscles although, when a variable considers muscle mass (M/P_o) in its equation, the apes have higher values despite the functional unit, but when muscle and tendon lengths are represented in the equation of the variables (TL/MTU, h) the macaques are comparable to the apes (Figures 5.3 and 5.4). In particular, M1 seemed to have had very long tendons compared to all of the primates studied, followed by the female ape P1. Therefore for this sample, greater body mass was indicative of large and strong muscles, while smaller body mass was representative of smaller but faster and more isometrically contracting muscles of the forelimbs.

5.1.3 Bone measurements

Once the bones were skeletonized, it was observed that both male orangutans (P2 and P3) had very large humeri with very well defined crests and overall muscle attachment sites (Figure 5.5). Their bones were very thick (see cortical area measurements below), and the humerus of the large P2 was even slightly curved. P3 had very robust entheses with the appearance of exostosis, which was probably a factor of his old age. On the other hand, the female orangutan (P1) had a very gracile humerus compared to the two male apes and her muscle attachments were poorly developed despite her age. Both macaques had nicely defined muscle attachment sites with large crests and relatively robust bones (Figure 5.5). The crests and processes of both macaques were prominent and well defined. Many of the attachment sites, especially in the more gracile

specimens and in areas of overlapping muscles, would have been difficult to identify without the aid of the dissections and the digital photographs. For example, where the attachment for the brachialis starts and the attachment of the medial head of the triceps brachii begins was very difficult to distinguish without the prior knowledge of where the fibres were located. In order to study fibrous attachments, knowledge of variation within a species is needed to fully capture the entheseal morphology.

Briefly, the humeri were quantified by looking at the data from the midshaft of each primate (Figure 5.5; Appendix C). Most variables (except medullary area [MA], both index of circularity [I_{max}/I_{min} and Zy/Zx], and the orientation of the greatest bending rigidity [theta]) were significantly different among the primates. As predicted, orangutans had stronger (larger section moduli [Zp]) and more rigid (larger second moments of area [*J*]) in bending, torsion and axial compression/tension (cortical area [CA]) than the macaques at the midshaft. P3 had the largest cortical area (CA) followed by P2 and P1 with both monkeys having the lowest cortical area (M1 > M2). Cortical areas of the diaphyseal attachments sites were considered when looking at the surface entheseal measurements. No differences were found between the sexes in the cross-sectional properties.

Along with the midshaft analyses seen above, cross-sectional geometric differences were compared within an enthesis. The proximal and distal edges as well as the midpoint of the eight-diaphyseal entheses on the humerus (latissiumus dorsi, pectoralis major, deltoideus, teres major, coracobrachialis, lateral and medial heads of the triceps brachii and brachialis) were selected to analyse the cross-sectional geometry (Tables 5.21 – 5.29). First, consistently throughout the sample (for every enthesis), P3 was always stronger (larger section moduli [Zp]) and more rigid

(larger second moments of area [*J*]) in bending, torsion and axial compression/tension (cortical area [CA]) compared with the other primates. The orangutans, as predicted, were found to have stronger bones within each muscle attachment than the macaques. It was predicted, that for each primate, the fibrous muscle attachment sites would not change in shape along the location sequence (proximal, midpoint, and distal) however; most of the attachment sites were significantly different within their sequential bone cross-sectional properties (Tables 5.21 – 5.29). For example, total area [TA], cortical area (CA) and both index of circularity (I_{max}/I_{min} and Zy/Zx) along the location sequence were always found to be significantly different within each enthesis (Tables 5.21 – 5.29) and for all primates.

Three of the eight attachment sites had less significant values (latissimus dorsi [Table 5.21], medial head of the triceps brachii [Table 5.27], and brachialis [Table 5.28). Although the location sequence within an attachment site showed some significant differences, no regular pattern in bone shape could be determined. For example, within the deltoid tuberosity, the cortical area of the bone might have increased (from the proximal to the midpoint sections) and then decreased (from the midpoint to the distal sections) within the attachment for one primate (i.e., P3), while it might only have increased in cortical area in another (i.e., P1).

More variation was also observed within each primate; the macaques often overlapped the apes (latissimus dorsi, pectoralis major, teres major, brachialis, and both attachments of the triceps brachii). The only variable that was predictable was the angle of greatest bending rigidity (theta). For all attachment sites and for most primates, the angle stayed the same throughout the enthesis. Therefore, no matter where the data were taken (proximal, distal or at the midpoint) within the attachment site, the angle of greatest bending rigidity was always oriented in the same plane.

Observations on the entheseal surface morphology and the associated muscle structural anatomy were analysed next.

5.2 Shoulder muscular and entheseal anatomy

The following sections goes over the internal structure of some of the shoulder muscles (LD, D, Pmaj, Sb, Sp, If, Tmin, Tmaj, and Cb) along with the morphology of their attachment sites. For the muscles that insert on the diaphysis of the humerus (LD, D, Pmaj, Tmaj), bone cross-sectional properties of the enthesis were also analysed. The distal-most position of each attachment site expressed in percentages of length from the proximal end (insertions) or distal end (origins) of the humerus was also analysed to determine leverage of each muscle. Unless otherwise stated, comparisons for the soft- and hard-tissue variables were non-significant between primates and sexes.

5.2.1 Latissimus dorsi muscle

The latissimus dorsi muscle (LD) is a large back muscle that helps extend, adduct and medially rotate the humerus. It is a muscle that also helps raise the body towards the forelimbs during climbing. Considering these actions and the locomotions of the primates from this project, LD was predicted to be large and pennated in the orangutans, but longer and slender in the macaques. Therefore, the insertion of LD, which was found on the supero-anterior surface of the humerus within the intertubercular groove, should be larger, stronger, and more hypertrophied in the apes. The latissimus dorsi muscle could only be harvested from P1, P2 and M2 although all primates were used to analyse the entheseal morphology (Table 5.3).

For this muscle, both apes had greater muscle mass and muscle mass/predicted effective max tetanic tension (M and M/P_o), longer tendons (TL/MTU), and larger cross-sections (PCSA). On the other hand the Barbary macaque had a longer muscle belly (L_b) and surprisingly a larger angle of pennation (θ). All primates overlapped in their fibre length (L_f), index of force (*I*) and maximum distal tendon excursion (h) (Table 5.3). The general pattern for the internal structures of LD was that the orangutans (as predicted) had a slightly larger LD with greater potential force production than the macaque.

When looking at the body mass adjusted muscle attachment site measurements (absolute measurements can be found in Appendix B), the male orangutans had a longer enthesis, while the width of the attachment overlapped in size in all primates, and the monkeys along with P3 had the most surface area (Table 5.3). A slightly different picture was seen when the measurements considered the area of the underlying bone (using the midpoint CA of the attachment site). Considering cortical area of the enthesis, P1 and P2 had a longer attachment site, P3 a wider one, while both P3 and M1 had the larger surface area (Table 5.3). The point of insertion of LD on the humerus bears significantly on the biomechanical roles of the muscle since it acts as a lever arm. Although no differences were found in the architectural data, the location of the LD insertion was located slightly more distal in macaques (M2 > M1 > P2 > P1 = P3; Table 5.29).

5.2.2 Deltoideus muscle

The deltoideus muscle (D) is a relatively large triangular muscle that helps flex, medially rotate, abduct, extend, and laterally rotate the humerus. Considering these actions, the deltoid was predicted to be large and pennated in the orangutans, but longer and slender in the macaques.

Therefore, the insertion of D, which was found on the deltoid "tuberosity" (deltoid crest in macaques) of the humerus, should be larger, stronger, and more hypertrophied in the apes. The deltoid muscle was harvested from all primates and could be compared with all attachment site morphologies (Table 5.4).

For this muscle, all apes had greater muscle mass and muscle mass/predicted effective max tetanic tension (M and M/P_o), larger cross-sections (PCSA), and index of force (*I*) (Table 5.4). On the other hand, both macaques had longer fibre lengths (L_f). All primates overlapped in tendon length (TL/MTU) although females seemed to have longer tendons than males. Considering all of the muscle fibre architectural variables of the deltoid, the orangutans (as predicted) had a slightly larger D with greater potential force production than the macaques. The monkeys had greater excursion and contraction velocity of the deltoid than the apes. Although suspensory primates tend to have more distally located deltoid insertions, the opposite pattern was found in this sample. The macaques (M1 > M2 > P3 > P2 > P1) had the distal-most insertion (Table 5.29). Looking at the relative muscle attachment site measurements, P1 had the longest enthesis, while P2 had greater width of the attachment site, and M2 had the most surface area of the deltoid crest (Table 5.4). A slightly different picture was seen when the measurements considered the area of the underlying bone. Considering CA of the enthesis, M1 had a longer attachment site, P2 still had the widest enthesis, while both male orangutans had the larger surface area (Table 5.4).

5.2.3 Pectoral muscles

The pectoralis major (Pmaj) and pectoralis abdominalis (Pabd: monkeys only) are large pectoral muscles that help adduct, flex, and medially rotate the humerus. These muscles can also help

protract and retract the scapula and extend the forelimb from a flexed position. Considering these actions, Pmaj and Pabd were predicted to be large and pennated in the macaques, but long and slender in the apes. Therefore, the insertion of Pmaj, which is found superior to the deltoid muscle attachment on the humerus, should be larger, more hypertrophied and stronger in the macaques. The pectoralis major muscle could only be harvested from P1 and M2 though all primates were used to analyse the entheseal morphology (Table 5.5).

For this muscle, P1 had greater muscle mass and muscle mass/predicted effective max tetanic tension (M and M/P_o), longer tendons (TL/MTU and h), and larger cross-sections (PCSA). M2 had a longer muscle belly (L_b) and a larger angle of pennation (θ). Both primates overlapped in their fibre length (L_f) and index of force (*I*) (Table 5.5). Thus when considering the limited data from the pectoralis muscle, the female orangutan had a larger Pmaj with greater potential force production than the macaque, which is unlike what was predicted for this muscle.

When looking at the relative entheseal measurements, P3 had a longer enthesis, while the width of the attachment was greatest in the macaques, and P3 and M1 had the most surface area (Table 5.5). Once again, a slightly different picture was seen when the measurements considered the area of the underlying bone. Considering CA of the enthesis, P1 and P3 had a longer attachment site, all primates overlapped in their attachment width, while P3 had the largest surface area (Table 5.5). Overall, it seemed that the apes had larger pectoral entheses. All primates had overlapping percentages of the maximum humeral length for the distal-most insertion of Pmaj, therefore the apes and monkeys in this sample had similar leverages for the pectoralis major muscle (Table 5.29).

5.2.4 Subscapularis muscle

The subscapularis muscle (Sb) helps with the medial rotation of the humerus. Like all rotator cuff muscles it also provides stability of the shoulder. Considering these actions, Sb muscle was predicted to be large and pennated in the macaques, but longer and slender in the apes. Therefore, the insertion of Sb, which is found on the lesser tuberosity, should be larger in the macaques. The subscapularis muscle was harvested from all primates and could be compared with all attachment site morphologies (Table 5.6).

For this muscle, all apes had greater muscle mass and muscle mass/predicted effective max tetanic tension (M and M/P_o), longer distal tendons (h), and larger cross-sections (PCSA). The macaques as in other shoulder muscles had longer muscle bellies (L_b) (Table 5.6). Male orangutans seemed to have greater potential force production of the subscapularis, which is unlike what was predicted for this muscle. Looking at the relative entheseal measurements, the orangutans had a longer enthesis and more surface area (unlike what was predicted), while the width of the attachment was greatest in M2 (Table 5.6). The location of the Sb insertion was significantly different between primates ($P = 0.002$; Table 5.29) with the apes possessing the distal-most insertion (P3 > P1 > P2 > M2 > M1).

5.2.5 Supraspinatus muscle

The supraspinatus muscle (Sp) helps abduct the forelimb and like all rotator cuff muscles it also provides stability of the shoulder. Considering these actions, Sp muscle was predicted to be large and pennated in the macaques, but longer and slender in the apes. Therefore, the insertion of Sp, which is found on the most superior facet of the greater tuberosity, should be larger in the

macaques. The supraspinatus muscle was harvested from all primates and could be compared with all attachment site morphologies (Table 5.7).

For this muscle, all apes had greater muscle mass/predicted effective max tetanic tension (M/P_o), and longer tendons (TL/MTU and h). The macaques had longer muscle bellies (L_b) (Table 5.7). Females had slightly longer fibres while the males had somewhat higher force index (Table 5.7). Male orangutans therefore had slightly greater potential force production of the supraspinatus, which is unlike what was predicted for this muscle. Looking at the relative entheseal measurements, both male orangutans had overall larger attachment sites (Table 5.7). Therefore, male orangutans seemed to be associated with a larger supraspinatus enthesis (contrary to prediction). Surprisingly, all primates had overlapping percentages of the maximum humeral length for the distal-most insertion, therefore the apes and monkeys in this sample had similar leverages for the supraspinatus muscle (Table 5.29).

5.2.6 Infraspinatus muscle

The infraspinatus muscle (If) helps with the lateral rotation of the humerus. Like all rotator cuff muscles it also provides stability of the shoulder. Considering these actions, the If muscle was predicted to be large and pennated in the macaques, but longer and slender in the apes. Therefore, the insertion of If, which is found on the greater tuberosity, should be larger in the macaques. The infraspinatus muscle was harvested from all primates and could be compared with all attachment site morphologies (Table 5.8).

For this muscle, the apes had greater muscle mass/predicted effective max tetanic tension (M/P_o), and slightly longer tendons (TL/MTU and h). As seen in all of the rotator cuff muscles so far, the

macaques had longer muscle bellies (L_b) (Table 5.8) Like supraspinatus, fibre lengths and index of force differed vaguely between sexes; females had longer fibres while the males had higher force index (Table 5.9). The orangutans therefore had slightly greater potential force production of the infraspinatus, which is unlike what was predicted for this muscle. Looking at the relative entheseal measurements, the female orangutan was the animal with the largest attachment site (Table 5.8). The location of the If insertion was significantly different between primates (P = 0.036; Table 5.29) with the apes possessing the distal-most insertion (P3 > P1 > P2 > M1 > M2).

5.2.7 Teres minor muscle

The teres minor muscle (Tmin) is similar to the infraspinatus muscle and helps with the lateral rotation of the humerus. Like all rotator cuff muscles it also provides stability of the shoulder. Like the infraspinatus muscle, Tmin was predicted to be large and pennated in the macaques, but longer and slender in the apes. Therefore, the insertion of Tmin, which is found inferior to the infraspinatus muscle on the greater tuberosity, should be larger in the macaques. The teres minor muscle was harvested from all primates and could be compared with all attachment site morphologies (Table 5.9).

For this muscle, the apes had longer distal tendons (h). On the other hand, the macaques had longer muscle bellies (L_b), longer tendon to muscle unit (TL/MTU), higher angle of pennation, and greater potential force production (M/P_o and I) (Table 5.9). The macaques seem to have the most powerful teres minor, which was as predicted for this muscle. Looking at the relative entheseal measurements, the orangutan had the largest overall attachment site (Table 5.9). Thus, this muscle with higher excursion and contraction velocity was associated with a smaller entheseal surface. All primates had overlapping percentages of the maximum humeral length for

the distal-most insertion, therefore the apes and monkeys in this sample had similar leverages for the teres minor muscle (Table 5.29).

5.2.8 Teres major muscle

The teres major (Tmaj) is a large shoulder muscle, similar to the latissimus dorsi, it helps extend, adduct and medially rotate the humerus. Like the latissimus dorsi muscle, Tmaj was predicted to be large and pennated in the orangutans, but longer and slender in the macaques. Therefore, the insertion of Tmaj, which is found superior to the latissimus dorsi attachment on the humerus of the apes, should be larger than the macaques attachment site. The teres major muscle was harvested from all primates and could be compared with all attachment site morphologies (Table 5.10).

For this muscle, all apes had greater muscle mass/predicted effective max tetanic tension (M/P_o), wider cross-sections (PCSA), and larger index of force (*I*). Both macaques had longer muscle bellies (L_b) and fibres (L_f), as well as longer tendons (TL/MTU) (Table 5.10). As predicted, the macaques seem to have greater excursion potential and contracting velocity while the orangutans have greater force potential for the teres major muscle. Looking at the relative entheseal measurements, the female orangutan seemed to have the largest overall attachment site (Table 5.10). When considering the bone underlying the enthesis, the female orangutan still seemed to have greater attachment area (Table 5.10). However, all primates had overlapping percentages of the maximum humeral length for the distal-most insertion, therefore the apes and monkeys in this sample had similar leverages for the teres major muscle (Table 5.29).

5.2.9 Coracobrachialis muscles

The coracobrachialis muscles (Cb = medius, Cbm = mini) help adduct and flex the humerus. Considering these actions and the locomotions of the primates from this study, Cb was predicted to be large and pennated in the orangutans, but long and slender in the macaques. Therefore, the insertion of Cb, which is found supero-medially on the humerus (relatively close to the anatomical neck), should be larger and more hypertrophied in the orangutans. The coracobrachialis muscle was harvested from all primates and could be compared with all attachment site morphologies (Table 5.11).

For this muscle, the apes had greater muscle mass and muscle mass/predicted effective max tetanic tension (M/P_o) as well as wider cross-sections (PCSA) (Table 5.12). Looking at the relative entheseal measurements, the orangutans had larger width and surface area of the attachment site (Table 5.11). The location of the Cb insertion was significantly different between primates ($P = 0.004$; Table 5.29) with the apes possessing the distal-most insertion (P2 > P3 > P1 > M1 > M2).

5.3 Elbow muscular and entheseal anatomy

The following sections will go over the internal structure of the elbow muscles (B, TB, De, BB, An, PT, Br, ECRL, common flexors and extensors) along with the morphology of their attachment sites. For the muscles that insert on the diaphysis of the humerus (medial and lateral head of triceps brachii and brachialis), bone cross-sectional properties of the enthesis are also analysed. The distal-most position of each attachment site expressed in percentages of length

from the proximal end (insertions) or distal end (origins) of the humerus was also analysed to determine leverage of each muscle.

5.3.1 Brachialis muscle

The brachialis muscle (B) is a large elbow muscle that helps flex the elbow. Considering that action and the locomotions of the primates from this project, B was predicted to be large and pennated in the orangutans, but longer and slender in the macaques. Therefore, the origin of B, which occupies most of the anterior surface of the diaphysis below the deltoid attachment on the humerus, should be larger, more hypertrophied and stronger in the orangutans. The brachialis muscle was harvested from all primates and could be compared with all attachment site morphologies (Table 5.12).

For this muscle, the apes had greater muscle mass and muscle mass/predicted effective max tetanic tension (M/P_o) as well as wider cross-sections (PCSA) (Table 5.12). The apes therefore seemed to have the most powerful brachialis muscles, which was as predicted for this muscle. Looking at the relative entheseal measurements, the orangutans had larger width and surface area of the attachment site and the males seemed to have wider entheses than the females (Tables 5.12). The location of the B origin was significantly different between primates ($P = 0.006$; Table 5.29) with the monkeys possessing the distal-most origin (M2 > M1 > P2 > P3 > P1).

5.3.2 Biceps brachii muscle

The biceps brachii (BB) is a large arm muscle that helps supinate the forearm and flex the shoulder and forearm. It is a muscle that also resists dislocation of the humerus. Considering

these actions and the locomotions of the primates, BB was predicted to be large and pennated in the orangutans, but long and slender in the macaques. Biceps brachii does not attach on the humerus; therefore, no attachments could be analysed with this muscle but it was harvested from all primates for internal structural analysis (Table 5.13).

For this muscle, the apes had greater muscle mass/predicted effective max tetanic tension (M/P_o) and slightly larger index of force (*I*). The macaques had longer fibre lengths (L_f) and pennation angle (Table 5.13). As predicted, the biceps brachii muscle may have greater excursion potential in the macaques, but greater force potential in the orangutans.

5.3.3 Triceps brachii and dorsoepitrochlearis muscles

The triceps brachii (TB) is very a large muscle of the arm that helps extend and adduct the humerus, as well as extend the forearm. It is a muscle that also resists dislocation of the humerus. Dorsoepitrochlearis (De) is a smaller muscle that aids in the extension of the forearm. Considering these actions and the locomotions of the primates from this study, TB and De were predicted to be large and pennated in the macaques, but long and slender in the apes. Therefore, the attachments of TB (lateral and medial head = most of the lateral and posterior surface of the humeral shaft) on the humerus of the monkeys should be larger, stronger and more hypertrophied than the apes. The triceps brachii muscle was harvested from all primates and could be compared with all attachment site morphologies (Table 5.14), however the dorsoepitrochlearis was too damaged in the Barbary macaque to be analysed.

For the triceps muscle, the apes had greater muscle mass/predicted effective max tetanic tension (M/P_o) while the macaques had significantly longer muscle bellies (L_b) (Table 5.14). Males

seemed to have slightly larger muscle mass and PCSA, while the females had longer muscle fibres and pennation angles (Table 5.14). For the dorsoepitrochlearis muscle, similar patterns were observed; except that M2 has a larger muscle mass, muscle belly, and pennation angle than the orangutans (Table 5.14). The apes seemed to have the more force potential, and the macaques seemed to have greater excursion potential (unlike what was predicted) for these extensors.

Looking at the relative entheseal measurements, all of the morphologies of the lateral head of the triceps entheses overlapped (Tables 5.14). Contrary to the lateral head, all of the variables were found to be larger in the orangutans for the medial head of the triceps entheses (Table 5.14). The males did seem to have wider entheses than the females for both attachment sites. The location of the TBmed origin was significantly different between primates ($P = 0.012$; Table 5.29) with the monkeys possessing the distal-most origin (M2 > M1 > P2 > P3 > P1). However, all primates had overlapping percentages of the maximum humeral length for the distal-most origin, therefore the apes and monkeys in this sample had similar leverages for the lateral head of the triceps brachii muscle (Table 5.29).

5.3.4 Anconeus muscle

The anconeus (An) is a small muscle of the elbow that helps extend the elbow and abduct the ulna in pronation. Considering these actions, An was predicted to be large and pennated in the macaques, but long and slender in the orangutans. Therefore, the origin of An on the lateral epicondyle of the humerus should be larger in the monkeys. The anconeus muscle was too damaged in the Barbary macaque to be analysed (Table 5.15).

For this muscle, the apes had greater muscle mass and muscle mass/predicted effective max tetanic tension (M/P_o) as well as longer fibre lengths (L_f) and distal tendons (h). The macaque had slightly long tendon-muscle unit (TL/MTU) and pennation angle (Table 5.15). M2 seemed to have overall a larger attachment site (Table 5.15). All primates had overlapping percentages of the maximum humeral length for the distal-most origin, therefore the apes and monkeys in this sample had similar leverages for the anconeus muscle (Table 5.29). Furthermore, all anconeus entheseal morphologies were overlapping in size.

5.3.5 Pronator teres muscle

The pronator teres muscle (PT) is the main pronator of the wrist. Considering its action, PT was predicted to be large and pennated in the orangutans, but long and slender in the macaques. Therefore, the origin of PT, which is found medially on the epicondylar ridge of the humerus (just above the common flexors of the elbow and wrist muscles), should be larger in the apes. The pronator teres muscle was harvested from all primates and could be compared with all attachment site morphologies (Table 5.16).

For this muscle, the apes had greater muscle mass and muscle mass/predicted effective max tetanic tension (M/P_o) and longer tendons (TL/MTU). On the other hand, macaques had longer belly lengths (L_b) (Table 5.16). Muscle mass, PCSA, and *I* seemed to to be greater in males, while fibre length longer in females (Table 5.16). The apes therefore may have larger muscles with longer tendons (as predicted) while the macaques have longer belly lengths. P2 seemed to have overall a larger attachment site (Table 5.16). P2 also had the greatest PCSA value. However, all primates had overlapping percentages of the maximum humeral length for the

distal-most origin, therefore the apes and monkeys in this sample had similar leverages for the pronator teres muscle (Table 5.29).

5.3.6 Brachioradialis muscle

The brachioradialis (Br) is an elbow muscle that helps with forearm flexion. Considering its action, Br was predicted to be large and pennated in the orangutans, but long and slender in the macaques. Therefore, the insertion of Br, which is superior to the supracondylar ridge on the humerus, should be larger, more hypertrophied and stronger in the apes. The brachioradialis muscle was harvested from all primates and could be compared with all attachment site morphologies (Table 5.17).

For this muscle, the apes had greater muscle mass and muscle mass/predicted effective max tetanic tension (M/P_o), longer tendons (TL/MTU), and wider cross-sections (PCSA). On the other hand, macaques had longer belly lengths (L_b) (Tables 5.17). The apes therefore may have had larger muscles with longer tendons and wider cross-sectional area (as predicted) while the macaques had longer belly lengths. However, all primates had overlapping percentages of the maximum humeral length for the distal-most origin, therefore the apes and monkeys in this sample had similar leverages for the brachioradialis muscle (Table 5.29). All of the entheseal measurements overlapped (Table 5.17) and none of the contrasts between species or sexes were different.

5.3.7 Extensor carpi radialis longus muscle

The extensor carpi radialis longus muscle (ECRL) helps extend and abduct the wrist. Considering these actions, ECRL was predicted to be large and pennated in the macaques with long tendons, but a longer and slender muscle belly in the orangutans. Therefore, the insertion of ECRL, which is inferior and deep to the brachioradialis on the supracondylar ridge of the humerus, should be larger in the monkeys. The ECRL muscle was harvested from all primates and could be compared with all attachment site morphologies (Table 5.18).

For this muscle, the apes had greater muscle mass/predicted effective max tetanic tension (M/P_o), and slightly wider cross-sections (PCSA). On the other hand, macaques had longer belly lengths (L_b) (Table 5.18). Fibre lengths were slightly longer in the females compared to the males. The male apes had larger muscles and wider cross-sectional area while the macaques had longer belly lengths (unlike what was predicted). Looking at the entheseal measurements, the male orangutans had longer attachment sites covering more surface area (Tables 5.18) and all primates had overlapping percentages of the maximum humeral length for the distal-most origin. Therefore the apes and monkeys in this sample had similar leverages for the ECRL muscle (Table 5.29).

5.3.8 Common flexors

The common flexors (PL, FCR, FCU, FDS; see Table 5.1 for abbreviations) all help flex the wrist and the elbow. Considering their action and the locomotions of the primates from this study, the common flexors (CFO) were predicted to be large and pennated in the orangutans with long tendons, but longer and slender muscle bellies in the macaques. Therefore, the origin of

CFO on the medial epicondyle of the humerus should be larger in the apes. The flexor muscles were harvested from all primates and could be compared with all attachment site morphologies (Table 5.19).

For PL, FCU, and FCR muscles, the apes had greater muscle mass/predicted effective maximum tetanic tension (M/P_o) while the macaques had significantly longer belly lengths (L_b). The FCR muscle is a little controversial as it also had longer fibre lengths (L_f) and distal tendon (h) in the orangutans, but larger pennation angles in the macaques. Finally, the FDS muscle had larger tendons (TL/MTU), pennation angle, and greater muscle mass/predicted effective max tetanic tension (M/P_o) in the apes (Table 519). Muscle masses were observed to be larger in the males while fibre lengths were longer in the females (Tables 5.19). Overall, the muscle fibre architecture of the elbow and wrist flexors was as predicted, somewhat stronger, larger, and more pennated in the orangutans. Looking at the entheseal measurements, the males had slightly longer attachment sites covering more surface area (Table 5.19). The location of the common flexors' origin was not significantly different between primates (Table 5.29) though the apes had a slightly more distal origin (P1 > P2 > P3 > M1 > M2).

5.3.9 Common extensors

The common extensors (ECRB, ECU, ED, EDM; see Table 5.1 for abbreviations) all help extend the wrist and the elbow. The supinator (Sup), which also shares an origin with the common extensors, helps with the supination of the wrist. Considering these actions, the common extensors (CEO) were predicted to be large and pennated in the macaques with long tendons, but longer and slender muscle bellies in the orangutans. Therefore, the origin of CEO on the lateral epicondyle of the humerus should be larger in the monkeys. The extensor and supinator muscles

were harvested from all primates and could be compared with all attachment site morphologies (Table 5.20).

For all of the above muscles, the macaques had longer belly lengths (L_b). For the Sup, ED, and EDM muscles the apes had greater muscle mass and muscle mass/predicted effective maximum tetanic tension (M/P_o). Sup also had wider pennation angles in the macaques, but longer distal tendons (h) and index of force (*I*) in the apes. On the other hand ECRB had wider pennation angles and longer tendon lengths (TL/MTU) in the orangutans. Finally, EDM had longer muscle fibres in the ape (Tables 5.20). Similar to the extensor muscles, muscle masses were generally found to be larger in the males while fibre lengths were longer in the females (Table 5.20). The location of the common extensors' origin was significantly different between primates (P = 0.009; Table 5.29) with the monkeys possessing the distal-most origin (M2 > M1 > P3 > P2 > P1). Overall, the muscle fibre architecture of the elbow and wrist extensors was quite unpredictable. Looking at the entheseal measurements, the orangutans had slightly longer attachment sites compared to the macaques (Tables 5.20).

5.4 Summary

This research looked at a female orangutan, two male orangutans, and two female macaques (*M. fuscata* and *M. sylvanus*) of different age and body mass to investigate in greater details the relationship between internal muscle structure and entheseal morphology. Surprisingly, many of the predictions for this project were not supported and very little contrasts were significant. The general trend for the functional muscle unit was that when a variable considered muscle mass (e.g., M/P_o) in its equation, the apes had higher values despite the functional unit, but when muscle and tendon lengths were represented in the equation of the variables (e.g., TL/MTU, h)

the macaques were comparable to the apes. Rarely did the macaques ever surpass the orangutans in muscle strength. Despite the different modes of locomotion, larger and stronger muscles (except for the pectoralis major, teres minor and some of the flexors and extensors of the elbow and wrist) were found to be associated more often with the larger species. Most of the orangutans' muscles were associated with greater potential force: larger muscle mass and muscle mass/predicted effective maximum tetanic tension, wider physiological cross-sectional areas and at times larger index of force and longer tendons (isometric contraction). On the other hand, macaques' muscles were usually associated with greater potential excursion and contraction velocity: longer belly and fibre lengths, often surprisingly wider pennation angles, and at times longer tendons.

The biomechanical leverages of the muscle attachment sites were also considered. Although many of the attachment sites overlapped in their distal-most length percentage of maximal humeral length within the sample, the apes seemed to have better leverage of the rotator cuff muscles (especially subscapularis and infraspinatus) along with the muscles that flex the elbow and wrist. On the other hand, the monkeys seemed to have better leverage in the large muscles of the arm such as the latissimus dorsi, deltoideus, brachialis, triceps brachii and the extensors of the forearm. The better biomechanical leverage of these muscles in the macaques may help explain their internal muscular structures (e.g., long isometric musculature).

Interesting results were found when looking at the muscle attachment sites. First, ape humeri were stronger (larger section moduli [Zp]) and more rigid (larger second moments of area [*J*]) in bending, torsion and axial compression/tension (cortical area [CA]) at the midshaft. This pattern was found all throughout the attachment sites as well. Interestingly, this study found that the

diaphyseal cross-sectional properties within an attachment site varied from the proximal to the distal end of the enthesis. Though cortical area, total area, and index of circularity were always significantly different in the attachment site, no consistent pattern was observed. The only variable that was predictable was the angle of greatest bending rigidity (theta). For all attachment sites and for most primates, the angle stayed the same throughout the enthesis. Therefore, no matter where the data were taken (proximal, distal or at the midpoint) within the attachment site, the angle of greatest bending rigidity was always oriented in the same plane. Second, both the sex and the species had some impact on the morphology of the entheses, but not in a consistent matter. Larger and stronger muscles (higher values for M, M/P_o, PCSA) were sometimes associated with larger muscle attachment sites (especially wider entheses) while interestingly, muscles associated with greater excursion and contracting velocity (Lb, Lf, h) were most often associated with smaller entheses. However, many of these associations were random. Finally, when considering the underlying bone of a diaphyseal enthesis, a more accurate relationship between the muscle and the attachment site was often found. This study has shown how variable muscle and bone can be even when considering factors such as age, sex, species, body mass, and locomotion.

Table 5.1 Twenty-two muscles and abbreviations used to compare internal muscle structure among individuals and species.

Muscle	Abbreviation
Deltoid	D
Subscapularis	Sb
Supraspinatus	Sp
Infraspinatus	If
Teres minor	Tmin
Teres major	Tmaj
Coracobrachialis	Cb
Biceps brachii	BB
Triceps brachii	TB
Brachialis	B
Brachioradialis	Br
Pronator teres	PT
Supinator	Sup
Palmaris longus	PL
Flexor carpi radialis	FCR
Flexor carpi ulnaris	FCU
Flexor digitorum superficialis	FDS
Extensor carpi radialis longus	ECRL
Extensor carpi radialis brevis	ECRB
Extensor carpi ulnaris	ECU
Extensor digitorum	ED
Extensor digitorum mini	EDM

Table 5.2 Body mass adjusted biomechanical variables for the midshaft cross sections in all primates.

Variable	P1	P2	P3	M1	M2
TA	34.61	30.71	33.73	27.19	21.55
CA	20.37	20.85	23.37	16.70	14.69
MA	14.24	9.87	10.36	10.49	6.86
Ix	4594.70	11559.72	8566.27	490.20	437.16
Iy	4612.60	7815.26	7063.39	373.81	307.22
Imax	5085.27	11592.95	8679.71	530.75	438.36
Imin	4122.03	10536.82	6949.95	333.26	306.01
Imax/Imin	1.23	1.49	1.25	1.59	1.43
J	9207.30	19374.98	15629.66	864.01	744.38
Theta	44.47	-84.642	-75.16	-63.06	-84.5246
Zx	332.81	809.86	496.47	75.14	68.26
Zy	311.99	650.17	430.66	65.43	56.90
Zy/Zx	0.94	0.80	0.87	0.87	0.83
Zp	2470.07	4174.04	4200.52	287.05	280.51

Table 5.3 Body mass adjusted hard and soft-tissue data for the latissimus dorsi muscle. The insertion for the latissimus dorsi muscle to the humerus was via a tendinous sheet on the humeral shaft: fibrocartilaginous attachment.

Primate	M	L_b	L_f	TL/MTU	θ	PCSA	M/P_0	*I*	h
P1	9.16	50.69	18.20	0.30	5.23	0.47	3.29	0.11	0.08
P2	8.09	52.83	14.65	0.27	4.97	0.52	3.59	0.13	0.06
P3	-	-	-	-	-	-	-	-	-
M1	-	-	-	-	-	-	-	-	-
M2	5.14	69.08	18.06	0.24	8.39	0.27	1.91	0.09	0.06

M = muscle mass; Lb = muscle belly length; Lf = sarcomere adjusted fibre length; TL/MTU = tendon length to muscle-tendon unit ratio; θ = pennation angle; PCSA = sarcomere adjusted physiological cross-sectional area; M/P_0 = muscle mass/predicted effective maximum tetanic tension; *I* = priority index of force; h = estimated excursion during muscle contraction.

Primate	Length*	Width*	Area*	Length°	Width°	Area°
P1	1.163	0.162	0.158	0.307	0.043	0.160
P2	1.258	0.176	0.172	0.290	0.041	0.206
P3	1.285	0.324	0.239	0.248	0.063	0.208
M1	1.100	0.359	0.281	0.150	0.049	0.078
M2	1.179	0.201	0.253	0.239	0.041	0.114

* Body mass adjusted variables
° CA adjusted variables

Table 5.4 Body mass adjusted hard and soft-tissue data for the deltoideus muscle. The insertion of the deltoid muscle on the humerus was via direct attachment of muscle fibres to the humeral shaft: fibrous attachment.

Primate	M	L_b	L_f	TL/MTU	θ	PCSA	M/P_0	*I*	h
P1	6.91	23.12	13.98	0.44	10.41	0.46	2.56	0.13	0.14
P2	7.05	21.66	16.61	0.40	7.61	0.40	4.09	0.11	0.18
P3	7.38	20.98	15.34	0.43	8.17	0.45	3.29	0.12	0.17
M1	1.61	33.98	26.68	0.49	3.50	0.06	2.55	0.04	0.18
M2	3.06	37.16	20.30	0.31	6.29	0.14	2.13	0.07	0.13

M = muscle mass; Lb = muscle belly length; Lf = sarcomere adjusted fibre length; TL/MTU = tendon length to muscle-tendon unit ratio; θ = pennation angle; PCSA = sarcomere adjusted physiological cross-sectional area; M/P_0 = muscle mass/predicted effective maximum tetanic tension; *I* = priority index of force; h = estimated excursion during muscle contraction.

Primate	Length*	Width*	Area*	Length°	Width°	Area°
P1	2.518	0.535	0.747	0.475	0.101	0.541
P2	1.616	0.746	0.820	0.345	0.159	0.910
P3	2.318	0.578	0.985	0.387	0.097	0.744
M1	1.925	0.672	1.013	0.235	0.082	0.251
M2	3.027	0.547	1.254	0.489	0.088	0.451

* Body mass adjusted variables
° CA adjusted variables

Table 5.5 Body mass adjusted hard and soft-tissue data for the pectoralis major muscle. The insertions for the pectoralis muscles to the humerus were via a tendinous sheet on the humeral shaft: fibrocartilaginous attachment.

Primate/Muscle	M	L_b	L_f	TL/MTU	θ	PCSA	M/P_0	*I*	h
P1	5.48	27.50	17.26	0.37	3.99	0.30	3.12	0.10	0.15
P2	-	-	-	-	-	-	-	-	-
P3	-	-	-	-	-	-	-	-	-
M1	-	-	-	-	-	-	-	-	-
M2	3.35	44.86	17.33	0.29	5.63	0.18	1.82	0.08	0.09

M = muscle mass; Lb = muscle belly length; Lf = sarcomere adjusted fibre length; TL/MTU = tendon length to muscle-tendon unit ratio; θ = pennation angle; PCSA = sarcomere adjusted physiological cross-sectional area; M/P_0 = muscle mass/predicted effective maximum tetanic tension; *I* = priority index of force; h = estimated excursion during muscle contraction.

.

Primate	Length*	Width*	Area*	Length°	Width°	Area°
P1	1.594	0.131	0.283	0.366	0.030	0.250
P2	1.266	0.182	0.204	0.239	0.034	0.200
P3	2.057	0.177	0.398	0.351	0.030	0.307
M1	1.755	0.226	0.332	0.211	0.027	0.081
M2	1.461	0.203	0.159	0.277	0.038	0.067

* Body mass adjusted variables
° CA adjusted variables

Table 5.6 Body mass adjusted hard and soft-tissue data for the subscapularis muscle. The insertion for the subscapularis muscle to the humerus was via a tendinous sheet by the proximal epiphysis: fibrocartilaginous attachment.

Primate	M	L_b	L_f	TL/MTU	θ	PCSA	M/P_0	*I*	h
P1	3.84	31.77	11.89	0.32	13.84	0.30	2.20	0.12	0.09
P2	3.58	24.11	10.88	0.41	11.20	0.31	2.70	0.13	0.11
P3	3.82	26.05	11.16	0.36	11.70	0.32	2.42	0.13	0.10
M1	2.07	38.41	11.35	0.46	10.69	0.17	1.10	0.10	0.07
M2	2.10	39.20	9.03	0.31	16.76	0.21	0.98	0.13	0.06

M = muscle mass; Lb = muscle belly length; Lf = sarcomere adjusted fibre length; TL/MTU = tendon length to muscle-tendon unit ratio; θ = pennation angle; PCSA = sarcomere adjusted physiological cross-sectional area; M/P_0 = muscle mass/predicted effective maximum tetanic tension; *I* = priority index of force; h = estimated excursion during muscle contraction.

Primate	Length	Width	Area
P1	0.709	0.342	0.202
P2	0.659	0.294	0.162
P3	0.711	0.491	0.215
M1	0.384	0.278	0.114
M2	0.177	0.456	0.071

Table 5.7 Body mass adjusted hard and soft-tissue data for the supraspinatus muscle. The insertion for the supraspinatus muscle to the humerus was via a tendinous sheet by the proximal epiphysis: fibrocartilaginous attachment.

Primate	M	L_b	L_f	TL/MTU	θ	PCSA	M/P_0	*I*	h
P1	1.67	17.60	13.71	0.37	7.15	0.11	2.49	0.08	0.18
P2	1.12	18.47	10.83	0.31	7.04	0.10	2.66	0.09	0.14
P3	1.30	16.80	11.90	0.35	6.42	0.10	2.54	0.09	0.17
M1	1.24	41.48	15.03	0.22	6.18	0.08	1.44	0.07	0.09
M2	1.23	33.75	9.88	0.24	16.82	0.11	1.08	0.10	0.07

M = muscle mass; Lb = muscle belly length; Lf = sarcomere adjusted fibre length; TL/MTU = tendon length to muscle-tendon unit ratio; θ = pennation angle; PCSA = sarcomere adjusted physiological cross-sectional area; M/P_0 = muscle mass/predicted effective maximum tetanic tension; *I* = priority index of force; h = estimated excursion during muscle contraction.

Primate	Length	Width	Area
P1	0.446	0.416	0.150
P2	0.987	0.363	0.252
P3	0.479	0.921	0.397
M1	0.443	0.164	0.079
M2	0.348	0.213	0.087

Table 5.8 Body mass adjusted hard and soft-tissue data for the infraspinatus muscle. The insertion for the infraspinatus muscle to the humerus was via a tendinous sheet by the proximal epiphysis: fibrocartilaginous attachment.

Primate	M	L_b	L_f	TL/MTU	θ	PCSA	M/P_0	*I*	h
P1	2.89	32.55	21.29	0.30	5.33	0.13	3.85	0.06	0.15
P2	2.89	32.31	11.36	0.25	10.31	0.24	2.81	0.12	0.08
P3	3.01	31.09	15.42	0.27	6.89	0.18	3.30	0.09	0.12
M1	1.33	42.52	19.24	0.32	4.12	0.07	1.84	0.05	0.11
M2	1.56	46.39	7.52	0.21	17.36	0.19	0.82	0.14	0.04

M = muscle mass; Lb = muscle belly length; Lf = sarcomere adjusted fibre length; TL/MTU = tendon length to muscle-tendon unit ratio; θ = pennation angle; PCSA = sarcomere adjusted physiological cross-sectional area; M/P_0 = muscle mass/predicted effective maximum tetanic tension; *I* = priority index of force; h = estimated excursion during muscle contraction.

Primate	Length	Width	Area
P1	0.665	0.838	0.382
P2	0.616	0.670	0.305
P3	0.522	0.483	0.221
M1	0.410	0.428	0.198
M2	0.232	0.301	0.118

Table 5.9 Body mass adjusted hard and soft-tissue data for the teres minor muscle. The insertion for the teres minor muscle to the humerus was via a tendinous sheet by the proximal epiphysis: fibrocartilaginous attachment.

Primate	M	L_b	L_f	TL/MTU	θ	PCSA	M/P_0	*I*	h
P1	0.62	19.25	12.37	0.30	4.75	0.05	2.23	0.06	0.15
P2	0.53	15.10	12.09	0.34	4.80	0.04	2.96	0.06	0.19
P3	0.53	15.57	12.06	0.33	4.09	0.04	2.57	0.06	0.18
M1	0.15	16.40	6.18	0.37	4.84	0.02	0.59	0.08	0.09
M2	1.70	20.67	4.76	0.38	18.06	0.32	0.52	0.23	0.06

M = muscle mass; Lb = muscle belly length; Lf = sarcomere adjusted fibre length; TL/MTU = tendon length to muscle-tendon unit ratio; θ = pennation angle; PCSA = sarcomere adjusted physiological cross-sectional area; M/P_0 = muscle mass/predicted effective maximum tetanic tension; *I* = priority index of force; h = estimated excursion during muscle contraction.

Primate	Length	Width	Area
P1	0.799	0.193	0.180
P2	0.858	0.231	0.167
P3	0.451	0.332	0.110
M1	0.277	0.204	0.038
M2	0.361	0.148	0.084

Table 5.10 Body mass adjusted hard and soft-tissue data for the teres major muscle. The insertion for the teres major muscle to the humerus was via a tendinous sheet on the humeral shaft: fibrocartilaginous attachment.

Primate	M	L_b	L_f	TL/MTU	θ	PCSA	M/P_0	*I*	h
P1	2.59	32.59	16.44	0.24	7.12	0.15	2.98	0.08	0.12
P2	2.22	32.12	12.19	0.31	7.53	0.17	3.00	0.10	0.09
P3	2.41	31.00	13.84	0.27	6.74	0.16	2.96	0.09	0.10
M1	0.82	33.08	22.04	0.42	5.08	0.04	2.11	0.04	0.16
M2	1.91	36.07	18.40	0.39	15.26	0.09	1.99	0.06	0.12

M = muscle mass; Lb = muscle belly length; Lf = sarcomere adjusted fibre length; TL/MTU = tendon length to muscle-tendon unit ratio; θ = pennation angle; PCSA = sarcomere adjusted physiological cross-sectional area; M/P_0 = muscle mass/predicted effective maximum tetanic tension; *I* = priority index of force; h = estimated excursion during muscle contraction.

Primate	Length*	Width*	Area*	Length°	Width°	Area°
P1	1.923	0.291	0.457	0.391	0.059	0.356
P2	1.090	0.127	0.199	0.222	0.026	0.210
P3	1.541	0.230	0.276	0.283	0.042	0.229
M1	1.314	0.163	0.207	0.174	0.022	0.056
M2	1.594	0.121	0.204	0.296	0.023	0.084

* Body mass adjusted variables
° CA adjusted variables

Table 5.11 Body mass adjusted hard and soft-tissue data for the coracobrachialis muscles. The insertion of the coracobrachialis muscle on the humerus was via direct attachment of muscle fibres to the humeral shaft: fibrous attachment.

Primate/Muscle	M	L_b	L_f	TL/MTU	θ	PCSA	M/P_0	*I*	h
Cb medius									
P1	1.36	24.89	8.31	0.51	9.10	0.15	1.52	0.12	0.08
P2	1.02	19.24	13.87	0.52	6.50	0.07	3.40	0.07	0.17
P3	1.12	28.42	7.87	0.44	9.53	0.13	1.69	0.12	0.07
M1	0.11	203.86	9.82	0.11	6.93	0.01	0.94	0.05	0.01
M2	0.17	19.96	7.94	0.57	9.26	0.02	0.84	0.07	0.09
Cb profundus									
P1	-	-	-	-	-	-	-	-	-
P2	-	-	-	-	-	-	-	-	-
P3	-	-	-	-	-	-	-	-	-
M1	0.07	11.01	7.76	0.41	7.61	0.01	0.75	0.05	0.17
M2	0.05	12.04	6.03	0.44	11.96	0.01	0.64	0.05	0.12

M = muscle mass; Lb = muscle belly length; Lf = sarcomere adjusted fibre length; TL/MTU = tendon length to muscle-tendon unit ratio; θ = pennation angle; PCSA = sarcomere adjusted physiological cross-sectional area; M/P_0 = muscle mass/predicted effective maximum tetanic tension; *I* = priority index of force; h = estimated excursion during muscle contraction.

Primate/Muscle	Length*	Width*	Area*	Length°	Width°	Area°
Cb medius						
P1	2.149	0.302	0.466	0.430	0.060	0.357
P2	1.143	0.305	0.305	0.225	0.060	0.312
P3	1.348	0.252	0.246	0.225	0.042	0.185
M1	1.182	0.108	0.120	0.140	0.013	0.029
M2	0.766	0.067	0.097	0.130	0.011	0.037
Cb profundus						
P1	-	-	-	-	-	-
P2	-	-	-	-	-	-
P3	-	-	-	-	-	-
M1	0.364	0.206	0.056	-	-	-
M2	0.336	0.107	0.020	-	-	-

* Body mass adjusted variables

° CA adjusted variables

Table 5.12 Body mass adjusted hard and soft-tissue data for the brachialis muscle. The origin of the brachialis muscle on the humerus was via direct attachment of muscle fibres to the humeral shaft: fibrous attachment.

Primate	M	L_b	L_f	TL/MTU	θ	PCSA	M/P_0	*I*	h
P1	2.56	27.03	14.21	0.43	8.47	0.17	2.59	0.09	0.12
P2	4.39	26.78	15.12	0.42	6.36	0.27	3.71	0.10	0.13
P3	4.05	45.10	11.85	0.29	8.22	0.32	2.54	0.13	0.06
M1	0.80	54.15	19.55	0.30	7.04	0.04	1.88	0.04	0.08
M2	0.94	35.54	10.59	0.31	12.91	0.08	1.13	0.09	0.07

M = muscle mass; Lb = muscle belly length; Lf = sarcomere adjusted fibre length; TL/MTU = tendon length to muscle-tendon unit ratio; θ = pennation angle; PCSA = sarcomere adjusted physiological cross-sectional area; M/P_0 = muscle mass/predicted effective maximum tetanic tension; *I* = priority index of force; h = estimated excursion during muscle contraction.

Primate	Length*	Width*	Area*	Length°	Width°	Area°
P1	3.439	0.716	3.062	0.656	0.136	2.239
P2	3.098	0.834	1.872	0.625	0.168	1.961
P3	3.549	0.853	2.528	0.635	0.153	2.047
M1	2.662	0.570	1.368	0.301	0.064	0.314
M2	3.216	0.492	1.460	0.539	0.083	0.544

* Body mass adjusted variables
° CA adjusted variables

Table 5.13 Body mass adjusted soft-tissue data for the biceps brachii muscle (does not have an attachment on the humerus).

Primate	M	L_b	L_f	TL/MTU	θ	PCSA	M/P_0	*I*	h
P1	2.90	30.18	18.02	0.55	4.98	0.15	3.26	0.07	0.14
P2	2.93	24.78	16.78	0.53	5.28	0.16	4.11	0.08	0.16
P3	3.04	36.95	14.26	0.46	5.61	0.20	3.04	0.10	0.09
M1	2.30	7.27	21.84	0.83	6.49	0.10	2.10	0.06	0.71
M2	3.37	55.03	23.35	0.37	10.00	0.13	2.48	0.06	0.10

M = muscle mass; Lb = muscle belly length; Lf = sarcomere adjusted fibre length; TL/MTU = tendon length to muscle-tendon unit ratio; θ = pennation angle; PCSA = sarcomere adjusted physiological cross-sectional area; M/P_0 = muscle mass/predicted effective maximum tetanic tension; *I* = priority index of force; h = estimated excursion during muscle contraction.

Table 5.14 Body mass adjusted hard and soft-tissue data for the triceps brachii and dorsoepitrochlearis muscles. The medial origin of the triceps muscle on the humerus was via direct attachment of muscle fibres to the humeral shaft: fibrous attachment. The lateral origin of the triceps muscle and the insertion of the dorsoepitrochlearis muscle on the humerus was a tendinous sheet on the humeral shaft towards the distal metaphysis: fibrocartilaginous attachment.

Primate/Muscle	M	L_b	L_f	TL/MTU	θ	PCSA	M/P_0	*I*	h
TB									
P1	6.28	27.12	19.89	0.58	6.19	0.30	3.60	0.09	0.17
P2	7.51	21.75	18.60	0.57	10.11	0.38	4.61	0.10	0.20
P3	7.54	48.94	15.65	0.39	9.67	0.45	3.37	0.12	0.08
M1	4.37	63.54	22.03	0.45	5.82	0.19	2.11	0.07	0.08
M2	7.75	57.42	16.54	0.42	14.60	0.43	1.78	0.11	0.07
De									
P1	0.78	21.55	16.12	0.50	3.13	0.05	2.91	0.05	0.17
P2	0.67	29.36	12.16	0.37	4.53	0.05	2.97	0.07	0.10
P3	0.69	24.89	13.66	0.43	3.23	0.05	2.90	0.06	0.13
M1	-	-	-	-	-	-	-	-	-
M2	0.92	34.42	14.42	0.49	8.19	0.06	1.52	0.06	0.10

M = muscle mass; Lb = muscle belly length; Lf = sarcomere adjusted fibre length; TL/MTU = tendon length to muscle-tendon unit ratio; θ = pennation angle; PCSA = sarcomere adjusted physiological cross-sectional area; M/P_0 = muscle mass/predicted effective maximum tetanic tension; *I* = priority index of force; h = estimated excursion during muscle contraction.

Primate/Muscle	Length*	Width*	Area*	Length°	Width°	Area°
TB lateral						
P1	2.911	0.212	0.542	0.587	0.043	0.419
P2	2.603	0.156	0.247	0.543	0.033	0.268
P3	2.561	0.171	0.417	0.416	0.028	0.306
M1	2.317	0.189	0.234	0.268	0.022	0.055
M2	2.568	0.196	0.461	0.406	0.031	0.162
TB medial						
P1	5.306	0.712	2.852	0.971	0.130	2.001
P2	4.137	0.726	2.538	0.966	0.169	3.076
P3	4.229	0.827	2.578	0.701	0.137	1.933
M1	2.653	0.641	1.410	0.317	0.077	0.342
M2	0.388	0.181	0.048	0.040	0.019	0.011

* Body mass adjusted variables
° CA adjusted variables

Table 5.15 Body mass adjusted hard and soft-tissue data for the anconeus muscle. The origin for the anconeus muscle to the humerus was via a tendinous sheet by the distal epiphysis: fibrocartilaginous attachment.

Primate	M	L_b	L_f	TL/MTU	θ	PCSA	M/P_0	*I*	h
P1	0.04	8.99	5.72	0.40	7.04	0.01	1.04	0.05	0.15
P2	0.10	7.44	4.86	0.44	10.39	0.02	1.20	0.09	0.16
P3	0.08	7.89	5.10	0.42	7.27	0.01	1.09	0.08	0.15
M1	-	-	-	-	-	-	-	-	-
M2	0.05	8.53	4.23	0.47	12.15	0.01	0.45	0.08	0.12

M = muscle mass; Lb = muscle belly length; Lf = sarcomere adjusted fibre length; TL/MTU = tendon length to muscle-tendon unit ratio; θ = pennation angle; PCSA = sarcomere adjusted physiological cross-sectional area; M/P_0 = muscle mass/predicted effective maximum tetanic tension; *I* = priority index of force; h = estimated excursion during muscle contraction.

Primate	Length	Width	Area
P1	0.366	0.226	0.061
P2	0.443	0.169	0.067
P3	0.380	0.284	0.111
M1	0.206	0.113	0.025
M2	0.701	0.469	0.244

Table 5.16 Body mass adjusted hard and soft-tissue data for the pronator teres muscle. The origin for the pronator teres muscle to the humerus was via direct attachment of muscle fibres to the humeral shaft: fibrous attachment.

Primate	M	L_b	L_f	TL/MTU	θ	PCSA	M/P_0	*I*	h
P1	0.39	15.80	12.23	0.60	5.41	0.03	2.21	0.06	0.18
P2	0.90	20.76	9.65	0.50	7.07	0.09	2.37	0.09	0.11
P3	0.74	17.36	10.59	0.54	5.50	0.07	2.26	0.08	0.14
M1	0.43	35.18	20.80	0.45	2.86	0.02	1.99	0.03	0.14
M2	0.70	28.27	7.37	0.47	2.61	0.08	0.85	0.10	0.07

M = muscle mass; Lb = muscle belly length; Lf = sarcomere adjusted fibre length; TL/MTU = tendon length to muscle-tendon unit ratio; θ = pennation angle; PCSA = sarcomere adjusted physiological cross-sectional area; M/P_0 = muscle mass/predicted effective maximum tetanic tension; *I* = priority index of force; h = estimated excursion during muscle contraction.

Primate	Length	Width	Area
P1	0.474	0.158	0.079
P2	0.606	0.223	0.158
P3	0.448	0.097	0.050
M1	0.390	0.104	0.048
M2	0.589	0.108	0.071

Table 5.17 Body mass adjusted hard and soft-tissue data for the brachioradialis muscle. The origin for the brachioradialis muscle to the humerus was via direct attachment of muscle fibres to the humeral shaft: fibrous attachment.

Primate	M	L_b	L_f	TL/MTU	θ	PCSA	M/P_0	*I*	h
P1	2.07	53.05	15.67	0.43	7.19	0.12	2.84	0.08	0.07
P2	3.92	50.27	13.48	0.40	7.24	0.27	3.31	0.11	0.06
P3	3.53	45.10	18.07	0.44	5.25	0.18	3.85	0.08	0.09
M1	1.08	58.50	27.61	0.36	3.83	0.04	2.64	0.04	0.11
M2	0.77	55.97	14.69	0.32	8.22	0.05	1.55	0.06	0.06

M = muscle mass; Lb = muscle belly length; Lf = sarcomere adjusted fibre length; TL/MTU = tendon length to muscle-tendon unit ratio; θ = pennation angle; PCSA = sarcomere adjusted physiological cross-sectional area; M/P_0 = muscle mass/predicted effective maximum tetanic tension; *I* = priority index of force; h = estimated excursion during muscle contraction.

Primate	Length	Width	Area
P1	2.291	0.135	0.308
P2	1.321	0.207	0.180
P3	1.724	0.132	0.194
M1	1.505	0.152	0.208
M2	1.585	0.129	0.159

Table 5.18 Body mass adjusted hard and soft-tissue data for the extensor carpi radialis longus muscle. The origin for the extensor carpi radialis longus muscle to the humerus was via a tendinous sheet by the distal metaphysis: fibrocartilaginous attachment.

Primate	M	L_b	L_f	TL/MTU	θ	PCSA	M/P_0	*I*	h
P1	0.49	31.71	20.52	0.69	4.45	0.02	3.71	0.04	0.15
P2	0.46	28.12	15.73	0.73	5.49	0.03	3.85	0.05	0.13
P3	0.44	28.32	17.60	0.72	4.51	0.02	3.75	0.04	0.15
M1	0.32	39.29	21.94	0.63	5.25	0.01	2.10	0.03	0.13
M2	0.44	37.45	17.43	0.61	6.32	0.02	1.83	0.04	0.11

M = muscle mass; Lb = muscle belly length; Lf = sarcomere adjusted fibre length; TL/MTU = tendon length to muscle-tendon unit ratio; θ = pennation angle; PCSA = sarcomere adjusted physiological cross-sectional area; M/P_0 = muscle mass/predicted effective maximum tetanic tension; *I* = priority index of force; h = estimated excursion during muscle contraction.

Primate	Length	Width	Area
P1	0.413	0.199	0.046
P2	0.956	0.149	0.118
P3	0.544	0.124	0.061
M1	0.184	0.249	0.038
M2	0.161	0.117	0.020

Table 5.19 Body mass adjusted hard and soft-tissue data for the common flexor muscles. Palmaris longus, flexor carpi radialis, flexor carpi ulnaris, and flexor digitorum superficialis all share a common origin on the medial epicondyle of the humerus. All flexors share a common tendinous sheet: fibrocartilaginous attachment.

Primate/Muscle		M	L_b	L_f	TL/MTU	θ	PCSA	M/P_0	*I*	h
PL										
	P1	0.34	27.76	18.73	0.66	5.93	0.02	3.39	0.04	0.16
	P2	0.50	27.18	15.37	0.61	9.31	0.03	3.80	0.05	0.13
	P3	0.42	26.11	16.63	0.64	7.23	0.02	3.56	0.04	0.15
	M1	0.23	41.74	24.10	0.61	2.66	0.01	2.30	0.02	0.13
	M2	0.35	49.29	6.79	0.53	15.13	0.05	0.73	0.10	0.03
FCR										
	P1	0.44	39.02	14.40	0.51	6.57	0.03	2.61	0.05	0.09
	P2	1.08	29.27	12.02	0.51	6.00	0.08	2.95	0.08	0.10
	P3	0.89	32.08	12.88	0.52	5.64	0.07	2.75	0.07	0.09
	M1	0.49	45.93	11.14	0.51	9.12	0.04	1.08	0.07	0.06
	M2	0.58	44.93	9.51	0.50	8.46	0.06	1.00	0.08	0.05
FCU										
	P1	0.78	29.72	18.28	0.59	3.58	0.04	3.30	0.05	0.14
	P2	1.03	38.46	14.64	0.50	5.19	0.07	3.58	0.06	0.09
	P3	0.95	33.42	16.02	0.54	3.90	0.06	3.41	0.06	0.11
	M1	0.40	68.70	26.94	0.48	2.84	0.01	2.57	0.03	0.09
	M2	1.16	51.61	11.21	0.51	16.46	0.09	1.22	0.09	0.05
FDS										
	P1	0.76	52.53	15.56	0.65	14.77	0.04	2.90	0.05	0.07
	P2	2.74	41.49	12.13	0.65	15.63	0.21	3.07	0.11	0.07
	P3	1.70	44.83	13.43	0.66	14.68	0.12	2.95	0.08	0.07
	M1	0.81	45.47	15.47	0.57	7.11	0.05	1.49	0.06	0.08
	M2	1.09	53.07	13.91	0.55	8.68	0.07	1.47	0.07	0.06

M = muscle mass; Lb = muscle belly length; Lf = sarcomere adjusted fibre length; TL/MTU = tendon length to muscle-tendon unit ratio; θ = pennation angle; PCSA = sarcomere adjusted physiological cross-sectional area; M/P_0 = muscle mass/predicted effective maximum tetanic tension; *I* = priority index of force; h = estimated excursion during muscle contraction.

Primate	Length	Width	Area
P1	0.580	0.267	0.188
P2	0.914	0.405	0.319
P3	0.681	0.460	0.289
M1	0.663	0.358	0.204
M2	0.666	0.525	0.253

Table 5.20 Body mass adjusted hard and soft-tissue data for the common extensor muscles. Supinator, extensor carpi radialis brevis, extensor carpi radialis longus, extensor digitorum, and extensor digitorum mini all share a common origin on the lateral epicondyle of the humerus. All extensors and supinator share a common tendinous sheet: fibrocartilaginous attachment.

Primate/Muscle	M	L_b	L_f	TL/MTU	θ	PCSA	M/P_0	*I*	h
Supinator									
P1	0.39	12.86	6.17	0.47	7.43	0.06	1.12	0.11	0.11
P2	0.90	11.76	5.68	0.54	9.33	0.15	1.40	0.16	0.11
P3	0.74	10.94	5.74	0.51	7.12	0.12	1.23	0.15	0.12
M1	0.27	27.33	7.00	0.51	14.37	0.04	0.69	0.09	0.06
M2	0.22	23.39	5.35	0.48	19.69	0.04	0.59	0.10	0.06
ECRB									
P1	0.43	26.24	18.04	0.70	9.05	0.02	3.29	0.04	0.16
P2	1.08	20.55	13.64	0.72	10.92	0.07	3.39	0.07	0.16
P3	0.89	21.66	15.35	0.72	9.49	0.05	3.30	0.06	0.17
M1	0.42	51.89	24.40	0.57	4.17	0.02	2.33	0.03	0.11
M2	0.49	42.24	14.76	0.57	7.60	0.03	1.56	0.05	0.08
ECU									
P1	0.36	46.80	11.98	0.37	12.26	0.03	2.21	0.06	0.06
P2	0.80	50.56	9.38	0.31	11.98	0.08	2.34	0.09	0.04
P3	0.66	47.61	10.33	0.33	11.40	0.06	2.24	0.08	0.05
M1	0.40	68.70	26.94	0.48	2.84	0.01	2.57	0.03	0.09
M2	0.45	66.87	10.05	0.42	9.42	0.04	1.06	0.07	0.04
ED									
P1	0.62	53.09	19.45	0.62	6.46	0.03	3.52	0.04	0.09
P2	1.25	47.63	14.94	0.61	6.94	0.08	3.67	0.07	0.07
P3	1.07	48.59	16.69	0.61	6.22	0.06	3.57	0.06	0.08
M1	0.46	54.21	15.21	0.61	4.99	0.03	1.46	0.05	0.07
M2	0.45	57.34	14.00	0.46	7.40	0.03	1.47	0.05	0.06
EDM									
P1	0.25	55.81	23.32	0.51	4.77	0.01	4.21	0.03	0.10
P2	0.54	59.77	18.06	0.46	5.41	0.03	4.42	0.04	0.07
P3	0.42	56.71	20.12	0.48	4.69	0.02	4.29	0.04	0.08
M1	0.17	45.80	15.41	0.61	4.76	0.01	1.48	0.03	0.08
M2	0.14	54.17	14.51	0.48	5.42	0.01	1.52	0.03	0.06

M = muscle mass; Lb = muscle belly length; Lf = sarcomere adjusted fibre length; TL/MTU = tendon length to muscle-tendon unit ratio; θ = pennation angle; PCSA = sarcomere adjusted physiological cross-sectional area; M/P_0 = muscle mass/predicted effective maximum tetanic tension; *I* = priority index of force; h = estimated excursion during muscle contraction.

Primate	Length	Width	Area
P1	0.577	0.306	0.126
P2	0.792	0.254	0.186
P3	0.477	0.409	0.145
M1	0.383	0.306	0.161
M2	0.354	0.522	0.161

Table 5.21 Body mass adjusted biomechanical variables for the cross sections at the latissimus dorsi attachment with the one sample t-test (two-tailed) comparing the proximal, midpoint and distal properties of the enthesis. Bold = significant ($P \leq 0.05$).

Variable	P1	P2	P3	M1	M2
Proximal					
TA	92.20	85.88	100.55	35.11	28.36
CA	24.23	19.87	26.82	15.84	11.31
MA	67.97	66.01	73.73	19.28	17.05
Ix	16311.16	30925.89	39002.36	734.08	568.58
Iy	20012.16	32544.13	31833.10	475.61	362.50
Imax	21002.77	32667.17	39957.30	768.60	581.19
Imin	15320.54	41706.83	30878.17	441.08	349.89
Imax/Imin	1.37	1.06	1.29	1.74	1.66
J	36323.32	63470.01	70835.47	1209.68	931.08
Theta	24.68	14.886	-71.08	-71.05	-76.50
Zx	633.41	1287.69	1270.34	87.07	70.76
Zy	778.38	1461.40	1129.85	68.10	55.46
Zy/Zx	1.23	1.13	0.89	0.78	0.78
Zp	5413.69	7767.75	10882.16	319.03	284.22
Midpoint					
TA	41.60	29.64	39.95	31.64	21.83
CA	14.54	22.51	23.46	14.89	10.97
MA	27.06	7.14	16.50	16.76	10.86
Ix	4412.32	8879.23	8981.97	669.75	422.40
Iy	4628.10	10083.06	11098.60	384.31	244.55
Imax	4704.31	10817.29	11161.72	675.43	424.57
Imin	4336.11	11028.27	8918.85	378.63	242.38
Imax/Imin	1.08	1.33	1.25	1.78	1.75
J	9040.42	18962.29	20080.57	1054.05	666.95
Theta	27.06	-31.612	-9.66	-82.05	83.74
Zx	307.25	678.58	534.52	78.27	61.08
Zy	313.80	778.64	640.67	56.67	42.22

	Zy/Zx	1.02	1.15	1.20	0.72	0.69
	Zp	2382.02	4125.85	5322.13	279.40	233.45
Distal						
	TA	34.18	37.39	34.50	32.71	23.06
	CA	15.72	27.54	21.77	16.84	12.08
	MA	18.46	9.85	12.73	15.86	10.99
	Ix	4126.82	15238.43	8729.48	763.27	476.33
	Iy	3306.26	14821.51	6893.71	455.05	296.76
	Imax	4145.31	19289.28	9195.46	772.79	482.99
	Imin	3287.77	14583.40	6427.73	445.53	290.10
	Imax/Imin	1.26	1.79	1.43	1.73	1.66
	J	7433.08	30059.94	15623.19	1218.32	773.09
	Theta	-81.56	-46.403	-65.78	-80.18	79.29
	Zx	300.07	1083.82	523.28	87.32	69.57
	Zy	257.09	1052.53	474.27	62.23	50.13
	Zy/Zx	0.86	0.97	0.91	0.71	0.72
	Zp	2142.22	6050.77	4526.69	308.56	269.35
			One sample t test			
	TA	0.092	0.101	0.11	**0.001**	**0.007**
	CA	**0.027**	**0.009**	**0.004**	**0.001**	**0.001**
	MA	0.132	0.286	0.224	**0.003**	**0.024**
	Ix	0.175	0.107	0.201	**0.001**	**0.008**
	Iy	0.224	0.107	0.164	**0.004**	**0.013**
	Imax	0.214	0.081	0.181	**0.002**	**0.008**
	Imin	0.185	0.147	0.186	**0.003**	**0.011**
	Imax/Imin	**0.005**	0.023	**0.002**	**<0.001**	**<0.001**
	J	0.201	0.107	0.183	**0.002**	**0.009**
	Theta	0.807	0.373	0.131	**0.002**	0.639
	Zx	0.064	**0.03**	0.088	**0.001**	**0.002**
	Zy	0.112	**0.031**	0.063	**0.003**	**0.006**
	Zy/Zx	**0.011**	**0.003**	**0.01**	**0.001**	**0.001**
	Zp	0.088	**0.03**	0.074	**0.002**	**0.003**

Table 5.22 Body mass adjusted biomechanical variables for the cross sections at the pectoralis attachment with the one sample t-test (two-tailed) comparing the proximal, midpoint and distal properties of the enthesis. Bold = significant ($P \leq 0.05$).

Variable	P1	P2	P3	M1	M2
Proximal					
TA	41.08	29.68	38.37	33.13	21.91
CA	14.79	22.94	22.88	16.43	12.35
MA	26.29	6.73	15.49	16.70	9.56
Ix	4474.34	9066.90	8799.94	737.92	456.85
Iy	4485.50	10152.95	9769.46	431.13	262.90
Imax	4499.80	11093.40	10011.53	759.28	458.70
Imin	4460.05	11003.15	8557.87	409.76	261.05
Imax/Imin	1.01	1.37	1.17	1.85	1.76
J	8959.85	19219.85	18569.40	1169.04	719.75
Theta	-36.85	-34.264	-24.08	-75.69	84.45
Zx	314.99	683.49	529.60	91.19	63.26
Zy	308.80	753.02	594.22	63.86	44.30
Zy/Zx	0.98	1.10	1.12	0.70	0.70
Zp	2391.96	4070.27	5080.94	320.20	243.33
Midpoint					
TA	34.21	37.26	35.31	32.91	22.14
CA	16.69	27.54	26.50	16.93	11.73
MA	17.52	9.73	8.82	15.98	10.41
Ix	4175.76	14977.34	9765.87	776.43	447.24
Iy	3615.93	14868.69	7804.39	450.68	267.82
Imax	4188.77	19237.19	9866.61	782.02	450.49
Imin	3602.92	14364.28	7703.65	445.09	264.56
Imax/Imin	1.16	1.81	1.28	1.76	1.70
J	7791.70	29846.02	17570.26	1227.11	715.05
Theta	-81.43	-45.361	-77.54	-82.60	82.40
Zx	307.36	1061.20	539.95	87.85	63.16
Zy	280.41	1069.37	521.51	60.06	46.76

	Zy/Zx	0.91	1.01	0.97	0.68	0.74
	Zp	2256.74	6034.28	4808.34	305.27	248.32
Distal						
	TA	36.66	29.68	37.19	31.34	23.40
	CA	21.42	22.94	25.27	17.59	12.67
	MA	15.25	6.73	11.92	13.75	10.74
	Ix	4110.87	9066.90	10710.40	651.81	494.33
	Iy	6324.33	10152.95	9741.00	462.67	314.54
	Imax	6449.70	11093.40	13377.19	694.85	500.48
	Imin	3985.49	11003.15	7074.20	419.64	308.39
	Imax/Imin	1.62	1.37	1.89	1.66	1.62
	J	10435.19	19219.85	20451.39	1114.49	808.87
	Theta	13.04	-34.264	-49.42	-66.71	79.69
	Zx	299.90	683.49	571.14	81.77	70.35
	Zy	403.60	753.02	533.15	68.40	53.53
	Zy/Zx	1.35	1.10	0.93	0.84	0.76
	Zp	2724.46	4070.27	4996.41	307.48	278.86
				One sample t test		
	TA	**0.003**	**0.006**	**0.001**	**<0.001**	**<0.001**
	CA	**0.012**	**0.004**	**0.002**	**<0.001**	**0.001**
	MA	**0.028**	**0.016**	**0.025**	**0.003**	**0.001**
	Ix	**0.001**	**0.03**	**0.003**	**0.003**	**0.001**
	Iy	**0.026**	**0.018**	**0.005**	**<0.001**	**0.003**
	Imax	**0.019**	**0.037**	**0.011**	**0.001**	**0.001**
	Imin	**0.004**	**0.008**	**0.003**	**0.001**	**0.003**
	Imax/Imin	**0.02**	**0.009**	**0.023**	**0.001**	**0.001**
	J	**0.007**	**0.023**	**0.002**	**0.001**	**0.002**
	Theta	0.327	**0.009**	0.083	**0.004**	**<0.001**
	Zx	**<0.001**	**0.023**	**0.001**	**0.001**	**0.001**
	Zy	**0.012**	**0.015**	**0.002**	**0.001**	**0.003**
	Zy/Zx	**0.016**	**0.001**	**0.003**	**0.005**	**0.001**
	Zp	**0.003**	**0.019**	**<0.001**	**<0.001**	**0.002**

Table 5.23 Body mass adjusted biomechanical variables for the cross sections at the deltoideus attachment with the one sample t-test (two-tailed) comparing the proximal, midpoint and distal properties of the enthesis. Bold = significant ($P \leq 0.05$).

Variable	P1	P2	P3	M1	M2
Proximal					
TA	34.21	37.89	39.93	31.66	21.99
CA	17.59	27.68	21.44	14.89	12.56
MA	16.62	10.22	18.49	16.77	9.43
Ix	4352.11	15696.44	8562.04	652.12	475.12
Iy	3714.41	14996.20	10323.51	376.77	272.47
Imax	4352.63	19811.74	10471.51	654.37	481.67
Imin	3713.89	14732.67	8414.03	374.52	265.92
Imax/Imin	1.17	1.82	1.24	1.75	1.81
J	8066.52	30692.65	18885.55	1028.89	747.59
Theta	-88.36	-47.249	-15.56	-84.85	79.97
Zx	320.35	1092.88	503.32	80.05	66.89
Zy	285.00	1072.17	611.90	54.26	48.16
Zy/Zx	0.89	0.98	1.22	0.68	0.72
Zp	2324.31	6132.92	5041.59	277.20	260.58
Midpoint					
TA	35.50	34.23	35.81	32.90	20.91
CA	20.32	24.30	27.08	16.67	13.76
MA	15.18	9.93	8.73	16.22	7.14
Ix	4218.52	13765.00	9135.65	695.40	398.97
Iy	5264.90	10548.46	8965.59	475.88	288.05
Imax	5707.95	14290.51	10099.44	726.43	403.14
Imin	3775.47	13571.01	8001.79	444.85	283.88
Imax/Imin	1.51	1.43	1.26	1.63	1.42
J	9483.42	24313.46	18101.23	1171.28	687.02
Theta	28.61	69.457	-47.33	-70.61	-79.22
Zx	321.63	927.72	519.00	81.87	63.62
Zy	348.79	780.10	554.47	67.59	53.88

	Zy/Zx	1.08	0.84	1.07	0.83	0.85
	Zp	2578.30	4856.51	4848.01	306.54	263.03
Distal						
	TA	34.03	30.85	33.41	26.46	19.50
	CA	21.07	20.70	24.05	18.31	13.99
	MA	12.96	10.16	9.36	8.15	5.51
	Ix	4311.63	11849.76	8533.31	454.68	254.18
	Iy	4782.38	7701.87	7081.01	405.11	406.88
	Imax	4851.89	11859.63	8622.36	506.22	421.83
	Imin	4242.12	10414.91	6991.95	353.56	239.24
	Imax/Imin	1.14	1.54	1.23	1.43	1.76
	J	9094.01	19551.63	15614.31	859.78	661.07
	Theta	19.73	-87.210	-76.48	-54.47	-16.63
	Zx	315.66	820.05	497.63	73.81	46.40
	Zy	329.88	653.93	425.90	68.28	54.43
	Zy/Zx	1.05	0.80	0.86	0.93	1.17
	Zp	2477.24	4222.75	4181.71	289.05	227.01
			One sample t test			
	TA	**<0.001**	**0.003**	**0.003**	**0.004**	**0.001**
	CA	**0.003**	**0.007**	**0.005**	**0.004**	**0.001**
	MA	**0.005**	**<0.001**	0.061	**0.039**	**0.023**
	Ix	**<0.001**	**0.006**	**0.001**	**0.015**	**0.028**
	Iy	**0.01**	**0.035**	**0.011**	**0.005**	**0.017**
	Imax	**0.006**	**0.023**	**0.003**	**0.01**	**0.003**
	Imin	**0.002**	**0.01**	**0.003**	**0.005**	**0.002**
	Imax/Imin	**0.009**	**0.005**	**<0.001**	**0.003**	**0.005**
	J	**0.002**	**0.016**	**0.003**	**0.008**	**0.001**
	Theta	0.757	0.69	0.118	**0.015**	0.919
	Zx	**<0.001**	**0.007**	**<0.001**	**0.001**	**0.011**
	Zy	**0.003**	**0.021**	**0.011**	**0.005**	**0.001**
	Zy/Zx	**0.003**	**0.004**	**0.01**	**0.008**	**0.021**
	Zp	**0.001**	**0.012**	**0.003**	**0.001**	**0.002**

Table 5.24 Body mass adjusted biomechanical variables for the cross sections at the teres major attachment with the one sample t-test (two-tailed) comparing the proximal, midpoint and distal properties of the enthesis. Bold = significant ($P \leq 0.05$).

Variable	P1	P2	P3	M1	M2
Proximal					
TA	37.19	31.24	39.93	41.69	32.29
CA	14.35	21.73	21.77	17.43	12.17
MA	22.84	9.51	18.16	24.26	20.12
Ix	4140.38	8613.91	8559.22	991.85	704.67
Iy	3652.15	11814.80	10605.11	682.14	447.96
Imax	4257.65	11975.83	10674.79	1057.25	711.04
Imin	3534.87	11445.14	8489.54	616.74	441.59
Imax/Imin	1.20	1.42	1.26	1.71	1.61
J	7792.53	20428.71	19164.33	1673.98	1152.63
Theta	-66.25	-12.345	-10.29	-67.34	-81.16
Zx	294.85	674.46	504.20	100.30	83.22
Zy	276.05	806.75	622.98	87.02	68.05
Zy/Zx	0.94	1.20	1.24	0.87	0.82
Zp	2191.53	4220.87	5098.48	383.91	340.65
Midpoint					
TA	35.24	32.94	33.94	31.60	21.88
CA	18.86	25.52	24.68	15.32	11.97
MA	16.38	7.42	9.26	16.28	9.90
Ix	4248.16	11627.33	9716.76	675.18	461.99
Iy	4610.23	11935.98	6570.02	394.23	257.58
Imax	4673.84	14189.59	9807.02	680.99	467.05
Imin	4184.55	12691.95	6479.77	388.42	252.52
Imax/Imin	1.12	1.51	1.51	1.75	1.85
J	8858.40	23563.31	16286.79	1069.41	719.56
Theta	21.13	-43.163	-80.52	-81.90	81.17
Zx	304.37	886.61	512.15	80.95	66.83
Zy	326.80	913.03	459.59	59.62	44.14

	Zy/Zx	1.07	1.03	0.90	0.74	0.66
	Zp	2420.93	5097.04	4428.16	290.77	251.05
Distal						
	TA	35.65	38.10	37.27	33.36	23.92
	CA	20.06	28.27	25.41	16.69	13.60
	MA	15.59	9.83	11.85	16.67	10.32
	Ix	4048.86	16210.68	10677.89	744.27	502.84
	Iy	5441.18	15000.21	9959.15	480.94	350.33
	Imax	5728.37	20067.58	13574.98	750.84	502.85
	Imin	3761.67	15087.97	7062.06	474.36	350.33
	Imax/Imin	1.52	1.80	1.92	1.58	1.44
	J	9490.04	31210.89	20637.04	1225.21	853.18
	Theta	22.47	-48.898	-48.17	-81.13	-89.57
	Zx	316.58	1121.16	568.37	87.59	73.02
	Zy	348.19	1072.41	531.35	64.62	59.35
	Zy/Zx	1.10	0.96	0.93	0.74	0.81
	Zp	2561.44	6215.21	4973.71	312.49	296.72
			One sample t test			
	TA	**<0.001**	**0.004**	**0.002**	**0.008**	**0.015**
	CA	**0.009**	**0.006**	**0.002**	**0.001**	**0.002**
	MA	**0.015**	**0.007**	**0.038**	**0.018**	0.056
	Ix	**<0.001**	**0.031**	**0.004**	**0.014**	**0.018**
	Iy	**0.013**	**0.006**	**0.019**	**0.026**	**0.024**
	Imax	**0.008**	**0.024**	**0.01**	**0.019**	**0.018**
	Imin	**0.002**	**0.007**	**0.007**	**0.018**	**0.024**
	Imax/Imin	**0.009**	**0.005**	**0.015**	**0.001**	**0.005**
	J	**0.003**	**0.016**	**0.005**	**0.018**	**0.019**
	Theta	0.821	0.092	0.15	**0.004**	0.645
	Zx	**<0.001**	**0.02**	**0.001**	**0.004**	**0.004**
	Zy	**0.005**	**0.007**	**0.008**	**0.014**	**0.015**
	Zy/Zx	**0.002**	**0.004**	**0.011**	**0.003**	**0.005**
	Zp	**0.002**	**0.012**	**0.002**	**0.007**	**0.008**

Table 5.25 Body mass adjusted biomechanical variables for the cross sections at the coracobrachialis attachment with the one sample t-test (two-tailed) comparing the proximal, midpoint and distal properties of the enthesis. Bold = significant ($P \leq 0.05$).

Variable	P1	P2	P3	M1	M2
Proximal					
TA	40.51	36.18	33.71	37.70	21.92
CA	15.12	27.06	23.63	14.71	11.77
MA	25.39	9.12	10.08	22.99	10.15
Ix	4631.10	14034.70	9288.31	734.80	443.19
Iy	4311.42	14258.62	6499.51	515.67	260.09
Imax	4653.59	18025.93	9434.66	777.65	448.24
Imin	4288.93	13901.97	6353.15	472.82	255.05
Imax/Imin	1.09	1.76	1.49	1.64	1.76
J	8942.52	28293.32	15787.82	1250.47	703.28
Theta	-75.62	-44.173	-77.41	-67.98	80.70
Zx	326.13	1031.84	499.89	81.78	63.01
Zy	292.69	1012.32	466.17	69.50	43.54
Zy/Zx	0.90	0.98	0.93	0.85	0.69
Zp	2370.79	5788.75	4390.76	309.90	240.49
Midpoint					
TA	35.25	37.20	36.07	31.70	23.27
CA	19.19	26.40	27.10	17.19	13.06
MA	16.06	10.80	8.97	14.51	10.21
Ix	4216.86	13846.80	9404.89	743.69	502.95
Iy	4767.85	14133.97	8744.59	427.41	319.18
Imax	4807.91	14514.48	9982.52	747.63	511.60
Imin	4176.80	18233.25	8166.96	423.46	310.53
Imax/Imin	1.15	1.08	1.22	1.77	1.65
J	8984.71	27980.77	18149.48	1171.10	822.13
Theta	14.59	-37.050	-55.66	-83.66	78.03
Zx	304.72	936.49	541.53	89.50	71.36
Zy	332.40	1000.22	551.53	64.10	53.74

	Zy/Zx	1.09	1.07	1.02	0.72	0.75
	Zp	2445.21	5481.29	4941.33	317.91	281.58
Distal						
	TA	35.47	33.04	37.86	33.87	23.79
	CA	19.24	23.29	27.43	17.22	14.17
	MA	16.23	9.75	10.42	16.66	9.62
	Ix	4131.05	14225.30	10275.23	775.76	495.42
	Iy	5028.93	8809.06	11268.55	497.75	354.04
	Imax	5524.92	14449.29	13867.42	783.37	495.43
	Imin	3635.05	11624.12	7676.35	490.15	354.03
	Imax/Imin	1.52	1.68	1.81	1.60	1.40
	J	9159.98	23034.37	21543.78	1273.52	849.46
	Theta	30.82	78.730	-40.38	-80.73	-89.73
	Zx	311.47	954.18	557.93	89.10	74.17
	Zy	339.29	687.19	588.66	67.18	61.38
	Zy/Zx	1.09	0.72	1.06	0.75	0.83
	Zp	2501.54	4705.88	5188.16	321.27	303.55
			One sample t test			
	TA	**0.002**	**0.001**	**0.001**	**0.003**	**0.001**
	CA	**0.006**	**0.002**	**0.002**	**0.003**	**0.003**
	MA	**0.025**	**0.002**	**0.002**	**0.019**	**<0.001**
	Ix	**0.001**	**<0.001**	**0.001**	**<0.001**	**0.002**
	Iy	**0.002**	**0.02**	**0.023**	**0.003**	**0.008**
	Imax	**0.003**	**0.006**	**0.015**	**<0.001**	**0.002**
	Imin	**0.002**	**0.017**	**0.005**	**0.002**	**0.009**
	Imax/Imin	**0.011**	**0.02**	**0.013**	**0.001**	**0.004**
	J	**<0.001**	**0.004**	**0.008**	**0.001**	**0.003**
	Theta	0.79	0.985	**0.033**	**0.004**	0.723
	Zx	**<0.001**	**0.001**	**0.001**	**0.001**	**0.002**
	Zy	**0.002**	**0.014**	**0.005**	**0.001**	**0.009**
	Zy/Zx	**0.004**	**0.013**	**0.001**	**0.003**	**0.003**
	Zp	**<0.001**	**0.004**	**0.002**	**<0.001**	**0.004**

Table 5.26 Body mass adjusted biomechanical variables for the cross sections at the triceps brachii (lateral head) attachment with the one sample t-test (two-tailed) comparing the proximal, midpoint and distal properties of the enthesis. Bold = significant ($P \leq 0.05$).

Variable	P1	P2	P3	M1	M2
Proximal					
TA	34.49	33.01	35.96	32.06	22.13
CA	14.11	25.39	22.67	15.23	11.42
MA	20.38	7.63	13.28	16.83	10.70
Ix	3847.87	11611.35	8818.02	690.71	422.83
Iy	3079.76	11865.41	7904.41	408.56	256.75
Imax	3884.93	14195.72	9581.26	697.42	424.02
Imin	3042.69	12566.46	7141.18	401.85	255.56
Imax/Imin	1.28	1.53	1.34	1.74	1.66
J	6927.62	23476.76	16722.43	1099.27	679.58
Theta	-77.89	-43.518	-55.99	-81.34	85.18
Zx	275.47	894.87	533.79	80.72	58.47
Zy	241.28	910.83	536.80	56.78	43.26
Zy/Zx	0.88	1.02	1.01	0.70	0.74
Zp	1987.62	5114.42	4841.00	283.72	229.56
Midpoint					
TA	35.44	34.51	35.92	31.34	23.86
CA	19.03	24.89	27.87	17.61	14.08
MA	16.41	9.61	8.04	13.73	9.79
Ix	4206.65	13661.80	9167.40	660.68	504.74
Iy	4884.02	11063.95	9164.79	457.66	352.15
Imax	5429.36	14251.55	10335.51	707.14	504.81
Imin	3661.32	14181.98	7996.68	411.20	352.08
Imax/Imin	1.48	1.36	1.29	1.72	1.43
J	9090.67	24725.75	18332.19	1118.34	856.89
Theta	33.74	66.726	-45.03	-66.66	-88.78
Zx	318.38	933.07	521.27	85.27	73.77
Zy	326.47	826.75	556.51	68.44	61.79

	Zy/Zx	1.03	0.89	1.07	0.80	0.84
	Zp	2474.89	4997.92	4869.06	314.97	303.90
Distal						
	TA	32.80	29.81	35.53	26.26	19.13
	CA	18.54	21.15	25.64	18.07	13.28
	MA	14.26	8.66	9.89	8.19	5.85
	Ix	3569.63	10322.50	10762.14	444.22	321.05
	Iy	4431.44	8078.93	8024.03	401.05	269.91
	Imax	4443.84	10530.53	11539.12	498.85	347.90
	Imin	3557.24	10657.14	7247.04	346.43	243.06
	Imax/Imin	1.25	1.34	1.59	1.44	1.43
	J	8001.08	18401.43	18786.17	845.27	590.96
	Theta	-6.79	-73.759	-64.82	-53.23	-59.60
	Zx	285.95	782.46	529.44	73.15	53.59
	Zy	306.87	666.57	457.96	66.78	50.82
	Zy/Zx	1.07	0.85	0.87	0.91	0.95
	Zp	2279.24	4118.05	4489.51	284.52	232.58
			One sample t test			
	TA	**0.001**	**0.002**	**<0.001**	**0.004**	**0.004**
	CA	**0.008**	**0.003**	**0.003**	**0.003**	**0.004**
	MA	**0.011**	**0.004**	**0.021**	**0.036**	**0.028**
	Ix	**0.002**	**0.007**	**0.004**	**0.016**	**0.016**
	Iy	**0.017**	**0.012**	**0.002**	**0.002**	**0.01**
	Imax	**0.01**	**0.009**	**0.003**	**0.011**	**0.011**
	Imin	**0.003**	**0.007**	**0.001**	**0.003**	**0.014**
	Imax/Imin	**0.003**	**0.002**	**0.004**	**0.003**	**0.003**
	J	**0.006**	**0.008**	**0.001**	**0.007**	**0.012**
	Theta	0.655	0.731	**0.011**	**0.014**	0.733
	Zx	**0.002**	**0.003**	**<0.001**	**0.002**	**0.009**
	Zy	**0.008**	**0.008**	**0.003**	**0.003**	**0.011**
	Zy/Zx	**0.003**	**0.003**	**0.004**	**0.006**	**0.005**
	Zp	**0.004**	**0.004**	**0.001**	**0.001**	**0.009**

Table 5.27 Body mass adjusted biomechanical variables for the cross sections at the triceps brachii (medial head) attachment with the one sample t-test (two-tailed) comparing the proximal, midpoint and distal properties of the enthesis. Bold = significant ($P \leq 0.05$).

Variable	P1	P2	P3	M1	M2
Proximal					
TA	63.40	30.14	44.35	45.62	82.11
CA	19.33	22.24	22.70	16.74	19.86
MA	44.07	7.90	21.65	28.88	62.24
Ix	9405.31	9476.77	10244.99	1066.35	2794.79
Iy	9996.00	10018.80	13114.43	743.84	2318.74
Imax	10084.56	11372.31	13176.69	1090.09	2903.85
Imin	9316.74	10998.84	10182.74	720.10	2209.67
Imax/Imin	1.08	1.40	1.29	1.51	1.31
J	19401.31	19495.57	23359.42	1810.19	5113.53
Theta	19.85	-40.198	8.29	-75.33	-66.65
Zx	488.00	707.03	578.26	103.14	214.10
Zy	488.55	747.65	721.02	89.08	206.34
Zy/Zx	1.00	1.06	1.25	0.86	0.96
Zp	3745.08	4120.10	5884.51	393.79	936.35
Midpoint					
TA	35.64	33.03	35.82	32.66	69.69
CA	20.96	23.05	27.27	17.03	21.34
MA	14.68	9.99	8.55	15.63	48.35
Ix	4233.77	14818.45	9116.75	780.22	2690.72
Iy	5489.32	8434.85	8975.65	450.03	1933.76
Imax	5891.73	15022.10	10073.84	786.73	2722.04
Imin	3831.36	11144.98	8018.57	443.51	1902.44
Imax/Imin	1.54	1.83	1.26	1.77	1.43
J	9723.09	23253.30	18092.41	1230.25	4624.48
Theta	26.23	80.028	-46.97	-82.08	78.73
Zx	323.98	978.56	524.53	88.13	209.94
Zy	360.53	682.72	555.04	59.97	181.66

	Zy/Zx	1.11	0.70	1.06	0.68	0.87
	Zp	2635.77	4790.26	4877.40	305.79	876.75
Distal						
	TA	31.85	29.26	33.30	28.13	39.38
	CA	21.36	22.93	23.42	18.11	13.60
	MA	10.49	6.33	9.88	10.02	25.78
	Ix	3485.09	8982.95	8098.70	552.50	1000.48
	Iy	4875.55	9800.58	7170.95	406.20	615.09
	Imax	4928.05	10837.61	8142.27	604.68	1003.16
	Imin	3432.59	10758.72	7127.39	354.02	612.41
	Imax/Imin	1.44	1.36	1.14	1.71	1.64
	J	8360.64	18783.53	15269.66	958.70	1615.57
	Theta	-10.80	-36.788	-78.04	-62.85	85.25
	Zx	294.68	701.09	495.79	79.89	104.70
	Zy	333.62	719.67	424.85	66.13	76.01
	Zy/Zx	1.13	1.03	0.86	0.83	0.73
	Zp	2425.27	4025.65	4158.34	298.49	407.20
			One sample t test			
	TA	**0.048**	**0.001**	**0.008**	**0.021**	**0.037**
	CA	**0.001**	**<0.001**	**0.003**	**0.001**	**0.016**
	MA	0.161	**0.017**	0.085	0.083	0.051
	Ix	0.092	**0.027**	**0.005**	**0.033**	0.065
	Iy	0.052	**0.003**	**0.031**	**0.037**	0.088
	Imax	**0.048**	**0.011**	**0.019**	**0.028**	0.068
	Imin	0.101	**<0.001**	**0.011**	**0.044**	0.084
	Imax/Imin	**0.01**	**0.01**	**0.001**	**0.002**	**0.004**
	J	0.069	**0.005**	**0.015**	**0.034**	0.074
	Theta	0.412	0.982	0.263	**0.006**	0.58
	Zx	**0.026**	**0.013**	**0.002**	**0.006**	**0.039**
	Zy	**0.014**	**0.001**	**0.022**	**0.015**	0.061
	Zy/Zx	**0.001**	**0.015**	**0.011**	**0.005**	**0.006**
	Zp	**0.019**	**0.003**	**0.01**	**0.008**	**0.048**

Table 5.28 Body mass adjusted biomechanical variables for the cross sections at brachialis attachment with the one sample t-test (two-tailed) comparing the proximal, midpoint and distal properties of the enthesis. Bold = significant ($P \leq 0.05$).

Variable	P1	P2	P3	M1	M2
Proximal					
TA	54.28	33.68	47.31	31.60	37.03
CA	13.88	21.07	23.90	15.46	12.18
MA	40.40	12.61	23.41	16.14	24.85
Ix	5360.14	8943.22	12194.50	691.66	838.13
Iy	6622.77	13755.40	14643.94	383.88	536.99
Imax	6624.81	13907.32	15697.67	693.99	842.44
Imin	5358.10	11903.35	11140.77	381.56	532.68
Imax/Imin	1.24	1.58	1.41	1.82	1.58
J	11982.91	22698.61	26838.44	1075.54	1375.12
Theta	2.30	-9.923	28.74	-85.05	-83.23
Zx	351.56	695.43	620.31	82.37	94.60
Zy	367.07	860.33	770.61	56.17	72.17
Zy/Zx	1.04	1.24	1.24	0.68	0.76
Zp	2760.90	4457.07	6278.95	287.09	375.24
Midpoint					
TA	36.13	36.43	35.98	32.69	23.83
CA	20.12	25.75	25.26	18.00	13.27
MA	16.02	10.69	10.72	14.70	10.56
Ix	4135.26	13741.26	8238.03	723.06	512.27
Iy	5568.01	13110.85	9541.31	495.24	339.86
Imax	5637.65	13926.33	10484.31	769.33	515.52
Imin	4065.62	17501.41	7295.02	448.97	336.61
Imax/Imin	1.39	1.08	1.44	1.71	1.53
J	9703.27	26852.11	17779.34	1218.30	852.13
Theta	12.15	64.528	-32.94	-67.66	82.25
Zx	297.71	922.38	464.93	88.36	71.85
Zy	358.31	937.72	561.24	70.33	56.46

	Zy/Zx	1.20	1.02	1.21	0.80	0.79
	Zp	2528.84	5267.02	4631.86	325.32	288.25
Distal						
	TA	35.17	29.61	32.62	26.78	18.92
	CA	19.57	21.42	23.74	18.17	12.95
	MA	15.60	8.19	8.88	8.61	5.97
	Ix	4668.49	10122.68	7020.91	465.54	312.05
	Iy	4600.20	8176.97	7740.63	406.59	263.31
	Imax	5407.37	10386.56	7954.27	517.29	336.14
	Imin	3861.32	10714.27	6807.27	354.85	239.22
	Imax/Imin	1.40	1.31	1.17	1.46	1.41
	J	9268.69	18299.65	14761.54	872.13	575.36
	Theta	46.27	-70.936	25.57	-55.64	-60.10
	Zx	334.78	769.15	467.42	75.93	52.66
	Zy	311.00	653.67	434.83	68.70	49.55
	Zy/Zx	0.93	0.85	0.93	0.90	0.94
	Zp	2473.85	4038.20	4067.96	294.27	227.70
			One sample t test			
	TA	**0.021**	**0.004**	**0.013**	**0.004**	**0.039**
	CA	**0.012**	**0.004**	**<0.001**	**0.003**	**0.001**
	MA	0.1	**0.015**	0.088	**0.029**	0.136
	Ix	**0.006**	**0.017**	**0.028**	**0.016**	0.069
	Iy	**0.011**	**0.022**	**0.036**	**0.006**	**0.043**
	Imax	**0.004**	**0.008**	**0.038**	**0.013**	0.062
	Imin	**0.011**	**0.024**	**0.026**	**0.005**	**0.05**
	Imax/Imin	**0.001**	**0.012**	**0.004**	**0.004**	**0.001**
	J	**0.007**	**0.012**	**0.032**	**0.009**	0.058
	Theta	0.268	0.902	0.756	**0.015**	0.732
	Zx	**0.002**	**0.007**	**0.01**	**0.002**	**0.026**
	Zy	**0.003**	**0.011**	**0.027**	**0.005**	**0.012**
	Zy/Zx	**0.005**	**0.012**	**0.008**	**0.006**	**0.004**
	Zp	**0.001**	**0.006**	**0.017**	**0.002**	**0.02**

Table 5.29 Distal positions of attachment sites expressed in percentages of length from the proximal end (insertions) or distal end (origins) of the humerus. Results from *t*-test comparing *Pongo* and *Macaca*. Significant results are shown in brackets.

Muscle	P1	P2	P3	M1	M2	*t*-test *Pongo* vs *Macaca*
LD	21.72	26.69	21.57	28.76	32.94	-2.815
Pmaj	31.89	36.04	41.89	42.50	34.30	-0.371
D	52.89	49.47	50.32	58.21	54.00	-2.536
Sb	12.80	12.22	13.55	6.74	7.27	**10.941 (0.002)**
Sp	2.38	3.34	4.57	2.41	2.56	1.152
If	12.47	15.17	11.11	7.61	5.08	**3.639 (0.036)**
Tmaj	36.88	28.28	34.26	32.07	37.87	-0.465
Tmin	12.74	13.08	15.89	10.45	11.60	2.119
Cb (med)	38.94	41.31	39.92	32.29	30.52	**7.823 (0.004)**
B	12.16	14.20	13.33	19.90	21.92	**-7.165 (0.006)**
TBlat	20.89	21.92	19.27	22.61	21.40	-1.2
TBmed	10.25	17.90	14.37	29.22	31.83	**-5.423 (0.012)**
PT	6.97	9.11	8.26	10.49	9.23	-1.877
CFO	3.20	2.90	2.00	1.41	1.30	2.878
Br	8.03	12.08	13.12	12.42	10.80	-0.255
ECRL	4.51	7.70	6.96	9.51	8.90	-2.225
CEO	1.22	1.30	2.32	6.24	8.45	**-6.085 (0.009)**
An	3.39	3.25	2.57	4.47	3.21	-1.346

Figure 5.1 Relative muscle mass distribution of the muscles studied in the primate sample. A) Relative muscle mass distribution of all forelimb muscles, B) Relative muscle mass distribution of all shoulder muscles, C) Relative muscle mass distribution of all elbow muscles, D) Relative muscle mass distribution of all wrist muscles.

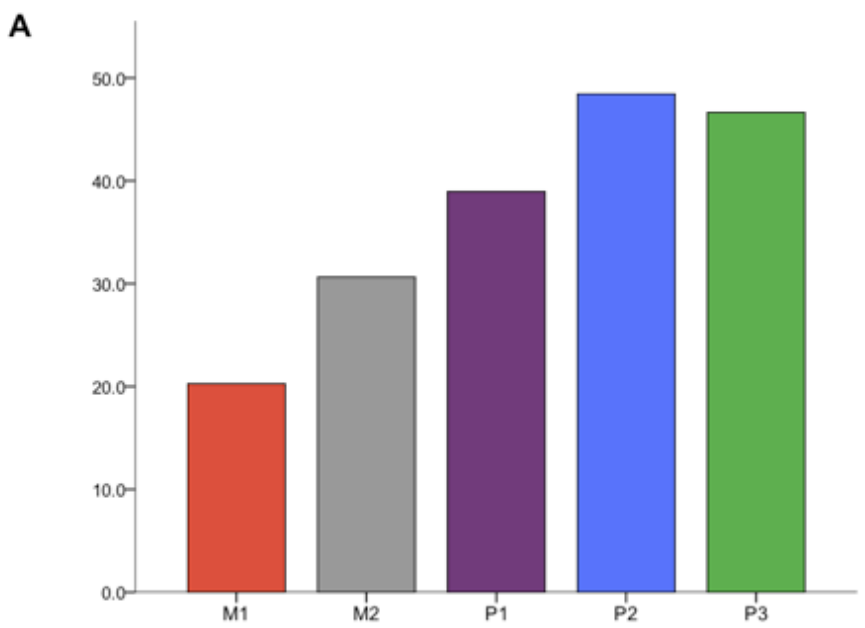

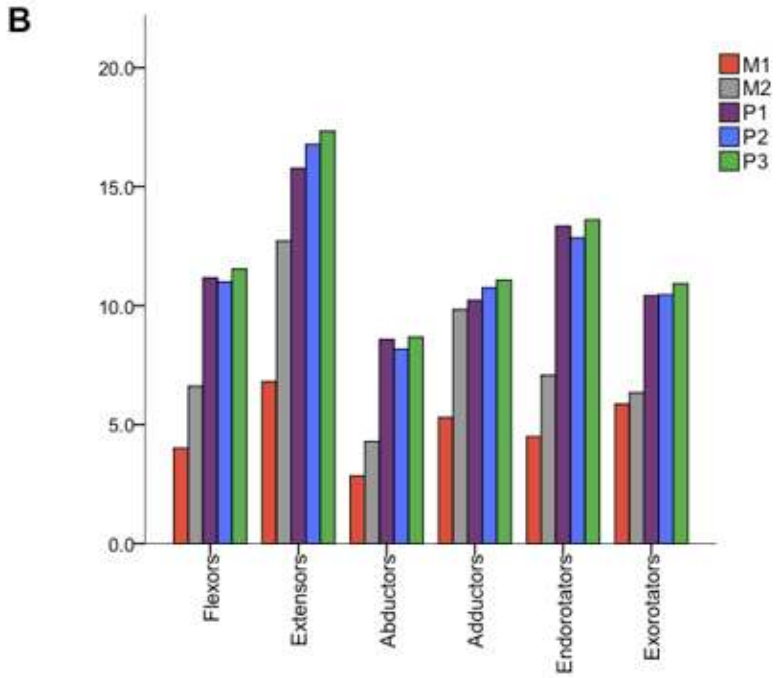

C

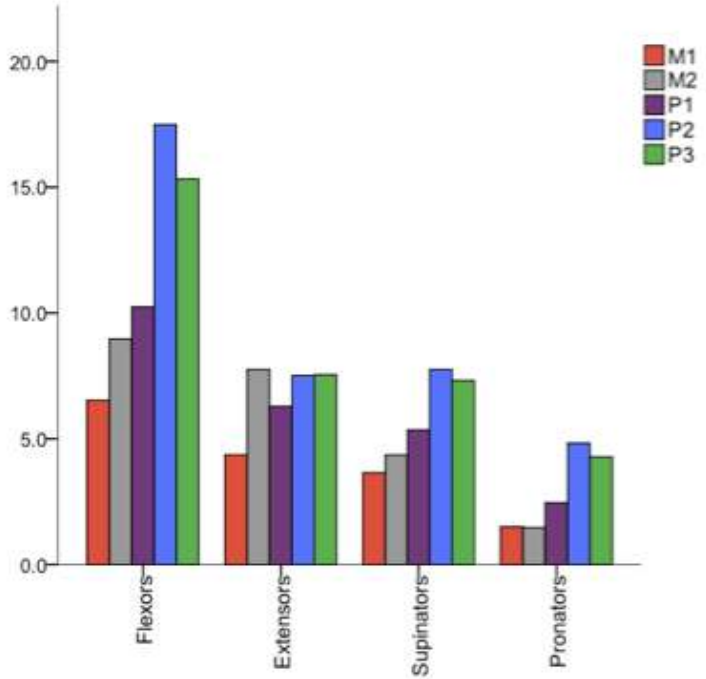
20.0
15.0
10.0
5.0
0.0
M1
M2
P1
P2
P3
Flexors
Extensors
Supinators
Pronators

D

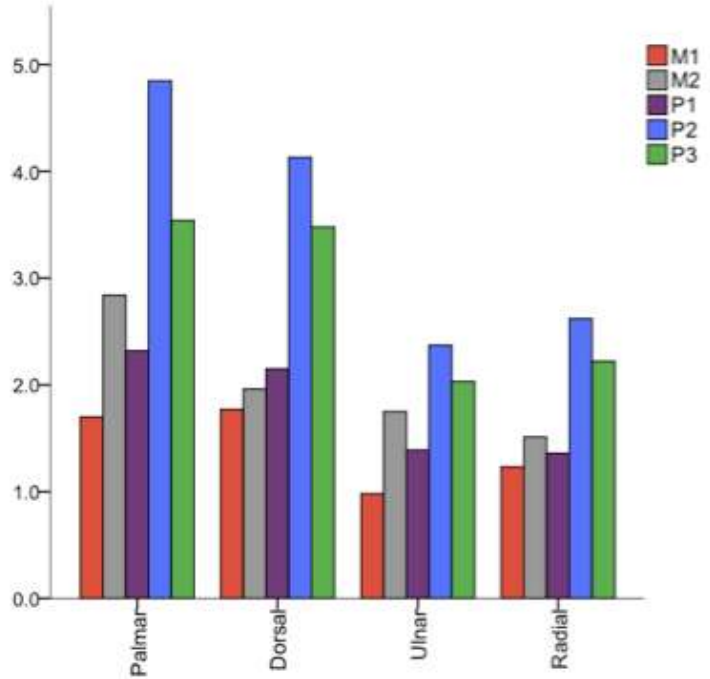
5.0
4.0
3.0
2.0
1.0
0.0
M1
M2
P1
P2
P3
Palmar
Dorsal
Ulnar
Radial

Figure 5.2 Body mass adjusted A) muscle belly lengths (L_b), B) fibre length (L_F), C) tendon length relative to muscle-tendon unit (TL/MTU), D) physiological cross-sectional area (PCSA), E) muscle mass/predicted effective maximal tetanic tension (M/P_0), F) estimated maximum excursion of the distal tendon of attachment (h), G) priority index for force (*I*) of each functional muscle group of the shoulder.

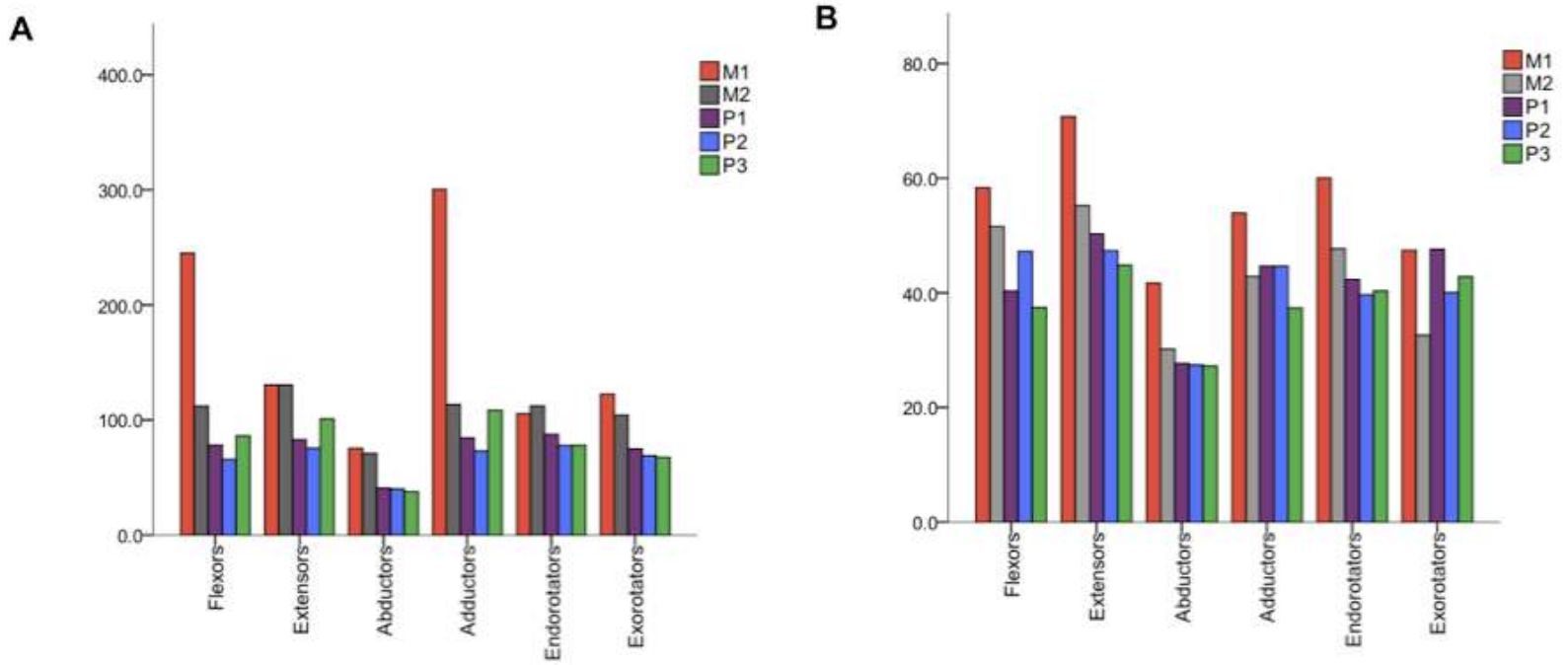

C

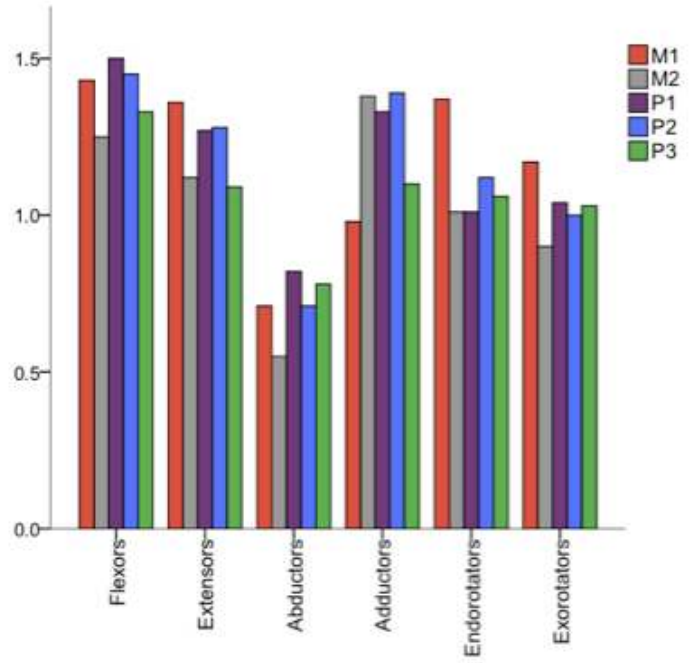
1.5
1.0
0.5
0.0
M1
M2
P1
P2
P3
Flexors
Extensors
Abductors
Adductors
Endorotators
Exorotators

D

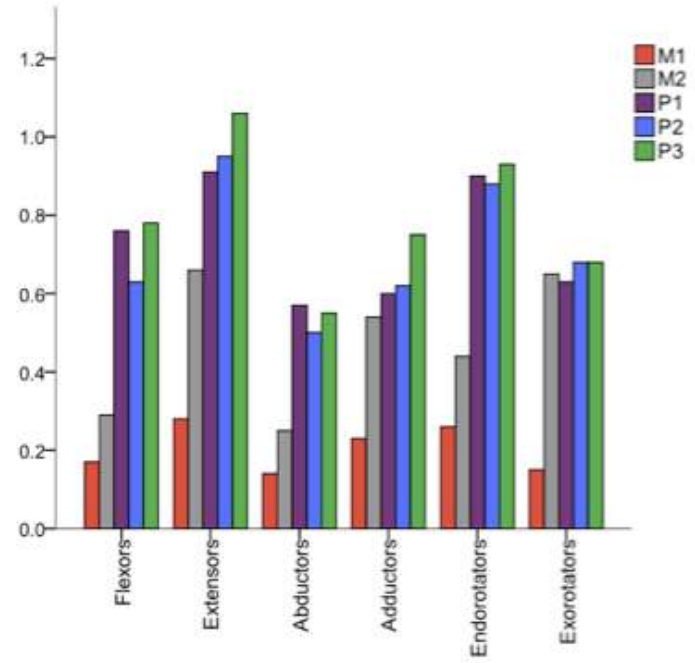
1.2
1.0
0.8
0.6
0.4
0.2
0.0
M1
M2
P1
P2
P3
Flexors
Extensors
Abductors
Adductors
Endorotators
Exorotators

E

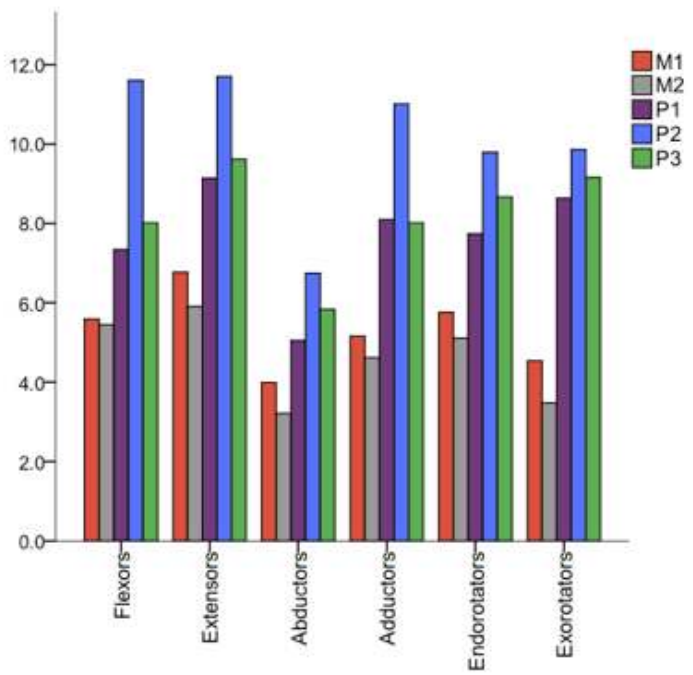
12.0
10.0
8.0
6.0
4.0
2.0
0.0
M1
M2
P1
P2
P3
Flexors
Extensors
Abductors
Adductors
Endorotators
Exorotators

F

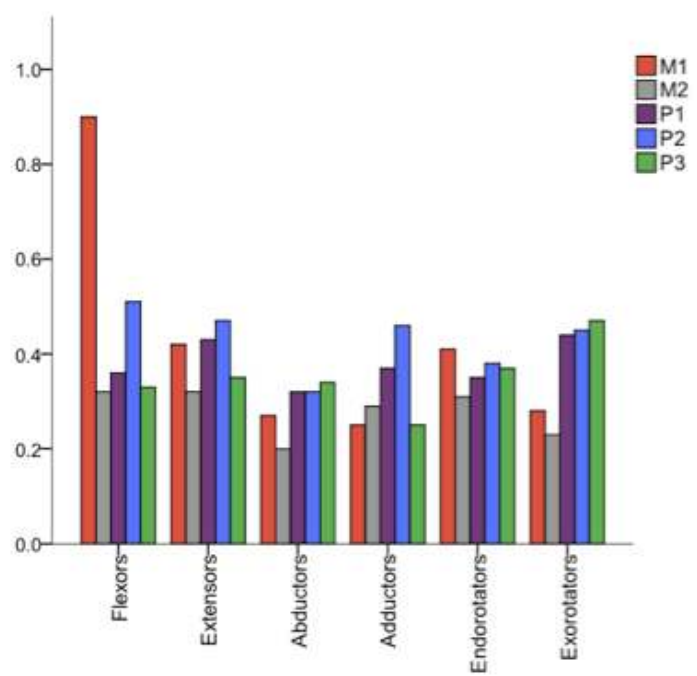
1.0
0.8
0.6
0.4
0.2
0.0
M1
M2
P1
P2
P3
Flexors
Extensors
Abductors
Adductors
Endorotators
Exorotators

G

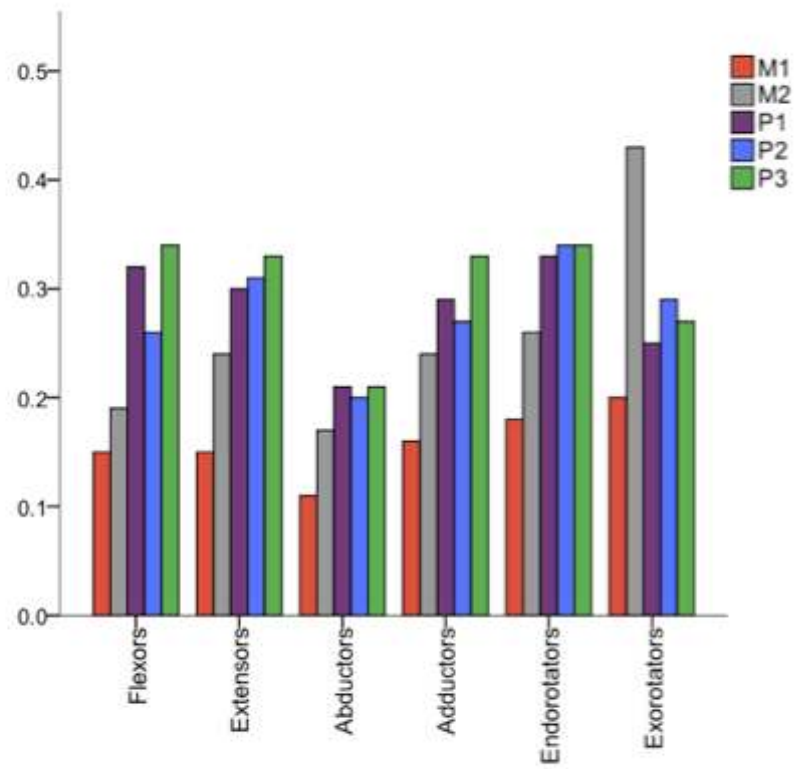
0.5
0.4
0.3
0.2
0.1
0.0
M1
M2
P1
P2
P3
Flexors
Extensors
Abductors
Adductors
Endorotators
Exorotators

Figure 5.3 Body mass adjusted A) muscle belly lengths (L_b), B) fibre length (L_F), C) tendon length relative to muscle-tendon unit (TL/MTU), D) physiological cross-sectional area (PCSA), E) muscle mass/predicted effective maximal tetanic tension (M/P_0), F) estimated maximum excursion of the distal tendon of attachment (h), G) priority index for force (*I*) of each functional muscle group of the elbow.

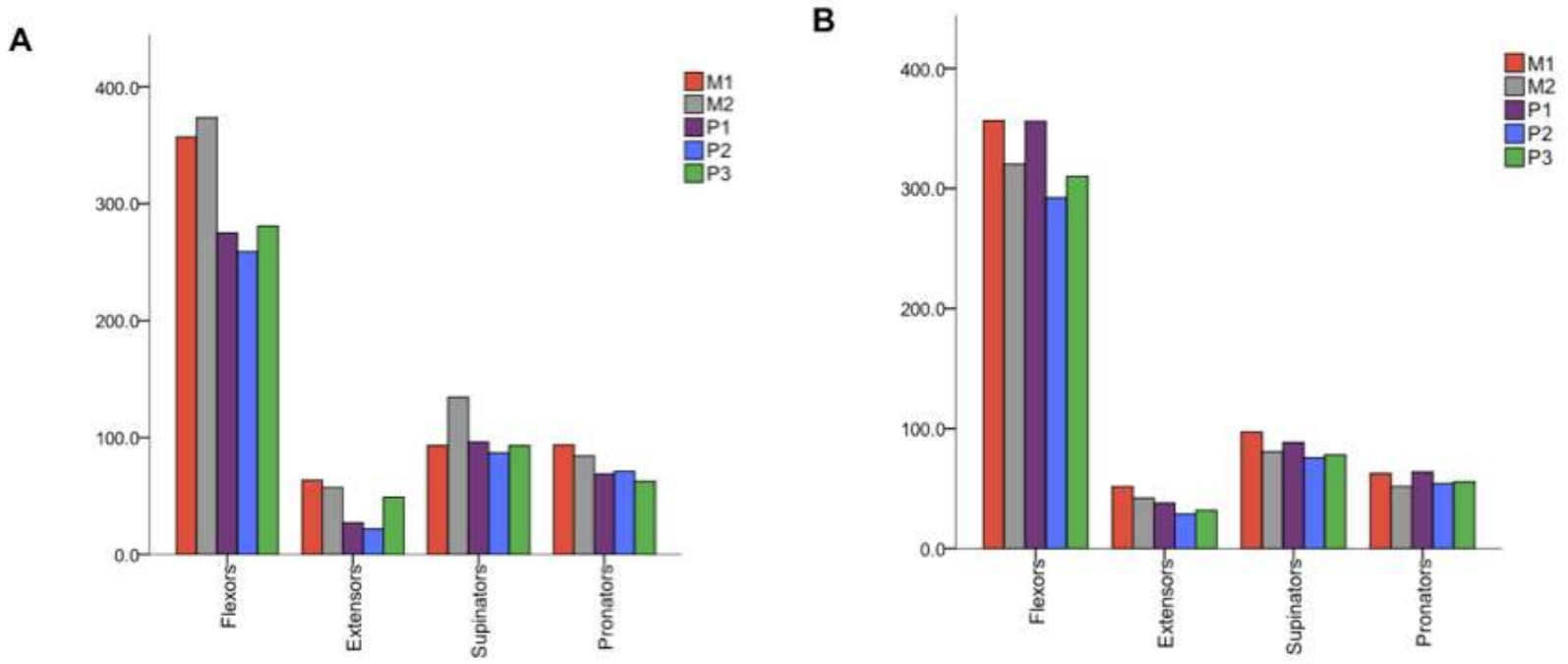

C

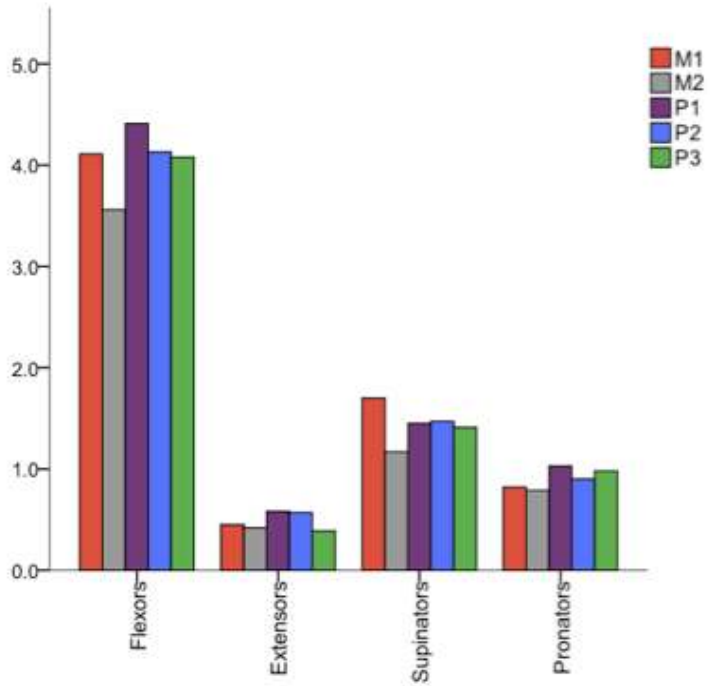
M1
M2
P1
P2
P3
5.0
4.0
3.0
2.0
1.0
0.0
Flexors
Extensors
Supinators
Pronators

D

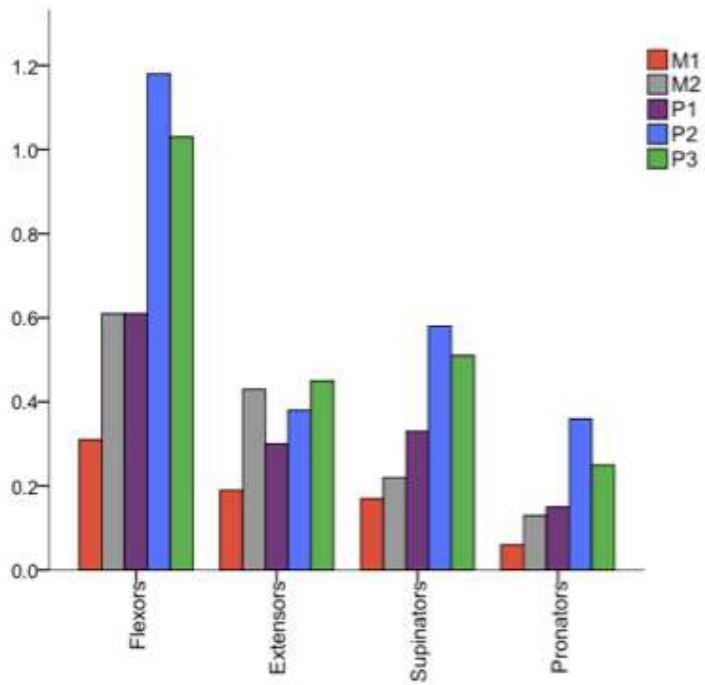
M1
M2
P1
P2
P3
1.2
1.0
0.8
0.6
0.4
0.2
0.0
Flexors
Extensors
Supinators
Pronators

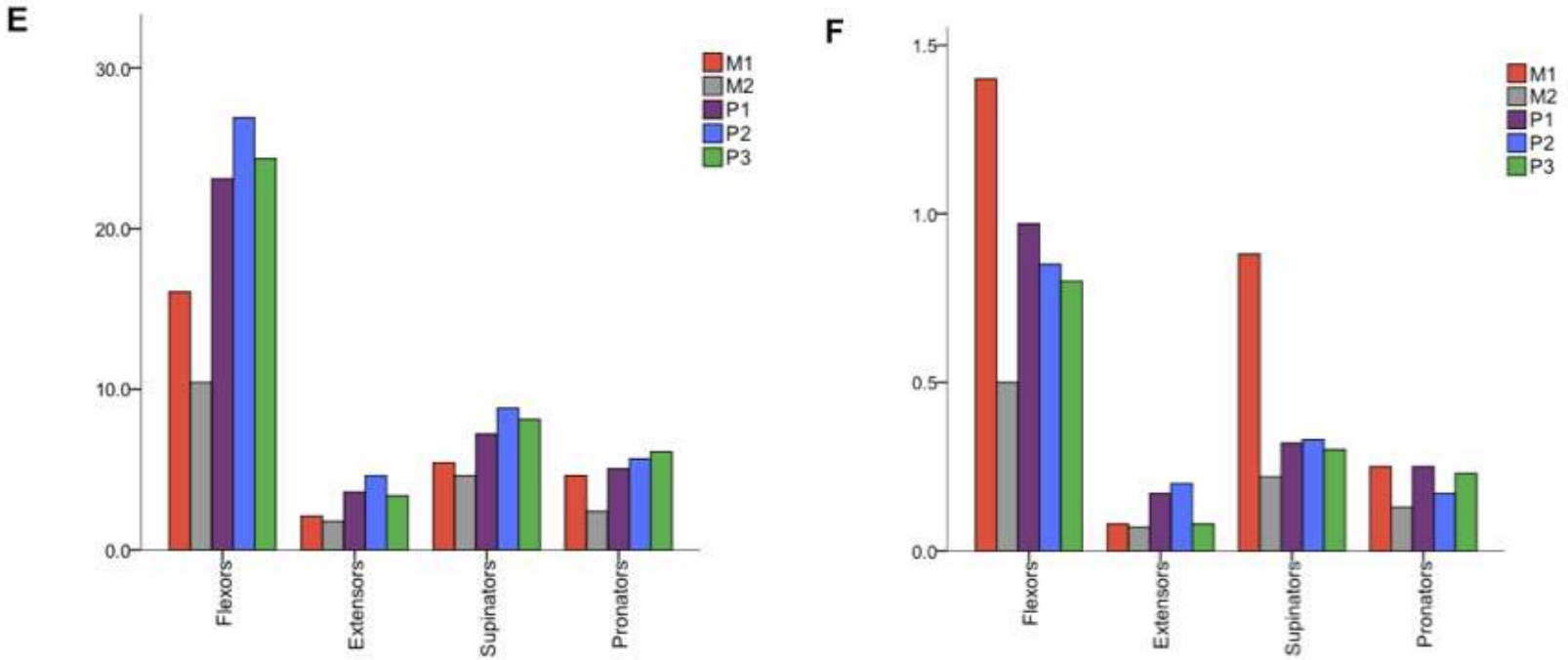
E
30.0
20.0
10.0
0.0
M1
M2
P1
P2
P3
Flexors
Extensors
Supinators
Pronators
F
1.5
1.0
0.5
0.0
M1
M2
P1
P2
P3
Flexors
Extensors
Supinators
Pronators

G

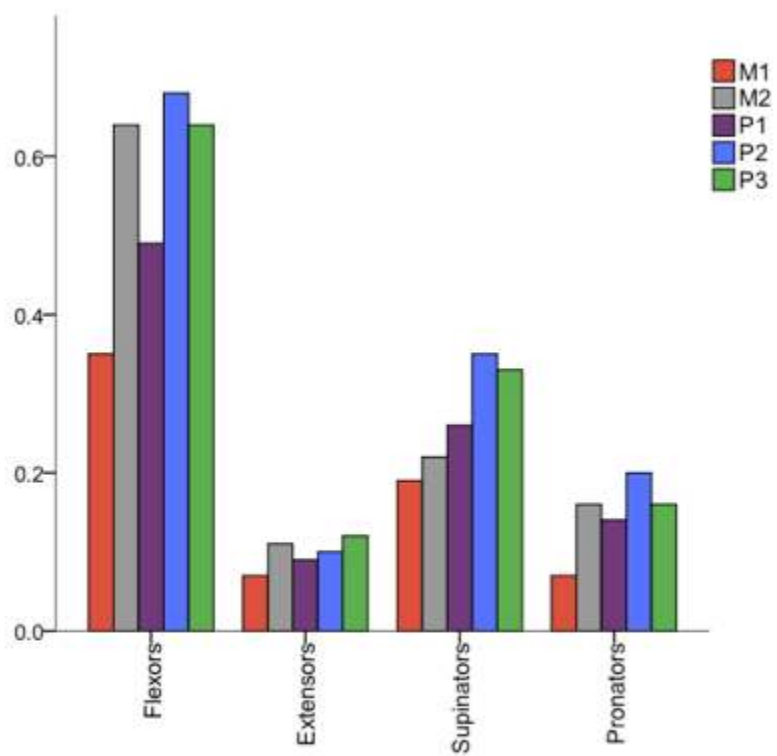
M1
M2
P1
P2
P3
0.6
0.4
0.2
0.0
Flexors
Extensors
Supinators
Pronators

Figure 5.4 Body mass adjusted A) muscle belly lengths (L_b), B) fibre length (L_F), C) tendon length relative to muscle-tendon unit (TL/MTU), D) physiological cross-sectional area (PCSA), E) muscle mass/predicted effective maximal tetanic tension (M/P_0), F) estimated maximum excursion of the distal tendon of attachment (h), G) priority index for force (*I*) of each functional muscle group of the wrist.

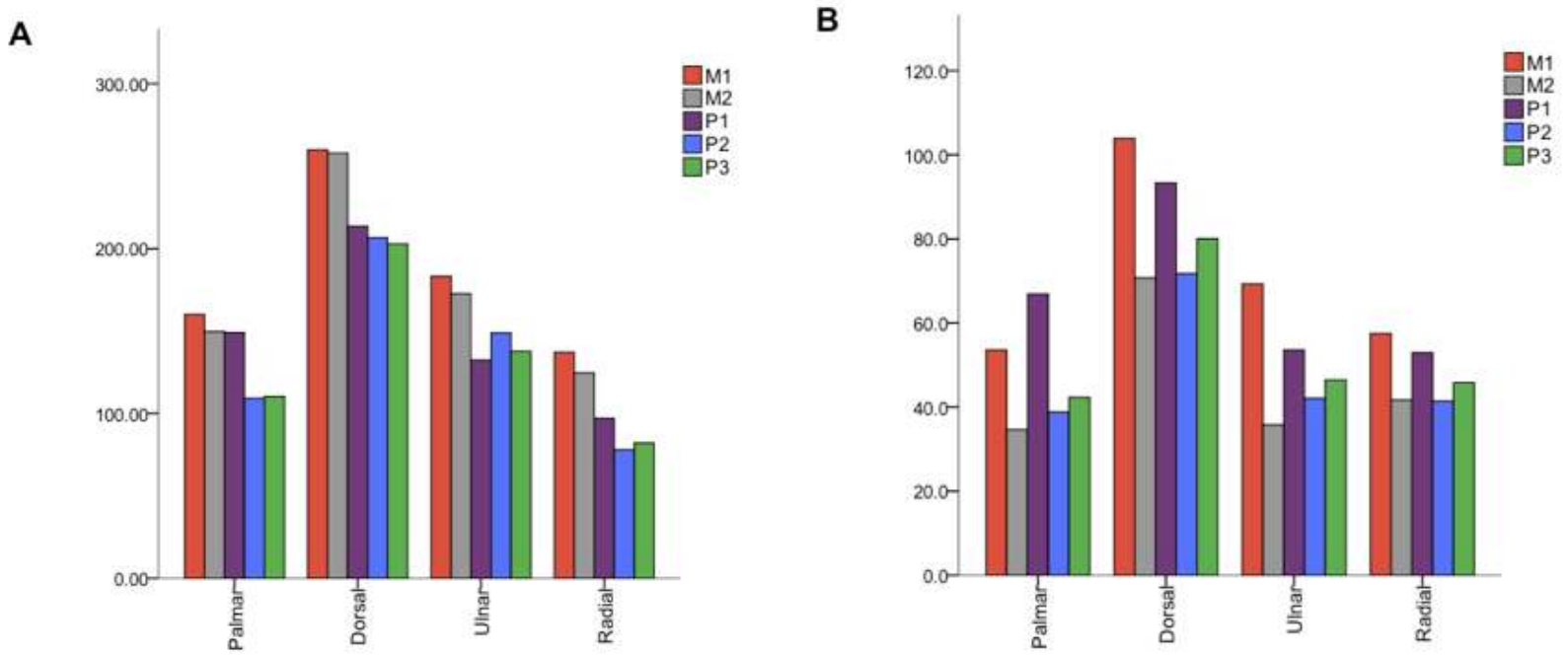

C

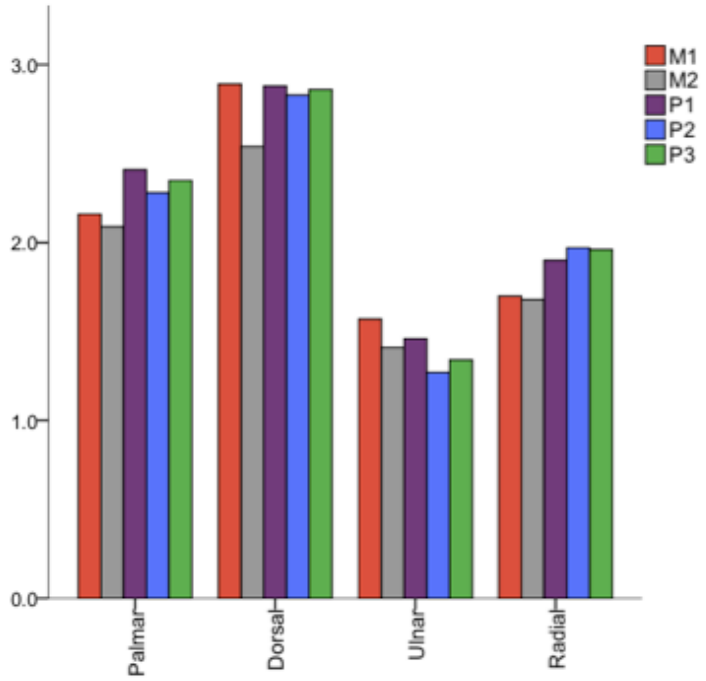
3.0
2.0
1.0
0.0
M1
M2
P1
P2
P3
Palmar
Dorsal
Ulnar
Radial

D

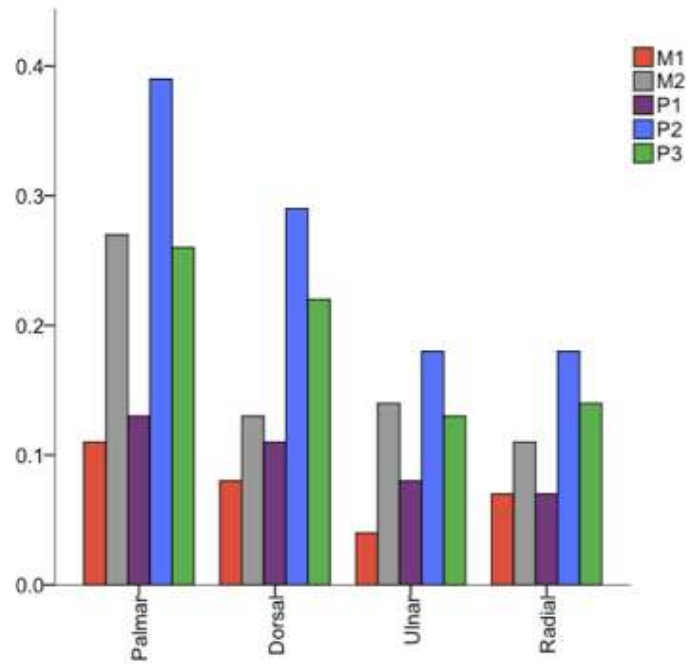
0.4
0.3
0.2
0.1
0.0
M1
M2
P1
P2
P3
Palmar
Dorsal
Ulnar
Radial

E

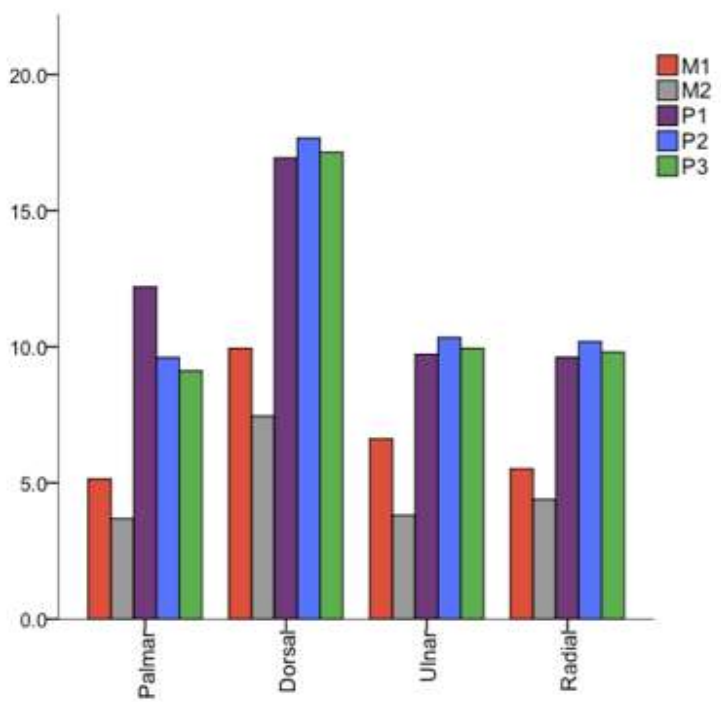
20.0
15.0
10.0
5.0
0.0
M1
M2
P1
P2
P3
Palmar
Dorsal
Ulnar
Radial

F

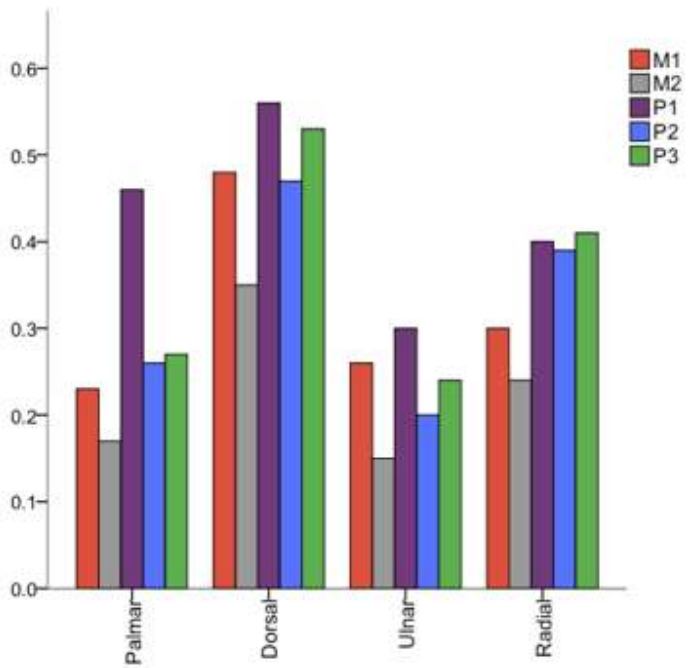
0.6
0.5
0.4
0.3
0.2
0.1
0.0
M1
M2
P1
P2
P3
Palmar
Dorsal
Ulnar
Radial

G

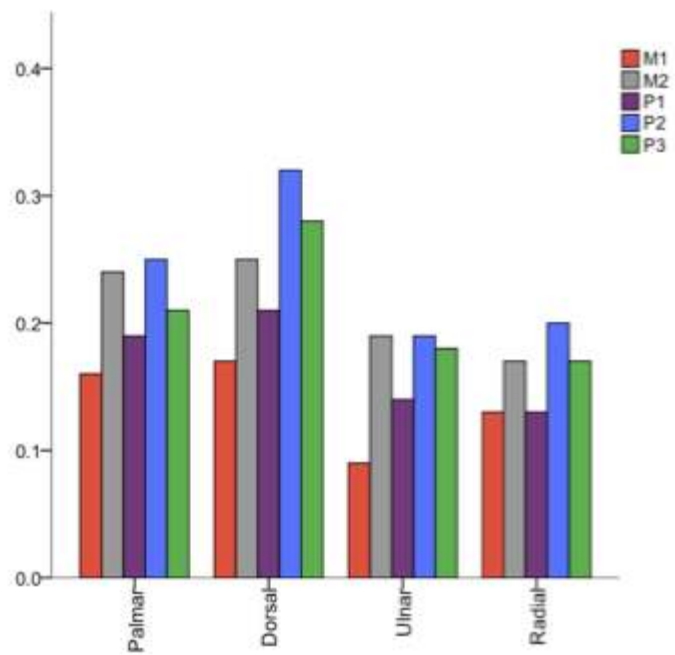

Figure 5.5 Whole humerus with midshaft CT scans for all primates: A) P1, B) P2, C) P3, D) M1, and E) M2.

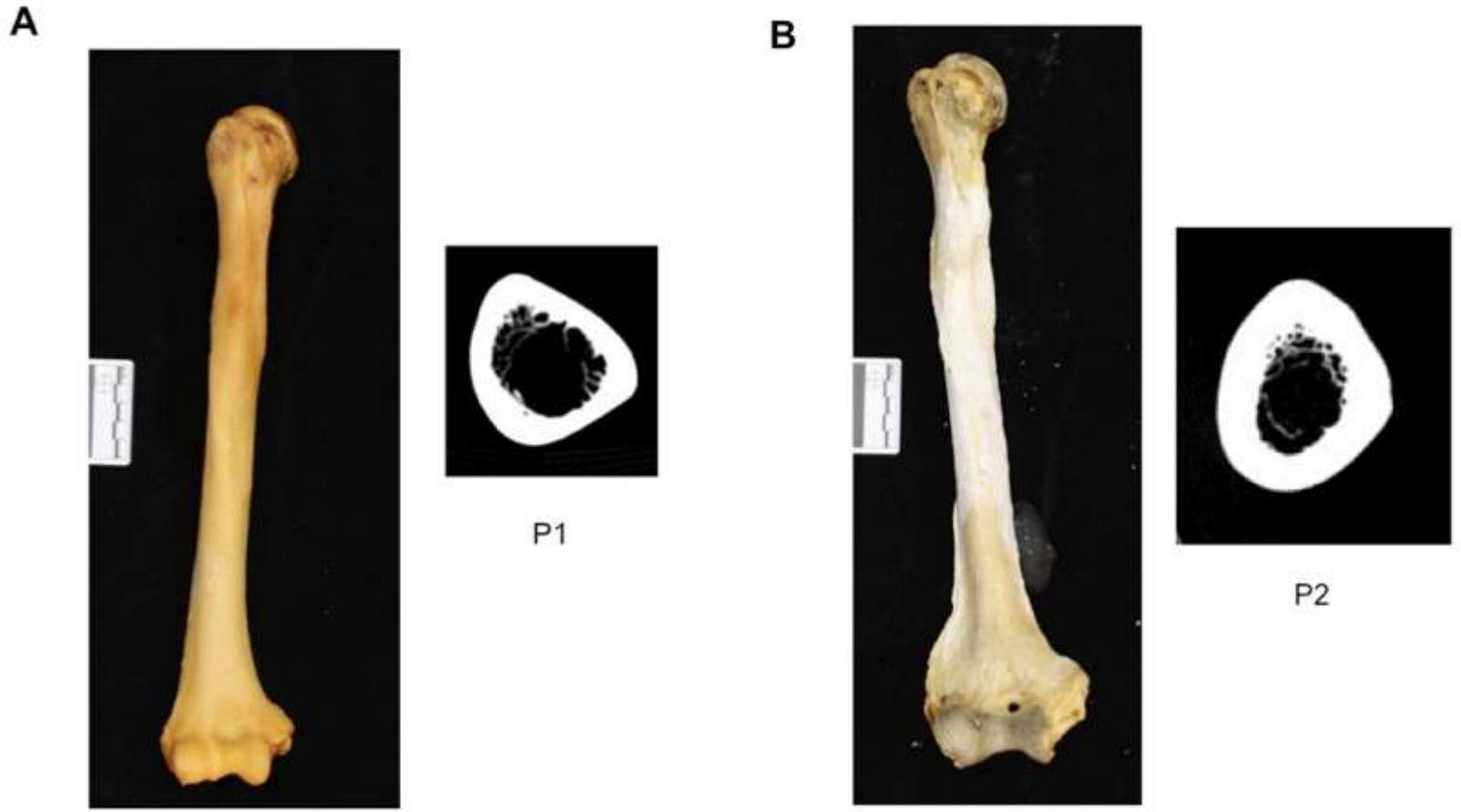

C

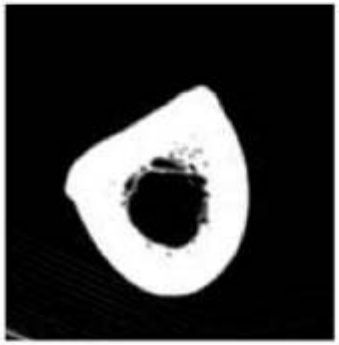

P3

D

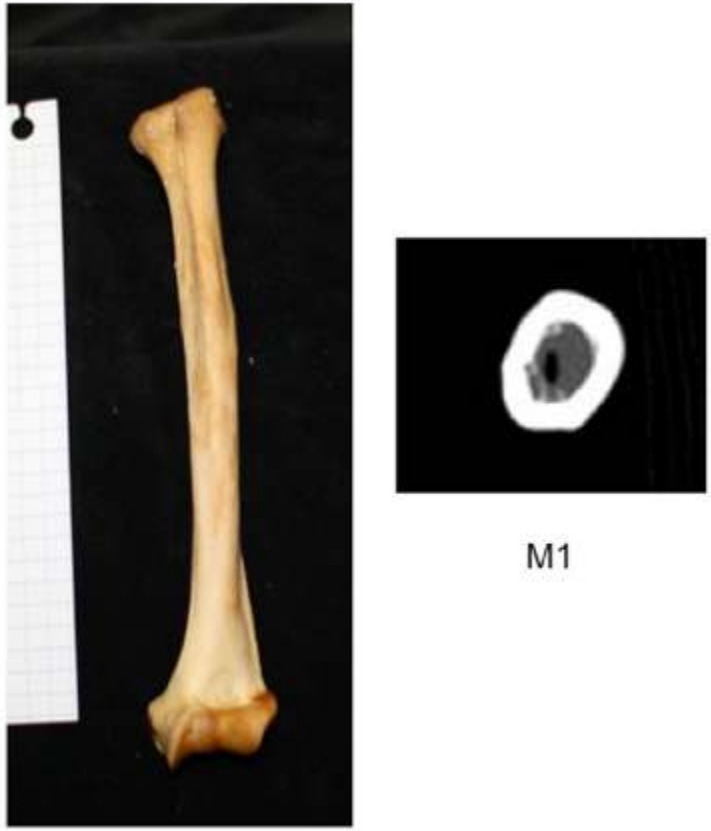

M1

E

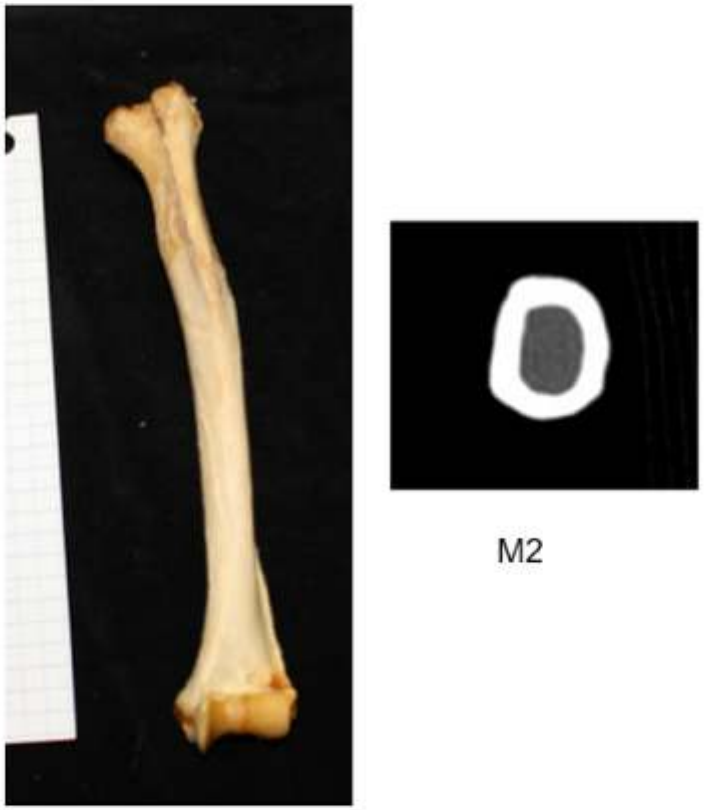

M2

Chapter 6

6. Mouse results

In this chapter, hard- and soft-tissue analyses of the left humerus are reported for the mouse sample. Thirty female wild-type mice doing different exercise regime were studied to investigate the relationship between activity, age, and muscle attachments. It was predicted that higher levels of exercise will result in the development of muscles with greater maximum force-generating potential output, higher rates of bone growth, stronger and faster growing bone, as well as hypertrophied deltoid crest with altered shape. Results from the anatomy and function of the muscles attaching to the deltoid crest are presented followed by deltoid entheseal surface morphology analyses. Next, biomechanical shape of the humerus (within the deltoid crest) is explored, and the results finish with the interpretations of the bone histology (variation and growth) from the humerus of the mouse sample. This chapter ends with a summary of the results found in the experimental mouse sample.

6.1 Muscle anatomy and function

Body mass of the mice and forelimb muscle variables were observed and results are presented here (Tables 6.1 - 6.4; Figures 6.1 – 6.3). On average and for all groups, superficial pectoralis was significantly the largest and longest muscle, followed by the spinodeltoideus, and then the acromiodeltoideus. Pennation angle was the only variable that showed a different pattern with acromiodeltoideus having a wider and higher range of angles. Overlapping values between the superficial pectoralis and the spinodeltoideus were found (Figure 6.1). Differences between groups are reported below.

6.1.1 Body and muscle masses

Body mass of mice (P = 0.007) varied slightly with the amount of exercise performed (Table 6.1), especially between the high-intensity runners and the control mice (P = 0.001). As predicted, on average the control (CON) group had the largest body mass ($\bar{x}$ = 33.93g), the wheel running (WHL) mice had the lowest body mass ($\bar{x}$ = 29.88g), and the climbing (CLB) animals were intermediate ($\bar{x}$ = 31.93g). Body mass did not differ with age (Table 6.4). In contrast, the experimental groups were found at opposite spectrums in absolute muscle masses (M). It was predicted that the experimental groups would have larger muscles, especially the high-intensity group. However, it was found that the intermediate-intensity climbers had the greatest absolute muscle masses while the high intensity runners had the lowest muscle masses (Table 6.1). For example, the average mass of the acromiodeltoideus muscle of the CLB group ($\bar{x}$ = 10.4 μg) significantly differed from both the WHL mice ($\bar{x}$ = 8.4 μg) and the CON group ($\bar{x}$ = 9.0 μg). The control and running groups had overlapping masses for all of the muscles observed. The control and climbing group did significantly differ for the absolute masses of the acromiodeltoideus (P = 0.001) and the superficial pectoralis (P = 0.005) muscles (Table 6.1). Body mass adjusted differences of muscle masses were less significant (Table 6.2 and Figure 6.2). Relative acromiodeltoideus muscle masses did not differ significantly between groups. Spinodeltoideus relative muscle mass did significantly differ between groups (P = 0.005) with the greatest contrast being between the intermediate-intensity climbers and the control mice (P = 0.01) as well as the CLB and the WHL groups (P = 0.013). High-intensity runners and controls overlapped in body mass adjusted spinodeltoideus mass (Table 6.2). Superficial pectoralis relative mass also significantly differed between groups (P = 0.006) with the greatest pairwise comparisons found between the CLB and CON mice (P = 0.004). There were no significant

differences (absolute [Table 6.3] or relative to body mass [Table 6.4]) between the juvenile and the adult groups for any of the muscle masses.

6.1.2 Muscle fibre architecture

Absolute belly lengths (L_b) of the muscles attaching to the deltoid crest differed significantly with the type of activity performed (Table 6.1). It was predicted that the exercise groups would have longer forelimb muscles, especially the vertical climbing group. However, the intermediate-intensity climbers had the shortest muscle bellies, but on average the high-intensity runners had the longest muscle bellies ($P \leq 0.001$). For example, the average length of the acromiodeltoideus muscle belly in the climbing mice ($\bar{x}$ = 7.2 mm) was significantly less than the control ($\bar{x}$ = 9.1 mm) and the running mice ($\bar{x}$ = 9.6 mm). The control and high-intensity running mice overlapped in belly lengths (Table 6.1). However, the control and intermediate-intensity climbing mice significantly differed ($P \leq 0.001$). Once again, controlling for body mass indicated similar significant differences: CON and WHL overlapped slightly and differed greatly from CLB (Table 6.2 and Figure 6.2). Superficial pectoralis was the only muscle to have significant contrasts between the relative belly lengths of the control and running mice ($P \leq 0.001$).

As predicted, absolute muscle fibres (L_f: potential excursion) of the forelimb muscles were longer in the WHL group than the CON group ($P \leq 0.001$; Table 6.1). However, the CLB group had the shortest fibres. For example, the fascicles of the acromiodeltoideus muscle were on average 5.2 mm in WHL mice, 4.3 mm in CON mice, and as short as 3.5 mm long in CLB mice. All L_f comparisons among groups were highly significant ($P \leq 0.001$). Body mass adjusted differences in L_f for all three muscles followed the same significant pattern (Table 6.2 and Figure

6.3). M/P_o (muscle mass/predicted effective maximum tetanic tension) considers how much muscle mass is due to longer fibres, and hence dedication to excursion depicted by longer parallel fascicles. The values for M/P_o ($P \leq 0.001$) followed a similar pattern as L_f, meaning that relative to their mass, the muscles of the high intensity WHL group facilitated contraction velocity. The biggest difference between muscle excursions was once again between the two exercise groups (WHL and CLB; $P \leq 0.001$). All group comparisons were highly significantly different (Table 6.1 and Figure 6.2).

The opposite pattern was found for physiological cross-sectional area (PCSA: potential maximum force output; Tables 6.1 and 6.2), which represents an architectural trade-off between potential excursion and potential maximum force production (Figure 6.3). It was predicted that the experimental groups would have the largest PCSA values, especially the high-intensity runners. Once again, the two exercise groups were found at each end of the spectrum, but this time, the intermediate-intensity climbing mice had the largest PCSA values. For example, absolute PCSA of the acromiodeltoideus muscle was widest in the CLB mice ($\bar{x}$ = 2.5 mm^2), intermediate in the CON ($\bar{x}$ = 1.6 mm^2), and smallest in the WHL mice ($\bar{x}$ = 1.3 mm^2). All groups' absolute PCSA comparisons were highly significant ($P \leq 0.001$; Table 6.1). Body mass adjusted differences followed the same pattern as absolute PCSA, again with the greatest differences being between the two exercise groups ($P \leq 0.001$; Table 6.2). The CON and WHL groups overlapped in their relative physiological cross-sectional areas of the spinodeltoideus and superficial pectoralis muscles, but the CON mice differed significantly from the CLB mice in all three muscles ($P \leq 0.001$).

Unlike what was predicted, exercise had little effect on pennation angles of the muscles that attach to the deltoid crest (Table 6.1 and Figure 6.2). Only acromiodeltoideus pennation angle differed significantly ($P \leq 0.001$), with the greatest contrast found between experimental groups ($P = 0.008$). Pennation angle did not differ for any muscles between the control and the exercise groups. Priority index of force (I) considers how much of a muscle volume is due to shorter more pennate fibres and enhancing force. The values for I followed the same pattern as absolute PCSA, meaning that the muscle of the intermediate-intensity climbers facilitated potential force production. All groups were found to be significantly different for all three muscles' priority index of force ($P \leq 0.001$; Table 6.1 and Figure 6.2). Therefore, for each muscle attaching to the deltoid crest, the climbers had the shortest fibres with the largest cross-sectional areas, while the runners had the opposite pattern with the longest fibres and smallest cross-sectional area, leaving the controls between the two experimental groups. (Tables 6.1 and 6.2; Figures 6.2 and 6.3). There were no significant differences (absolute [Table 6.3] or relative to body mass [Table 6.4]) among age groups in any of the muscle fibre architecture variables.

6.2 Enthesis anatomy and function

The lengths, areas, thickness, and angle of the deltoid crest were considered and results are presented here next (Tables 6.5 - 6.8; Figures 6.4 and 6.5). It was predicted that the experimental groups would have larger and thicker entheses, especially the high-intensity runners. In contrast to significant effects of activity on aspects of muscle architecture, all three groups demonstrated substantial overlap in entheseal morphology and there were no significant differences (absolute [Table 6.5] or relative to body mass [Table 6.6]) among groups in any measure of muscle attachment site (Figures 6.4 and 6.5). When looking a little closer at the data, the only contrast that came close to significance was the thickness of the crest. The deltoid crest was slightly

thicker in the intermediate-intensity climbers ($\bar{x}$ = 0.06 mm) compared to the control mice ($\bar{x}$ = 0.05 mm) (P = 0.023). Contrary to the predictions, the high-intensity runners overlapped greatly in crest thickness. There were also no significant differences (absolute [Table 6.7] or relative to body mass [Table 6.8]) among age groups in any measure of muscle attachment site.

6.2.1 Relationship between hard- and soft-tissue variables

General linear mixed model (GLM) multivariate analyses were performed between muscular and entheseal variables to further examine the relationship between the hard- and soft-tissue variables (Tables 6.9 and 6.10). Variables from the spinodeltoideus muscle were regressed with the measurements from the lateral side of the deltoid crest, while the variables from the acromiodeltoideus and the superficial pectoralis muscles were regressed with the measurements of the medial side of the crest. All muscles were regressed with the thickness and the angle of the deltoid crest. Absolute acromiodeltoideus values showed significant relationships with the thickness of the deltoid crest (Table 6.9). Muscle mass (M; P = 0.031), physiological cross-sectional area (PCSA; P = 0.002) and the priority index of force (I; P = 0.002) of the acromiodeltoideus muscle were positively associated with crest thickness. As predicted, potentially stronger muscles (potential maximum force output) might be a reason for thicker entheses. On the other hand, acromiodeltoideus belly length (L_b; P = 0.003), fibre length (L_f; P = 0.003), and M/P_o (muscle mass/predicted effective maximum tetanic tension; P = 0.003) were negatively associated with crest thickness. A muscle with greater excursion potential might have the opposite effect of force by decreasing the thickness of an enthesis. Results were similar for the spinodletoideus (Table 6.9). As for superficial pectoralis, only its mass negatively correlated with the maximum width of the crest (P = 0.021; Table 6.9), which is contrary to the predictions.

GLM of the body mass adjusted variables showed the same pattern for the acromiodeltoideus and the spinodeltoideus muscles (Table 6.10). Superficial pectoralis was less predictable. Muscle mass had a positive relationship with the area of the crest ($P = 0.002$), while pennation angle and PCSA had a slightly negative relationship with the length ($P = 0.041$) and width ($P = 0.042$) of the deltoid crest (Table 6.10). Therefore in this sample, variables associated to potential muscle force or potential excursion and contraction velocity were not always associated with larger, longer, wider and differently shaped deltoid crest (Tables 6.9 and 6.10).

6.3 Biomechanical shape

The results from the diaphyseal geometric analyses for the two cross-sections of the left humerus are presented in this next section (Tables 6.11-6.15; Figures 6.6 and 6.7). Due to the high number of variables, the results will be described under three separate sections: 1) cross-sectional areas, 2) second moment of areas, and 3) section moduli.

6.3.1 Cross-sectional areas

According to beam theory, cross-sectional areas of bone tissue determine resistance to pure axial tensile or compressive loading (Huiskes, 1982; Ruff and Hayes, 1983; Hamrick et al., 2000; Ruff, 2000, 2002, 2003; Stock, 2002; Lieberman et al., 2004; O'Neill and Ruff, 2004; Pearson and Lieberman, 2004; Stock and Shaw, 2007; Goldman et al., 2009; Shaw and Stock, 2009a, b; Harrington, 2010; Shaw and Ryan, 2012). It was predicted that the experimental groups (particularly the high-intensity runners) would have a bone with better force resistance by increasing the bone area in the cross-section. In general, total subperiosteal (TA) and cortical

area (CA) increased from the standard section (25% of maximum bone length) to the distal margin of the deltoid crest (located more distally), while the medullary area (MA) decreased (Tables 6.11 - 613; Figure 6.6). A significant increase in bone rigidity under axial loading of the humerus was therefore found at the distal margin of the enthesis compared to the more proximal section (Table 6.13). When looking more closely at each histological cut, it was found that none of the contrasts were significantly different for the distal margin of the deltoid crest section (Table 6.12). For the 25% of maximal bone length section (Table 6.11), only cortical area (P = 0.003) significantly differed between groups. Cortical bone was the thickest in the climbing group ($\bar{x}$ = 0.49 mm^2) and surprisingly the running group had the thinnest cortical bone area ($\bar{x}$ = 0.42mm^2) (P = 0.002). The running and control mice had overlapping cortical thickness (Table 6.11). Since TA and MA influence CA, it was no surprise to see that the medullary area values followed a slightly opposite trend; WHL group had the largest medullary cavity ($\bar{x}$ = 0.44 mm^2) and the CLB had the smallest medullary cavity ($\bar{x}$ = 0.36 mm^2). Once again, there were no significant differences between the control and the running mice and both groups overlapped in cortical and medullary values (Table 6.11). There were no significant differences (absolute [Table 6.14] or relative to body mass [Table 6.15]) among age groups in any of the variables for cross-sectional areas.

6.3.2 Second moment of areas

Second moment of area properties, which take into consideration both the amount of bone material (reflecting bending strength) and its distribution relative to the neutral axis, were examined next (Tables 6.11-6.13; Figure 6.7). Contrary to the prediction, all of the variables were significantly higher (except I_{min}) on the distal of the deltoid crest cross-section; meaning

that the area where all three muscles inserted on the crest can resist the greatest bending stresses (Table 6.13). However, none of the contrasts were found to be significantly different for the distal margin of the deltoid crest section among the groups (Table 6.12), but the general tendency for this section was similar to the 25% of maximum bone length section. A lot of commonalities were seen for these properties and the presence of many outliers in each activity group brought many nonsignificant results. Overall, results for second moment of area variables were similar to the cross-sectional area results, where the intermediate-intensity climbers were separated from the controls and high-intensity runners (Table 6.11). For this standard cross-section, I_x, bending rigidity in the A-P plane about the M-L axis ($P = 0.046$), I_{max}, axis across which bending rigidity is the greatest ($P = 0.044$), and theta (θ), angle of maximum bending rigidity, demonstrated important distinctions between the activity groups. All three variables classified CLB mice with potentially greatest maximum bending rigidity of all three groups, and located in the anterior-posterior (A-P) plane ($\theta = -72.21 \pm 7.5°$). The WHL and CON groups had overlapping and lower values for I_x, I_{max}, and their angle of maximum bending rigidity were located on a more anteromedial-posterolateral (AM-PL) plane (Table 6.11). Some slight differences between the two experimental groups could also be distinguished for the polar second moment of area (J); bones from the CLB group seemed to reflect greater torsional strength than bones from the WHL group ($P = 0.041$). Despite these trends, after correcting for multiple comparisons, none of the contrasts remained significantly different (Table 6.11). There were also no significant differences (absolute [Table 6.14] or relative to body mass [Table 6.15]) among age groups in any of the variables for second moment of area.

6.3.3 Section moduli

Section modulus variables take into account the perpendicular distance from the bone's neutral axis to the outer perimeter of the bone to predict maximum bending strains. As was seen in the cortical areas and the second moment of areas, the standard thin section had the lowest values between the two slides (Table 6.13). The end of the deltoid crest was found to be the site that could sustain the greatest amount of loading. However, once again in both cross-sections, there was a lot of overlap for these geometric properties with very little significance in the results (Tables 6.11 and6.12; Figure 6.7). Unlike the second moment of area variables, the section modulus variables show significant differences in the medio-lateral planes (M-L) between the experimental groups. Despite the emphasis on the opposite axis, the distinction between the groups remains the same, separating the CLB group from the other two groups. Z_y/Z_x representing the relative M-L bending rigidity of the bone was close to significant ($P = 0.045$) at the 25% of maximum bone length section (Table 6.11). The runners had the highest Z_y/Z_x ratio ($\bar{x} = 1.13$), followed by the controls ($\bar{x} = 1.11$), and then by a lower ratio for the climbers ($\bar{x} = 1.0$). Although there was no significance in the most distal bone cross-section, the trends were similar for both sections of the humerus (Table 6.12). There were no significant differences (absolute [Table 6.14] or relative to body mass [Table 6.15]) among age groups in any of the variables for section modulus.

6.4 Entheseal microanatomy

So far, gross morphology and diaphyseal geometric properties of the enthesis could not clearly indicate any significant changes with age or activity. Next, bone's microanatomy was studied

through 1) qualitative observations, 2) cortical drift, 3) periosteal bone growth, and 4) variation in secondary remodelling activity (Tables 6.16 - 6.20; Figures 6.8 - 6.11).

6.4.1 Histological description

The following are qualitative observations of cortical bone tissue organization within each activity and age groups (Figures 6.8 - 6.10). Looking at the cross-sections in circularly polarized light, some general features were seen in all activity groups (Figure 6.8). The cortical bone found in the humerus of these mice was defined mainly with primary bone tissue (tissue formed as a result of periosteal or endosteal growth during post-natal development). Within each cortex the orientation of the collagen fibres and the vascular canals were observed to classify the bone tissue. In the 25% of the maximum bone length (standard) cross-section, the prevalent tissue was endosteal compacted coarse cancellous (ECCC) bone. This convoluted tissue is indicative of inward endosteal growth, usually associated with metaphyseal remodelling in proximal and distal regions of the diaphysis (Enlow, 1963; Francillon-Vieillot et al., 1990; de Ricqlès et al., 1991). This tissue, as seen in this sample, is associated with osteons. All groups showed evidence of ECCC in the standard cross-section with several horizontal blood vessels. Some individuals (particularly the intermediate-intensity climbing group) demonstrated evidence of ECCC around the medullary cavity (on the medial quadrant of the cortex) in the distal margin of the deltoid crest section (Figure 6.8). This detail became an interesting feature for later quantification (see below).

Collagen fibre organization defined most of the remaining tissue (especially in the distal margin of the deltoid crest) as parallel-fibre to lamellar bone (PFL). This type of tissue, which is intermediate in organization between woven and lamellar bone, is characterized by closely

packed collagen fibres within a single orientation and running approximately parallel to one another (Enlow, 1963; Francillon-Vieillot et al., 1990; de Ricqlès et al., 1991). It was not surprising to find parallel-fibered tissue in the humeral cross-sections of the mice, since this tissue is considered to have a relatively fast depositional rate, which is typical of small rodents (Enlow, 1957). Some of the parallel-fibre tissue did transition to lamellar bone, especially in the lateral quadrant of the cortices. The high-intensity running group seemed to be the individuals with the most organized lamellar bone, which expended anteriorly and posteriorly at times (Figure 6.8). Lamellar bone is an organized tissue often associated with adult individuals since their layered appearance result from regular change (whether continuous or discontinuous) in the collagen fibre bundles, and by extension, their depositional orientation (which again could be conveniently quantified with the vital fluorescent dyes).

On the other hand, the other two groups (CLB and CON), and particularly the intermediate-intensity climbing group, had more fibro-lamellar bone (Figure 6.8) than lamellar tissue. Like the ECCC, this tissue is a composite of woven bone and lamellar, where vascularization is dense and the compaction of lamellar bone over the spaces in the woven bone result in the formation of primary osteons (Enlow, 1963; Francillon-Vieillot et al., 1990; de Ricqlès et al., 1991). Lamellar-zonal and fibro-lamellar tissues are not mutually exclusive, and these cross-sections were nicely showing the interaction between the two tissue types, especially within the enthesis. A mixture of these tissues represented the deltoid crests with the addition of Sharpey's fibre (SF) tissue. Although Sharpey's fibres were present throughout the periosteal border of the cortices, the deltoid crests seem to have a significantly greater amount of this tissue. In most cases, the SF tissue was located on the lateral side of the crest (where fibro-lamellar tissue was located). Before quantifying osteon density, observations indicated that when present, the osteons and

drifting osteons were often located in the prominent deltoid crest within SF bone. They were also often found on the medial side of the cross-sections, with Sharpey fibres in the periosteal bone tissue. Osteons appeared to mainly form underneath muscle attachment sites for this mice sample.

There did not seem to be any striking differences in the bone tissue of the two age groups. For the most part, all of the cortices from the WHL group were commonly characterized with organized lamellar bone, while the cortices of the CLB group were associated with more disorganized tissue (fibro-lamellar) with signs of secondary remodelling activity. The cortices of the CON mice were intermediate, showing considerable variability and overlap in their tissue organization.

6.4.2 Cortical drift and bone turnover

Bone tissue features that indicated recently deposited bone versus resorptive bone surfaces (as well as the direction of the fluorescent labels – see below) could be identified to help determine the cortical drift patterns of the humeral cross-sections. As previously discussed, cortical drift is the change in shape of the bone associated with growth. For each cross-section, where sites of bone deposition were seen, pluses were drawn, and then minuses showed bone resorption (Figure 6.9). The bone deposited therefore showed the direction of drift. All groups had the same posterior-lateral cortical drift pattern.

Finally, before quantifying the above histological variations, visual examination of the superimposed images revealed clear differences in the patterns of growth between the groups (Figure 6.10). First, it could be seen that the CLB mice almost always preserved all three

fluorescent labels (Alizarin-red, DCAF-green, Xylenol-orange) in their cortices, while the CON mice were more variable in the presence of labels. However, the Xylenol-orange label (which was administered last in the sequence) was often the only label present in the WHL mice. The bone from the runners was resorbed more quickly during earlier growth stages of the bone. Since the high exercise level of these mice resorbed most of the bone, only four (JV = 1; AD = 3) individuals had a minimum of two labels preserved and could be included in the osteogenesis analysis (see below).

6.4.3 Rates of osteogenesis

The following investigated the periosteal bone growth of the cross-sections to determine if there would be differences among the three groups (Tables 6.16 - 6.18; Figure 6.11). As mentioned earlier (section 6.4.1), qualitative inspection of humeral microanatomy at the two section levels revealed clear differences in the growth of bone between the groups (Figure 6.10). Quantification of these observations was accomplished by measuring the distance between adjacent fluorescent labels. It was predicted that the experimental groups (specifically the high-intensity runners) would have a faster growing deltoid crest. As predicted, when growth rate measurements collected across all cortices and labels were averaged, the two exercise groups had faster periosteal bone growth than the controls ($P < 0.001$). Although the two experimental groups overlapped periosteal bone growth rates ($P = 0.014$), the WHL group had the fastest rates ($\bar{x}$ = 3.16 μm/day), followed by the CLB ($\bar{x}$ = 2.8 μm/day), while the control mice were characterized by slower bone growth ($\bar{x}$ = 2.1 μm/day) (Table 6.15 and Figure 6.11). The mean growth in the standard ($P = 0.004$) and the distal of deltoid crest ($P = 0.003$) sections followed a similar pattern. Although the juvenile group (JV) exhibited a faster bone growth rate than the

adults (AD), the differential growth between age groups was not statistically significant (Table 6.16).

In addition to total growth rate, rates of osteogenesis were calculated for every quadrant of the cross-sections, and the region immediately underlying the deltoid crest specifically. The Kruskal-Wallis (Table 6.16) results showed highly significant different contrasts between the activity groups across all regions of the cross-sections ($P \leq 0.007$). In every region, the same pattern was observed: the WHL mice had faster rate of bone growth while the CON mice had slower bone growth on average. The WHL and CLB groups often overlapped in their rate of osteogenesis (Figure 6.11). The deltoid crest was the site of the quickest periosteal osteogenesis for every group ($P = 0.007$) (Tables 6.16 and 6.17). At the crest, runners deposited on average 3.46 μm of periosteal bone a day, the climbers 2.99 μm/day, and controls 2.46 μm/day. Although the exercised mice had faster bone growth rates than the controls under the deltoid crest, no significant contrasts were found in post-hoc pairwise comparisons (Table 6.16). Again, the juvenile groups had faster bone growth on average than the adult groups, but this trend was not found to be statistically significant (Table 6.18).

6.4.4 Secondary remodelling activity

Lastly, secondary remodelling activity was investigated to see if exercise quantitatively changed remodelling of the humerus, and the deltoid crest specifically (Tables 6.19 and 6.20). Due to the small number of secondary osteon present within the cortices, osteon density was easy to calculate by simply counting the Haversian canals present across the cross-sections. Results showed that the intermediate-intensity climbing group had the highest number of osteons ($\bar{x}$ =

3.95), followed by the control group ($\bar{x}$ = 1.15), leaving the high-intensity running group with the least number of osteons ($\bar{x}$ = 0.5). All contrasts were highly significant ($P \leq 0.001$) and only the runners and the controls overlapped in osteon density (Table 6.19). A similar pattern was observed for the number of drifting osteons in both cross-sections with the largest gap in the number of secondary osteons found between the two different exercise groups ($P \leq 0.001$). The running group never had any drifting osteons, while the control group had the presence of one or two drifting osteon, but the climbing group almost always showed at least one drifting osteon in their cross-sections. Finally, there were once again no significant contrasts between age groups (Table 6.20).

6.5 Summary

This research looked at thirty female wild-type mice doing different exercise regime to investigate in greater details the relationship between activity, age, and muscle attachments. First, results showed that body mass were influenced by the amount of exercise practiced by the animals: lower body mass with higher amounts of exercise. Second, it was shown that the muscles attaching to the deltoid crest significantly differed between activity levels and types. An architectural trade-off was observed between potential maximum force output (M, PCSA, *I*) and potential excursion and contraction velocity (L_b, L_f, M/P_o) of the muscles studied. Activity had no effect on the pennation angles of the muscles attaching to the deltoid crest. None of the muscle fibre architectural variables differed among age groups.

This project started out with the idea of looking at the effect of exercise on entheseal morphology. Surprisingly, no differences were found between activity patterns associated with

the gross morphology of the crest. Some correlations were found between the acromiodeltoideus and the spinodeltoideus muscle variables with the thickness of the crest. Potential excursion and contraction velocity seemed to decrease the crest thickness, while potential maximum force output seemed to positively correlate with the thickness of the crest. On the other hand, superficial pectoralis was much less predictable. Overall, all exercise and age groups had overlapping morphology of the deltoid crest.

Since the gross morphology of the enthesis did not indicate any changes with activity, the bone's shape and microanatomy were observed. The results showed that diaphyseal geometric results were not very significant and differed only slightly between types of activities. Despite the many commonalities seen in the diaphyseal geometric properties, clear differences in histological properties between activity groups were observed, especially within the deltoid crest. First, the type of bone tissue found in the humerus and the prominent crest varied between the level (more organized lamellar tissue) and the type of activity (more disorganized fibro-lamellar bone) practiced by the mice. Second, bone growth differences were seen between the activity groups and were associated with the amount of activity each group experienced: more exercise was matched with faster periosteal bone growth. Finally, bone remodelling within the deltoid crest differed the most between the two activity types: increased number of secondary osteons with vertical climbing. However, no significant differences were noted between the juvenile and adult mice groups for any of the above bony variables. This study has shown how muscle and bone can vary with the amount and type of activity performed.

Table 6.1 Results of Kruskal-Wallis and two-tailed Mann-Whitney contrasts between groups for body mass, acromiodeltoideus, spinodeltoideus, and superficial pectoralis absolute measurements and muscle fibre architectural properties. Means ± standard deviations are reported for all three groups. Z scores are given with significance in brackets (when $P \leq 0.05$) for the pairwise results.

Variable	Control (CON)	Running (WHL)	Climbing (CLB)	Kruskal-Wallis	Mann-Whitney CON vs WHL	Mann-Whitney CON vs CLB	Mann-Whitney WHL vs CLB
Body mass (g)	33.93 ± 2.27	29.88 ± 1.82	31.94 ± 4.05	**0.007**	-3.326 **(0.001)**	-1.436	-1.285
Acromiodeltoideus							
M (μg)	9.0 ± 0.67	8.4 ± 0.7	10.4 ± 0.7	**< 0.001**	-1.975	-3.461 **(0.001)**	-3.719 **(<0.001)**
L_b (mm)	9.05 ± 0.61	9.56 ± 0.69	7.23 ± 0.71	**< 0.001**	-1.587	-3.780 **(<0.001)**	-3.78 **(<0.001)**
L_f (mm)	4.29 ± 0.26	5.21 ± 0.32	3.54 ± 0. .31	**< 0.001**	-3.628 **(<0.001)**	-3.78 **(<0.001)**	-3.78 **(<0.001)**
θ (°)	34.73 ± 8.42	34.7 ± 3.89	26.07 ± 6.75	**< 0.001**	-.076	-2.268 (0.023)	-2.646 (0.008)
PCSA (mm^2)	1.61 ± 0.15	1.26 ± 0.14	2.49 ± 0.22	**< 0.001**	-3.553 **(<0.001)**	-3.78 **(<0.001)**	-3.78 **(<0.001)**
M/P_o	0.25 ± 0.03	0.3 ± 0.02	0.19 ± 0.02	**< 0.001**	-3.024 **(0.002)**	-3.704 **(<0.001)**	-3.78 **(<0.001)**
I	0.037 ± 0.004	0.03 ± 0.002	0.052 ± 0.004	**< 0.001**	-3.25 **(0.001)**	-3.78 **(<0.001)**	-3.78 **(<0.001)**
Spinodeltoideus							
M (μg)	18.8 ± 2.9	17.9 ± 1.2	22.1 ± 3.96	0.05	-0.347	-1.947 (0.05)	-2.222 (0.026)
L_b (mm)	12.24 ± 0.76	12.24 ± 0.73	10.35 ± 0.92	**< 0.001**	-0.227	-3.477 **(0.001)**	-3.404 **(0.001)**
L_f (mm)	7.41 ± 0.77	8.47 ± 0.33	6.01 ± 0.75	**< 0.001**	-3.628 **(<0.001)**	-3.099 **(0.002)**	-3.78 **(<0.001)**
θ (°)	10.32 ± 1.68	11.45 ± 2.83	11.0 ± 3.67	NS	-0.907	-0.227	-0.832 **(<0.001)**
PCSA (mm^2)	2.37 ± 0.29	1.96 ± 0.17	3.43 ± 0.63	**< 0.001**	-3.024 **(0.002)**	-3.553 **(<0.001)**	-3.78 **(<0.001)**
M/P_o	0.35 ± 0.04	0.41 ± 0.01	0.29 ± 0.04	**< 0.001**	-3.402 **(0.001)**	-3.024 **(0.002)**	-3.78 **(<0.001)**
I	0.034 ± 0.003	0.029 ± 0.0014	0.044 ± 0.0049	**< 0.001**	-3.477 **(0.001)**	-3.553 **(<0.001)**	-3.78 **(<0.001)**
Superficial pectoralis							
M (μg)	101.9 ± 6.15	101.0 ± 9.06	111.5 ± 6.45	0.009	-0.532	-2.84 **(0.005)**	-2.424 (0.015)
L_b (mm)	22.72 ± 0.73	22.93 ± 0.74	20.71 ± 1.19	**0.001**	-0.529	-3.175 **(0.001)**	-3.139 **(0.002)**
L_f (mm)	13.21 ± 0.31	14.84 ± 0.68	11.86 ± 0.77	**< 0.001**	-3.780 **(<0.001)**	-3.553 **(<0.001)**	-3.78 **(<0.001)**
θ (°)	10.4 ± 2.39	10.15 ± 2.04	10.79 ± 2.01	NS	-0.227	-0.907	-0.681
PCSA (mm^2)	7.18 ± 0.4	6.33 ± 0.35	8.75 ± 0.49	**< 0.001**	-3.704 **(<0.001)**	-3.78 **(<0.001)**	-3.78 **(<0.001)**
M/P_o	0.63 ± 0.02	0.71 ± 0.03	0.57 ± 0.04	**< 0.001**	-3.78 **(<0.001)**	-3.477 **(<0.001)**	-3.78 **(<0.001)**
I	0.033 ± 0.0008	0.029 ± 0.0008	0.038 ± 0.002	**< 0.001**	-3.78 **(<0.001)**	-3.78 **(<0.001)**	-3.78 **(<0.001)**

M = muscle mass; L_b = belly length; L_f = sarcomere adjusted fibre length; θ = pennation angle; PCSA = sarcomere adjusted physiological cross-sectional area; M/P_o = muscle mass/predicted effective maximum tetanic tension; *I* = priority index of force.
Bold = significant differences after the Dunn-Šidák correction method ($P \leq 0.007$ for 7 comparisons per muscle contrast); NS = non-significant.

Table 6.2 Results of Kruskal-Wallis and two-tailed Mann-Whitney contrasts between groups for body mass adjusted acromiodeltoideus, spinodeltoideus, and superficial pectoralis measurements and muscle fibre architectural properties. Resulting numbers are dimensionless. Means ± standard deviations are reported for all three groups. Z scores are given with significance in brackets (when $P \leq 0.05$) for the pairwise results.

Variable	Control (CON)	Running (WHL)	Climbing (CLB)	Kruskal-Wallis	Mann-Whitney CON vs WHL	Mann-Whitney CON vs CLB	Mann-Whitney WHL vs CLB
Acromiodeltoideus							
M	0.28 ± 0.05	0.29 ± 0.03	0.32 ± 0.05	NS	-0.227	-1.89	-1.739 **(<0.001)**
L_b	2.8 ± 0.19	3.08± 0.23	2.28 ± 0.19	**< 0.001**	-2.495 (0.013)	-3.628 **(<0.001)**	-3.78 **(<0.001)**
L_f	1.33 ± 0.1	1.68 ± 0.11	1.12 ± 0.11	**< 0.001**	3.704 **(<0.001)**	-3.704 **(0.001)**	-3.78 **(<0.001)**
PCSA	0.15 ± 0.02	0.13 ± 0.02	0.25 ± 0.03	**< 0.001**	-2.797 (**0.005**)	-3.78 **(<0.001)**	-3.78 **(<0.001)**
Spinodeltoideus							
M	0.56± 0.08	0.6 ± 0.04	0.69 ± 0.11	**0.005**	-2.041 (0.041)	-2.57 (**0.01**)	-2.495 (0.013)
L_b	3.78 ± 0.23	3.94 ± 0.19	3.26 ± 0.2	**< 0.001**	-1.587	-3.553 **(<0.001)**	-3.78**(<0.001)**
L_f	2.29 ± 0.23	2.73 ± 0.14	1.9 ± 0.24	**< 0.001**	-3.628 **(<0.001)**	-2.797 (**0.005**)	-3.78 **(<0.001)**
PCSA	0.23 ± 0.03	0.2 ± 0.01	0.34 ± 0.05	**< 0.001**	-1.739	-3.628 **(<0.001)**	-3.78 **(<0.001)**
Superficial pectoralis							
M	3.01 ± 0.23	3.38 ± 0.26	3.53 ± 0.38	**0.006**	-2.495 (0.013)	-2.873 **(0.004)**	-0.907
L_b	7.02 ± 0.12	7.39 ± 0.24	6.54 ± 0.19	**< 0.001**	-3.326 **(0.001)**	-3.628 **(<0.001)**	-3.78 **(<0.001)**
L_f	4.08 ± 0.13	4.78 ± 0.23	3.75 ± 0.29	**< 0.001**	-3.78 **(<0.001)**	-2.646 (**0.008**)	-3.78 **(<0.001)**
PCSA	0.69 ± 0.04	0.66 ± 0.02	0.87 ± 0.06	**< 0.001**	-1.587	-3.704 **(<0.001)**	-3.78 **(<0.001)**

M = body mass adjusted muscle mass; L_b = body mass adjusted belly length; L_f = body mass and sarcomere adjusted fibre length; PCSA = body mass and sarcomere adjusted physiological cross-sectional area.

Bold = significant differences after the Dunn-Šidák correction method ($P \leq 0.01$ for 4 comparisons per muscle contrast); NS = non-significant.

Table 6.3 Results of two-tailed Mann-Whitney contrasts between age groups for body mass, acromiodeltoideus, spinodeltoideus, and superficial pectoralis absolute measurements and muscle fibre architectural properties. Means ± standard deviations are reported for both groups. Z scores are given and all results are found non-significant ($P > 0.05$)

Variable	Juvenile (JV)	Adult (AD)	Mann-Whitney JV vs AD
Body mass (g)	31.43 ± 3.63	32.4 ± 2.86	-0.684
Acromiodeltoideus			
M (μg)	9.4 ± 1.06	9.13 ± 1.12	-0.866
L_b (mm)	8.54 ± 1.28	8.69 ± 1.17	-0.228
L_f (mm)	4.41 ± 0.64	4.28 ± 0.87	-0.477
θ (°)	30.1 ± 7.62	33.56 ± 7.46	-0.933
PCSA (mm^2)	1.79 ± 0.47	1.79 ± 0.65	-0.27
M/P_o	0.24 ± 0.05	0.25 ± 0.06	-0.311
I	0.04 ± 0.009	0.04 ± 0.01	-0.27
Spinodeltoideus			
M (μg)	18.87 ± 2.77	20.33 ± 3.81	-0.797
L_b (mm)	11.24 ± 1.31	11.98 ± 0.98	-1.39
L_f (mm)	7.37 ± 1.29	7.22 ± 1.15	-0.477
θ (°)	10.89 ± 2.27	10.96 ± 3.3	-0.518
PCSA (mm^2)	2.47 ± 0.69	2.7 ± 0.8	-0.85
M/P_o	0.35 ± 0.06	0.36 ± 0.05	-0.643
I	0.03 ± 0.007	0.04 ± 0.007	-0.601
Superficial pectoralis			
M (μg)	102.2 ± 8.01	107.4 ± 8.58	-1.684
L_b (mm)	21.84 ± 1.45	22.4 ± 1.21	-1.079
L_f (mm)	13.22 ± 1.16	13.38 ± 1.6	-0.311
θ (°)	10.35 ± 2.07	10.54 ± 2.18	-0.145
PCSA (mm^2)	7.27 ± 1.06	7.57 ± 1.15	-0.892
M/P_o	0.632 ± 0.055	0.639 ± 0.077	-0.187
I	0.033 ± 0.003	0.033 ± 0.004	-0.104

M = muscle mass; L_b = belly length; L_f = sarcomere adjusted fibre length; θ = pennation angle; PCSA = sarcomere adjusted physiological cross-sectional area; M/P_o = muscle mass/predicted effective maximum tetanic tension; *I* = priority index of force.

Table 6.4 Results two-tailed Mann-Whitney contrasts between age groups for body mass adjusted acromiodeltoideus, spinodeltoideus, and superficial pectoralis measurements and muscle fibre architectural properties. Resulting numbers are dimensionless. Means ± standard deviations are reported for both groups. Z scores are given and all results are found non-significant ($P > 0.05$).

Variable	Juvenile (JV)	Adult (AD)	Mann-Whitney JV vs AD
Acromiodeltoideus			
M	0.31 ± 0.05	0.28 ± 0.04	-1.804
L_b	2.71 ± 0.39	2.73 ± 0.4	-0.021
L_f	1.4 ± 0.22	1.35 ± 0.3	-0.726
PCSA	0.18 ± 0.05	0.18 ± 0.06	-0.726
Spinodeltoideus			
M	0.6 ± 0.08	0.63 ± 0.12	-0.518
L_b	3.57 ± 0.39	3.76 ± 0.3	-1.39
L_f	2.34 ± 0.42	2.27 ± 0.39	-0.436
PCSA	0.25 ± 0.07	0.27 ± 0.08	-0.933
Superficial pectoralis			
M	3.28 ± 0.38	3.33 ± 0.35	-0.809
L_b	6.93 ± 0.38	7.04 ± 0.43	-0.477
L_f	4.2 ± 0.41	4.21 ± 0.57	-0.021
PCSA	0.73 ± 0.12	0.75 ± 0.1	-0.684

M = body mass adjusted muscle mass; L_b = body mass adjusted belly length; L_f= body mass and sarcomere adjusted fibre length; PCSA = body mass and sarcomere adjusted physiological cross-sectional area.

Table 6.5 Results of Kruskal-Wallis and two-tailed Mann-Whitney contrasts between groups for absolute humeral and deltoid crest measurements. Mean ± standard deviations are reported for all three groups. Z scores are also given with significance in brackets (when $P \leq 0.05$) for the pairwise results.

Variable	Control (CON)	Running (WHL)	Climbing (CLB)	Kruskal-Wallis	Mann-Whitney		
					CON vs WHL	CON vs CLB	WHL vs CLB
Humerus length (mm)	12.43 ± 0.4	12.31 ± 0.31	12.46 ± 0.51	NS	-0.832	-0.983	-0.378
Lateral							
Max length (mm)	1.44 ± 0.08	1.42 ± 0.06	1.4 ± 0.083	NS	-0.832	-0.265	-1.211
Max width (mm)	0.41 ± 0.04	0.42 ± 0.03	0.42 ± 0.01		-0.227	-1.25	-0.644
Area (mm^2)	0.38 ± 0.04	0.38 ± 0.034	0.37± 0.035	NS	-0.227	-0.756	-1.209
Medial							
Max length (mm)	1.39 ± 0.11	1.41 ± 0.09	1.36 ± 0.09	NS	-0.378	-0.227	-0.644
Max width (mm)	0.36 ± 0.04	0.33 ± 0.03	0.33 ± 0.01	NS	-0.983	-1.176	-1.401
Area (mm^2)	0.3 ± 0.037	0.3 ± 0.032	0.31± 0.04	NS	-0.378	-0.189	-0.605
Thickness (mm)	0.052 ± 0.004	0.05 ± 0.005	0.056 ± 0.006	NS	-0.832	-2.269 (0.023)	-1.817
Angle (º)	145.28 ± 18.34	147.21 ± 10.51	148.01 ± 9.6	NS	-0.151	-0.151	-0.302

Non-significant after the Dunn-Šidák correction method ($P \leq 0.006$ for 8 contrast activity group contrast); NS = non-significant.

Table 6.6 Results of Kruskal-Wallis and two-tailed Mann-Whitney contrasts between groups for body mass adjusted deltoid crest measurements. Resulting numbers are dimensionless. Mean ± standard deviations are reported for all three groups. Z scores are also given with significance in brackets (when $P \leq 0.05$) for the pairwise results.

Variable	Control (CON)	Running (WHL)	Climbing (CLB)	Kruskal-Wallis	Mann-Whitney		
					CON vs WHL	CON vs CLB	WHL vs CLB
Humerus length	3.84 ± 0.12	3.97 ± 0.14	3.94 ± 0.19	NS	-2.384 (0.017)	-0.983	-0.378
Lateral							
Max length	0.45 ± 0.029	0.46 ± 0.019	0.44 ± 0.03	NS	-0.946	-0.265	-1.211
Max width	0.13 ± 0.012	0.13 ± 0.008	0.13 ± 0.006	NS	-1.668	-1.25	-0.644
Area	0.04 ± 0.004	0.04 ± 0.004	0.04 ± 0.005	NS	-1.663	-0.756	-1.209
Medial							
Max length	0.43 ± 0.04	0.45 ± 0.032	0.43 ± 0.038	NS	-1.362	-0.227	-1.401
Max width	0.11 ± 0.01	0.11 ± 0.01	0.11 ± 0.007	NS	-0.379	-1.176	-0.644
Area	0.03 ± 0.004	0.03 ± 0.003	0.03 ± 0.006	NS	-1.475	-0.189	-0.605
Thickness	0.015 ± 0.001	0.016 ± 0.002	0.018 ± 0.002	NS	-0.227	-2.269 (0.023)	-1.817

Non-significant after the Dunn-Šidák correction method ($P \leq 0.006$ for 8 activity group contrast); NS = non-significant.

Table 6.7 Results of two-tailed Mann-Whitney contrasts between age groups for absolute humeral and deltoid crest measurements. Mean ± standard deviations are reported for both groups. Z scores are also given with significance in brackets (when $P \leq 0.05$) for the pairwise results.

Variable	Juvenile (JV)	Adult (AD)	Mann-Whitney JV vs AD
Humerus length (mm)	12.51 ± 0.47	12.28 ± 0.3	-1.514
Lateral			
Max length (mm)	1.43 ± 0.07	1.41 ± 0.08	-0.684
Max width (mm)	0.42 ±0.03	0.41 ± 0.03	-0.643
Area (mm^2)	0.38 ± 0.04	0.37 ± 0.03	-1.099
Medial			
Max length (mm)	1.38 ± 0.1	1.39 ± 0.1	-0.353
Max width (mm)	0.35 ± 0.03	0.34 ± 0.03	-0.975
Area (mm^2)	0.31 ± 0.04	0.29 ± 0.04	-0.56
Thickness (mm)	0.053 ± 0.005	0.052 ± 0.006	-1.016
Angle (º)	140.82 ± 13.52	152.86 ± 9.44	-2.551 (0.011)

Non-significant after the Dunn-Šidák correction method ($P \leq 0.006$ for 8 contrast activity group contrast).

Table 6.8 Results of two-tailed Mann-Whitney contrasts between age groups for body mass adjusted deltoid crest measurements. Resulting numbers are dimensionless. Mean ± standard deviations are reported for both groups. Z scores are given and all results are found non-significant (*P* > 0.05).

Variable	Juvenile (JV)	Adult (AD)	Mann-Whitney JV vs AD
Humerus length	3.97 ± 0.17	3.86 ± 0.13	-1.785
Lateral			
Max length	0.45 ± 0.027	0.44 ± 0.028	-0.934
Max width	0.133 ± 0.009	0.13 ± 0.01	-1.621
Area	0.039 ± 0.005	0.036 ± 0.004	-1.245
Medial			
Max length	0.44 ± 0.04	0.44 ± 0.037	-0.062
Max width	0.11 ± 0.008	0.11 ± 0.01	-1.226
Area	0.031 ± 0.005	0.029 ± 0.004	-0.809
Thickness	0.017 ± 0.001	0.016 ± 0.002	-1.328

Table 6.9 Results of general linear mixed models (GLM) for multivariate variables between absolute attachment site morphology measurements and muscular variables. *P*-values are always shown and when significant ($P \leq 0.05$) partial et-squared (η^2) is provided in brackets and the parameter estimate value (β) is given underneath.

Muscle variable	Deltoid variable							
	Lateral			Medial				
	Max length (mm)	Max width (mm)	Area (mm^2)	Max length (mm)	Max width (mm)	Area (mm^2)	Thickness (mm)	Angle (º)
Acromiodeltoideus								
M (μg)	-	-	-	0.605	0.917	0.86	**0.031 (0.179) 83.47**	0.98
L_b (mm)	-	-	-	0.733	0.408	0.493	**0.003 (0.312) -123.0**	0.988
L_f (mm)	-	-	-	0.54	0.855	0.576	**0.003 (0.312) -52.81**	0.55
θ (°)	-	-	-	0.36	0.15	0.349	0.112	0.322
PCSA (mm^2)	-	-	-	0.349	0.494	0.961	**0.002 (0.328) 59.41**	0.896
M/P_o	-	-	-	0.445	0.633	0.985	**0.003 (0.314) -3.7**	0.962
I	-	-	-	0.309	0.435	0.931	**0.002 (0.34) 1.04**	0.926
Spinodeltoideus								
M (μg)	0.502	0.737	0.827	-	-	-	0.166	0.105
L_b (mm)	0.262	0.749	0.791	-	-	-	0.122	0.41
L_f (mm)	0.783	0.946	0.231	-	-	-	**0.028 (0.186) -65.72**	0.856
θ (°)	0.47	0.547	0.307	-	-	-	0.84	0.571
PCSA (mm^2)	0.701	0.865	0.514	-	-	-	**0.019 (0.208) 62.47**	0.136
M/P_o	0.734	0.991	0.279	-	-	-	**0.031 (0.180) -3.15**	0.82
I	0.932	0.988	0.293	-	-	-	**0.018 (0.213) 0.59**	0.0
Superficial pectoralis								
M (μg)	-	-	-	0.222	**0.021 (0.202)**	0.411	0.176	0.61

M (μg)					**-136.85**			
L_b (mm)	-	-	-	0.83	0.426	0.413	0.345	0.71
L_f (mm)	-	-	-	0.763	0.867	0.7	0.355	0.663
θ (°)	-	-	-	0.825	0.063	0.506	0.557	0.334
PCSA (mm^2)	-	-	-	0.27	0.176	0.764	0.103	0.424
M/P_o	-	-	-	0.777	0.759	0.719	0.379	0.709
I	-	-	-	0.518	0.729	0.958	0.236	0.478

M = muscle mass; L_b = belly length; L_f = sarcomere adjusted fibre length; θ = pennation angle; PCSA = sarcomere adjusted physiological cross-sectional area; M/P_o = muscle mass/predicted effective maximum tetanic tension; *I* = priority index of force.

Table 6.10 Results of general linear mixed models (GLM) for multivariate variables between body mass adjusted attachment site morphology measurements and muscular variables. *P*-values are always shown and when significant ($P \leq 0.05$) partial et-squared (η^2) is provided in brackets and the parameter estimate value (β) is given underneath.

Muscle variable	Deltoid variable							
	Lateral			Medial				
	Max length	Max width	Area	Max length	Max width	Area	Thickness	Angle
Acromiodeltoideus								
M	-	-	-	0.112	0.464	0.144	0.197	0.641
L_b	-	-	-	0.212	0.357	0.685	**0.001 (0.355) -138.78**	0.764
L_f	-	-	-	0.138	0.86	0.892	**0.011 (0.241) -215.71**	0.358
θ (°)	-	-	-	0.309	0.17	0.191	0.099	0.325
PCSA	-	-	-	0.177	0.437	0.648	**0.003 (0.308) 183.24**	0.652
M/P_o	-	-	-	0.164	0.576	0.717	**0.012 (0.236) -15.063**	0.763
I	-	-	-	0.143	0.37	0.616	**0.004 (0.303) 3.25**	0.643
Spinodeltoideus								
M	0.829	0.646	0.299	-	-	-	0.383	0.166
L_b	0.451	0.803	0.951	-	-	-	**0.026 (0.19) -92.19**	0.532
L_f	0.439	0.983	0.543	-	-	-	**0.027 (0.188) -309.49**	0.533
θ (°)	0.381	0.566	0.285	-	-	-	0.916	0.477
PCSA	0.21	0.755	0.635	-	-	-	**0.034 (0.173) 175.74**	0.154
M/P_o	0.484	0.935	0.602	-	-	-	**0.027 (0.187) -14.93**	0.502
I	0.312	0.918	0.555	-	-	-	**0.02 (0.206) 1.895**	0.308
Superficial pectoralis								
M	-	-	-	0.173	0.145	**0.002 (0.335) 45.73**	0.631	0.772

L_b	-	-	-	0.168	0.423	0.618	0.076	0.952
L_f	-	-	-	0.121	0.45	0.889	0.077	0.857
θ (°)	-	-	-	0.986	**0.041 (0.161) -91.14**	0.547	0.781	0.415
PCSA	-	-	-	**0.042 (0.161) -11.28**	**0.043 (0.16) -44.68**	0.511	0.057	0.696
M/P_o	-	-	-	0.124	0.554	0.868	0.081	0.898
I	-	-	-	0.079	0.221	0.682	0.062	0.755

M = body mass adjusted muscle mass; L_b = body mass adjusted belly length; L_f = body mass and sarcomere adjusted fibre length; PCSA = body mass and sarcomere adjusted physiological cross-sectional area.

Table 6.11 Results of Kruskal-Wallis and two-tailed Mann-Whitney contrasts between groups for the biomechanical shape (bone strength) of the histological cut made at the 25% of maximum humeral length. Mean ± standard deviations are reported for all three groups. Z scores are also given with significance in brackets (when $P \leq 0.05$) for the pairwise results.

Variable	Control (CON)	Running (WHL)	Climbing (CLB)	Kruskal-Wallis	Mann-Whitney		
					CON vs WHL	CON vs CLB	WHL vs CLB
TA (mm^2)	0.838 ± 0.084	0.85 ± 0.102	0.848 ± 0.054	NS	0.683	-0.327	-0.454
CA (mm^2)	0.426 ± 0.042	0.415 ± 0.045	0.492 ± 0.046	**0.003**	0.624	-2.694 (0.007)	**-3.099 (0.002)**
MA (mm^2)	0.412 ± 0.062	0.435 ± 0.095	0.356 ± 0.034	0.024	0.568	-2.368 (0.018)	-2.268 (0.023)
Ix (mm^4)	0.059 ± 0.02	0.058 ± 0.015	0.077 ± 0.018	0.046	0	-1.96 (0.05)	-2.268 (0.023)
Iy (mm^4)	0.041 ± 0.004	0.042 ± 0.004	0.043 ± 0.005	NS	-0.653	-0.735	-0.151
Imax (mm^4)	0.064 ± 0.02	0.066 ± 0.011	0.081 ± 0.018	0.044	-0.816	-1.796	-2.419 (0.016)
Imin (mm^4)	0.036 ± 0.006	0.035 ± 0.007	0.038 ± 0.005	NS	-0.163	-0.49	-0.605
Imax/Imin	1.79 ± 0.5	1.94 ± 0.42	2.12 ± 0.32	NS	-0.735	-1.633	-0.983
J (mm^4)	0.1 ± 0.023	0.1 ± 0.016	0.119 ± 0.023	NS	-0.163	-1.715	-2.041 (0.041)
Theta (°)	-67.12 ± 13.43	-61.06 ± 10.77	-72.21 ± 7.49	NS	-1.143	-0.408	-2.268 (0.023)
Zx (mm^3)	0.068 ± 0.014	0.068 ± 0.013	0.074 ± 0.013	NS	-0.735	-1.388	-0.605
Zy (mm^3)	0.072 ± 0.008	0.075 ± 0.008	0.073 ± 0.008	NS	-0.98	-0.408	-0.529
Zp (mm^3)	0.14 ± 0.021	0.141 ± 0.021	0.147 ± 0.021	NS	-0.572	-0.653	-0.227
Zy/Zx	1.107 ± 0.179	1.125 ± 0.157	1.00 ± 0.107	0.045	-0.245	-1.96 (0.05)	-2.268 (0.023)

See text for description of each variable.

Bold = significant differences after the Dunn-Šidák correction method ($P \leq 0.004$ for 14 activity group contrast); NS = non-significant.

Table 6.12 Results of Kruskal-Wallis and two-tailed Mann-Whitney contrasts between groups for the biomechanical shape of the histological cut made at the distal margin of deltoid crest. Mean ± standard deviations are reported for all three groups. Z scores are also given with significance in brackets (when $P \leq 0.05$) for the pairwise results.

Variable	Control (CON)	Running (WHL)	Climbing (CLB)	Kruskal-Wallis	Mann-Whitney		
					CON vs WHL	CON vs CLB	WHL vs CLB
TA (mm^2)	0.996 ± 0.126	1.006 ± 0.107	1.045 ± 0.123	NS	-0.378	-0.983	-1.134
CA (mm^2)	0.672 ± 0.096	0.695 ± 0.121	0.736 ± 0.162	NS	-0.605	-1.436	-0.983
MA (mm^2)	0.324 ± 0.058	0.311 ± 0.053	0.309 ± 0.069	NS	-0.643	-0.605	-0.227
Ix (mm^4)	0.232 ± 0.099	0.264 ± 0.096	0.283 ± 0.117	NS	-0.605	-1.134	-0.151
Iy (mm^4)	0.056 ± 0.009	0.06 ± 0.01	0.064 ± 0.015	NS	-0.68	-1.587	-0.907
Imax (mm^4)	0.25 ± 0.102	0.287 ± 0.1	0.309 ± 0.122	NS	-0.68	-1.209	-0.227
Imin (mm^4)	0.038 ± 0.005	0.038 ± 0.004	0.039 ± 0.005	NS	-0.302	-0.605	-0.454
Imax/Imin	6.49 ± 2.12	7.35 ± 2.07	7.71 ± 2.53	NS	-1.285	-1.361	-0.454
J (mm^4)	0.288 ± 0.106	0.325 ± 0.104	0.348 ± 0.127	NS	-0.756	-1.285	-0.302
Theta (°)	-73.1 ± 4.58	-72.05 ± 3.79	-71.24 ± 5.14	NS	-0.378	-0.529	-0.227
Zx (mm^3)	0.181 ± 0.06	0.193 ± 0.06	0.21 ± 0.08	NS	-0.454	-0.907	-0.605
Zy (mm^3)	0.082 ± 0.01	0.088 ± 0.01	0.093 ± 0.02	NS	-1.361	-2.268 (0.023)	-1.058
Zp (mm^3)	0.293 ± 0.09	0.316 ± 0.09	0.341 ± 0.11	NS	-0.454	-0.983	-0.68
Zy/Zx	0.496 ± 0.135	0.492 ± 0.136	0.504 ± 0.188	NS	-0.151	-0.227	-0.151

See text for description of each variable.

Non-significant differences after the Dunn-Šidák correction method ($P \leq 0.004$ for 14 activity group contrast); NS = non-significant.

Table 6.13 Results of Wilcoxon's signed ranks contrasts for the biomechanical variables between the two histological cross-sections.

Variable	Wilcoxon's signed ranks	
	Z scores	*P*-values
TA (mm^2)	-4.314	**<0.001**
CA (mm^2)	-4.617	**<0.001**
MA (mm^2)	-4.119	**<0.001**
Ix (mm^4)	-4.703	**<0.001**
Iy (mm^4)	-4.617	**<0.001**
Imax (mm^4)	-4.703	**<0.001**
Imin (mm^4)	-1.546	0.122
Imax/Imin	-4.703	**<0.001**
J (mm^4)	-4.703	**<0.001**
Theta (°)	-2.714	**0.007**
Zx (mm^3)	-4.703	**<0.001**
Zy (mm^3)	-4.011	**<0.001**
Zp (mm^3)	-4.703	**<0.001**
Zy/Zx	-4.703	**<0.001**

See text for description of each variable.
Bold = significant differences after the Dunn-Šidák correction method ($P \leq 0.004$ for 14 activity group contrast)

Table 6.14 Results two-tailed Mann-Whitney contrasts between age groups for the biomechanical shape of the histological cut made at the 25% of maximum humeral length. Mean ± standard deviations are reported for both groups. Z scores are given and all results are found non-significant ($P > 0.05$).

Variable	Juvenile (JV)	Adult (AD)	Mann-Whitney JV vs AD
TA (mm^2)	0.84 ± 0.071	0.85 ± 0.089	-0.415
CA (mm^2)	0.44 ± 0.054	0.45 ± 0.058	-0.262
MA (mm^2)	0.41 ± 0.07	0.4 ± 0.081	-0.218
Ix (mm^4)	0.061 ± 0.015	0.069 ± 0.022	-0.655
Iy (mm^4)	0.041 ± 0.005	0.043 ± 0.004	-0.917
Imax (mm^4)	0.065 ± 0.014	0.075 ± 0.02	-1.222
Imin (mm^4)	0.036 ± 0.006	0.036 ± 0.006	-0.044
Imax/Imin	1.83 ± 0.37	2.08 ± 0.44	-1.44
J (mm^4)	0.1 ± 0.018	0.11 ± 0.025	-0.786
Theta (°)	-68.23 ± 9.67	-65.43 ± 12.94	-0.611
Zx (mm^3)	0.068 ± 0.01	0.071 ± 0.015	-0.349
Zy (mm^3)	0.073 ± 0.009	0.074 ± 0.007	-0.175
Zp (mm^3)	0.14 ± 0.019	0.15 ± 0.022	-0.349
Zy/Zx	1.08 ± 0.09	1.08 ± 0.2	-0.262

See text for description of each variable.

Table 6.15 Results of two-tailed Mann-Whitney contrasts between age groups for the biomechanical shape of the histological cut made at the distal margin of deltoid crest. Mean ± standard deviations are reported for both groups. Z scores are also given with significance in brackets (when $P \leq 0.05$) for the pairwise results.

Variable	Juvenile (JV)	Adult (AD)	Mann-Whitney JV vs AD
TA (mm^2)	1.02 ± 0.12	1.01 ± 0.12	-0.062
CA (mm^2)	0.68 ± 0.13	0.72 ± 0.13	-0.809
MA (mm^2)	0.34 ± 0.05	0.29 ± 0.06	-2.282 (0.023)
Ix (mm^4)	0.25 ± 0.11	0.27 ± 0.1	-0.394
Iy (mm^4)	0.057 ± 0.011	0.063 ± 0.012	-1.472
Imax (mm^4)	0.27 ± 0.11	0.29 ± 0.11	-0.684
Imin (mm^4)	0.038 ± 0.005	0.04 ± 0.005	-0.145
Imax/Imin	6.86 ± 2.33	7.51 ± 2. 16	-0.85
J (mm^4)	0.31 ± 0.11	0.33 ± 0.11	-0.726
Theta (°)	-72.79 ± 4.51	-71.47 ± 4.43	-0.56
Zx (mm^3)	0.19 ± 0.67	0.2 ± 0.066	-0.933
Zy (mm^3)	0.085 ± 0.011	0.091 ± 0.014	-0.975
Zp (mm^3)	0.3 ± 0.1	0.33 ± 0.095	-0.892
Zy/Zx	0.51 ± 0.17	0.48 ± 0.13	-0.27

See text for description of each variable.

Non-significant differences after the Dunn-Šidák correction method ($P \leq 0.004$ for 14 activity group contrast).

Table 6.16 Results of Kruskal-Wallis and two-tailed Mann-Whitney contrasts between groups for rates of osteogenesis at each quadrant, the deltoid crest, and averaged across all quadrants within cross-sections (μm/day). Means ± standard deviations are reported for all three groups. Z scores are also given with significance in brackets (when $P \leq 0.05$) for the pairwise results.

Variable	Control (CON: n = 8)	Running (WHL: n = 4)	Climbing (CLB: n = 9)	Kruskal-Wallis	Mann-Whitney CON vs WHL	Mann-Whitney CON vs CLB	Mann-Whitney WHL vs CLB
Mean 25%-section	1.95 ± 0.2	3.04 ± 0.07	2.41 ± 0.35	**0.004**	-2.049 (0.04)	-2.701 (0.007)	-2.126 (0.033)
Mean crest-section	2.12 ± 0.48	3.08 ± 0.34	2.65 ± 0.19	**0.003**	**-2.722 (0.006)**	-2.27 (0.023)	-2.318 (0.02)
Total mean growth	2.1 ± 0.292	3.16 ± 0.3	2.8 ± 0.141	**< 0.001**	-2.717 (0.007)	**-3.464 (0.001)**	-2.469 (0.014)
Crest	2.46 ± 0.334	3.46 ± 0.405	2.99 ± 0.378	**0.007**	-2.449 (0.014)	-2.359 (0.018)	-1.757
Superior	1.88 ± 0.5	2.89 ± 0.3	2.52 ± 0.16	**0.005**	-2.378 (0.017)	-2.598 (0.009)	-2.006 (0.045)
Lateral	2.14 ± 0.38	3.29 ± 0.84	2.98 ± 0.3	**0.003**	-2.467 (0.014)	**-3.131 (0.002)**	-0.387
Inferior	2.17 ± 0.28	3.22 ± 0.35	2.7 ± 0.14	**0.002**	-2.089 (0.037)	**-3.009 (0.003)**	-2.049 (0.04)
Medial	1.86 ± 0.28	3.18 ± 0.18	2.76 ± 0.33	**0.001**	-2.717 (0.007)	**-3.37 (0.001)**	-1.854

Bold = significant differences after the Dunn-Šidák correction method ($P \leq 0.006$ for 8 activity group contrast).

Table 6.17 Results of Wilcoxon's signed ranks contrasts for deltoid crest rates of osteogenesis against mean bone growth rate and growth across each quadrants (μm/day).

Variable	Wilcoxon's signed ranks	
	Z-scores	*P*-values
Total mean growth	-3.193	**0.001**
Superior	-3.697	**<0.001**
Lateral	-1.606	0.108
Inferior	-3.195	**0.001**
Medial	-3.501	**<0.001**

Bold = significant differences after the Dunn-Šidák correction method ($P \leq 0.01$ for 5 activity group contrast).

Table 6.18 Results of two-tailed Mann-Whitney contrasts between age groups for rates of osteogenesis at each quadrant, the deltoid crest, and averaged across all quadrants within cross-sections (μm/day). Means ± standard deviations are reported for all three groups. Z scores are also given with significance in brackets (when $P \leq 0.05$) for the pairwise results.

Variable	Juvenile (JV)	Adult (AD)	Mann-Whitney JV vs AD
Mean 25%-section	2.53 ± 0.29	2.16 ± 0.47	-2.039 (0.041)
Mean crest-section	2.79 ± 0.33	2.34 ± 0.52	-1.923
Total mean growth	2.81 ± 0.39	2.45 ± 0.5	-1.421
Crest	3.16 ± 0.4	2.59 ± 0.44	-2.47 (0.014)
Superior	2.57 ± 0.31	2.18 ± 0.6	-1.706
Lateral	3.08 ± 0.63	2.45 ± 0.54	-2.135 (0.033)
Inferior	2.75 ± 0.36	2.31 ± 0.39	-2.117 (0.034)
Medial	2.74 ± 0.52	2.32 ± 0.61	-1.671

25% = histological cut made at 25% of maximum bone length; Distal crest = histological cut made at the distal margin of the deltoid crest.
Non-significant differences after the Dunn-Šidák correction method ($P \leq 0.006$ for 8 activity group contrast).

Table 6.19 Results of Kruskal-Wallis and two-tailed Mann-Whitney contrasts between groups for the appearance of osteons across all cortices. Means ± standard deviations are reported for all three groups. Z scores are also given with significance in brackets (when $P \leq 0.05$) for the pairwise results.

Variable	Control (CON)	Running (WHL)	Climbing (CLB)	Kruskal-Wallis	Mann-Whitney		
					CON vs WHL	CON vs CLB	WHL vs CLB
Osteon (25%)	1 ± 1.05	0.4 ± 0.52	4.2 ± 2.3	**< 0.001**	-1.325	**-2.993 (0.003)**	**-3.581 (<0.001)**
Osteons (distal)	1.3 ± 1.06	0.6 ± 0.7	3.7 ± 1.06	**< 0.001**	-1.584	**-3.445 (0.001)**	**-3.822 (<0.001)**
Mean osteons	1.15 ± 0.88	0.5 ± 0.47	3.95 ± 1.04	**< 0.001**	-2.081 (0.037)	**-3.629 (<0.001)**	**-3.82 (<0.001)**
Drifting osteons (25%)	0.1 ± 0.32	0	0.9 ± 0.88	**0.001**	-1.0	**-2.675 (0.007)**	**-3.162 (0.002)**
Drifting osteons (distal)	0.4 ± 0.52	0	1.1 ± 0.88	**0.004**	-2.179 (0.029)	-1.875	**-3.127 (0.002)**
Mean drifting osteons	0.5 ± 0.71	0	2 ± 1.25	**< 0.001**	-2.169 (0.03)	**-2.711 (0.007)**	**-3.729 (<0.001)**

25% = histological cut made at 25% of maximum bone length; Distal crest = histological cut made at the distal margin of the deltoid crest.
Bold = significant differences after the Dunn-Šidák correction method ($P \leq 0.009$ for 6 activity group contrast).

Table 6.20 Results of two-tailed Mann-Whitney contrasts between age groups for the appearance of osteons across all cortices. Means ± standard deviations are reported for both groups. Z scores are given and all results are found non-significant (*P* > 0.05).

Variable	Juvenile (JV)	Adult (AD)	Mann-Whitney JV vs AD
Osteon (25%)	1.4 ± 1.84	2.33 ± 2.53	-1.116
Osteons (distal)	1.93 ± 1.83	1.8 ± 1.47	-0.021
Mean osteons	1.67 ± 1.59	2.07 ± 1.88	-0.886
Drifting osteons (25%)	0.4 ± 0.83	0.27 ± 0.46	-0.108
Drifting osteons (distal)	0.33 ± 0.62	0.67 ± 0.82	-1.212
Mean drifting osteons	0.73 ± 1.16	0.93 ± 1.22	-0.461

25% = histological cut made at 25% of maximum bone length; Distal crest = histological cut made at the distal margin of the deltoid crest.

Figure 6.1 Boxplots showing the variation found between each muscle studies. A) Body mass adjusted muscle mass, B) body mass adjusted muscle belly length, C) fibre length (L_f), D) PCSA (physiological cross-sectional area), and E) pennation angle (°). The centre horizontal line in each box marks the mean of the sample; the length of each box shows the range within which the central 50% of the values fall. Whiskers indicate 10th and 90th percentiles. Individuals outside of the whiskers are outliers. * *P* < 0.001; left white box = superficial pectoralis; middle grey box = acromiodeltoideus; right dark grey = spinodeltoideus.

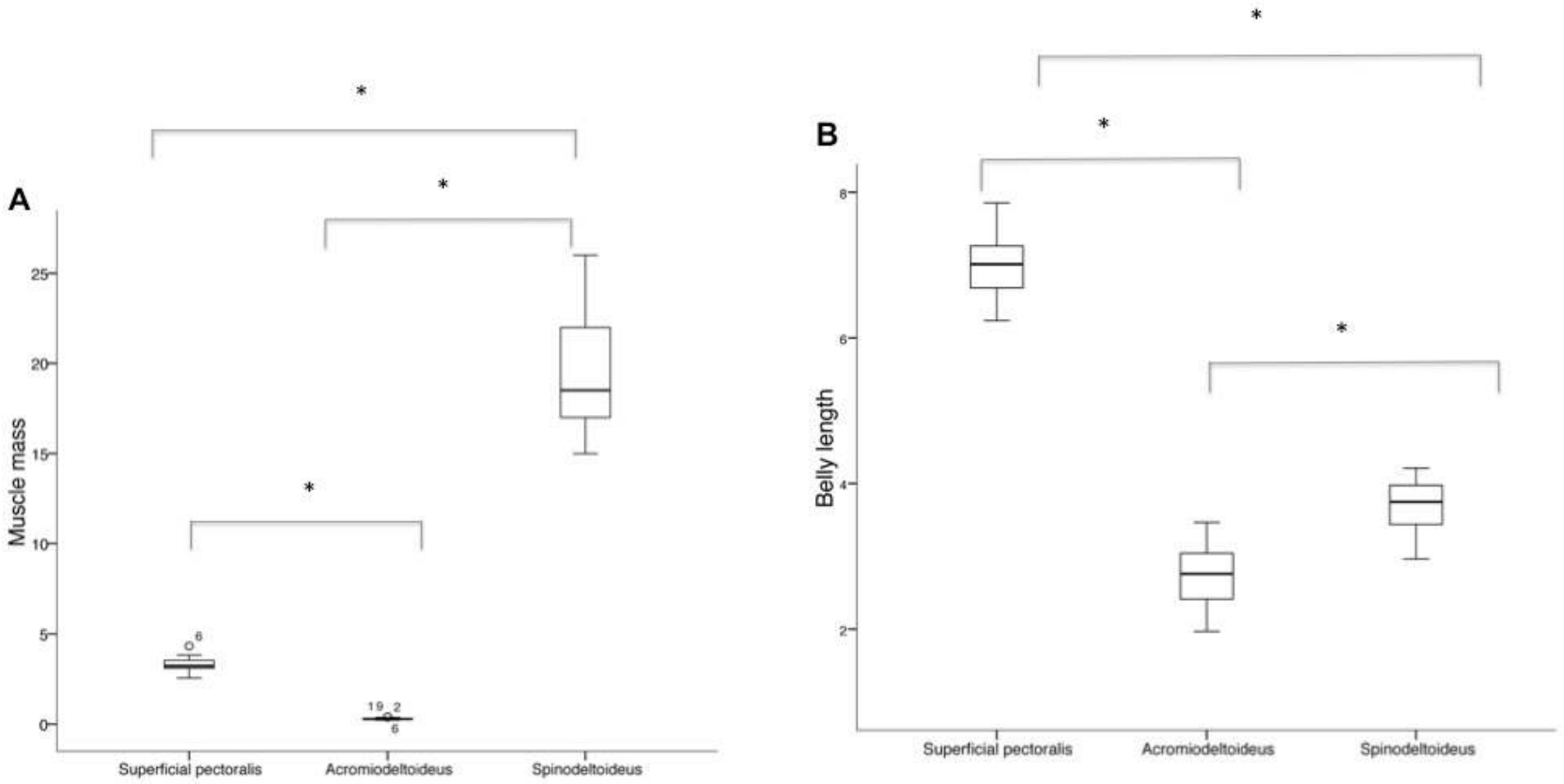

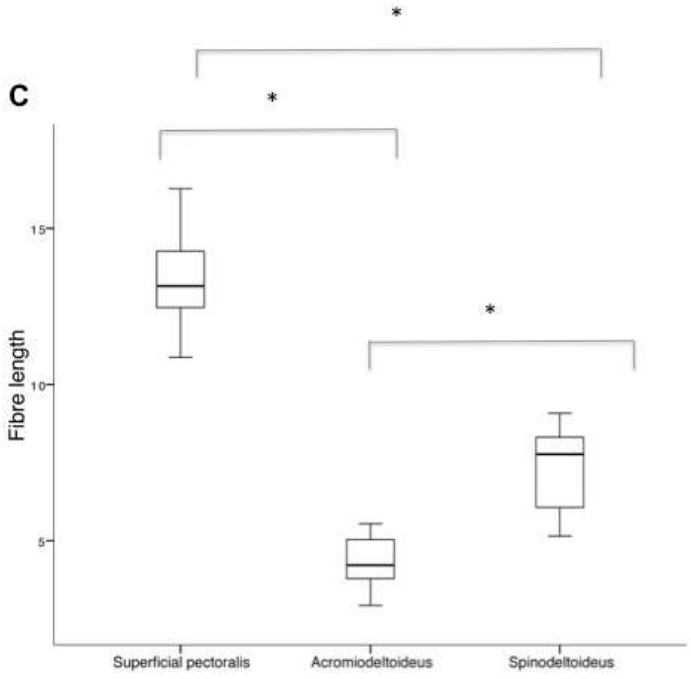
C
*
*
*
Fibre length
15
10
5
Superficial pectoralis
Acromiodeltoideus
Spinodeltoideus

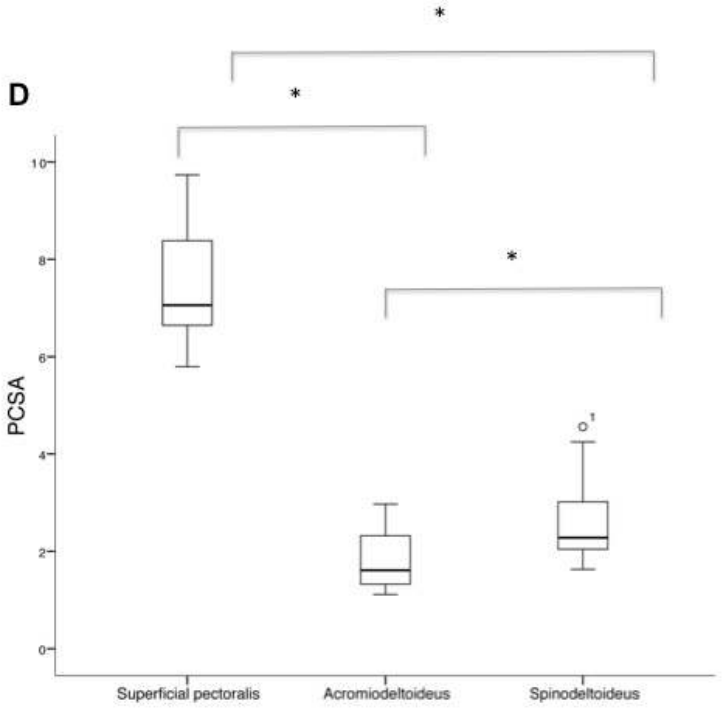
D
*
*
*
PCSA
10
8
6
4
2
0
1
Superficial pectoralis
Acromiodeltoideus
Spinodeltoideus

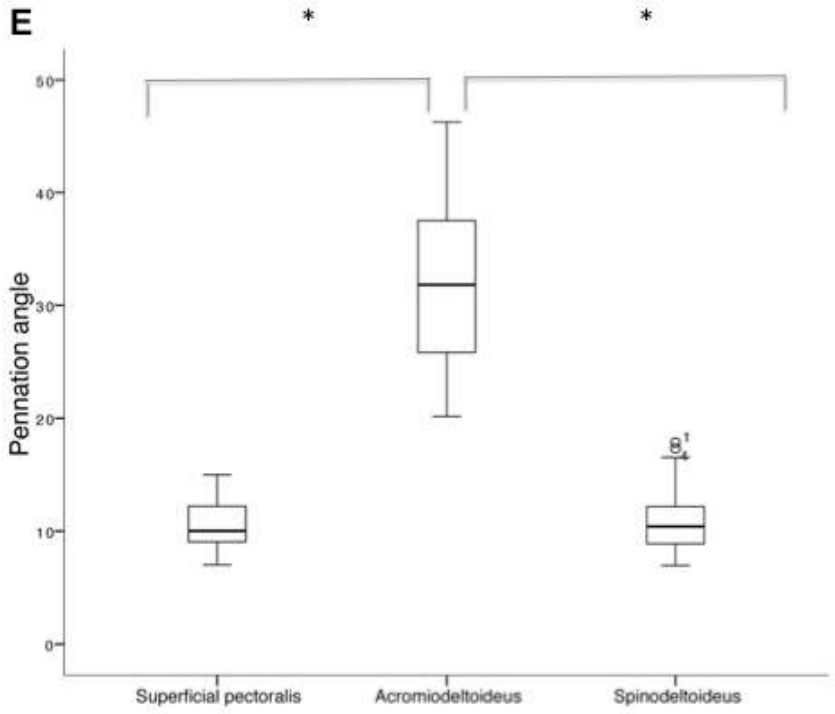
E
*
*
Pennation angle
50
40
30
20
10
0
Superficial pectoralis
Acromiodeltoideus
Spinodeltoideus

Figure 6.2 Boxplots showing the variation found in the muscle variables. A) Body mass adjusted muscle mass, B) body mass adjusted muscle belly length, C) pennation angle (°), D) M/P_o (muscle mass/predicted effective maximal tetanic tension), and E) priority index of force (*I*). The centre horizontal line in each box marks the mean of the sample; the length of each box shows the range within which the central 50% of the values fall. Whiskers indicate 10^{th} and 90^{th} percentiles. Individuals outside of the whiskers are outliers. CLB = climbing, CON = control, WHL = running.

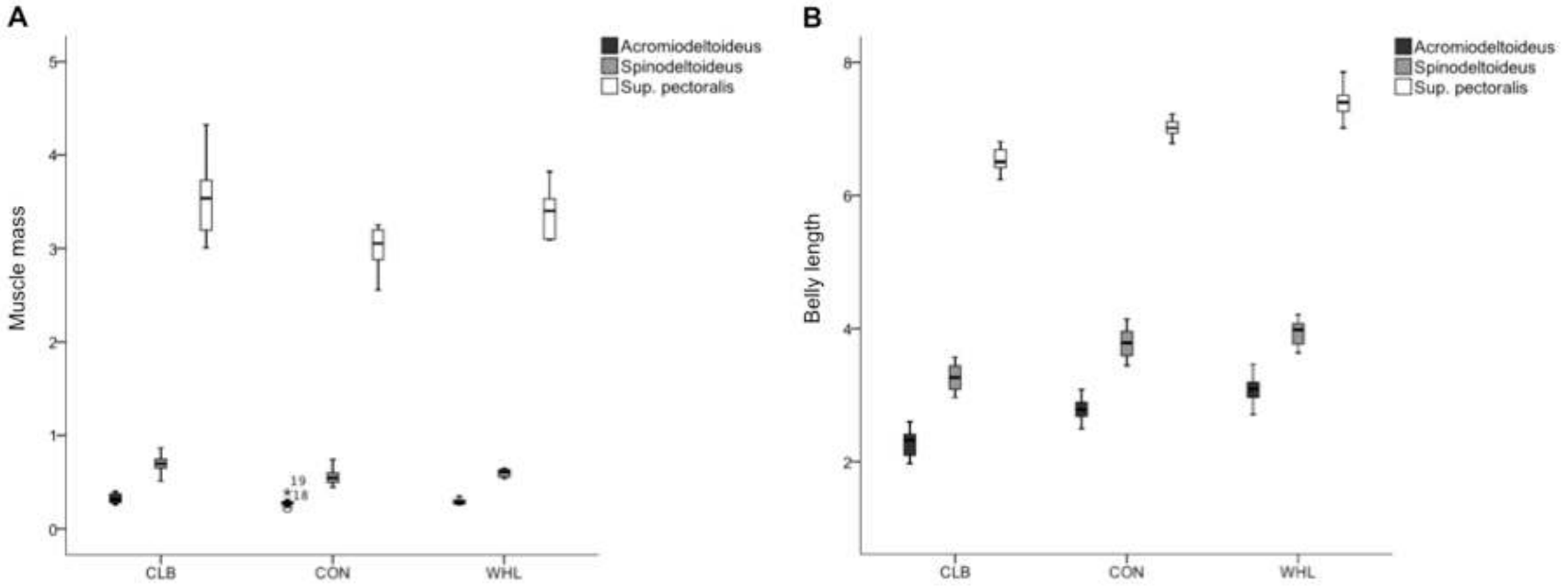

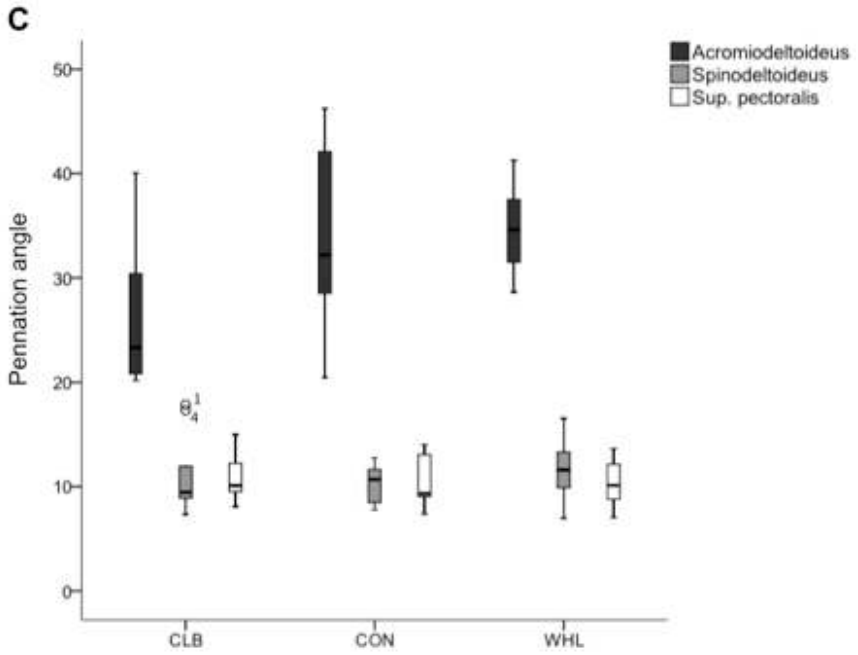
C
Acromiodeltoideus
Spinodeltoideus
Sup. pectoralis
Pennation angle
50
40
30
20
10
0
CLB
CON
WHL

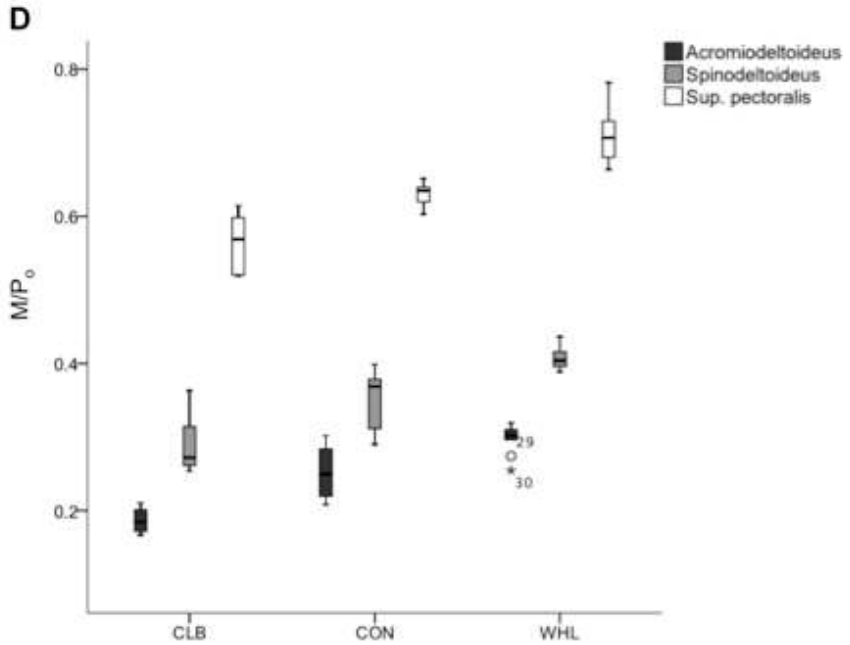
D
Acromiodeltoideus
Spinodeltoideus
Sup. pectoralis
M/P0
0.8
0.6
0.4
0.2
CLB
CON
WHL

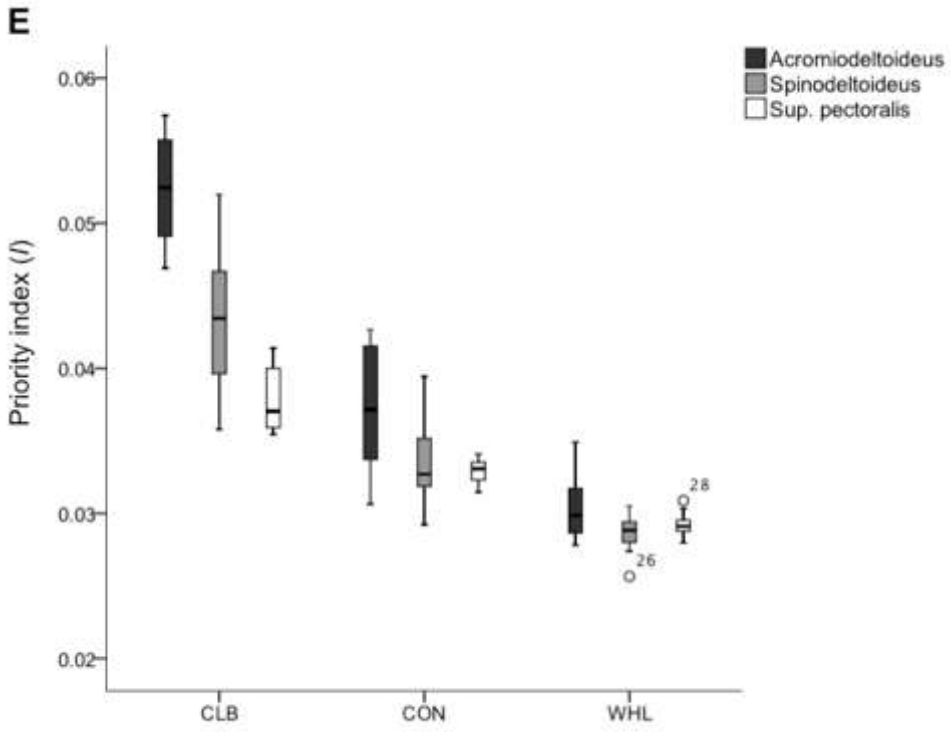
E
Acromiodeltoideus
Spinodeltoideus
Sup. pectoralis
Priority index (I)
0.06
0.05
0.04
0.03
0.02
28
26
CLB
CON
WHL

Figure 6.3 Bivariate plots showing that for a given muscle, there is an architectural trade-off between muscle force (represented by PCSA) and muscle excursion (represented L_f). A) Body mass adjusted fibre length (L_f) against body mass adjusted physiological cross-sectional area (PCSA) of the acromiodeltoideus, B) spinodeltoideus, and C) superficial pectoralis muscles. CLB = climbing, CON = control, WHL = running.

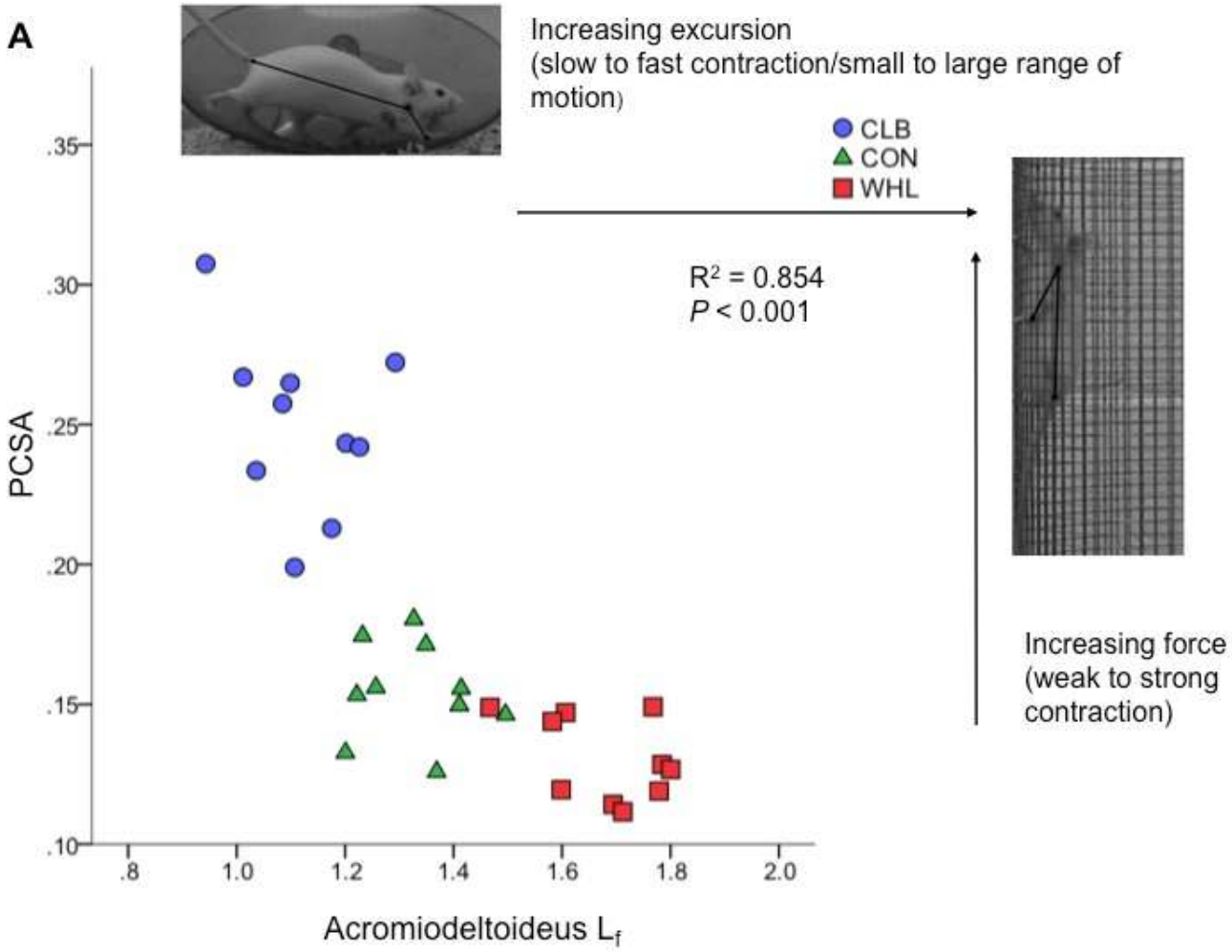

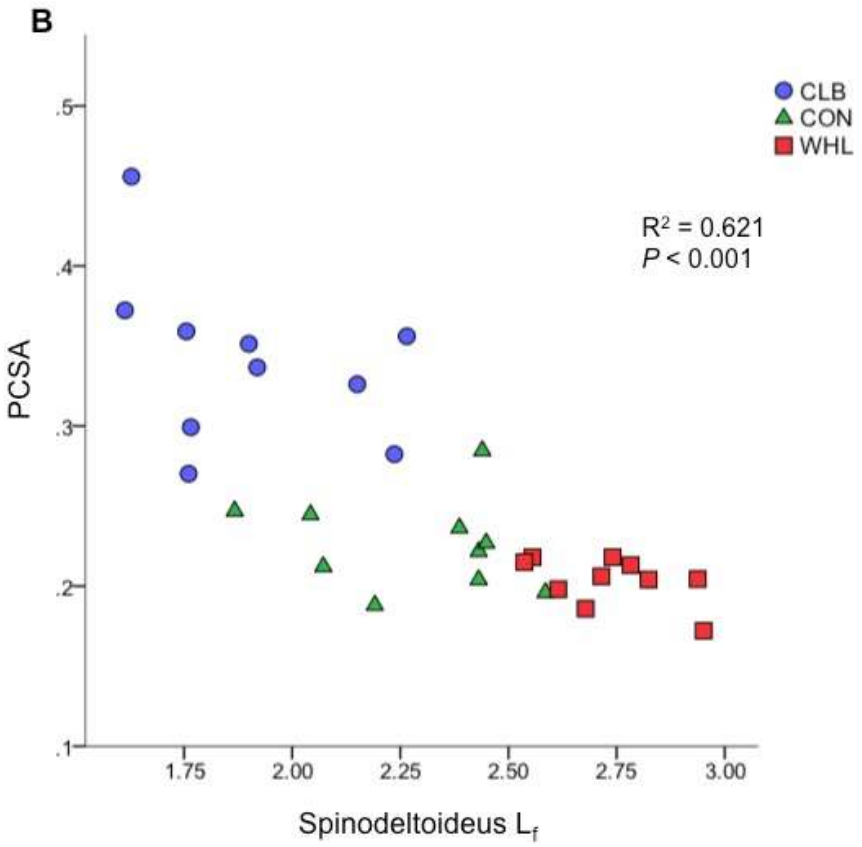
B
CLB
CON
WHL
R² = 0.621
P < 0.001
PCSA
.5
.4
.3
.2
.1
1.75
2.00
2.25
2.50
2.75
3.00
Spinodeltoideus L_f

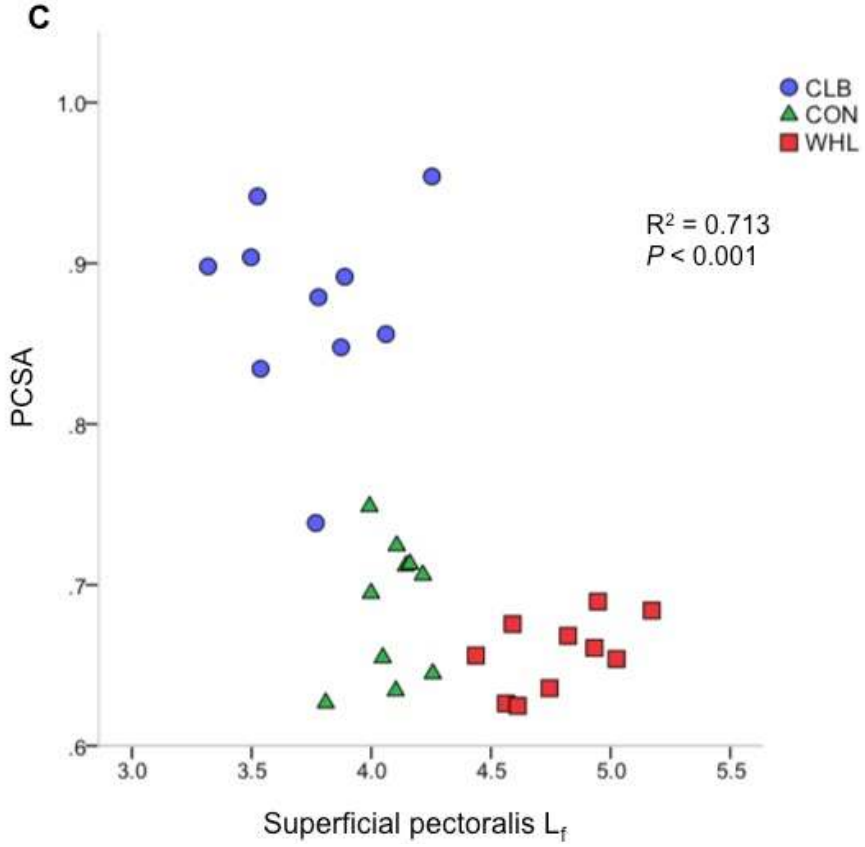
C
CLB
CON
WHL
R² = 0.713
P < 0.001
PCSA
1.0
.9
.8
.7
.6
3.0
3.5
4.0
4.5
5.0
5.5
Superficial pectoralis L_f

Figure 6.4 Boxplots showing the overlap in morphology for all of the deltoid crest surface measurements. A) Maximum length of deltoid crest, B) maximum width, C) area of the crest, D) distal angle, and E) thickness of the deltoid crest. The centre horizontal line in each box marks the mean of the sample; the length of each box shows the range within which the central 50% of the values fall. Whiskers indicate 10th and 90th percentiles. Individuals outside of the whiskers are outliers. CLB = climbing, CON = control, WHL = running.

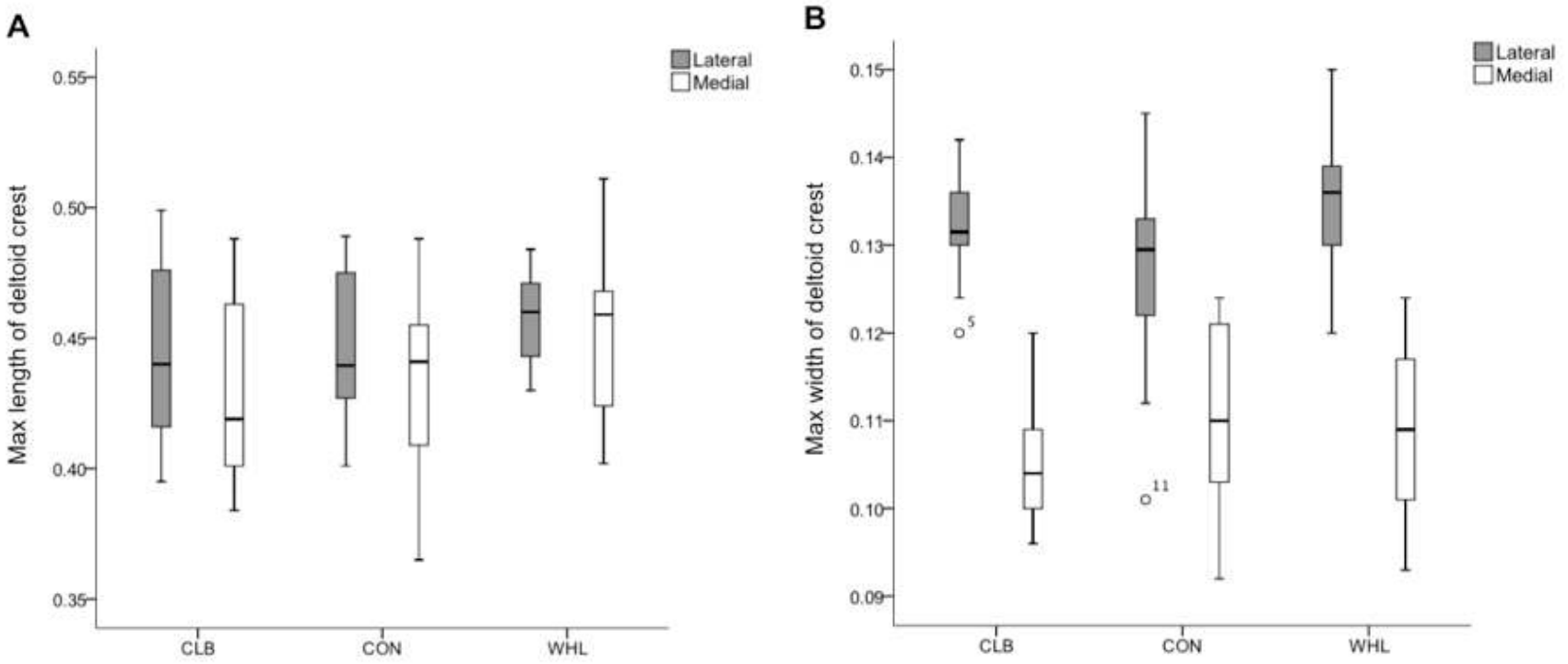

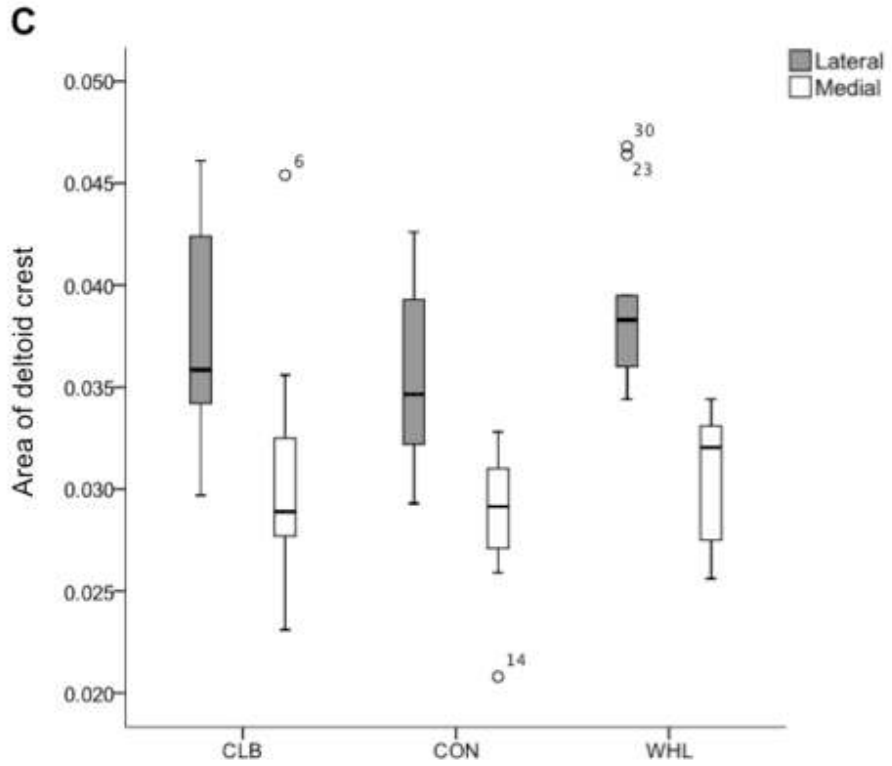
C
Lateral
Medial
Area of deltoid crest
0.050
0.045
0.040
0.035
0.030
0.025
0.020
6
30
23
14
CLB
CON
WHL

D

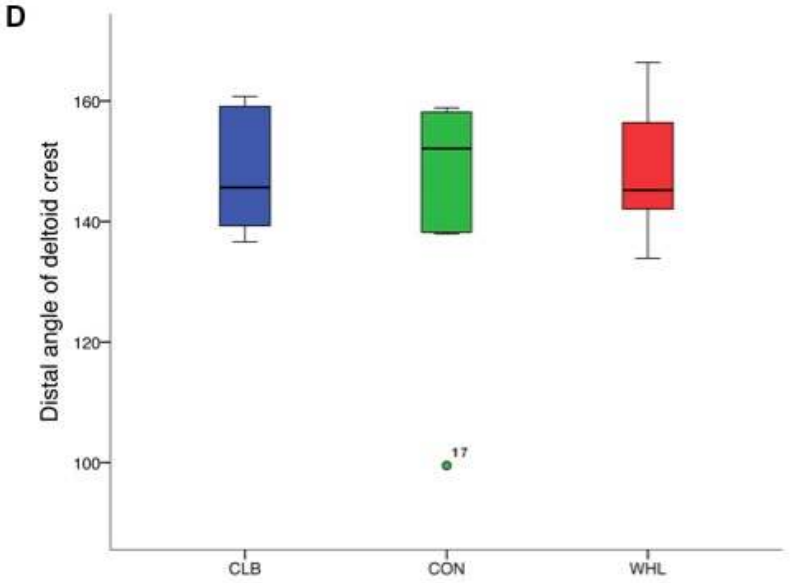
Distal angle of deltoid crest
160
140
120
100
17
CLB
CON
WHL

E

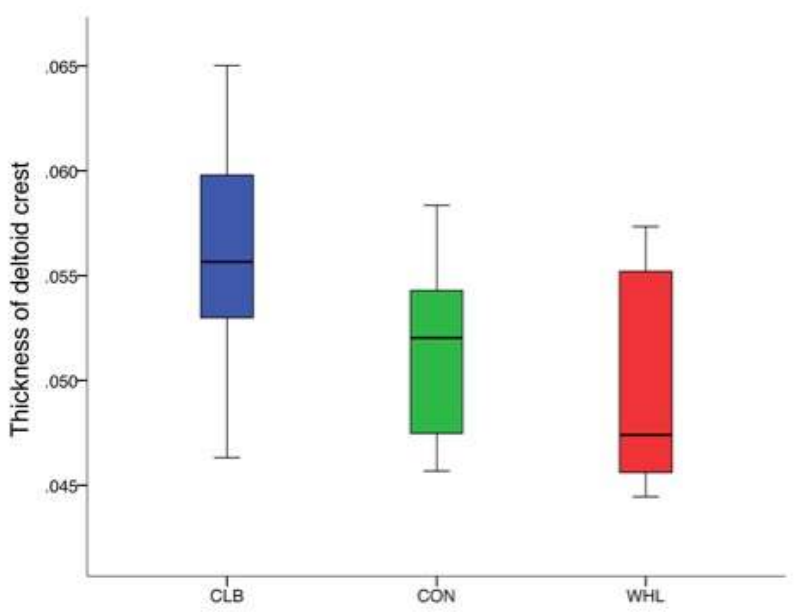
Thickness of deltoid crest
.065
.060
.055
.050
.045
CLB
CON
WHL

Figure 6.5 Example from each activity and age mouse group illustrating the overlap in morphology for the deltoid crest. The "juvenile" (JV) age groups are seen on the left, and the "adult" (AD) age groups are depicted on the right. Note that the humeral head from all specimens have been removed. Scale is in mm.

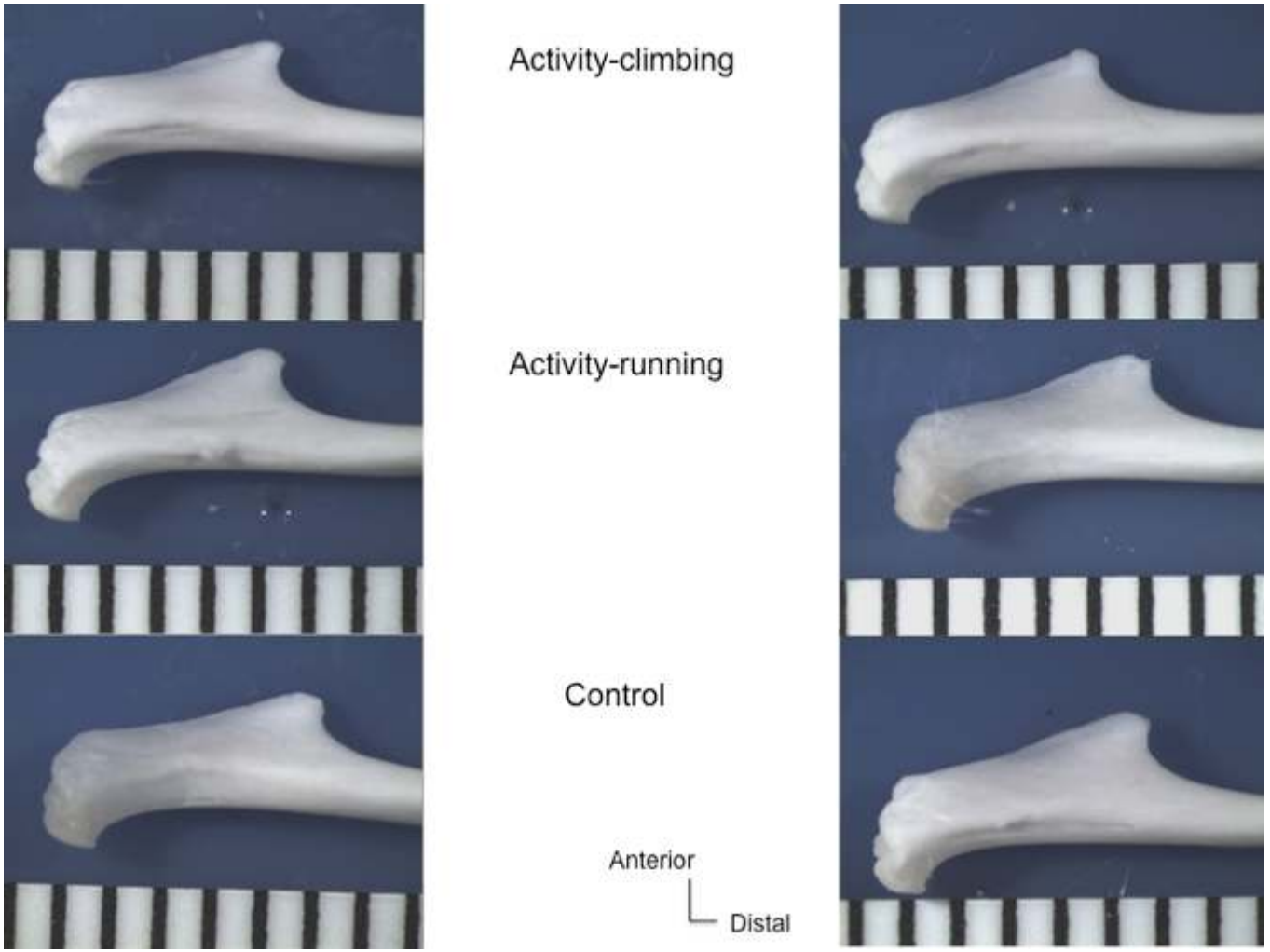

Figure 6.6 Boxplots showing areas of the cross-sections for all activity groups. A) Total area (TA), cortical area (CA), and medullary area (MA) for the cut at the 25% of maximal humeral length, and B) TA, CA, and MA for the distal margin of the deltoid crest section. The centre horizontal line in each box marks the mean of the sample; the length of each box shows the range within which the central 50% of the values fall. Whiskers indicate 10th and 90th percentiles. Individuals outside of the whiskers are outliers. CLB = climbing, CON = control, WHL = running.

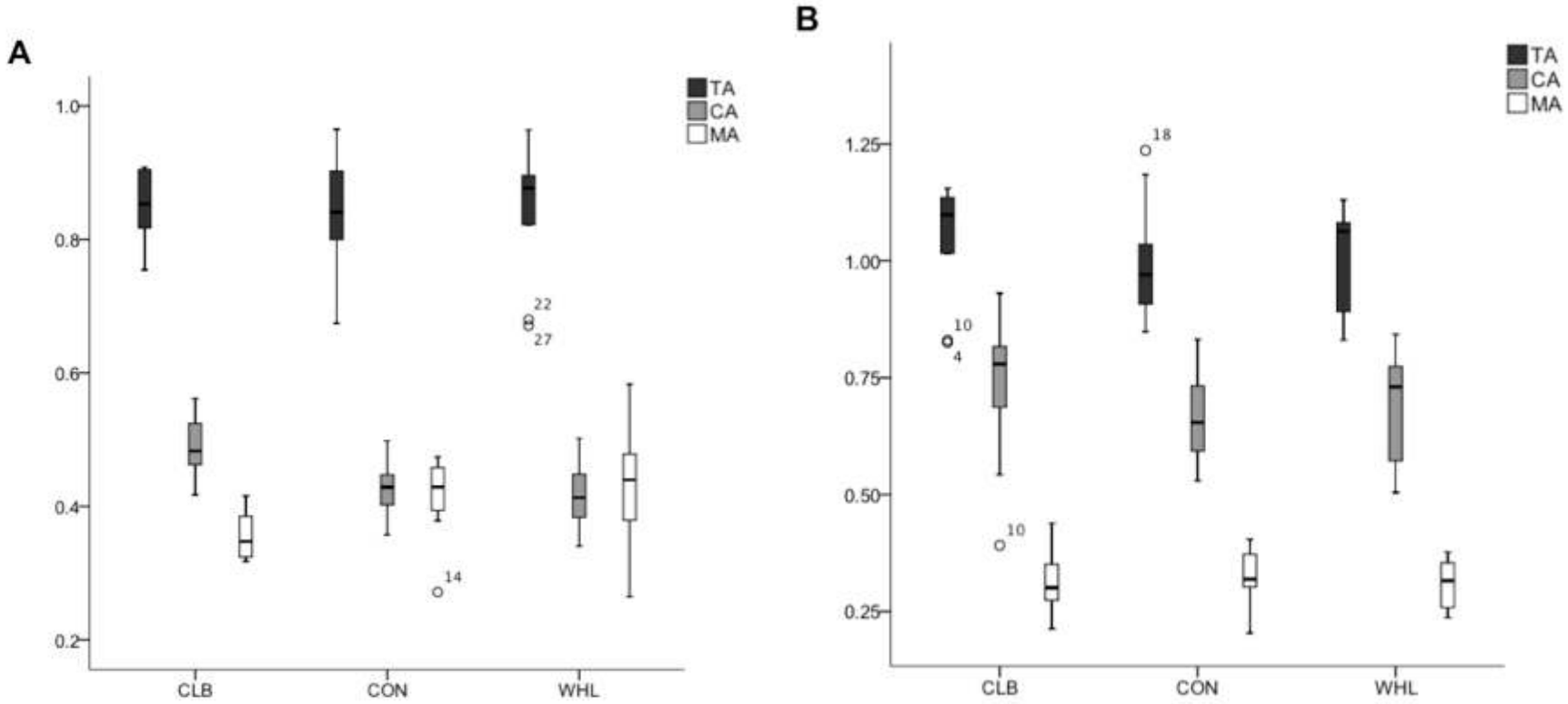

Figure 6.7 Boxplots showing biomechanical variables of the cross-sections for all activity groups. A) Zx (A-P bending strength) and Zy (M-L bending strength) for the 25% of maximal humeral length and distal margin of the crest sections, B) maximum bending rigidity (Imax) for both cuts, C) orientation plane of maximum bending rigidity (theta in degrees), D) index of circularity (Imax/Imin and Zy/Zx) for both sections, and E) *J* and Zp (torsional strength). The centre horizontal line in each box marks the mean of the sample; the length of each box shows the range within which the central 50% of the values fall. Whiskers indicate 10th and 90th percentiles. Individuals outside of the whiskers are outliers. CLB = climbing, CON = control, WHL = running.

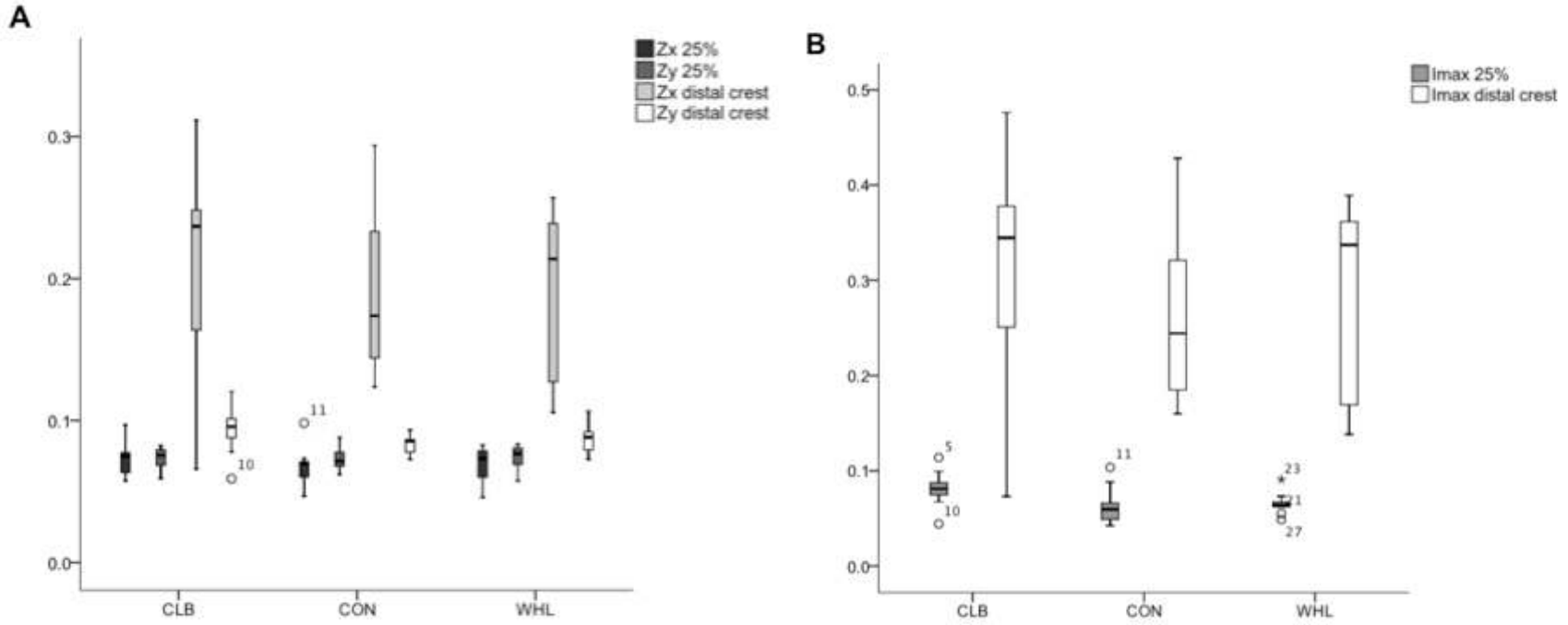

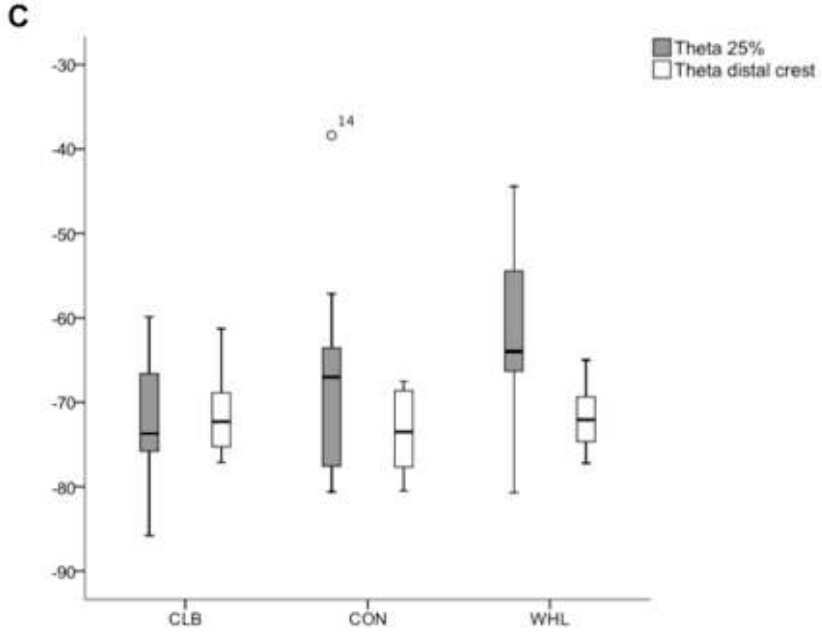
C
Theta 25%
Theta distal crest
-30
-40
-50
-60
-70
-80
-90
14
CLB
CON
WHL

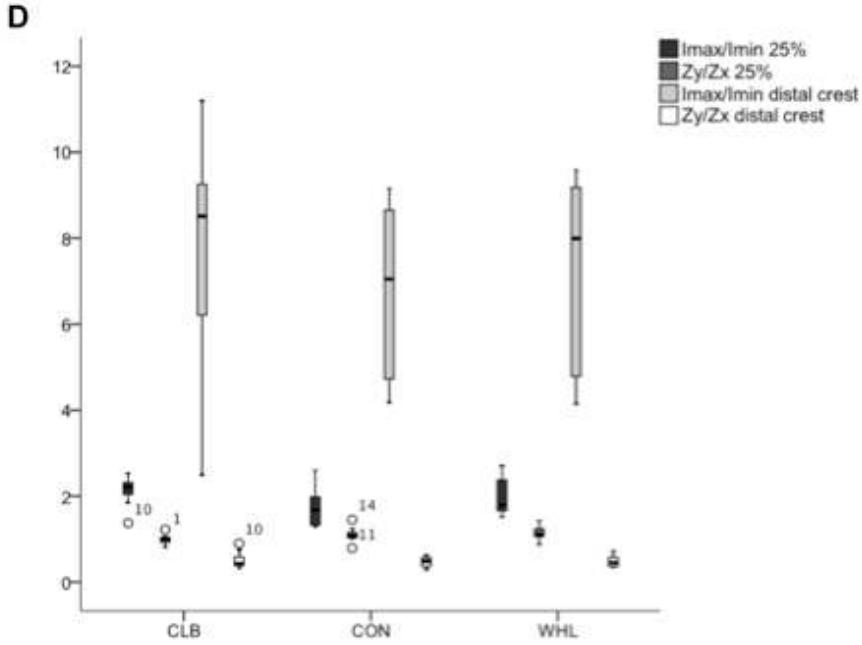
D
Imax/Imin 25%
Zy/Zx 25%
Imax/Imin distal crest
Zy/Zx distal crest
12
10
8
6
4
2
0
10
1
10
14
11
CLB
CON
WHL

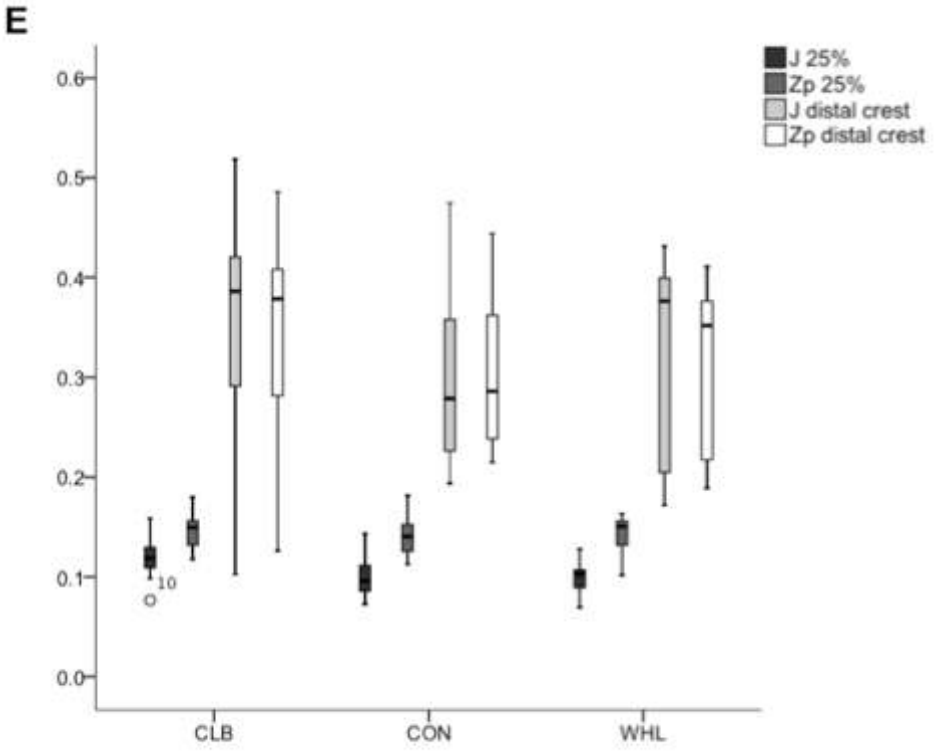
E
J 25%
Zp 25%
J distal crest
Zp distal crest
0.6
0.5
0.4
0.3
0.2
0.1
0.0
10
CLB
CON
WHL

Figure 6.8 Examples of the bone tissue found in the cross-sections. Cross-sections from the distal margin of the deltoid crest are shown here. A) In climbing (CLB) mice, both lamellar bone (left) and fibro-lamellar (right) tissue were found. B) The running mice (WHL) were mainly characterized by the organized lamellar bone, while CLB usually had more variation in their bone tissue (i.e., fibro-lamellar bone).

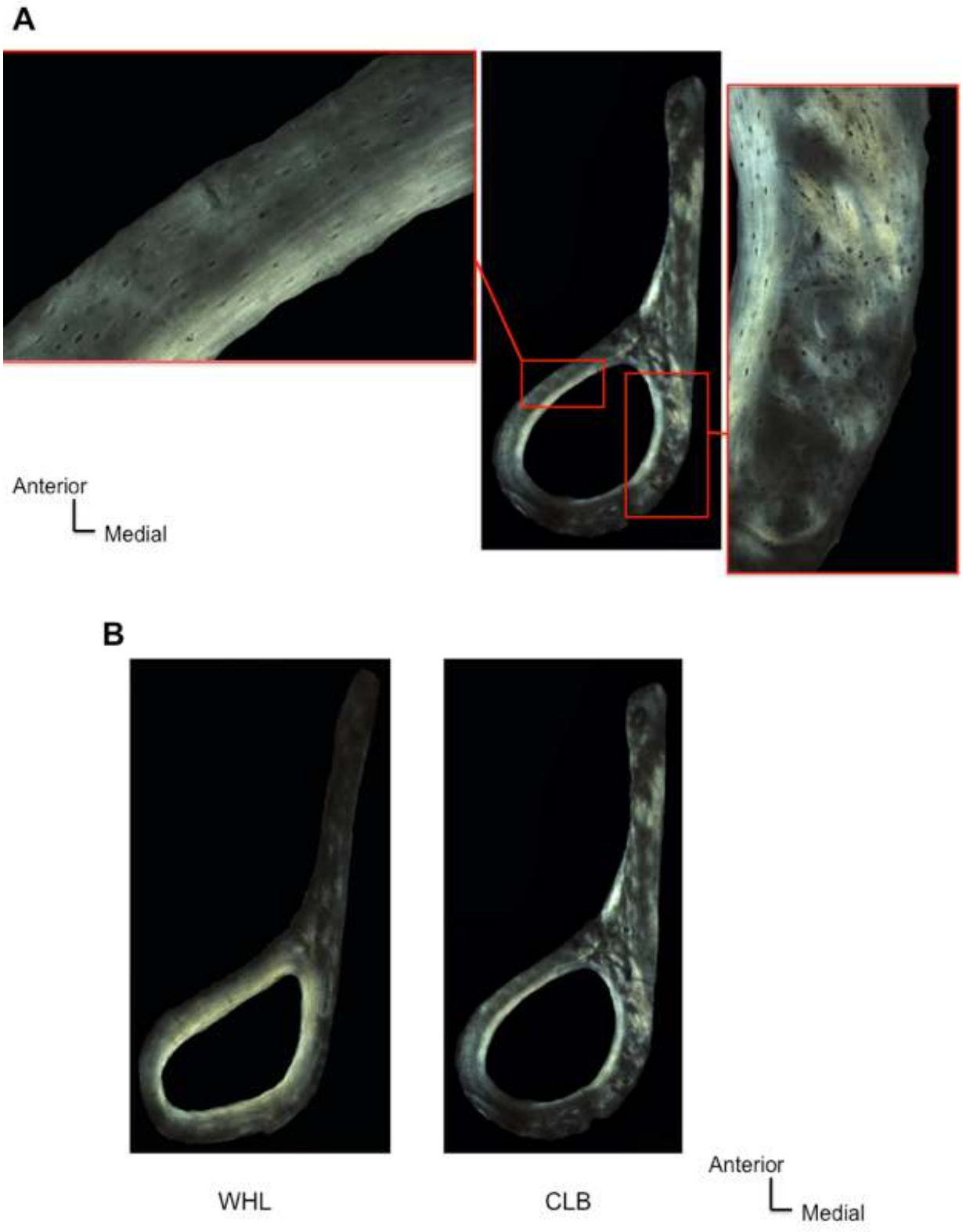

Figure 6.9 Example of cortical drift in a distal margin of the deltoid crest cross-section from a female climbing (CLB) mouse. Plusses are located at the sites of bone deposition while the minuses show bone resorption. The bone deposited shows the direction of drift, which in this case follows a posterior-lateral direction.

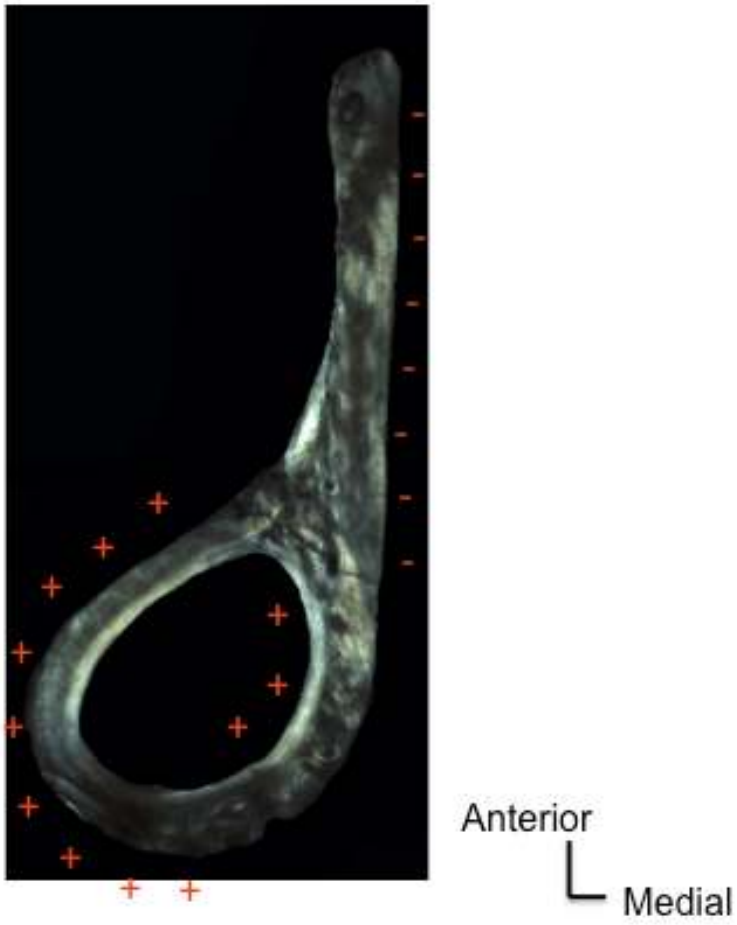

Figure 6.10 Example of the fluorochrome labeled cross-section for each activity groups. All examples are distal margin of the deltoid crest cross-section. Running mice (WHL) commonly only had the Xylenol-orange label (administered last in the sequence) present; climbing mice (CLB) usually had all three labels present; control mice (CON) showed a more variable pattern of labels.

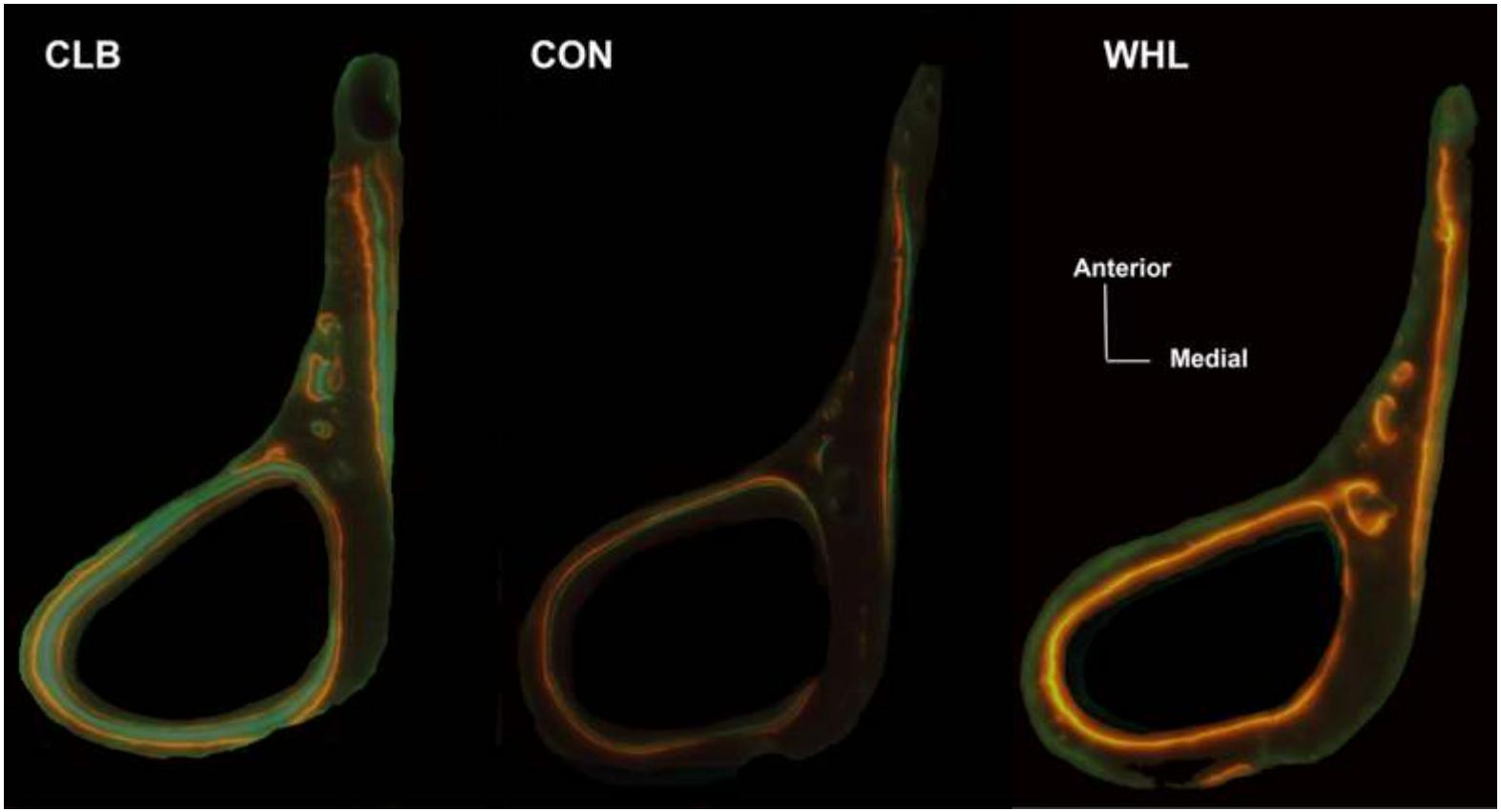

Figure 6.11 Boxplots showing the periosteal bone growth per day differences for the humerus in all activity groups. A) Mean growth (µm/day) within the 25% maximum bone length section, distal margin of the crest section, and the overall mean from both cross-sections (total), B) mean growth (µm/day) within the deltoid crest itself, and C) mean growth (µm/day) at every quadrant of both cross-sections. The centre horizontal line in each box marks the mean of the sample; the length of each box shows the range within which the central 50% of the values fall. Whiskers indicate 10th and 90th percentiles. CLB = climbing, CON = control, WHL = running.

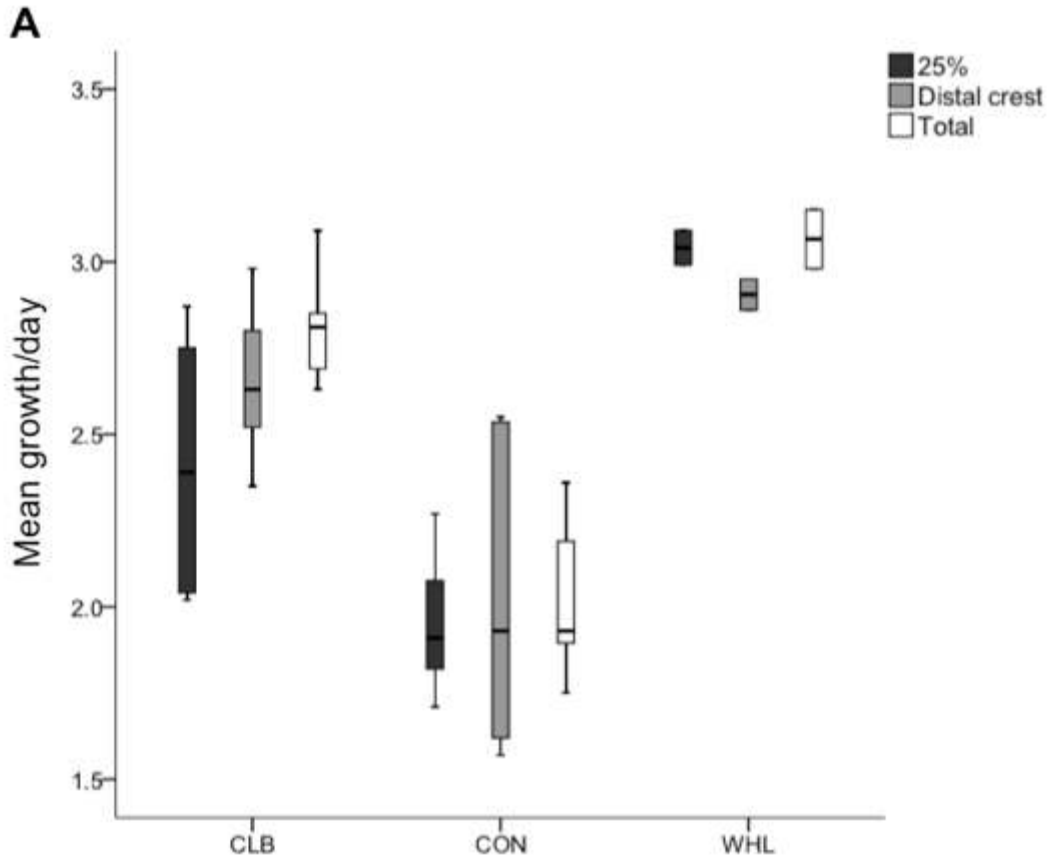

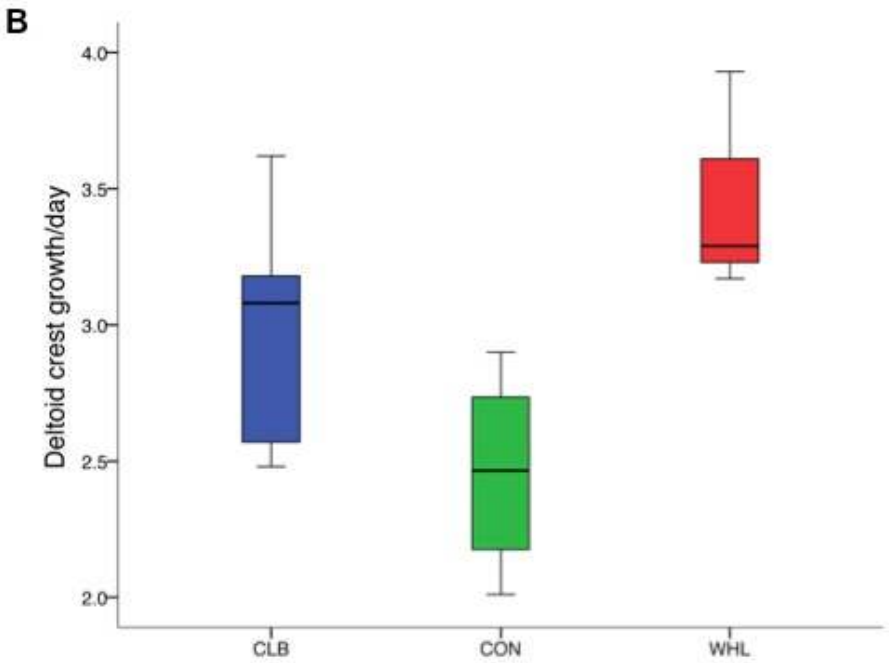
B
Deltoid crest growth/day
4.0
3.5
3.0
2.5
2.0
CLB
CON
WHL

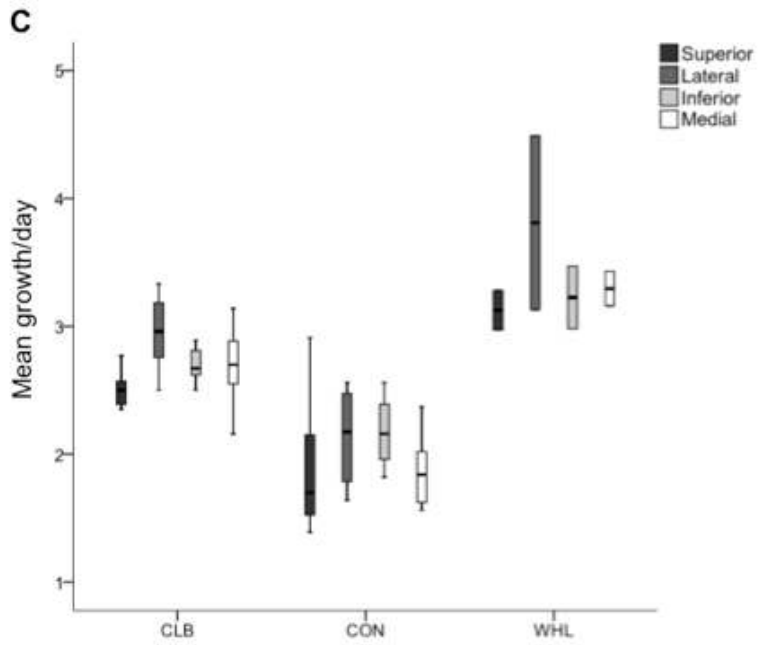
C
Mean growth/day
5
4
3
2
1
Superior
Lateral
Inferior
Medial
CLB
CON
WHL

Chapter 7

7. Discussion and Conclusions

This chapter summarizes the main results from Chapters 5 and 6 and their significance. This is followed by a discussion of the broader implications and limitation of this research for the study of muscle attachment in bioarchaeological and fossil samples, and the avenues for future investigations.

7.1 Primate discussion

Three species of primates (*Pongo pygmeaus abelii, Macaca sylvanus* and *Macaca fuscata*) were used to examine whether muscular differences stemming from different locomotion can be reliably inferred from muscle attachment site morphology. Muscle fibre architecture and entheseal morphology data were collected on the muscles that attach to the humerus. A total of eight fibrocartilaginous insertions (latissimus dorsi, pectoralis major, subscapularis, supraspinatus, infraspinatus, teres minor, teres major, dorsoepitrochlearis), two fibrous insertions (deltoideus, coracobrachialis), four fibrocartilaginous origins (anconeus, extensor carpi radialis longus, common extensor origin, common flexor origin) and five fibrous origins (brachialis, lateral and medial head of the triceps brachii, pronator teres, brachioradialis) were investigated. Although extant primates are often used to infer behaviour from fossils (Pilbeam et al., 1990; Begun, 1992; Rose 1994; Larson, 1993, 1995, 1996, 1998; Antón, 1996; Madar et al., 2002; Kunimatsu et al., 2007) currently, little is understood about the relationship between the gross appearance of the bony features and the structure and function of the associated soft-tissues. This research incorporated aspects of both macro and micro structural features of muscle and bone in relation to locomotion, species, sex, and body mass. Results demonstrate that, although sex had a

small impact on the fibre architecture of the muscle studied, body mass was the main factor influencing the internal muscular structures. In general, muscles from the apes were potentially more forceful while the muscles from the monkeys had greater excursion potential and contractile velocity. It should be re-noted that the body masses of the macaques were unavailable. Therefore, an average for the species and sex was used for both macaque specimens (Smith and Jungers, 1997). This might have underestimated the potential force of the muscles studied. However, when biomechanical leverages of the attachment sites were considered, the macaques had relatively distal attachments of many large arm and forearm muscles, which provide a mechanical advantage, favouring strong and deliberate movements (Youlatos, 2000). The lack of high values in the variables measuring potential force of muscles might be explained by their better muscular leverage on the humerus.

Finally, the relationship between the primates' internal muscle structures and the associated attachment sites is less clear[1]. Neither the fibrous or fibrocartilaginous entheses were predictable in their bony response to muscle contractions. The fibrous origins seemed to be the least predictable of all attachments studied. Controlling for the underlying bone thickness using cortical area of the enthesis allowed for another method of comparison without using body mass, which seemed to improve accuracy for the macaques. From the data, it was observed that greater potential force seems to increase with the width of an attachment site (i.e., wider) while greater potential velocity actually seems to decrease the potential size of an enthesis. The biomechanical leverage of the attachment, once again might relieve the forceful muscular contractions, thereby reducing the bone response at the enthesis. Although both monkeys and apes had different powerful forelimb muscles (apes = greater potential force, monkeys = greater potential velocity),

[1] These relationships are based on observation alone. No statistics could be run on such a small sample.

both had very different associations with their underlying attachment sites. Therefore, results from this dissertation do not seem to provide strong support for previous assumptions about the biology of musculoskeletal attachment sites (Hawkey and Merbs, 1995; Hawkey, 1998; Wilczak, 1998a, b; Knüsel, 2000; Eshed et al., 2004; Wang et al., 2004; Weiss, 2003, 2004, 2007, 2010; Molnar, 2006, 2010; Marzke et al., 2007; Havelková et al., 2011) linking muscle size and power with large and robust attachment site morphology. These results suggest caution when using entheseal morphology to reconstruct behaviour in fossils and bioarchaeological samples (Davis, 1964; McGowan, 1979; Zumwalt, 2005, 2006; Marzke and Shrewbury, 2006; Cardoso and Henderson, 2010; Meyer et al., 2011, Schlecht 2012a, b).

7.1.1 Primates and internal muscle structure

For this project, the forelimb musculature of large suspensory orangutans was compared to smaller quadrupedal macaques. In general, the forelimb musculature of the primates studied had similar organization as that of other primates found in the literature. When exceptions did occur, they seemed to be individually specific (e.g., lack of clavicular attachment on the clavicle of the pectoralis major muscle in the female orangutan). No consistent differences were found in the locations of the muscles, and those differences noted are examples of variation within each species (Ashton and Oxnard, 1962a, b, 1963; Oxnard, 1963, 1967; Swindler and Wood, 1973; Berringer et al., 1978).

Past research has concentrated on gross anatomy and muscle mass when considering muscle data and only some attention has been paid to architectural data of postcranial musculature in primates. The lack of architectural attention is often due to the destructive nature of the soft-

tissue when using this method. However, the arrangement of internal muscle structures influences the potential force and velocity production of a muscle (Gans, 1982; Gans, 1988; Lieber and Brown, 1992; Lieber, 2002; Williams et al., 2008; Lieber and Ward, 2011) and some studies show that muscle mass is not always the best correlate for muscle function (Bryant and Seymour, 1990; Lieber, 2002; Hamrick et al., 2006). Therefore, architectural muscle data are key to a better interpretation of muscle function.

Looking at their daily behaviours, orangutans and macaques use wide ranges of motion during their main locomotor behaviours. As mentioned in Chapter 2, orangutans do not brachiate while moving in their arboreal habitat due to their large size. Their main form of locomotion in the trees is quadrumanus climbing used to achieve maximal weight distribution across as many supports as possible. While terrestrial, the orangutans use the sides of their hands and feet as the main body support during "fist walking" quadrupedalism. They can also do some bipedal standing (Ashton and Oxnard, 1962a, b; Oxnard, 1963; Tuttle, 1986; Galdikas, 1988; Hunt et al., 1996; Rowe, 1996; Fleagle, 1999; Ankel-Simons, 2007). Macaques have a wide spread of locomotor repertoire and are highly adaptable to their environment (Ashton and Oxnard, 1962a, b; Oxnard, 1963; Hunt et al., 1996; Rowe, 1996; Fleagle, 1999; Chatani, 2003; Ankel-Simons, 2007). They are in general considered semiterrestrial capable of walking, running, leaping, hanging from all fours. Therefore, based on previous EMG research (Tuttle and Basmajian, 1978a, b; Jungers and Stern, 1980, 1981; Tuttle et al., 1983; Larson and Stern, 1986, 1989, 1992, 2006, 2007; Whitehead and Larson, 1994; Jouffroy et al., 1998; Larson et al., 2000, 2001; Stern and Larson, 2001) and gross dissection research (Kimura and Takai, 1970; Cheng and Scott, 2000; Youlatos, 2000; Gibbs et al., 2002; Oishi et al., 2008, 2009; Diogo et al., 2009; Michilsens et al., 2009) it was predicted that the orangutans would have highly pennated, shorter fibres, but

larger physiological cross-sectional areas of the elbow and wrist flexors in order to generate more potential force output. These (especially the wrist flexors) should be coupled with long tendons (isometric contraction and therefore maximal force production). It was predicted that the macaques would have highly pennated, shorter fibres, with larger physiological cross-sectional areas of the elbow and wrist extensors in order to generate more potential force output (opposite from the suspensory orangutan). Shoulder muscles were expected to have long and parallel (smaller PCSA) muscle fibres in the apes. And, contrary to the orangutans, the shoulder muscles of macaques particularly the protractors, were expected to have highly pennated, shorter fibres, with larger physiological cross-sectional areas (PCSA).

The forelimb muscles were analysed first as functional units. Generally, the apes, especially the males, had greater forelimb muscle masses than the monkeys. When a variable considered muscle mass (e.g., M/P_o) in its equation, the apes had higher values but when muscle and tendon lengths were represented in the equation of the variables (e.g., TL/MTU, h) the macaques were comparable to the apes. More specifically, the orangutans had greater shoulder muscle masses, more closely packed physiological cross-sectional areas (PCSA), a higher index of force (*I*), and a higher ratio of muscle mass over predicted effective maximal tetanic tension (M/P_0). These four variables are closely related (all use muscle mass in their formulation) and are all associated with priority of force production in a muscle (Gans, 1982; Anapol and Jungers, 1986; Hurov, 1986; Gans and De Vree, 1987; Antón, 1994; Lemelin, 1995; Anapol and Barry, 1997; Lieber, 2002; Medler, 2002; Anapol and Gray, 2003; Organ, 2007; Williams et al., 2008; Taylor et al., 2009). Generally the shoulder extensors (triceps brachii, teres major, latissimus dorsi, deltoideus), adductors (deltoideus and supraspinatus), and endorotators (subscapularis, pectoralis major, deltoideus, teres major, latissimus dorsi) have greater muscle mass when compared to

flexors (protractors), abductors and exorotators. However all primates often overlapped in their muscle-tendon ratio (TL/MTU) of the shoulder muscles. Muscles with long tendons (high capacity to store strain energy) may be able to contract nearly isometrically, leading to a low shortening velocity of the muscle fibres and hence a high force production (due to force-velocity relationship). In this case the contraction is possible at a high speed but not at maximal force production because the muscle fibres will typically not be operating at maximal myofilaments overlap (Lorenz and Campello, 2001). To complement this result, the macaques had long shoulder muscles and tendons (long belly length [L_b], fibre length [L_f] and distal tendon [h]) compared to the apes. Therefore, the macaques were still able to have powerful shoulder muscles with an increase in tendon and belly lengths instead of an increase in muscle weights.

The same general pattern was also observed in the elbow and wrist musculature, but the female orangutan more often overlapped with the female macaques than the male orangutans. Also, the Barbary macaque (M2) was often comparable to the two male orangutans. Overall, the macaques did have relatively large elbow extensors (triceps brachii) and ulnar (extensor carpi ulnaris, flexor carpi ulnaris, extensor digitorum) muscles. Rarely did the macaques ever surpass the orangutans in muscle strength. Despite the different modes of locomotion, larger and stronger muscles were usually found to be associated more often with the larger species. In this region, the flexors (e.g., biceps brachii, brachialis) and supinators (supinator, biceps brachii, brachioradialis) had the highest muscle mass. There are some possible explanations to this interesting pattern observed in this sample. First, the lack of body mass of the monkeys is a factor that cannot be ignored. However, many of the inter-specific researches on musculature also lack in body mass and use average body masses to compare the internal musculature of the primates studied (e.g., Michilsens et al., 2009). All of the original architectural muscle data

(Appendix A) that could be compared were within the ranges found in previous researches in macaques (Kimura and Takai, 1970; Cheng and Scott, 2000) and in orangutans (Oishi et al., 2008, 2009) (note that P2 was unusually large and weighed more than any typical range of orangutans in past researches). Thus, some of the measurements might be over or under estimated but the data presented do represent a range of values for those species and sexes. Second, despite the complete fixation of all the muscles before being measured (Ward and Lieber, 2005), the macaques and P1 were much older in terms of preservation (had been fixed in the laboratory for many years) and could have been more dried out. This means that their musculature could have been measured as being smaller in size, especially when both P2 and P3 had been new additions to the laboratory during the collection of soft-tissue data.

When looking at the individual muscles of the forelimb, the general pattern observed with the functional units was further emphasized. Attachment location was also considered when analysing each muscle. The apes had distal attachments of the rotator cuff muscles (especially subscapularis and infraspinatus) and the muscles that flex the elbow and wrist. They also had larger shoulder extensors, adductors, and endorotators (deltoideus, pectoralis major, subscapularis, supraspinatus and teres major) and larger flexors and supinators of the elbow and wrist. These muscles had either longer belly lengths or fibre lengths in the macaques.

Deltoideus: EMG data show functional differentiation of the three heads of the deltoideus muscle (Tuttle and Basmajian, 1978a, b; Larson and Stern, 1986, 2006, 2007; Whitehead and Larson, 1994). The anterior part of the deltoideus muscle acts as an arm elevator, raising the arm and reaching during postural behaviour in the swing phase of vertical climbing, or in suspended quadrupedalism (and silent during quadrupedal walking). The middle part acts as a humeral

abductor during quadrupedal walk, vertical climbing and arm swinging (active during the second half of swing phase). Finally, the posterior part provides propulsive humeral retraction in both vertical climbing and arm swinging or can help the middle deltoid with abduction of the arm in the support phase of quadrupedal walk. Arm elevation and humeral retraction are habitual movements of orangutans during suspensory and climbing locomotor activities. Coupled with a proximal insertion on the humerus, the large and powerful deltoideus in the orangutans would provide a significant advantage in these frequent forelimb movements and would favour rapid arm movements. On the other hand, a more distal insertion of the deltoideus in the macaques, along with a longer deltoideus, would favour strong and deliberate movements of humeral abduction for quadrupedal walking.

Pectoralis major: EMG data demonstrate that the pectoral muscles are active during the support phase of both arm swinging and vertical climbing in most suspensory primates, as well as during late swing phase slowing the arm for touchdown and humeral abduction during quadrupedal walking (Jungers and Stern, 1980, 1981; Larson and Stern, 1989; Whitehead and Larson, 1994). Thus the large pectoralis major in the orangutans would favour powerful and controlled humeral retraction necessary during suspensory activities. The longer pectoralis major in the macaques might provide fast muscular contraction during propulsion (retracting and abducting the arm) while walking or running.

Supraspinatus and subscapularis: According to EMG data, supraspinatus is active during the initial phases of arm rising during reaching or during the swing phases of vertical climbing and arm swinging when the arm is elevated against gravity and abducted. It can also assist deltoideus in abducting the humerus and stabilising the glenohumeral joint (Tuttle and Basmajian, 1978a, b;

Larson and Stern, 1986, 1989, 1992). Once again, the larger supraspinatus in the orangutans would favour suspensory postural behaviours requiring frequent abduction and arm elevation against gravity. EMG data also show that subscapularis is active during the later phases of arm reaching by lowering the arm via medial rotation as it is dropping from overhead suspension, and very important during the support phase (e.g., medially rotating the arm during climbing). This muscle also serves regularly as a postural muscle during static terrestrial quadrupedalism, especially in orangutans (Tuttle and Basmajian, 1978a, b; Larson and Stern, 1986, 1989, 2006). Coupled with a distal insertion on the humerus, the large subscapularis in the apes found in this sample would provide a significant advantage in these frequent forelimb movements and favour powerful and deliberate movements during reaching postural behaviours.

Teres major: Past EMG data show that teres major is active during the support phase by providing propulsive humeral retraction and medial humeral rotation in both vertical climbing and arm swinging (Larson and Stern, 1986, 1989). As the previous shoulder muscles have shown, the large powerful teres major found in the orangutans would favour these movements during suspensory postural behaviours.

Elbow and wrist flexors: Differences were also found in the elbow flexors. Both biceps brachii and brachialis are found to be active during the support phase of arm swinging providing controlled extension of the elbow as well as elevating the centre of gravity. They are also active in the support phase of vertical climbing, providing elbow flexion when the body is pulled upwards. Elbow flexors are found to be silent in the propulsive phase of quadrupedal walking (Jungers and Stern, 1980, 1981; Tuttle et al., 1983; Youlatos, 2000; Stern and Larson, 2001). Strong digital and wrist flexors are usually associated with powerful and hook-like grasp

facilitating arm swinging and suspensory activities in general. EMG also supports this data and show that the flexors are active during support phase establishing a firm handgrip on an arboreal substrate (Jungers and Stern, 1980). The distal origin of the flexors along with the large muscles provides more evidence that the orangutans would favour these movements required during suspensory locomotion and feeding.

Supinators: Supinators should be well developed in suspensory primates facilitating movements of the forearm necessary in hanging activities (Tuttle et al., 1992). A more quadrupedal primate requires powerful pronation of the forearm in order to place the hand above a support (and therefore active during support phase to maintain the forearm above the substrate). It is therefore not surprising that the apes had more powerful supinators than the macaques in this sample.

The only difference found between the sexes was fibre length (L_f); females seemed to have longer muscle fibres than the males. L_f reflects the possibility of the muscle generating force over a wider range of motion and to the shortening velocity of the muscle (Anapol and Jungers, 1986; Antón, 1994, 1999, 2000; Anapol and Barry, 1996; Gibbs et al., 2002; Lieber, 2002; Anapol and Gray, 2003; Taylor and Vinyard, 2004; Organ, 2007, 2009; Taylor et al., 2009). However, both macaques were female and most likely were driving this relationship. The macaques did have distal attachments of the large muscles of the arm (latissimus dorsi, deltoideus, brachialis, triceps brachii) and the extensors of the forearm. These more distal attachments allowed the delivery of strong and deliberate movements necessary during quadrupedal locomotion. For example, a distal insertion of the latissimus dorsi muscle provides powerful humeral retraction during the propulsive phase of walking by pulling the body forward (Youlatos, 2000). Along with their long slender muscle fibres, the macaques had forelimb

muscles that could contract over a wider range of motion and shorten at a faster velocity, while still being able to be strong and precise during their quadrupedal behaviours. More details of gait parameters such as ground reaction forces, velocity, and loading rates in primate forelimbs (e.g., Biewener, 1992; Demes et al, 1998; Larson et al., 2000; Schmitt et al., 2010) would need to be collected in addition to EMG and internal structural data to more accurately interpret the variation in these primates.

7.1.2 Primates and bone structure

Following soft-tissue analyses, each attachment site on the humerus was investigated. One of the methodological problems found in entheseal research involves the relatively high percentage of measurement error since it is very difficult to distinguish where a fibrous attachment begins and ends (Jurmain et al., 2012). It was found that without the help of digital photographs, many of the fibrous attachments would have been difficult to accurately trace out. Each specimen had very different overlapping attachment sites and could only be distinguished with the help of photographs. Digital photographs also greatly reduced tracing errors. Since entheses are subjected to forces from the contracting muscles, it is presumed that blood flow will increase, stimulate local osteogenesis, and increase the mass of bone beneath the muscle, thereby producing an elevated or a robust area of insertion (Hawkey and Merbs, 1995, 1998; Zumwalt, 2005; Cardoso and Henderson, 2010; Jurmain et al., 2012). Using that assumption, it was predicted in Chapter 3 that the larger and stronger muscles (high M, PCSA, M/P_0, and *I* values) would be associated with more hypertrophied attachments sites. It was also predicted that the orangutan would be stronger (larger section moduli) and more rigid (larger second moments of area) in bending, torsion, and axial compression/tension (cortical area) than the macaques as a

result of the increased stress and strain incurred during suspensory locomotion. Finally, it was predicted that the fibrous muscle attachment sites in all primates would not change in shape along the location sequence (proximal, midpoint, and distal) since theoretically muscle fibres should enter the periosteum potentially at the same angle throughout the attachment (Benjamin et al., 2002).

The skeleton is thought to adapt to variable mechanical loadings associated with changes in positional behaviour by making appropriate adjustments in the quantity and distribution of bone tissue (see Frankel and Nordin, 2001; Currey, 2002; Huiskes and van Rietbergen, 2005 for review). Past studies have shown that species of macaques are reported to have lower bending rigidity at midshaft, while orangutans exhibit greater strength relative to humeral length when compared to other primates (Burr et al., 1981; Burr et al., 1989; Delson et al., 2000; Ruff, 2002, 2003; McFarlin 2006; McFarlin et al., 2008). In this study, the orangutan humeri were also found to be stronger (larger section moduli [Zp]) and more rigid (larger second moments of area [*J*]) in bending, torsion and axial compression/tension (cortical area [CA]) at the midshaft. The species with forelimb suspensory behaviours had stronger and larger humeri, than the terrestrial species. Those same researchers along with others (e.g., Carlson et al., 2006) have found that the humerus of primates has less variation in diaphyseal geometry among taxa characterized by different locomotor specializations than does the femur. Here, no differences were found between the primates when looking at the medullary area (MA), both the index of circularity (I_{max}/I_{min} and Zy/Zx), and the orientation of the greatest bending rigidity (theta). Therefore, not all variables showed clear relationships between specific locomotor behaviour (e.g., suspensory) and diaphyseal shape.

Relatively similar cross-sectional geometry patterns were found throughout the humerus and within attachment sites. Surprisingly, the diaphyseal cross-sectional properties within an attachment site varied within the location sequence (proximal, midpoint, and distal). The large muscles characterized by the fibrous entheses attach directly to the bone or via periosteum and are anchored by Sharpey's fibres (Hoyte and Enlow, 1966; Hems and Tillmann, 2000; Benjamin et al., 2002; Hieronymous, 2006). Blood vessels from the soft-tissue can then anastomose with those of the bone (Dörfl, 1969). It was thought that since those muscle fibres enter the bone or periosteum potentially at the same angle throughout the attachment and equally anastomose with the vessels of the bone, the entheseal surface along with the underlying bone should hypertrophy in response to locomotor and postural behaviour in a similar matter. Thus, the cross-sectional properties should stay relatively the same throughout the enthesis. However, that was not the case. Instead, the cortical area, total area, and index of circularity were significantly different in each primate for most attachment sites, but no consistent pattern was observed. For example, within the deltoid tuberosity, the cortical area of the bone might have increased (from the proximal to the midpoint sections) and then decreased (from the midpoint to the distal sections) within the attachment for one of the male orangutans, while it might only have increased in cortical area in the female orangutan. Therefore, not every section within the location sequence had the same bone thickness and distribution. The only variable that was predictable was the angle of greatest bending rigidity (theta). For all attachment sites, the angle stayed the same throughout the enthesis, perhaps because similar muscular contractions were experienced within each enthesis. Therefore, no matter where the data were taken (proximal, distal or at the midpoint) within the attachment site, the angle of greatest bending rigidity was always oriented in the same plane. The perception of an attachment site (i.e., being faint or well-developed) can be biased if the observer does not control for the relative robusticity of the underlying bone

(Robb, 1998; Weiss, 2003; Zumwalt, 2005, 2006). This research was unable to determine which aspect of the fibrous attachment site is the most meaningful for interpretation, since no consistent pattern was observed. Each fibrous muscle attachment site might have its own region of interest, and more research looking at each specific attachment is needed to understand the complexity of fibrous attachments. Therefore, for the purpose of this project, the cortical thickness found at the midpoint of each of the eight-diaphyseal attachments sites of the humerus (latissimus dorsi, pectoralis major, deltoideus, teres major, coracobrachialis, lateral and medial heads of the triceps brachii and brachialis) was considered to control for the underlying bone.

Results from the entheseal surface bone measurements showed that the sex and the species had some impact on the morphology of the attachment sites, but again, not in a predictable matter. Therefore, the null hypothesis could not be rejected. It was hypothesized that the larger orangutan males should have the largest attachment sites, since hypertrophy of bony attachments for larger and/or more active muscles is a theoretically advantageous mechanism to reduce stress or maintain acceptable stress magnitudes (Biewener, 1992; Hawkey and Merbs, 1995, 1998). However, the smaller female macaques had larger surface areas for the attachments of the latissimus dorsi and the deltoideus muscles. No associations were observed between the attachments of teres major, lateral head of the triceps brachii, pronator teres, and brachioradialis muscles with the sex and species of the primates. Larger and stronger muscles (higher values for M, M/P_o, PCSA or *I*) were sometimes associated with larger (especially wider entheses) muscle attachment sites (coracobrachialis and brachialis). However, the large muscles mentioned in the previous section (deltoideus, pectoralis major, teres major, subscapularis, supraspinatus, elbow and wrist flexors and supinators) were not all associated with larger entheses. Deltoideus had a larger surface area and the width of the pectoralis attachment was wider in the macaques, while

the attachments of the teres major and brachioradialis muscles overlapped in morphology. Surprisingly, muscles associated with greater excursion and contracting velocity (higher values for Lb, Lf, or h) were at times associated with smaller entheses (supraspinatus, teres minor, extensor carpi radialis longus), but sometimes with larger entheses as well (latissimus dorsi and deltoideus). Entheseal studies often fail to consider that long and slender muscles matched with long tendons are also very powerful muscles. If these muscles (low in muscle mass) are matched with a distal attachment on the long bone, their movements might in fact be very strong and their forceful contraction on the bone may have effects similar to those of a large muscle (high in muscle mass). It was seen in section 7.1.1 that the macaques often had great mechanical leverage without the need for large muscles. Good mechanical leverage probably reduces the amount of stress experienced by the attachment site, and may not hypertrophy the enthesis. It has been suggested that muscle attachments responsively develop to protect the underlying bone from injury during muscle contraction, and forceful muscle pulls may not impact enthesis morphology until they reach pathological levels (Zumwalt, 2005, 2006; Jurmain et al., 2012). Better mechanical leverage could explain why muscle attachments may not hypertrophy until it does reach pathological levels, such as accumulated muscle contraction forces associated with age.

Finally, when considering the underlying bone of a diaphyseal enthesis, a better association between the muscle and the attachment site seemed to be observed. Larger and stronger muscles (higher values for M, M/P_o, PCSA or *I*) seem to have some association with at least one of the entheseal measurements. However, no clear associations were found. At times, the width of the attachment was wide as was the muscles (teres major, brachialis), other times it was the length that was long when a muscle was large (coracobrachialis, pronator teres), and sometimes it was a greater area that could be observed with a large muscle (latissimus dorsi, deltoideus, triceps

brachii). Therefore, the underlying bone of an enthesis does seem to be important, however, each fibrous attachment site appears to deposit bone differently. Having a better understanding of how each muscle is pulling on the bones could help determine if bone is deposited where the muscle contractions are the largest. Considering the underlying bone in fibrocartilaginous attachment sites should be explored. Including microscopic analyses (as seen in the mice model in this project – see below) could also help shed light on whether or not, and if so, how, primate bones respond to daily behaviours. Again, more details of strain analyses and kinematics of primate forelimbs (e.g., Biewener, 1992; Demes et al, 1998; Larson et al., 2000; Abdulaliyev et al., 2007) need to be collected to more accurately interpret the variation found in the bones of these primates. In general, it was found that many of these associations were random and not specifically associated to the mode of locomotion, sex, body size, age, or species of the primates.

7.1.3 Summary of primates

A major goal of musculoskeletal research is to link daily behaviours to the anatomy of the enthesis. The results from the primates have shown how variable muscle and bone can be even when considering factors such as age, sex, species, body mass, and locomotion. They also emphasized the lack of clear relationship between daily locomotor and postural behaviours and the overall size and shape of a muscle attachment site. The results demonstrated the need to include as much information as possible when interpreting entheses: internal muscle structures, kinematic and EMG data, location of the insertion on the bone for biomechanical leverage, underlying cortical bone, and microscopic analyses. The functional significance of enthesis morphology is much more complex than what is typically assumed, and these results show that gross enthesis morphology is not enough to assume daily patterned activities.

7.2 Mouse model discussion

A mouse experimental model was also used to examine whether muscular differences stemming from different activity patterns can be reliably inferred from enthesis morphology. Activity levels, muscle fibre architecture, and entheseal morphology data were collected in two experimental groups (high intensity running and intermediate intensity climbing) and one control group of female wild-type mice. Human preclinical studies rely heavily on data from mouse models; therefore, it is useful to have comparative info regarding the composition and architecture of mouse muscle and bone (Mathewson et al., 2012). Currently, little is understood on whether enthesis morphology responds in predictable ways to muscle action, and if the surface morphology of bone underlying muscle attachments is dependent on the type of activity. Also, if activity does dictate bony morphology, it is not clear if the morphology represents activity over many years, or simply activity that occurred shortly before death. This experiment enabled controlled settings where age, weight, growth, and activity could be accurately recorded, which is ideal for studying how entheses may change in response to these factors. Mice are ideal for this study due to: 1) their small body size and rapid development (Carlson et al., 2008), 2) their bones being able to experience the same amount of strain as other vertebrates, making them valuable to study bone adaptation to material and mechanical properties (Lee et al., 2002), and 3) the ability to have voluntary exercise settings that can allow observation of changes in muscle and bone growth. Results demonstrated that activity pattern could influence aspects of muscular development (e.g., fibre length, physiological cross-sectional area), as well as rate of osteogenesis and bone microanatomy beneath an enthesis, yet have no observable effect on the external shape or size of the muscle attachments site. Therefore, results from this dissertation do

not provide experimental support for previous musculoskeletal research (Hawkey and Merbs, 1995; Hawkey, 1998; Wilczak, 1998a, b; Knüsel, 2000; Eshed et al., 2004; Wang et al., 2004; Weiss, 2003, 2004, 2007, 2010; Molnar, 2006, 2010; Marzke et al., 2007; Havelková et al., 2011) linking muscle size and attachment site morphology. In addition, neither activity intensity nor type (running and climbing) produced an appreciable effect on the gross bony morphology of fibrous entheses.

7.2.1 Activity and internal muscle structure

Mice undertaking different exercise regimes in the current study showed differences in body mass, with the largest differences found between the running group (lowest body mass) and the control mice (highest body mass). Therefore, on average the greatest amount of activity lowered the weight of the individuals more than the intermediate (climbing) to low (control) level of exercise. Mathewson and colleagues (2012) found that the forelimb flexor muscles in mice were larger and better at potential force production, while the extensors were better conducted for excursion and contraction speed. However, they did not look at the spinodeltoideus, acromiodeltoideus, or the superficial pectoralis. Based on Mathewson and colleagues' result (2012), it was predicted that the protracting muscles studied (acromiodeltoideus and superficial pectoralis) would be larger and stronger than the retracting muscle (spinodeltoideus). Although this was true for the superficial pectoralis muscle, the acromiodeltoideus had the smallest muscle mass, belly length, fibre length, and physiological cross-sectional area for all mouse groups. The superficial pectoralis was therefore the most powerful protracting muscle in this sample.

For the muscle fibre architecture variables between age groups, the null hypothesis could not be rejected. Although both groups of mice were not of the same age at the end of the experiment and despite neither group having reached full skeletal maturity yet, all mice were of adult body size and sexually mature (Kilborn et al., 2002). The results indicate that the age at onset does not significantly change the development of internal muscle structures. Whether or not exercise affects differently early (before sexual maturity) or later development (after closure of epiphyseal growth plate) of the internal muscle structures in wild-type mice requires further investigations. A wider range of ages (e.g., non sexually mature [less than a month], aged mice [over 5 months]) would help explore the ontogenetic relationship between muscle and bone.

For most of the internal muscle structure, the null hypothesis between exercise groups and controls could be rejected. Although the exercised animals did differ in most muscle fibre architectural organization from the controls, the differences found did not follow the predictions outlined in Chapter 2. Absolute muscle masses (M) differed among groups, but only acromiodeltoideus differed significantly between exercise groups following multiple comparison correction. The intermediate intensity-climbing mice had the largest absolute and relative muscle masses, while contrary to the prediction; the high intensity running mice had the lowest muscle masses (both absolute and relative). Frequency of exercise did not increase the mass of the muscles studied, although the magnitude of the exercise due to vertical climbing (going against gravity) did have some impact in higher muscle masses. These results further support previous research and experimental models (e.g. Hamrick et al., 2006) indicating that muscle mass is not always the best correlate for muscle function (Bryant and Seymour, 1990; Lieber, 2002). Contrary to muscle mass, the vertical climbers had the shortest belly lengths (L_b), while the high intensity runners had the longest length (both absolute and relative). However, the controls and

the running mice had overlapping muscle belly lengths. Although L_b was a better indicator of contractile properties between locomotor groups (climbing versus walking/running), overall results showed that muscles were not getting absolutely larger or longer with an increase in frequency of an activity.

Interestingly, despite minimal influence on muscle mass and belly length, activity differences did have a significant effect on muscle fibre architectural properties attaching to the deltoid crest. Changes in motor function, such as changes in gait (e.g., speed, degree of shoulder flexion), were met by a change in contractile behaviour of individual muscles (Biewener and Gills, 1999). As mentioned in Chapter 2, muscle growth can occur by myofibrils adding sarcomere at the tendon sites, thereby increasing length of the muscle fibre (Goldspink, 1968; Williams and Goldspink, 1971, 1973, 1976, 1978; Antón, 1994; Lieber, 2002; Marini and Veicsteinas, 2010). In fact, sarcomeres can be serially added to a fibre within days of a muscle being stretched (Williams et al., 1986), and these additions have a greater effect on architectural muscular properties than the overall mass or belly length of the muscle. As predicted, results showed differences in potential muscle force and excursion/contraction velocity between activity groups. Both the running and control mice had absolutely and relatively longer fibered (L_f) muscles than the intermediate intensity climbers, perhaps reflecting the shorter forelimb excursions involved in climbing (Green, 2010; Green et al., 2012). The same results were seen for the muscle mass over predicted effective maximum tetanic tension (M/P_0), which compares the priority of force production versus contraction velocity. These data are consistent with the observation that running and control groups practiced similar types (quadrupedalism) of daily locomotion. Overall, the running mice had significantly longer fibres than both the control and climbing mice. Therefore, contrary to the intermediate intensity vertical climbing activity, higher intensity running

promoted the development of longer fibres in the forelimb muscles. Fibres of the acromiodeltoideus, spinodeltoideus, and the superficial pectoralis could shorten over greater lengths with theoretically higher velocity than the climbers. These findings are consistent with significant kinematic differences observed previously between the climbing and running groups, including significantly more flexed (protracted) shoulders during touchdown and lift-off during running (Green, 2010; Green et al., 2012). Fibre length is also dependent on muscle type, which was not analysed in this study. However, since Type IIA (fast-twitch oxidative-glycolytic [FOG]) is a type of fibre associated with a higher resistance to fatigue and endurance training (without dramatic muscle hypertrophy) (Anapol and Jungers, 1986; Jouffroy and Médina, 1996; Jouffroy et al., 1998; Lorenz and Campello, 2001; Lieber 2002; Higham and Biewener, 2011), it is possible that the high-intensity runners had a higher quantity of these types of fibres. More research is needed in fibre typing to test if endurance in this sample did increase Type IIA fibres in the shoulder muscles.

A basic trade-off exists between a muscle's ability to shorten actively and it's ability to generate mechanical power (Gans, 1982; Biewener and Gills, 1999; Lieber, 2002; Williams et al., 2008; Taylor et al., 2009). Muscle cannot be simultaneously optimized for maximum force generation (PCSA) and excursion/contraction velocity (L_f). This architectural trade-off was observed among the experimental and control groups as activity type significantly influenced the potential maximum force-generating capacity of the muscles analysed in this study. The climbers developed muscles comprising absolutely and relatively larger physiological cross-sectional areas (PCSA) and higher index of force (*I*), but absolutely and relatively shorter fibres compared to the running and control groups, as might be predicted with the vertical activity that required mice to move up (and down) the meshed-cages. It was mentioned in Chapter 2, that muscle could

also grow by hypertrophy by increasing fibre diameter (Goldspink, 1968; Williams and Goldspink, 1971, 1973, 1976, 1978; Antón, 1994; Lieber, 2002; Marini and Veicsteinas, 2010). Therefore, in the absence of differences in muscle pennation angles, climbing appears to have increased the potential force output of the muscles, largely by increasing in fibre diameter (therefore adding muscle mass) without altering the orientation of the fibres relative to the muscle's force generating axis. A complementary conclusion could be that the intermediate intensity climbers had more Type IIB (fast twitch glycolytic [FG]) fibres, which are associated with bursts of strong force over a shorter period of time (which can also result in muscle hypertrophy) (Anapol and Junger, 1986; Jouffroy and Médina, 1996; Jouffroy et al., 1998; Lorenz and Campello, 2001; Lieber 2002; Higham and Biewener, 2011). As mentioned in Chapter 2, power production of muscle also depends on the metabolic properties of the fibres. Future research should include fibre typing of the muscles studied to add to the factors of muscle function.

Overall, muscle architecture data compiled in this study indicated that as predicted, increased activity influenced the development of more powerful muscles (Williams et al., 2008); in potential maximum force generating (intermediate intensity climbers) or potential excursion/contraction velocity (high intensity runners) of each individual muscle. Control mice were left with the least powerful muscles in all of the groups studied here. This project emphasizes that, researchers seeking to reconstruct muscle function need to consider more than muscle mass to more accurately define habitual behaviours.

7.2.2 Activity and bone structure

Bone has been shown to be responsive to mechanical stresses, such that elevated amounts of muscle contraction ought to influence bone morphology (see Frankel and Nordin, 2001; Currey, 2002; Huiskes and van Rietbergen, 2005 for review). As mentioned previously, tension exerted by muscles is presumed to increase blood flow, stimulate local osteogenesis, and increase the mass of bone beneath the muscle, thereby producing an elevated or a robust area of insertion (Hawkey and Merbs, 1995, 1998; Zumwalt, 2005; Cardoso and Henderson, 2010; Jurmain et al., 2012).

The results of this study show very interesting variation at the microscopic levels, but lack in macroscopic differences. It was found that elevated activity influenced differential periosteal growth in the humerus and throughout the deltoid crest. However, no differences in the gross size or shape of the deltoid crest across the experimental conditions were found, rejecting the hypothesis that attachment site morphology reflects in vivo activity. All groups (exercise and age groups) demonstrated substantial overlap in the deltoid crest morphology. Although the deltoid crest serves as the attachment site for three large powerful muscles - all of which attach directly to the periosteum and anastomose with the vessels of the bone (Dörfl, 1969) - no evidence of entheseal surface hypertrophy in response to increased activity was found.

Before discussing the lack of differences in the gross morphology of the deltoid crest, some important microscopic differences are worth noting. All cross-sections of mice were analysed based on collagen fibre orientation, density, and vascularization of the tissue. Primary bone tissue, which is considered to have a relatively fast depositional rate (typical of rodents), was the main tissue present in all cross-sections (Enlow, 1957). Circumferential lamellar bone dominated

across both cross-sections and for all activity groups. High intensity runners did present more parallel lamellar bone remodelling, while the vertical climbers had more "disorganized" tissue remodelling with a larger presence of secondary osteons and drifting osteons. Disorganized tissue was especially present at the 25% of the maximum bone length cross-section. This convoluted tissue called endosteal compacted coarse cancellous bone (ECCC) is indicative of inward endosteal growth, usually associated with metaphyseal remodelling in proximal and distal regions of the diaphysis (Enlow, 1963; McFarlin, 2006; Goldman et al., 2009). During compaction (in-filling of cancellous spaces), lamellar tissue is deposited along the contours of cancellous trabeculae (which is itself composed of parallel-fibered or lamellar bone), giving this tissue type its distinctive convoluted appearance. This tissue, as seen in this sample, is associated with secondary osteons. These osteons are often of irregular shape, showing evidence of drift. ECCC is also a tissue portraying cement lines, which delineate discontinuities in cycles of bone deposition during cancellous compaction (Enlow, 1963). Cement lines were seen in these mice and were even more demarcated with the fluorescent-labelling dyes, especially in the vertical climbing mice. Therefore the lack of differences in cortical shape particularly for the standard cross-sections could be due to the fact that, at this bone location, growth and potential expansion of the metaphyses might have dominated the growth remodelling instead of contracting muscle attaching to the deltoid crest. This was probably the case since the growth plates of these mice were not yet fused (Kilborn et al., 2002). Another standardized location with less metaphyseal activity, such as the midshaft of these humeri, would be interesting to study and to better understand how the microanatomy of the cortical bone is affected by activity.

This research demonstrated that intrinsic rates of bone growth at the enthesis are influenced by activity. The two experimental groups often overlapped in their faster rate of osteogenesis, but

the controls were clearly depositing bone at a slower rate. This was true throughout the entire cortex, but especially for the bone underlying the deltoid crest. Therefore, the microscopic analyses of the humeral bone showed that the mice were all mainly characterized by circumferential lamellar bone, except close to the metaphysis. The amount of exercise seemed to dictate the speed of deposition of bone, since both exercise groups, and especially the highly exercised runners exhibited faster rates of osteogenesis. However, high amounts of running decreased secondary activity in these mice, while climbing vertically increased significantly the presence of secondary osteons and the presence of less organized tissue. The lack of differences in surface morphology could be due to the fact that different loadings on bone dictated variation in bone remodelling. Lee and colleagues (2002) found that varying peak strains on the bones affected differently bone tissue. Loading to peak strains of 2000 με (micro-strain) stimulated lamellar periosteal bone formation, whereas loading to 3000 με stimulated a combination of lamellar and woven periosteal bone formation and lamellar endosteal bone formation (Lee et al., 2002). More details of gait parameters such as ground reaction forces, velocity, and loading rates of each individual mouse (Schmitt et al., 2010) need to be collected to more accurately interpret the variation of bone tissue found in wild-type mice doing these two types of activities.

Finally, cortical drift was inspected by looking at the direction of the drifting osteons, as well as the features that indicate recently deposited bone versus resorptive bone surfaces (e.g., direction of the fluorescent labels). The deposition of bone showed a general postero-lateral cortical drift pattern for all activity and age groups. The lack of variation in the cortical drift of the humeral cortex, again can partly explain the lack of differences in the gross anatomy of the bone. Quantification of bone tissue type and cell types would be needed to clarify how these mice were reacting to their environment, especially the vertical climbers. Past research (Notomi et al., 2001;

Mori et al., 2003; Robling et al., 2006; Menukiet al., 2008; Plochocki, 2009; Robling, 2009) found that accelerated cortical drift by mechanical stimulation can result in different osteoblastic and osteoclastic activities, but the effect on bone formation seems to be site specific (i.e., midshaft of the femur). Such research has not been done on the humerus, and could shed light on the different tissue types and levels of remodelling found in this sample. Therefore, the amount of activity seemed to dictate the speed of deposition of bone, however, remodelling rates need to be further studied to fully understand how activity groups were reacting to their daily behaviours. Further research should focus on examinations of the microstructure of the entheseal surface to have a better understanding of how these entheses grow and maintain integrity throughout life.

The skeleton is thought to adapt to variable mechanical loadings associated with changes in positional behaviour by making appropriate adjustments in the quantity and distribution of bone. Using beam theory it is possible to estimate the resistance of a bone to axial compression, tension, bending and torsion, by considering the geometric distribution of bone tissue in a cross-section of a whole bone (e.g., Huiskes, 1982; Biewener, 1992; Ruff and Haynes, 1983). A lot of overlap was seen in the diaphyseal geometric analyses and the presence of many outliers in each group brought many non-significant results. The lack of significance from the 25% of maximum humeral length section could be due to location problem, since this cut was made close to the proximal end of the bone. Hamrick and colleagues (2006c) found that bone mass from the femurs of female wild-type mice increased more (35%) in the distal metaphyseal region than the mid-diaphysis (20%) with exercise. In this sample, all geometric properties of the humerus increased at the more distal cross-section compared to the proximal section. Therefore, osteogenic response of cortical bone to exercise can significantly vary along the length of a bone, where distal regions may exhibit more morphologic changes when loading conditions are altered

(Hamrick et al., 2006c). However, none of the contrasts were found to be significantly different for the distal margin of the deltoid crest section. The lack of significance at this more distal location of the deltoid crest could be due to the large prominent crest present and extending away from the centroid, causing an irregular shape for this cross-section, and very different than the typical "beam" shape that is used for these analyses (Ruff and Haynes, 1983; Biewener, 1992). Once again, the midshaft of these humeri could help to better understand how the cortical bone shape was affected by activity without the presence of the large prominent deltoid crest. Although there was very little significance in the geometric properties, a general trend could be seen. The vertical climbing mice were separated from the two other groups by having thicker cortical bone (the only significant result) with a generally greatest bending rigidity in the antero-posterior axis. The control and running mice had smaller cortices and their greatest bending rigidity was generally located in a more medio-lateral orientation. However, the lack of differences in geometric properties does call for further analysis and cautions the inference of locomotor and physical behaviours from bony morphology alone. Wallace and colleagues (2010) looked at mice that were artificially selected for high voluntary wheel running and found that diaphyseal structure was highly determined by genetic factors rather than simply by direct mechanical stimuli. Their results, like the ones from this dissertation, suggest that limb bone cross-sections may not always reflect the activity levels of past individuals.

Overall, the hard-tissue results call into question previous interpretations that differences in function among individuals in a species can be directly linked with differences in entheseal surfaces (Hawkey and Merbs, 1995; Hawkey, 1998; Wilczak, 1998a, b; Knüsel, 2000; Eshed et al., 2004; Wang et al., 2004; Weiss, 2003, 2004, 2007, 2010; Molnar, 2006, 2010; Marzke et al., 2007; Havelková et al., 2011). It is important to note that the experiments reported here involved

voluntary activity differences designed to produce physiologically normal variation in the intensity and type of activity, and to avoid activities that might induce pathology. This study confirms experimental evidence that show no effect of exercise on enthesis morphology in adult sheep (Zumwalt, 2005, 2006). It has been suggested that muscle attachments responsively develop to protect the underlying bone from injury during muscle contraction, and forceful muscle pulls may not impact enthesis morphology until they reach pathological levels (Zumwalt, 2005, 2006; Jurmain et al., 2012). This study demonstrated that intrinsic rates of bone growth at the enthesis are influenced by activity and some correlations were observed with the thickness of the crest and some of the internal muscle structure variables (e.g., fibre length, physiological cross-sectional area). Perhaps, as hypothesized in previous studies (Zumwalt, 2005, 2006; Jurmain et al., 2012), the stress that is exerted on the fibrous enthesis must be at a certain threshold in order to have a visible change on the cortex. Whether or not the surface morphology of the enthesis changes only in response to pathological levels requires further investigation. However, it is unclear how muscle attachment morphology can be used to make inferences about behaviour in past populations if the attachment sites only develop visible morphological differences in response to pathological damage.

These results show that it is unclear how daily behaviours influence the gross surface morphology of a fibrous enthesis. As it is well known, bone does not simply grow by adding new bone to all outer (periosteal) surfaces with corresponding removal from all inner (endosteal) surfaces. Rather it appears to grow through a combination of deposition and resorption on both the periosteal and endosteal surfaces (Enlow, 1962). As a result, tension from muscles can be associated with simultaneous bone deposition and removal, although it may not necessarily change the overall shape or size of the bony crest. Bone resorption is also often regarded as a

process where all tissues are completely removed. However, as Hoyte and Enlow (1966) demonstrated, Sharpey's fibres may be exempt from this type of resorptive destruction. They may remain unaltered even though superficial bone tissues are removed. Therefore, Sharpey's fibres provide an important mechanism for anchoring muscle attachments to bone during growth and remodelling of the bone surface. This may partially explain why entheseal surface morphology did not change in response to the type or degree of activity over time. More research on Sharpey's fibres is needed to better understand their role at the muscle-bone interface. Very little is currently known about Sharpey's fibres found in long bones, with most of the research focusing on theses fibres found in the alveolar socket of the teeth (Aaron, 2012). Currently there is reason to believe that Sharpey's fibres may alter the structural quality of the bone matrix they occupy, may be instrumental in early musculoskeletal development, may provide an integrated scaffold for skeletal repair, may be protected from resorption creating stability, may actually be a direct microanatomical link uniting the outer periosteal and inner endosteal membranes and thereby coordinating bone behaviour, may weaken and fragment in circumstances such as low oestrogen, and may strengthen and augment in circumstances such as increased activity (Hoyte and Enlow, 1966; Aaron, 2012). Sharpey's fibres can be identified on the surface of the bone (or by casting the surface of the bone) using scanning electron microscopy and then be correlated to their location and orientation in a cross-section of a bone. If such a relationship exists, more details could be interpreted on archaeological and fossil material without the destruction of the bone and could even be correlated to daily activities.

The deltoid crest was used to evaluate a fibrous attachment site with its attaching musculature. A wider range of fibrous attachment sites (e.g., linea aspera of the femur) should be investigated, which would add the currently sparse knowledge of these types of entheses (Benjamin et al.,

2002). Of course, more knowledge on fibrocartilaginous attachment sites is also needed, and mice models are a great experimental way of gathering such information with the control of many factors. Further research is required to determine how bone changes with muscular contraction throughout an individual's lifetime and with different activity. Different age groups and adding male mice to this study could also help better determine the influence of hormones, such as oestrogen, on the mechanical loading and bone formation of the entheses.

The lack of differences between age groups also needs to be further investigated: it is not well known how a fibrous enthesis develops with long bones. It is thought that during growth, muscles and tendons attach primarily to the periosteum and only after longitudinal bone growth is completed, do the muscles appear to pass through the periosteum and attach firmly to the underlying bone (Hoyte and Enlow, 1966; Wilczak, 1998a, b; Zumwalt, 2005, 2006). However, despite the lack of growth plate fusion in the mice, Sharpey's fibres were present in the cross-sections from this study, meaning that these extrinsic fibres were already anchoring the muscles onto the bone (agreeing with Hoyte and Enlow, 1966 ;McFarlin et al., 2008). Full knowledge of the variables that directly influence enthesis development will be needed to make more reliable inferences about muscle development and activity from hard tissue structures. Finally, future research should include observations of gait parameters for each individual mouse. In the current study, specific mice were not identified during the kinematic analyses. An average of the activities were identified for each exercise group (Green 2010; Green et al., 2012). As mentioned above, more details of gait parameters such as ground reaction forces, velocity, and loading rates (Schmitt et al., 2010) could be used to more accurately interpret changes in the musculoskeletal anatomy. This type of research would help determine more accurately how gait mechanics influence histological variability and diaphyseal shape of the bones

7.2.3 Summary of mice

A major goal of musculoskeletal research is to link daily behaviours to the anatomy of the enthesis. Based on the results from the mouse model, it is clear that a re-evaluation of basic concepts regarding muscle influence on bone development is needed. The functional significance of enthesis morphology is more complex than what is typically assumed, and gross enthesis morphology cannot be assumed to simply reflect variation in daily patterned activities. This study emphasized the need to add microstructural analyses to geometric and gross analyses to make refined inferences about activity and locomotor history from archaeological skeletal and fossil remains. Microanatomy could be more labile in response to variations in muscle activity during bone development; therefore future research should focus on the examinations of the microstructure of the entheseal surface. A general deficit in the understanding of muscle attachment site development has led to oversimplified and unsubstantiated interpretations of entheseal morphology and activity patterns from past populations. Further knowledge of the functional significance and development of entheseal morphology is needed if one is to accurately reconstruct behaviour based solely on skeletal and fossil remains.

7.4 Conclusions

Providing information on habitual activities of past populations from skeletal and fossil material is crucial to studies in biological anthropology. When faced with a scarcity of anatomical information due to the loss of soft tissue, researchers assume a functional relationship between bone morphology and the missing musculature. The results of this study indicate that the relationship between muscle activity and attachment size and shape is much more complex than

what has long been assumed. No other research has done this kind of work combining both soft- and hard-tissue along with macro and microanalyses to interpret muscle attachment sites in primates or mice. Results from both the primates and the mice models showed that activity produces no predictable surface morphology of an enthesis. The relationship between external load and surface osseous morphology is not clear and attachment sites do not appear to reflect lifetime muscle activity.

In order to have a better understanding of muscle-bone interfaces, more studies need to include muscular variables and ontogenetic bony surface analyses before classifying and scoring entheseal surfaces from past populations. More reliable methods to analyse entheses in living individuals (e.g., magnetic resonance imaging, ultrasound, kinematics) are crucial to the understanding of how muscles and bone interact together during a lifetime. Future research should aim to use these methods to study the effect of mechanical stress on entheseal surfaces. Also, more microstructural analyses are needed to better understand muscle and bone development and wear. Fibre typing to test power production, orientation of collagen fibres in bone (Sharpey's fibres), tissue typing in bones of primate and other mammals could all help shed light on the variations observed in this study.

There are a number of factors besides muscle size and activity that may contribute to the development of attachment sites. Bone does not respond to all stimuli, and when it does, similar or disparate conditions may lead to different bony responses (Turner, 1998, 2000; Burr et al., 2002; Currey, 2002; Robling, 2009). Growing bone seems to be more responsive to muscle contractions than mature bone, and bone may also respond only when a load has surpassed a certain threshold. Both genetic factors and phenotypic plasticity are also very important, as are

hormones, nutrition, sex, and age, and it is crucial to consider the non-mechanical influences on diaphyseal structure as more than confounding variables but as potential sources of scientific inquiry (Montgomery et al., 2005; Zumwalt 2005, 2006; Hamrick et al., 2006; Ravosa et al., 2008; Plochocki, 2009; Jurmain et al., 2012; Schlecht, 2012a, b). Therefore, although muscle attachment sites have the potential to be very informative to biological anthropologists, more clarification of the functional significance is necessary to be able to reconstruct the level and type of activity patterns experienced during the life of past populations.

Bibliography

Abdulaliyev Z, Çelik Ö, Göller G, Kayali ES. 2007. Investigation of forces and stresses acting on a shoulder-hand system considering strains in muscles. Turkish Journal of Engineering and Environmental Science 31:1-8.

Aiello L, Dean C. 2002. An introduction to human evolutionary anatomy. Amsterdam: Academic Press. 596 p.

Alexander RMcN. 2002. Tendon elasticity and muscle function. Comparative Biochemistry and Physiology Part A 133:1001-1011.

Allen DL, Harrison BC, Maass A, Bell ML, Byrnes WC, Leinwand LA. 2001. Cardiac and skeletal muscle adaptations to voluntary wheel running in the mouse. Journal of Applied Physiology 90:1900-1908.

Amis AA, Dowson D, Wright V. 1979a. Muscle strengths and musculo-skeletal geometry of the upper limb. Engineering in Medicine 8:41-48.

Amis AA, Dowson D, Wright V. 1979b. Elbow joint force predictions for some strenuous isometric actions. Biomechanics 13:765-775.

An KN, Hui FC, Morrey BF, Linscheid RL, Chao EY. 1981. Muscle across the elbow joint: a biomechanical analysis. Biomechanics 14:659-669.

Anapol FC, Barry K. 1996. Fiber architecture of the extensors of the hindlimb in the semiterrestrial and arboreal guenons. American Journal of Physical Anthropology 99:429-447.

Anapol F, Gray JP. 2003. Fiber architecture of the intrinsic muscles of the shoulder and arm in semiterrestrial and arboreal guenons. American Journal of Physical Anthropology 122:51-65.

Anapol FC, Jungers WL. 1986. Architectural and histochemical diversity within the quadriceps femoris of the brown lemur (*Lemur fulvus*). American Journal of Physical Anthropology 69:355-375.

Anderson JE, Lentz DL, Johnson RB. 1993. Recovery from disuse osteopenia coincident to restoration of muscle strength in Mdx mice. Bone 14:625-634.

Ankel-Simons F. 2007. Primate anatomy: an introduction. 3rd ed. Amsterdam: Academic Press. 724 p.

Antón SC. 1994. Masticatory muscle architecture and bone morphology in primates [dissertation]. Berkeley (CA): University of California. 334 p.

Antón SC. 1996. Tendon-associated bone features of the masticatory system in Neandertals. Journal of Human Evolution 31:391-408.

Antón SC. 1999. Macaque masseter muscle: internal architecture, fiber length and cross sectional area. International Journal of Primatology 20:441-462.

Antón SC. 2000. Macaque pterygoid muscles: internal architecture, fiber length, and cross-sectional area. International Journal of Primatology 21:131-156.

Ashton EH, Oxnard CE. 1962a. Locomotor patterns in primates. Proceedings of the Zoological Society of London 142:1-28.

Ashton EH, Oxnard CE. 1962b. Functional adaptations in the primate shoulder girdle. Proceedings of the Zoological Society of London 142:49-66.

Ashton EH, Oxnard CE. 1963. The musculature of the primate shoulder. The Transactions of the Zoological Society of London 29:552-650.

Asfour SS, Ayoub MM, Mital A. 1984. Effects of an endurance and strength training programme on lifting capability of males. Ergonomics 27:435-442.

Atzeva M, Demes B, Kirkbride ML, Burrows AM, Smith TD. 2007. Comparison of hind limb muscle mass in neonate and adult prosimian primates. Journal of Human Evolution 52:231-242.

Begun DR. 1992. Phylogenetic diversity and locomotion in primitive European hominids.

American Journal of Physical Anthropology 87:311-340.

Benjamin M, Evans EJ, Copp L. 1986. The histology of tendon attachments to bone in man. Journal of Anatomy 149:89-100.

Benjamin M, Kumai T, Milz S, Boszcyk BM, Boszcyk AA, Ralphs JR. 2002. The skeletal attachment of tendons – tendons 'entheses'. Comparative Biochemistry and Physiology Part A 133:931-945.

Benjamin M, Moriggl B, Brenner E, Emery P, McGonagle D, Redman S. 2004. The "enthesis organ" concept; why enthesopathies may not present as focal insertional disorders. Arthritis and Rheumatism 50:3306-3313.

Benjamin M, Ralphs JR. 1998. Fibrocartilage in tendons and ligaments - an adaptation to compressive load. Journal of Anatomy 193:481-494.

Benjamin M, Toumi H, Suzuki D, Redman S, Emery P, McGonagle D. 2007. Mircodamage and altered vascularity and the enthesis-bone interface provides an anatomic explanation for bone involvement in the HLA-B27 associated spondylarthritides and allied disorders. Arthritis and Rheumatism 56:224-233.

Bennett WF, Doherty N, Hallisey MJ, Fulkerson JP. 1993. Insertion orientation of terminal vastus lateralis obliquus and vastus medialis obliquus muscle fibers in human knees. Clinical Anatomy 6:129-134.

Benninghoff A, Rollhäuser H. 1952. Zur inneren Mechanik des gefiederten Musckels. Plfügers Archiv European Journal of Physiology 254:527-548.

Berringer OM, Browning FM, Schroeder CR.1978. An atlas and dissection manual of rhesus monkey anatomy. 3rd ed. Tallahassee (FL): Rose Printing Company Inc. 116 p.

Bertram JEA, Biewener AA. 1990. Differential scaling of long bones in the terrestrial Carnivora and other mammals. Journal of Morphology 204:157-169.

Bertram JEA, Swartz SM. 1991. The 'law of bone transformation': a case of crying Wolff? Biological Reviews 66:245-273.

Biewener AA. 1990. Biomechanics of mammalian terrestrial locomotion. Science 250:1097-1103.

Biewener AA. 1991. Musculoskeletal design in relation to body size. Journal of Biomechanics 24:19-29.

Biewener AA. 1992. *In vivo* measurement of bone strain and tendon force. In: Biewener AA, editor. Biomechanics - Structures and Systems: A Practical Approach. New York (NY): Oxford University Press. p 123-147

Biewener AA. 1998. Muscle-tendon stresses and elastic energy storage during locomotion in the

horse. Comparative Biochemistry and Physiology Part A 120:73-87.

Biewener AA. 2000. Future directions for the analysis of musculoskeletal design and locomotor performance. Journal of Morphology 252:38-51.

Biewener AA, Gills GB. 1999. Dynamics of muscle function during locomotion: accommodating variable conditions. Journal of Experimental Biology 202:3387-3396.

Botticelli R, Reggiani C. 2006. Skeletal muscle plasticity in health and disease: from genes to whole muscle. New York (NY): Springer. 376 p.

Bromage TG. 1991. Issues related to mineralized tissue biology in human evolutionary research. Journal of Human Evolution 6:165-174.

Bryant H, Seymour K. 1990. Observations and comments on the reliability of muscle reconstruction in fossil vertebrates. Journal of Morphology 206:109-117.

Burkholder TJ, Fingado B, Baron S, Lieber RL. 1994. Relationship between muscle fiber types and sizes and muscle architectural properties in the mouse hindlimb. Journal of Morphology 221:177-190.

Burkholder TJ, Lieber RL. 2001. Sarcomere length operating range of vertebrate muscles during movement. The Journal of Experimental Biology 204: 1529-1536.

Burr DB. 2002. Targeted and nontargeted remodelling. Bone 30:2-4.

Burr DB, Allen MR. 2013. Basic and Applied Bone Biology. London: Academic Press. 373 p.

Burr DB, Piotrowski G, Miller GJ. 1981. Structural strength of the macaque femur. American Journal of Physical Anthropology 30:781-786.

Burr DB, Robling AG, Turner CH. 2002. Effects of biomechanical stress in animals. Bone 30:781-786.

Burr DB, Ruff CB, Johnson C. 1989. Structural adaptations of the femur and humerus to arboreal and terrestrial environment in three species of macaque. American Journal of Physical Anthropology 79:357-367,.

Byron C, Kunz H, Matuszek H, Lewis S, Van Valkinburgh D. 2010. Rudimentary pedal grasping in mice and implications for terminal branch arboreal quadrupedalism. Journal of Morphology 272:230-240.

Caiozzo VJ. 2002. Plasticity of skeletal muscle phenotype: mechanical consequences. Muscle & Nerve 26:740-768.

Cardoso FA, Henderson CY. 2010. Enthesopathy formation in the humerus: data from known age-at-death and known occupation skeletal collections. American Journal of Physical Anthropology 141:550-560.

Carlson DS. 1983. Growth of the masseter muscle in rhesus monkeys (*Macaca mulatta*). American Journal of Physical Anthropology 60:401-410.

Carlson KJ. 2006. Muscle architecture of the common chimpanzee (*Pan troglodytes*): perspectives for investigating chimpanzee behavior. Primates 47:218-229.

Carlson KJ, Doran-Sheehy DM, Hunt KD, Nishida T, Yamanaka A, Boesch C. 2006. Locomotor behaviour and long bone morphology in individual free-ranging chimpanzees. Journal of Human Evolution 50:394-404.

Carlson KJ, Lublinsky S, Judex S. 2008. Do different locomotor modes during growth modulate trabecular architecture in the murine hind limb? Integrative and Comparative Biology 48:385-393.

Carry MR, Horan SE, Reed SM, Farrell RV. 1993. Structure, innervation, and age-related changes of mouse forearm muscles. The Anatomical Record 237:345-357.

Carter DS, Beaupré GS, 2001. Skeletal function and form: mechanobiology of skeletal development, aging, and regeneration. Cambridge: Cambridge University Press. 332 p.

Castanet J, Croci S, Aujard F, Perret M, Cubo J, de Margerie E. 2004. Lines of arrested growth in bone and age estimation in a small primate: *Microcebus murinus*. Journal of Zoology London 263:31-39.

Castanet J, Francillon-Vieillot H, Meunier FJ, de Ricqlès A. 1993. Bone and individual aging. In: Hall BK, editor. Bone. Boca Raton (FL): CRC Press Inc. p 245-284.

Cavagna GA, Heglund NC, Taylor R. 1977. Mechanical work in terrestrial locomotion: two basic mechanisms for minimizing energy expenditure. The American Journal of Physiology – Regulatory, Integrative and Comparative Physiology 233:243-261.

Chamay A, Tschantz P. 1972. Mechanical influences in bone remodelling. Experimental esearch on Wolff's law. Journal of Biomechanics 5:173-180.

Chatani K. 2003. Positional behaviour of free-ranging Japanese macaques (*Macaca fuscata*). Primates 44:12-23.

Chen X, Macica C, Nasiri A, Judex S, Broadus AE. 2007. Mechanical regulation of PTHrP expression in entheses. Bone41:752-759.

Cheng EJ, Scott SH. 2000. Morphometry of *Macaca mulatta* forelimb. I. Shoulder and elbow muscles and segment inertial parameters. Journal of Morphology 245:206-224.

Chiasson RB. 1975. Laboratory anatomy of the white rat. 3rd ed. Iowa : WM.C. Brown Company Publishers. 129 p.

Cho H. 2012. The histology laboratory and principles of microscope instrumentation. In:

Crowder C, Stout S, editors. Bone Histology: An Anthropological Perspective. Boca Raton (FL): Taylor & Francis Group, LLC. p 341-359.

Churchill SE, Morris AG. 1998. Muscle marking morphology and labour intensity in prehistoric Khoisan foragers. International Journal of Osteoarchaeology 8: 390-411.

Clarke KA, Still J. 1999. Gait analysis in the mouse. Physiology and Behavior 66:723-729.

Close RI. 1972. Dynamic properties of mammalian skeletal muscles. Physiological Review 52:129-197.

Cooper R, Misol S. 1970. Tendon and ligament insertion. Journal of Bone and Joint Surgery Part A 52:1-20.

Currey J. 1984. Comparative mechanical properties and histology of bone. American Zoologist 24:5-12.

Currey J. 2002. Bone: Structure and mechanism. New Jersey: Princeton University Press. 456 p.

D'Août K, Vereecke E, Schoonaert K, de Clercq D, Van Elsacker L, Aerts P. 2004. Locomotion in bonobos (*Pan paniscus*): differences and similarities between bipedal and quadrupedal terrestrial walking, and a comparison with other locomotor modes. Journal of Anatomy 204:353-361.

Davidson AG, Buford JA. 2006. Bilateral actions of the reticulospinal tract on arm and shoulder muscles in monkey: stimulus triggered averaging. Experimental Brain Research 173:25-39.

Davis CB, Shuler KA, Danforth ME, Hendron KE. 2013. Patterns of interobserver error in the scoring of entheseal changes. International Journal of Osteoarchaeology 23:147-151.

Davis DD. 1964. The giant panda. A morphological study of evolutionary mechanism. Fieldiana Zoology Memoirs 3:1-339.

de Ricqlès A, Meunier FJ, Castanet J, Francillon-Vieillot H. 1991. Comparative microstructure of bone. In: Hall BK, editor. Bone. Boca Raton (FL): CRC Press Inc. p 1-78.

Delson E, Terranova CJ, Jungers Wl, Sargis EJ, Jablonski NG, Dechow PC. 2000. Body mass in Cercopithecidae (Primates, Mammalia): Estimation and scaling in extinct and extant taxa. Anthropological Papers of the American Museum of Natural History 83:1-159.

Demes B, Stern JT Jr, Hausman MR, Larson SG, McLeod KJ, Rubin CT. 1998. Pattern of strain in the macaque ulna during functional activity. American Journal of Physical Anthropology 106:87-100.

Diederichsen LP, Norregaard J, Dyhre-Poulsen P, Winther A, Tufekovic G, Bandholm T, Rasmussen LR, Krogsgaarg M. 2007. The effect of handedness on electromyographic activity of human shoulder muscles during movement. Journal of Electromyography and Kinesiology 17:410-419.

Diogo R, Abdala V, Aziz MA, Lonergan N, Wood BA. 2009. From fish to modern humans – comparative anatomy, homologies and evolution of the pectoral and forelimb musculature. Journal of Anatomy 214:694-716.

Dörfl J. 1969. Vessels in the region of tendinous insertions. II Diaphysoperiosteal insertion. Folia Primatologica 17:70-82.

Dörfl J. 1980a. Migration of tendinous insertions. I. Cause and mechanism. Journal of Anatomy 131:179-195.

Dörfl J. 1980b. Migration of tendinous insertions. II. Experimental modifications. Journal of Anatomy 131:229-237.

Doschak MR, Zernicke RF. 2005. Structure, function and adaptation of bone-tendon and bone-ligament complexes. Journal of Musculoskeletal and Neuronal Interactions 5:35-40.

Drapeau M. 2008. Enthesis bilateral asymmetry in humans and African apes. HOMO Journal of Comparative Human Biology 59:93-109.

Dutour O. 1986. Enthesopathies (lesions of muscular insertions) as indicators of the activities of Neolithic Saharan populations. American Journal of Physical Anthropology 71:221-224.

Dysart PS, Harkness EM, Herbison GP. 1989. Growth of the humerus after denervation: an

experimental study in the rat. Journal of Anatomy 167:147-159.

Edman KAP. 2005. Contractile properties of mouse single muscle fibers, a comparison with amphibian muscle fibers. Journal of Experimental Biology 208:1905-1913.

Eliot DJ, Jungers WL. 2000. Fifth metatarsal morphology does not predict presence or absence of fibularis tertius muscle in hominids. Journal of Human Evolution 38:333-342.

Elkasrawy MN, Hamrick MW. 2010. Myostatin (GDF-8) as a key factor linking muscle mass and bone structure. Journal of Musculoskeletal and Neuronal Interactions 10:56-63.

Elliot DH. 1965. The growth of tendon after denervation or excision of its muscle. Proceedings of the Royal Society of London Series B, Biological Sciences 162:203-209.

Elliot DH, Crawford GNC. 1965. The thickness and collagen content of tendon relative to the cross-sectional area of muscle during growth. Proceedings of the Royal Society of London Series B, Biological Sciences 162:198-202.

Enlow DH. 1962. Functions of the Haversian system. American Journal of Anatomy 110:269 305.

Enlow DH. 1963. Principles of bone remodeling: an account of post-natal growth and remodeling processes in long bone and the mandible. Springfield (IL): Charles C. Thomas. 123p.

Enlow DH. 1976. The remodeling of bone. Yearbook of Physical Anthropology 20:19-34.

Enlow DH, Brown SO. 1956. A comparative histological study of fossil and recent bone tissues. Part I. The Texas Journal of Science 8:405-443.

Enlow DH, Brown SO. 1957. A comparative histological study of fossil and recent bone tissues. Part II. The Texas Journal of Science 9:186-214.

Enlow DH, Brown SO. 1958. A comparative histological study of fossil and recent bone tissues. Part III. The Texas Journal of Science 10:187-230.

Eshed V, Gopher A, Galili E, Israel H. 2004. Musculoskeletal stress markers in Natufian hunter gatherers and Neolithic farmers in the Levant: the upper limb. American Journal of Physical Anthropology 123:303-315.

Feik SA, Bruns TR, Clement JG. 2000. Regional variations in cortical modeling in the femoral mid-shaft: sex and age differences. American Journal of Physical Anthropology 112:191-205.

Felder A, Ward SR, Lieber RL. 2005. Sarcomere length measurement permits high resolution normalization of muscle fiber length in architectural studies. The Journal of Experimental Biology 208:3275-3279.

Fleagle JG. 1999. Primate adaptation and evolution, 2nd ed. San Diego (CA): Academic Press. 596 p.

Francillon-Vieillot H, de Buffrénil V, Castanet J, Géraudie, Meunier FJ, Sire JY, Zylberberg L, de Ricqlès A. 1990. Microstructure and mineralization of vertebrate skeletal tissues. In: Carter JG, editor. Skeletal Biomineralization: Patterns, Processes and Evolutionary Trends. New York (NY): Van Nostrand Reinhold. p 471-530.

Frankel VH, Nordin M. 2001. Biomechanics of bone. In Nordin M, Frankel VH, editors. Basic Biomechanics of the Musculoskeletal System. 3rd ed. Baltimore (MD): Lippincott Williams and Wilkins. p 26-59.

Fricke O, Schoenau E. 2006. Influence of mechanical signalling on bone development in children and adolescents. Current Opinion in Orthopaedics 17:443-450.

Fricke O, Schoenau E. 2007. The 'functional muscle-bone unit': probing the relevance of mechanical signals for bone development in children and adolescents. Growth and Hormone and IGF Research 17:1-9.

Frost HM. 1990. Skeletal structural adaptations to mechanical usage (SATMU): 2. Redefining Wolff's law: the remodeling problem. Anatomical Record 226: 414-422.

Galdikas BM. 1988. Orangutan diet, range and activity at Tanjung Puting, Central Borneo. International Journal of Primatology 9:1-35.

Gans C. 1982. Fiber architecture and muscle function. Exercise and Sport Science Review 10:160-207.

Gans C. 1988. Adaptation and form-function relation. American Zoologist 22:681-697.

Gans C, Brock WJ. 1965. The functional significance of muscle architecture – a theoretical analysis. Advances in Anatomy, Embryology and Cell Biology 38:115-142.

Gans C, de Vree F. 1987. Functional bases of fiber length and angulation in muscle. Journal of Morphology 192:63-85.

Gans C, Gaunt AS. 1991. Muscle architecture in relation to function. Journal of Biomechanics 24:53-65.

Gibbs S, Collard M, Wood B. 2002. Sot-tissue anatomy of the extant hominoids: a review and phylogenetic analysis. Journal of Anatomy 200:3-49.

Gillies AR, Lieber RL. 2011. Structure and function of the skeletal muscle extracellular matrix. Muscle Nerve 44:318-331.

Gokhin DS, Ward SR, Bremmer SN, Lieber RL. 2008. Quantitative analysis of neonatal skeletal muscle functional improvement in the mouse. The Journal of Experimental Biology 211:837-843.

Goldman HM, Kindsvater J, Bromage TG. 1998. Correlative light and backscattered electron microscopy of bone – Part I: Specimen preparation methods. Scanning 21:40-43.

Goldman HM, McFarlin SC, Cooper DML, Thomas CDL, Clement JG. 2009. Ontogenetic patterning of cortical bone microstructure and geometry at the human mid-shaft femur. The Anatomical Record 292:48-64.

Goldspink G. 1968. Sarcomere length during post-natal growth of mammalian muscle fibres. Journal of Cell Science 3:539-548.

Gordon AM, Huxley AF, Julian FJ. 1966. The variation in isometric tension with sarcomere length in vertebrate muscle fibers. The Journal of Physiology 184:170-192.

Goulding D, Bullard B, Gautel M. 1997. A survey of *in situ* sarcomere extension in mouse skeletal muscle. Journal of Muscle Research and Cell Motility 18:465-472.

Grand TI. 1977. Body weight: its relation to tissue composition, segment distribution, and motor function. American Journal of Physical Anthropology 47:211-240.

Green DJ. 2010. Shoulder functional anatomy and development: implications for interpreting early hominin locomotion [dissertation]. Washington (DC): The George Washington University. 377 p.

Green DJ, Hamrick MW, Richmond BG. 2011. The effects of hypermuscularity on shoulder morphology in myostatin-deficient mice. Journal of Anatomy 218:544-557.

Green DJ, Richmond BG, Miran SL. 2012. Mouse shoulder morphology responds to locomotor activity and kinematic differences in climbing and running. Journal of Experimental Zoology 318:621-638.

Greene EC. 1935. Anatomy of the rat. New Jersey: Prentice Hall. 370 p.

Gurkan UA, Akkus O. 2008. The mechanical environment of bone marrow: a review. Annals of Biomedical Engineering 36:1978-1991.

Hamrick MW, Ding K-H, Pennington C, Chao YJ, Wu Y-D, Howard B, Immel D, Borlongan C, McNeil PL, Bollag WB, Curl WW, Yu J, Isales CM. 2006a. Age-related loss of muscle mass and bone strength in mice is associated with a decline in physical activity and serum leptin. Bone 39:845-853.

Hamrick MW, McNeil PL, Patterson SL. 2010. Role of muscle-derived growth factors in bone formation. Journal of Musculoskeletal and Neuronal Interactions 10:64-70.

Hamrick MW, McPherron AC, Lovejoy CO. 2002. Bone mineral content and density in the humerus of adult myostatin-deficient mice. Calcified Tissue International 71:63-68.

Hamrick MW, McPherron AC, Lovejoy CO, Hudson J. 2000. Femoral morphology and cross

sectional geometry of adult myostatin-deficient mice. Bone 27:343-349.

Hamrick MW, Samaddar T, Pennington C, McCormick J. 2006b. Increased muscle mass with myostatin deficiency improves gains in bone strength with exercise. Journal of Bone and Mineral Research 21:477-483.

Hamrick MW, Skedros JG, Pennington C, McNeil PL. 2006c. Increased osteogenic response to exercise in metaphyseal versus diaphyseal cortical bone. Journal of Musculoskeletal and Neuronal Interactions 6:258-263.

Hansen P, Aagaard P, Kjaer M, Larsson B, Magnusson SP. 2003. Effect of habitual running on human Achilles tendon load-deformation properties and cross-sectional area. Journal of Applied Physiology 95:2375-2380.

Harber MP, Konopka AR, Undem MK, Hinkley JM, Minchev K, Kaminsky LA, Trappe TA, Trappe S. 2012. Aerobic exercise training induces skeletal muscle hypertrophy and age-dependent adaptations in myofiber function in young and older men. Journal of Applied Physiology 113:1495-1504.

Harrington L. 2010. Ontogeny of postcranial robusticity among Holocene hunter-gatherers of southernmost Africa [dissertation]. Toronto (Canada): University of Toronto. 142 p.

Havelková P, Hladík M, Velemínský P. 2013. Entheseal changes: do they reflect socioeconomic

status in the early medieval central European population? (Mikulčice – Kláteřisko, Great Moravian Empire, 9th-10th century). International Journal of Osteoarchaeology 23:237-251.

Havelková P, Vilotte S, Velemínský P, Polácek L, Dobisíková M. 2011. Enthesopathies and activity patterns in the Early Medieval Great Moravian population: evidence of division of labour. International Journal of Osteoarchaeology 21:487-504.

Hawkey DE. 1998 Disability, compassion and the skeletal record: using musculoskeletal stress markers (MSM) to construct an osteobiography from early New Mexico. International Journal of Osteoarchaeology 8:326-340.

Hawkey, DE, Merbs CF. 1995. Activity induced musculoskeletal stress markers (MSM) and subsistence strategy changes among ancient Hudson Bay Eskimos. International Journal of Osteoarchaeology 5:324-338.

Hedgecock NL, Hadi T, Chen AA, Curtiss SB, Martin RB, Hazelwood SJ. 2007. Quantitative regional associations between remodeling, modeling, and osteocyte apoptosis and density in rabbit tibial midshaft. Bone 40: 627-637.

Hegarty PHJ, Hooper AC. 1971. Sarcomere length and fiber diameter distributions in four different mouse skeletal muscles. Journal of Anatomy 110:249-257.

Hems T, Tillmann B. 2000. Tendon entheses of the human masticatory muscles. Anatomical

Embryology 202:201-208.

Henderson CY, Craps DD, Caffell AC, Millard AR, Gowland R. 2013a. Occupational mobility in the 19th century rural England: the interpretation of entheseal changes. International Journal of Osteoarchaeology 23:197-210.

Henderson CY, Mariotti V, Pany-Kucera D, Villotte S, Wilczak C. 2013b. Recording specific entheseal changes of fibrocartilaginous entheses: initial tests using Coimbra method. International Journal of Osteoarchaeology 23:152-162.

Hieronymus TL. 2006. Quantitative microanatomy of jaw muscle attachment in extant Diapsids. Journal of Morphology 267:954-967.

Higham TE, Biewener AA. 2011. Functional and architectural complexity within and between muscles: regional variation and intermuscular force transmission. Philosophical Transaction of the Royal Society B: Biological Sciences 366:1477-1487.

Hill AV. 1953. The mechanics of active muscle. Proceedings of the Royal Society of London Series B, Biological Sciences 141:104-117.

Holzbaur KRS, Delp SL, Gold GE, Murray WM. 2007a. Moment-generating capacity of upper limb muscles in healthy adults. Journal of Biomechanics 40:2442-2449.

Holzbaur KRS, Murray WM, Gold GE, Delp SL. 2007b. Upper limb muscle volumes in adult

subjects. Journal of Biomechanics 40:742-749.

Hoyte DAN, Enlow DH. 1966. Wolff's law and the problem of muscle attachment on resorptive surfaces of bone. American Journal of Physical Anthropology 24:205-214.

Hunt KD, Cant JG, Gebo DL, Rose MD, Walker SE, Youlatos D. 1996. Standardized descriptions of primate locomotor and postural modes. Primates 37:363-387.

Hurov JR. 1986. Soft-tissue bone interface: how do attachments of muscles, tendons, and ligaments change during growth? Journal of Morphology 189:313-325.

Huiskes R. 1982. On meodelling long bones in structural analyses. Journal of Biomechanics 15:65-69.

Huiskes R, van Rietbergen B. 2005. Biomechanics of bone. In: Mow VC, Huiskes R, editors. Basic Orthopaedic Biomechanics and Mechano-biology. Philadelphia (PA): Lippincott Williams & Wilkins. p 123-179.

Huxley HE. 1972. Molecular basis of contraction in cross-striated muscles. In: GH Bourne, editor. The Structure and Function of Muscle, 2nd ed. New York (NY): Academy Press, p 301-387.

Ishihara A, Roy BB, Ohira Y, Ibata Y, Edgerton VR. 1998. Hypertrophy of rat plantaris muscle

fibres after voluntary running with increasing loads. Journal of Applied Physiology 84:2183-2189.

Isler K, Payne RC, Günther MM, Thorpe SKS, Li, Y, Savage R, Crompton RH. 2006. Inertial properties of hominoid limb segments. Journal of Anatomy 209:201-218.

Jaworski ZFG, Liskova-Kiar M, Uhthoff HK. 1980. Effect of long term immobilisation on the pattern of bone loss in older dogs. The Journal of Bone and Joint Surgery 62:104-110

Jouffroy FK, Médina MF. 1996. Developmental changes in the fibre composition of elbow, knee, and ankle extensor muscles in Cercopithecoid monkeys. Folia Primatologica 66:55-67.

Jouffroy FK, Stern JT Jr, Médina MF. 1998. Function and cytochemical characteristics of postural limb muscles of the rhesus monkey: a telemetered EMG and immunofluorescence study. Folia Primatologica 70:235-253.

Jungers WL, Stern JT Jr. 1980. Telemetered electromyography of forelimb muscle chains in gibbons (*Hylobates lar*). Science 208:617-619.

Jungers WL, Stern JT Jr. 1981. Preliminary electromyographical analysis of brachiation in gibbon and spider monkey. International Journal of Primatology 2:19-33.

Jurmain R, Cardoso FA, Henderson C, Villotte S. 2012. Bioarchaeology's Holy Grail: The

reconstruction of activity. In: Grauer AL, editor. A companion to paleopathology. Massachusetts: Wiley-Blackwell. p 531-552.

Jurmain R, Villotte S. 2010. Terminology – Entheses in medical literature: a brief review. *In* Workshop in Musculoskeletal Stress Markers (MSM): Limitations and Achievements in the Reconstruction of Past Activity Patterns. University of Coimbra July 2-3, 2009. Available from http://uc.pt/en/cia/msm/MSM_teminology3.

Kennedy KAR. 1989. Skeletal markers of occupational stress. In Iscan MY, Kennedy KAR, editors. Reconstruction of life from the skeleton. New York (NY): Wiley-Liss. p. 129-160

Kelley G. 1996. Mechanical overload and skeletal muscle fiber hyperplasia: a meta-analysis. Journal of Applied Physiology 81:1584-1588.

Kilborn SH, Trudel G, Uhthoff H. 2002. Review of growth plate closure compared with age and sexual maturity and lifespan in laboratory animal. Journal of American Association for Laboratory Animal Science 41:21-26.

Kiliaridis S. 1989. Muscle function as a determinant of mandibular growth in normal and hypocalcaemic rat. European Journal of Orthodontics 11:298-308.

Kimes KR, Siegel MI, Sadler DL. 1981. Alteration of scapular morphology through experimental behavioural modification in the laboratory mouse (*Mus musculus*). Acta Anatomica: 109:161-165.

Kimura K, Takai S. 1970. On the musculature of the forelimb of the crab-eating monkey. Primates 11:145-170.

Knüsel, C. 2000. Bone adaptation and its relationship to physical activity in the past. In: Cox M, Mays S, editors. Human Osteology in Archaeology and Forensic Science. London: Greenwich Medical Media Limited. p 381-402.

Kunimatsu Y, Nakastukasa M, Sawada Y, Sakai T, Hyodo M, Hyodo H, Itaya T, Nakaya H, Saegusa H, Mazurier A, Saneyoshi M, Tsujikawa H, Yanamoto A, Mbua E. 2007. A new Late Miocene great ape from Kenya and its implications for the origins of African great apes and humans. Proceedings for the National Academy of Sciences 104:19220-19225.

Kurtzer I, Pruszynski AJ, Herter TM, Scott SH. 2006. Primate upper limb muscles exhibit activity patterns that differ from their anatomical action during postural task. Journal of Neurophysiology 95:493-504.

Langenderfer JE, Jerabek SA, Thangamani VB, Kuhn JE, Hughes RE. 2004. Musculoskeletal parameters of muscles crossing the shoulder and elbow and the effect of sarcomere length sample size on estimation of optimal muscle length. Clinical Biomechanics 19:664-670.

Langenderfer JE, Pattanacharoenphon C, Carpenter JE, Hughes RE. 2006. Variability in isometric force and moment generating capacity of glenohumeral external rotator muscles. Clinical Biomechanics 21:701-709.

Laros GS, Tipton CM, Cooper RR. 1971. Influence of physical activity on ligament insertions in the knees of dogs. The Journal of Bone and Joint Surgery 53A:273-286.

Larson SG. 1993. Functional morphology of the shoulder in primates. In: Gebo DL, editor. Postcranial Adaptation in Nonhuman Primates. Dekalb (IL): Northern Illinois University Press. p 45-69.

Larson SG. 1995. New characters for the functional interpretation of primate scapulae and proximal humeri. American Journal of Physical Anthropology 98:13-35.

Larson SG. 1996. Estimating humeral torsion on incomplete fossil anthropoid humeri. Journal of Human Evolution 31:239-257.

Larson SG. 1998. Parallel evolution of the hominoid trunk and forelimb. Evolutionary Anthropology 6:87-99.

Larson SG, Schmitt D, Lemelin P, Hamrick MW. 2000. Uniqueness of primate forelimb posture during quadrupedal locomotion. American Journal of Physical Anthropology 112:87-101.

Larson SG, Schmitt D, Lemelin P, Hamrick MW. 2001. Limb excursion during quadrupedal walking: how primates compare to other mammals? Journal of Zoology London 255:353-365.

Larson SG, Stern JT Jr. 1986. EMG of scapulohumeral muscles in the chimpanzee during reaching and arboreal locomotion. The American Journal of Anatomy 176:171-190.

Larson SG, Stern JT Jr. 1989. The role of propulsive muscles of the shoulder during quadrupedalism in vervet monkeys (*Cercopithecus aethiops*): implications for neural control of locomotion in primates. Journal of Motor Behavior 21:457-472.

Larson SG, Stern JT Jr. 1991. EMG of serratus anterior and trapezius in the chimpanzee: scapular rotators revisited. American Journal of Physical Anthropology 85:71-84.

Larson SG, Stern JT Jr. 1992. Further evidence for the role of supraspinatus in quadrupedal monkeys. American Journal of Physical Anthropology 87:359-363.

Larson SG, Stern JT Jr. 2006. Maintenance of above-branch balance during primate arboreal quadrupedalism: coordinated use of forearm rotators and tail motion. American Journal of Physical Anthropology 129:71-81.

Larson SG, Stern JT Jr. 2007. Humeral retractor EMG during quadrupedal walking in primates. The Journal of Experimental Biology 210:1204-1215.

Lee KCL, Maxwell A, Lanyon LE. 2002. Validation of a technique for studying functional adaptation of the mouse ulna in response to mechanical loading. Bone 31:1-9.

Lemelin P. 1995. Comparative and functional myology of the prehensile tail in New World

monkeys. Journal of Morphology 224:351-368.

Lieber RL. 2002. Skeletal muscle structure, function, and plasticity. 2nd ed. Baltimore (MD): Lippincott Williams & Wilkins. 369 p.

Lieber RL, Brown CG. 1992. Quantitative method for comparison of skeletal muscle architectural properties. Journal of Biomechanics 25:557-560.

Lieber RL, Fridén J. 2000. Functional and clinical significance of skeletal muscle architecture. Muscle Nerve 23:1647-1666.

Lieber RL, Loren GJ, Fridén J. 1994. In vivo measurement of human wrist extensor muscle sarcomere length changes. Journal of Neurophysiology 71: 874-881.

Lieber RL, Ward SR. 2011. Skeletal muscle design to meet functional demands. Philosophical Transactions of the Royal Society B: Biological Sciences 366:1466-1476.

Lieberman, DE, Crompton AW. 1998. Responses of bone to stress: constraints on symmorphosis. In: Weibel ER, Taylor CR, Bolis L, editors. Principles of Animal Design: The Optimization and Symmorphosis Debate. Cambridge: Cambridge University Press. p 78-86.

Lieberman DE, Polk JD, Demes B. 2004. Predicting long bone loading from cross-sectional geometry. American Journal of Physical Anthropology 123:156-171.

Lorenz T, Campello M. 2001. Biomechanics of skeletal muscle. In Nordin M, Frankel VH, editors. Basic Biomechanics of the Musculoskeletal System. 3rd ed. Baltimore (MD): Lippincott Williams and Wilkins. p 148-171.

Madar SI, Rose MD, Kelley J, MacLatchy L, Pilbeam D. 2002. New *Sivapithecus* postcranial specimens from Siwaliks of Pakistan. Journal of Human Evolution 42:705-752.

Maggiano CM. 2012. Making the mold: a microstructural perspective on bone modeling during growth and mechanical adaptation. In: Crowder C, Stout S, editors. Bone Histology: An Anthropological Perspective. Boca Raton (FL): Taylor & Francis Group, LLC. p. 45-90.

Marini M, Veicsteinas A. 2010 The exercised skeletal muscle: a review. European Journal Translational Myology – Myology Reviews 20:105-120.

Mariotti V, Facchini F, Belcastro MG. 2004. Enthesopathies – proposal of standardized scoring method and applications. Collegium Anthropologicum 28:145-159.

Mariotti V, Facchini F, Belcastro MG. 2007. The study of entheses: proposal of a standardised scoring method for twenty-three entheses of the postcranial skeleton. Collegium Anthropologium 31:291-313.

Martin RB. 2000. Toward a unifying theory on bone remodeling. Bone 26:1-6.

Martin RB. 2007. Fatigue failure and skeletal evolution. International Journal of Fatigue 29:1019-1023.

Martin RB, Burr DB, Sharkey NA. 1998. Skeletal tissue mechanics. New York (NY): Springer-Verlag Inc. 392 p.

Marzke MW, Shrewsbury MM. 2006. The *Oreopithecus* thumb: pitfalls in reconstructing muscle and ligament attachments from fossil bones. Journal of Human Evolution 51:213-215.

Marzke MW, Shrewsbury MM, Horner KE. 2007. Middle phalanx skeletal morphology in the hand: can it predict flexor tendon size and attachments? American Journal of Physical Anthropology 134:141-151.

Mathewson MA, Chapman MA, Hentzen ER, Fridén J, Lieber RL. 2012. Anatomical, architectural, and biomechanical diversity of the murine forelimb muscles. Journal of Anatomy 221:443-451.

McFarlin SC. 2006. Ontogenetic variation in long bone microstructure in catarrhines and its significance for life history research [dissertation]. New York (NY): The City University of New York. 687 p.

McFarlin SC, Terranova CJ, Zihlman AL, Enlow DH, Bromage TG. 2008. Regional variability

in secondary remodeling within long bone cortices of catarrhine primates: the influence of bone growth history. Journal of Anatomy 213:308-324.

McGowan C. 1979. The hind limb musculature of the brown kiwi, *Apteryx australis mantelli*. Journal of Morphology 160:22-73.

Medler S. 2002. Comparative trends in shortening velocity and force production in skeletal muscles. The American Journal of Physiology – Regulatory, Integrative and Comparative Physiology 238:368-378.

Mendez RA, Keys A. 1960. Density and composition of mammalian muscle. Metabolism Clinical and Experimental 9:184-188.

Menuki K, Mori T, Sakai A, Sakuma M, Okimoto N, Shimizu Y, Kunugita N, Nakamura T. 2008. Climbing exercise enhances osteoblast differentiation and inhibits adipogenic differentiation with high expression of PTH/PTHrP receptor in bone marrow cells. Bone 43:613-620.

Meyers C, Nicklish N, Held P, Fritsch B, Alt KW. 2011. Tracing patterns of activity in the human skeleton: an overview of methods, problems, and limits to interpretations. HOMO Journal of Comparative Human Biology 62:202-217.

Michilsens F, Vereecke EE, D'Août K, Aerts P. 2009. Functional anatomy of the gibbon forelimb: adaptations to a brachiating lifestyle. Journal of Anatomy 215:335-354.

Michilsens F, Vereecke EE, D'Août K, Aerts P. 2010. Muscle moment arms and function of the siamang forelimb during brachiation. Journal of Anatomy 217:521-535.

Miller, RA. 1932. Evolution of the pectoral girdle and forelimb in the primates. American Journal of Physical Anthropology 17: 1-56.

Molnar P. 2006. Tracing prehistoric activities: musculoskeletal stress marker analysis of a Stone-Age population on the island of Gotland in the Baltic Sea. American Journal of Physical Anthropology 129:12-23.

Molnar P. 2010. Patterns of physical activity and material culture on Gotland, Sweden, during the Middle Neolithic. International Journal of Osteoarchaeology 20:1-14.

Molnar P, Ahlstrom TP, Leden I. 2011. Osteoarthritis and activity – an analysis of the relationship between eburnation, musculoskeletal stress markers (MSM) and age in two Neolithic hunter-gatherer populations from Gotland, Sweden. International Journal of Osteoarchaeology 21:283-291.

Montgomery E, Pennington C, Isales CM, Hamrick MH. 2005. Muscle-bone interactions in drystrophin-deficient and myostatin-deficient mice. The Anatomical Record 286A:814-822.

Moore KL, Agur AMR. 2007. Essential clinical anatomy. 3rd ed. Baltimore (MD): Lippincott

Williams and Wilkins. 692 p.

Mori T, Okimoto N, Sakai A, Okazaki, Nakura N, Notomi T, Nakamura T. 2003. Climbing exercise increase bone mass and trabecular bone turnover through transient regulation of marrow osteogenic and osteoclastogenic potentials in mice. Journal of Bone and Mineral Research 18:2002-

Mulh ZF. 1982. Active length-tension relation and the effect of muscle pinnation on fiber lengthening. Journal of Morphology 173:285-292.

Mulhern DM, Ubelaker DH. 2012. Differentiating human from nonhuman bone microstructure. In: Crowder C, Stout S, editors. Bone Histology: An Anthropological Perspective. Boca Raton (FL): Taylor & Francis Group, LLC. p 109-134.

Murphy RA, Beardsley AC. 1974. Mechanical properties of the cat soleus muscle in situ. American Journal of Physical Anthropology 227:1008-1013.

Nawata K, Minamizaki T, Yamashita Y, Teshima R. 2002. Development of the attachment zones in the rat anterior cruciate ligament: changes in the distributions of proliferating cells and fibrillar collagens during postnatal growth. Journal of Orthopaedic Research 20:1339-1344.

Newell-Morris L, Sirianni JE. 1982. Parameters of bone growth in the fetal and infant macaque

(*Macaca nemestrina*) humerus as documented by trichromatic bone labels. In: Dixon AD, Sarnat BG, editors. Factors and Mechanisms Influencing Bone Growth. New York (NY): Alan R. Liss Inc. p. 243-258.

Niinimäki S. 2011. What do muscle marker ruggedness scores actually tell us? International Journal of Osteoarchaeology 21:292-299.

Niinimäki S, Sotos LB. 2013. The relationship between intensity of physical activity and entheseal changes on the lower limb. International Journal of Osteoarchaeology 23:221-228.

Nolte MLS, Wilczak C. 2013. Three-dimensional surface area of the biceps enthesis, relationship to body size, sex, age, and secular changes in a 20th century American sample. International Journal of Osteoarchaeology 23:163-174.

Notomi T, Okimoto N, Okazaki Y, Tanaka Y, Nakamura T, Suzuki M. 2001. Effect of tower climbing exercise on bone mass, strength, and turnover in growing rats. Jounral of Bone and Mineral Research 16:166-174

Ogihara N, Kumai T, Nakatsukasa M. 2005. Muscle dimensions in the chimpanzee hand. Primates 46:275-280.

Oishi M, Ogihara N, Endo H, Asari M. 2008. Muscle architecture of the upper limb in the orangutan. Primates 49:204-209.

Oishi M, Ogihara N, Endo H, Ichihara N, Asari M. 2009. Dimensions of the forelimb muscles in orangutans and chimpanzees. Journal of Anatomy 215:373-382.

Oizumi N, Tadano S, Narita Y, Suenaga N, Iwasaki N, Minami A. 2006. Numerical analysis of cooperative abduction muscle forces in a human shoulder joint. Journal of Shoulder and Elbow Surgery 15:331-338.

O'Neill MC, Ruff CB. 2004. Estimating human long bone cross-sectional geometric properties: a comparison of noninvasive methods. Journal of Human Evolution 47:221-235.

Organ JM. 2007. The functional anatomy of prehensile and nonprehensile tails of the Platyrrhini (Primates) and Procyonidae (Carnivora) [dissertation]. Baltimore (MD): Johns Hopkins University. 361 p.

Organ JM, Teaford MF, Taylor AB. 2009. Functional correlates of fiber architecture of the lateral caudal musculature in the prehensile and nonprehensile tails of the Platyrrhini (Primates) and Procyonidae (Carnivora). The Anatomical Record 292:827-841.

Oxnard CE. 1963. Locomotor adaptations in the primate forelimb. Symposia of the Zoological Society of London 10:165-182.

Oxnard CE. 1967. The functional morphology of the primate shoulder as revealed by

comparative anatomical osteometric and discriminant function techniques. American Journal of Physical Anthropology 26:219-240.

Ozcivici E, Luu YK, Adler B, Qin Y-X, Rubin J, Judex S, Rubin CT. 2010. Mechanical signals as anabolic agents in bone. Nature Reviews Rheumatology 6:50-59.

Parfitt AM. 1994. Osteonal and hemi-osteonal remodelling: the spatial and temporal framework for signal traffic in adult human bone. Journal of Cellular Biochemistry 55:273-286.

Parfitt AM. 2004. The attainment of peak bone mass: what is the relationship between muscle growth and bone growth? Bone 34: 767-770.

Payne RC, Crompton RH, Isler K, Savage R, Vereecke EE, Günther MM, Thorpe SKS, D'Août K. 2006a. Morphological analysis of the hindlimb in apes and humans I. Muscle architecture. Journal of Anatomy 208:709-724.

Payne RC, Crompton RH, Isler K, Savage R, Vereecke EE, Günther MM, Thorpe SKS, D'Août K. 2006b. Morphological analysis of the hindlimb in apes and humans II. Moment arms. Journal of Anatomy 208:725-742.

Pearson OM, Lieberman DE. 2004. The aging of Wolff's "law": ontogeny and responses to mechanical loading in cortical bone. Yearbook of Physical Anthropology 47:63-99.

Pfeiffer S, Crowder C, Harrington L, Brown M. 2006. Secondary osteon and haversian canal

dimensions as behavioral indicators. American Journal of Physical Anthropology 131: 460-468.

Pfeiffer S, Lazenby R, Chiang J. 1996. Brief communication: cortical remodeling data are affected by sampling location. American Journal of Physical Anthropology 96: 89-92.

Pfeiffer S, Zehr MK. 1996. A morphological and histological study of the human humerus from Border Cave. Journal of Human Evolution 31: 49-59.

Pilbeam D, Rose MD, Barry JC, Shah SMI. 1990. New *Sivapithecus* humeri from Pakistan and the relationship of *Sivapithecus* and *Pongo*. Nature 348:237-239.

Plochocki JH. 2009. Mechanically-induced osteogenesis in the cortical bone of pre- to peripubertal stage and peri- to postpubertal stage mice. Journal of Orthopaedic Surgery and Research 4:22.

Plochocki JH, Rivera JP, Zhang C, Ebba SA. 2008. Bone modeling response to voluntary exercise in the hindlimb of mice. Journal of Mophology 269:313-318.

Powell PL, Roy RR, Kanim P, Bello M, Edgerton VR. 1984. Predictability of skeletal tension from architectural determinations in guinea pig hindlimbs. Journal of Applied Physiology 57:1715-1721.

Puetzer J, Williams J, Gillies A, Bernacki S, Loboa EG. 2013. The effects of cyclic hydrostatic

pressure on chondrogenesis and viability of human adipose- and bone marrow-derived mesenchymal stem cells in three-dimentional agarose contructs. Tissue Engineering Part A 19:299-306.

Rauch F, Travers R, Glorieux FH. 2007. Intracortical remodeling during human bone development - a histomorphometric study. Bone 40:274-280.

Ravosa MJ, López EK, Menegaz RA, Stock SR, Stack MS, Hamrick MW. 2008. Using "mighty mouse" to understand masticatory plasticity: myostatin-deficient mice and musculoskeletal function. Integrative and Comparative Biology 48:345-359.

Reid DC, Oedekove G, Kramer JF, Saboe LA. 1989. Isokinetic muscle strength parameters for shoulder movements. Clinical Biomechanics 4:97-104.

Robb J. 1998. The interpretation of skeletal muscle sites: a statistical approach. International Journal of Osteoarchaeology 8:363-377.

Roberts TJ. 2002. The integrated function of muscles and tendons during locomotion. Comparative Biochemistry and Physiology Part A 133:1087-1099.

Robling AG. 2009. Is bone's response to mechanical signals dominated by muscle forces? Medicine and Science in Sports and Exercise 41:2044-2049.

Robling AG, Castillo AB, Turner CH. 2006 Biomechanical and molecular regulation of bone

remodelling. Annual Review of Biomedical Engineering 8:455-498.

Robling AG, Hinant FM, Burr DB, Turner CH. 2002. Improved bone structure and strength after long term mechanical loading is greatest if loading is separated into short bouts. Journal of Bone and Mineral Research 17:1545-1554.

Robling AG, Stout SD. 1999. Morphology of the drifting osteon. Cell Tissues Organs 164:192 204.

Rose MD. 1988. Another look at the anthropoid elbow. Journal of Human Evolution 17:193 224.

Rose MD. 1993. Functional morphology of the elbow and forearm in primates. In: Gebo DL, editor. Postcranial Adaptation in Nonhuman Primates. Dekalb (IL): Northern Illinois University Press. p 70-95.

Rose MD. 1994. Quadrupedalism in some Miocene catarrhines. Journal of Human Evolution 26:387-411.

Rowe N. 1996. The pictorial guide to living primates. Charlestown (SC): Pogonias Press. 263 p.

Rubin CT, Lanyon LE. 1982. Limb mechanics as a function of speed and gait: a study of functional strains in the radius and tibia of horse and dog. Journal of Experimental Biology 101:187-211.

Ruff CB. 2000. Biomechanical analyses of archaeological human skeletons. In: Katzenberg MA, Saunders SR, editors. Biological Anthropology of the Human Skeleton. New York (NY): Wiley Liss Inc. p 71-102.

Ruff CB. 2002. Long bone articular and diaphyseal structure in Old World monkeys and apes. I: locomotor effects. American Journal of Physical Anthropology 119:305-342.

Ruff CB. 2003. Long bone articular and diaphyseal structure in Old World monkeys and apes. II: estimation of body mass. American Journal of Physical Anthropology 120:16-37.

Ruff CB, Hayes WC. 1983. Cross-sectional geometry of Pecos Pueblo femora and tibiae – a biomechanical investigation: I. Method and general patterns of variation. American Journal of Physical Anthropology 60:359-381.

Salmons S, Henriksson J. 1981. The adaptive response of skeletal muscle to increased use. Muscle Nerve 4:94-105.

Scheuer L, Black S. 2000. Developmental juvenile osteology. San Diego: Academic Press. 587p.

Schlecht SH. 2012a. A histomorphometric analysis of muscular insertion regions: understanding enthesis etiology [dissertation]. Columbus (OH): The Ohio State University. 178 p.

Schlecht SH. 2012b. Understanding entheses: bridging the gap between clinical and anthropological perspectives. The Anatomical Record 295:1239-1251.

Schmidt M, Schilling N. 2007. Fibre type distribution in the shoulder muscles of the tree shrew, the cotton-top tamarin, and the squirrel monkey related to shoulder movements and forelimb loading. Journal of Human Evolution 52:401-419.

Schmitt D, Zumwalt AC, Hamrick MW. 2010. The relationship between bone mechanical properties and ground reaction forces in normal and hypermuscular mice. Journal of Experimental Zoology 313A:339-351.

Schoenau E, Fricke O. 2008. Mechanical influences on bone development in children. European Journal of Endocrinology 159:S27-S31.

Schoenau E, Neu CM, Beck B, Manz F, Rauch F. 2002. Bone mineral content per muscle cross sectional area as an index of the functional muscle-bone unit. Journal of Bone and Mineral Research 17:1095-1101.

Schoenau E, Neu CM, Mokov E, Wassmer G, Manz F. 2000. Influence of puberty on muscle area and cortical bone area of the forearm in boys and girls. Journal of Clinical Endocrinology and Metabolism 85:1095-1098.

Schultz AH. 1942. Morphological observations on a gorilla and an orang of closely known ages. American Journal of Physical Anthropology 39:1-21.

Schultz AH. 1962. The relative weights of the skeletal parts in adult primates. American Journal of Physical Anthropology 20:1-10.

Shaw CN, Ryan TM. 2012. Does skeletal anatomy reflect adaptation to locomotor patterns? Cortical and trabecular architecture in human and nonhuman anthropoids. American Journal of Physical Anthropology 147:187:200.

Shaw CN, Stock JT. 2009a. Intensity, repetitiveness, and directionality of habitual adolescent mobility patterns influence the tibial diaphysis morphology of athletes. American Journal of Physical Anthropology 140:149-159.

Shaw CN, Stock JT. 2009b. Habitual throwing and swimming correspond with upper limb diaphyseal strength and shape in modern human athletes. American Journal of Physical Anthropology 140:160-172.

Shaw CN, Stock JT. 2011. The influence of body proportions on femoral and tibial midshaft shape in hunter-gatherers. American Journal of Physical Anthropology 144:22-29.

Shaw HM, Vázquez OT, McGonagle D, Bydder G, Santer RM, Benjamin M. 2008. Development of the human Achilles tendon enthesis organ. Journal of Anatomy 213:718-724.

Skedros JG. 2012. Interpreting load history in limb-bone diaphyses: important

considerations and their biomechanical foundations. In: Crowder C, Stout S, editors. Bone Histology: An Anthropological Perspective. Boca Raton (FL): Taylor & Francis Group, LLC. p 153-220.

Smith RJ, Jungers WL. 1997. Body mass in comparative primatology. Journal of Human Evolution 32:523-559.

Smith NC, Wilson AM, Jespers KJ, Payne RC. 2006. Muscle architecture and functional anatomy of the pelvic limb of the ostrich (*Struthio camelus*). Journal of Anatomy 209:265-279.

Sokal RR, Rohlf FJ. 2012. Biometry: the principles and practice of statistics in biological research. 4th ed. New York (NY): W.H. Freeman and Company. 937 p.

Stern JT Jr. 1971. Functional myology of the hip and thigh of cebid monkeys and its implications for the evolution of erect posture. Basel: S. Karger. 318 p.

Stern JT Jr, Larson SG. 2001. Telemetered electromyography of the supinators and pronators of the forearm in gibbons and chimpanzees: implications for the fundamental positional adaptation of hominoids. American Journal of Physical Anthropology 115:253-368.

Stock JT. 2002. A test of two methods of radiographically deriving long bone cross-sectional properties compared to direct sectioning of the diaphysis. International Journal of Osteoarchaeology 12:335-342.

Stock JT, Pfeiffer S. 2001. Linking structural variability in long bone diaphyses to habitual behaviors: foragers from the southern African Later Stone Age and the Andaman islands. American Journal of Physical Anthropology 115:337-348.

Stock JT, Shaw CN. 2007. Which measures of diaphyseal robusticity are robust? A comparison of external methods of quantifying the strength of long bone diaphyses to cross-sectional geometric properties. American Journal of Physical Anthropology 134:412-423.

Stout S, Crowder C. 2012. Bone remodeling, histomorphology, and histomorphometry. In: Crowder C, Stout S, editors. Bone Histology: An Anthropological Perspective. Boca Raton (FL): Taylor & Francis Group, LLC. p 1-21.

Susman RL, Jungers WL, Stern JT Jr. 1982. The functional morphology of the accessory interosseous muscle in the gibbon hand: determination of locomotor and manipulatory compromises. Journal of Anatomy 143:111-120.

Susman RL, Stern JT Jr. 1980. EMG of the interosseous and lumbrical muscles in the chimpanzee (*Pan troglodytes*) hand during locomotion. The American Journal of Anatomy 157:389-397.

Suzuki D, Murakami G, Minoura N. 2002. Histology of the bone-tendon interfaces of limb muscles in lizards. Annals of Anatomy 184:363-377.

Suzuki D, Murakami G, Minoura N. 2003. Crocodilian bone-tendon and bone-ligament interfaces. Annals of Anatomy 185:425-433.

Swindler DR, Wood CD. 1973. An atlas of primate gross anatomy: baboon, chimpanzee and man. Seattle (WA): University of Washington Press. 370 p.

Taylor AB, Eng CM, Anapol FC, Vinyard CJ. 2009. The functional correlates of jaw-muscle fiber architecture in tree-gouging and nongouging callitrichid monkeys. American Journal of Physical Anthropology 139:353-367.

Taylor AB, Vinyard CJ. 2004. Comparative analysis of masseter fiber architecture in tree gouging (*Callithrix jacchus*) and nongouging (*Saguinus oedipus*) callitrichids. Journal of Morphology 261:276-285.

Thorpe SKS, Crompton RH. 2006. Orangutan positional behavior and the nature of arboreal locomotion in Hominoidea. American Journal of Physical Anthropology 131:384-401.

Thorpe SKS, Crompton RH, Günther MM, Ker RF, Alexander RMc. 1999. Dimensions and moment arms of the hind- and forelimb muscles of common chimpanzee (*Pan troglodytes*). American Journal of Physical Anthropology 110:179-199.

Tubbs RS, Caycedo FJ, Oakes WJ, Salter EG. 2006. Descriptive anatomy of the insertion of the biceps femoris muscle. Clinical Anatomy 19:517-521.

Turner CH. 1998. Three rules of bone adaption to mechanical stimuli. Bone 23:399-407.

Turner CH. 2000. Muscle-bone interactions, revisited. Bone 27:339-340.

Turner CH. 2007. Skeletal adaptation to mechanical loading. Clinical Reviews in Bone and Mineral Metabolism 5:181-194.

Tuttle RH. 1969. Quantitative and functional studies on the hands of Anthropoidea I: the Homoidea. Journal of Morphology 128:309-364.

Tuttle RH. 1972. Functional and evolutionary biology of hylobatid hands and feet. In: Rumbauch DM, editor. Gibbon and Siamang, vol 1. Basel: S. Karger. p 136-206.

Tuttle RH. 1986. Apes of the world: their social behaviour, communication, mentality, and ecology. New Jersey: Noyes Publications. 421 p.

Tuttle RH, Basmajian JV. 1978a. Electromyography of pongid shoulder muscles II. Deltoid, rhomboid and “rotator cuff”. American Journal of Physical Anthropology 49:47-56.

Tuttle RH, Basmajian JV. 1978b. Electromyography of pongid shoulder muscles III. Quadrupedal positional behavior. American Journal of Physical Anthropology 49:57-70.

Tuttle RH, Velte MJ, Basmajian JV. 1983. Electromyography of brachial muscles in *Pan troglodytes* and *Pongo pygmaeus*. American Journal of Physical Anthropology 61:75-83.

van der Meulen CH, Prendergast PJ. 2000. Mechanics in skeletal development, adaptation and disease. Philosophical Transactions: Mathematical, Physical and Engineering Sciences 358:565-578.

van Eijden TM, Korfage JA, Brugman P. 1997. Architecture of the human jaw-closing and jaw opening muscles. Anatomical Records 248:464-474.

van Gaalen SM, Kruyt MC, Geuze RE, de Bruijn JD, Alblas J, Dhert JA. 2010. Use of fluorochrome labels in *in vivo* bone tissue engineering research. Tissue Engineering Part B 16:209-217.

van Oers RFM, Ruimerman R, Tanck E, Hilbers PAJ, Huiskes R. 2008. A unified theory of osteonal and hemi-osteonal remodeling. Bone 42:250-259.

Villotte S. 2006. Connaissance médicales actuelles, cotation des enthésopathies. Bulletins et mémoires de la Société d'Anthropologie de Paris. 18 :65-85.

Villotte S. 2008. Enthésopathies et activités des hommes préhistoriques – recherche méthodologique et application aux fossiles européens du Paléolithique supérieur et du Mésolithique [dissertation]. Bordeaux (France): Université de Bordeaux. 381 p.

Villotte S, Castex D, Couallier V, Dutour OJ, Knüssel CJ, Henry-Gambier D. 2010a.

Enthesopathies as occupational stress markers: Evidence from the upper limb. American Journal of Physical Anthropology 142:224-234.

Villotte S, Churchill SE, Dutour OJ, Henry-Gambier D. 2010b. Subsistence activities and the sexual division of labor in the European Upper Paleolithic and Mesolithic: evidence from the upper limb enthesopathies. Journal of Human Evolution 59:35-43.

Villotte S, Knüsel J. 2013. Understanding entheseal changes: definition and life course changes. International Journal of Osteoarchaeology 23:135-146.

Waldron T. 1994. Counting the dead. The epidemiology of skeletal populations. New York: John Wiley & Sons. 109 p.

Walker SM, Schrodt GR. 1974. I segment lengths and thin filament periods in skeletal muscle fibers of the rhesus monkey and the human. Anatomical Records 178:63-81.

Wallace IJ, Middleton KM, Lublinsky S, Kelly SA, Judex S, Garland TJr, Demes B. 2010. Functional significance of genetic variation underlying limb bone diaphyseal structure. American Journal of Physical Anthropology 143:21-30.

Wang LC, Kernell D. 2001. Fibre type regionalisation in lower hindlimb muscles of rabbit, rat and mouse: a comparative study. Journal of Anatomy 199:631-643.

Wang W, Crompton RH, Carey TS, Günther MM, Li Y, Savage R, Sellers WI. 2004.

Comparison of inverse-dynamics musculo-skeletal models of AL 288-1 *Australopithecus afarensis* and KNM-WT 15000 *Homo ergaster* to modern humans, with implications for the evolution of bipedalism. Journal of Human Evolution 47:453-478.

Ward SR, Lieber RL. 2005. Density and hydration of fresh and fixed human skeletal muscle. Journal of Biomechanics 38:2317-2320.

Weijs WA, Brugman P, Klok EM. 1987. The growth of the skull and jaw muscles and its functional consequences in the New Zealand rabbit (*Oryctolagus cuniculus*). Journal of Morphology 194:143-161.

Weiss E. 2003. Understanding muscle markers: aggregation and construct validity. American Journal of Physical Anthropology 121:230-240.

Weiss E. 2004. Understanding muscle markers: lower limbs. American Journal of Physical Anthropology 125:232-238.

Weiss E. 2007. Muscle markers revisited: Activity pattern reconstruction with controls in a Central California Amerind population. American Journal of Physical Anthropology 133:931-940.

Weiss E. 2010. Cranial muscle markers: A preliminary examination of size, sex, and age effects. Journal of Comparative Human Biology 61:48-58.

Whitehead PF, Larson SG. 1994. Shoulder motion during quadrupedal walking in *Cercopithecus aethiops*: integration of cineradiographic and electromyographic data. Journal of Human Evolution 26:525-544.

Wingerd BD. 1988. Rat dissection manual. Baltimore (MD): The John Hopkins University Press. 62 p.

Wilczak CA. 1998a. Consideration of sexual dimorphism, age, and asymmetry in quantitative measurements of muscle insertion sites. International Journal of Osteoarchaeology 8:311-325.

Wilczak CA. 1998b. A new method for quantifying musculoskeletal stress markers (MSM): a test of the relationship between enthesis size and habitual activity in archaeological populations [dissertation]. Ithaca (NY): Cornell University. 233 p.

Williams PE, Goldspink G. 1971. Longitudinal growth of striated muscle fibres. Journal of Cell Science 9:751-767.

Williams PE, Goldspink G. 1973. The effect of immobilization on the longitudinal growth of striated muscle fibres. Journal of Anatomy 116:45-55.

Williams PE, Goldspink G. 1976. The effect of denervation and dystrophy on the adaptation of sarcomere number to the functional length of the muscle in young and adult mice. Journal of Anatomy 122:455-465.

Williams PE, Goldspink G. 1978. Changes in sarcomere length and physiological properties in immobilized muscle. Journal of Anatomy 127:459-468.

Williams SB, Wilson AM, Rhodes L, Andrews J, Payne RC. 2008. Functional anatomy and muscle moment arms of the pelvic limb of an elite athlete: the racing greyhound (*Canis familiaris*). Journal of Anatomy 213:361-372.

Woittiez RD, Heerkens YF, Huijing PA, Rijnsburger WH, Rozendal RH. 1986. Functional morphology of the m. gastrocnemius medialis of the rat during growth. Journal of Morphology 187:247-258.

Woo SL, Kuei SC, Amiel D, Gomez MA, Hayes WC, White FC, Akeson WH. 1981. The effect of prolonged physical training on the properties of bone: a study of Wolff's law. The Journal of Bone and Joint surgery 63A:780-787.

Youlatos D. 2000. Functional anatomy of forelimb muscles in Guianan Atelines (Platyrrhini: Primates). Annales des Sciences Naturelles 21:137-151.

Zajac FE. 1992. How musculotendon architecture and joint geometry affect the capacity of muscles to move and exert force on objects: a review with application to arm and forearm tendon transfer. Journal of Hand Surgery 17A:799-804.

Zihlman AL. 1992. Locomotion as a life history character: the contribution of anatomy. Journal

of Human Evolution 22:315-325.

Zilhman AL, McFarland RK. 2000. Body mass in lowland gorillas: a quantitative analysis. American Journal of Physical Anthropology 113:61-78.

Zumwalt A. 2005. The effect of endurance exercise on the morphology of muscle attachment sites: an experimental study in sheep (*Ovis aries*) [dissertation]. Baltimore (MD): Johns Hopkins University. 292 p.

Zumwalt A. 2006. The effect of endurance exercise on the morphology of muscle attachment sites. Journal of Experimental Biology 209:444-454.

Appendix A

A1. Absolute soft-tissue variables for P1.

Muscle	M (g)	L_b (mm)	L_f (mm)	TL (mm)	MTU (mm)	PCSA (cm^2)
LD	516.87	194.39	69.81	85.00	279.39	6.98
D	389.67	88.66	53.63	70.81	159.47	6.76
Pmaj	308.87	105.47	66.21	61.01	166.48	4.41
Sb	216.43	121.84	45.58	58.09	179.93	4.36
Sp	93.93	67.49	52.57	39.91	107.40	1.68
If	163.00	124.81	81.65	52.68	177.49	1.88
Tmin	34.80	73.83	47.42	31.99	105.82	0.69
Tmaj	146.00	125.00	63.03	40.03	165.03	2.18
Cb	76.63	95.44	31.88	97.76	193.20	2.25
BB	163.50	115.75	69.12	140.35	256.10	2.23
TB	354.47	104.00	76.27	145.29	249.29	4.37
An	2.00	34.49	21.94	22.88	57.37	0.09
B	144.60	103.66	54.50	77.04	180.70	2.48
De	44.20	82.63	61.81	81.71	164.34	0.68
Br	116.83	203.43	60.11	154.36	357.79	1.83
Sup	21.80	49.33	23.66	44.08	93.41	0.86
PT	21.80	60.60	46.90	89.69	150.29	0.44
PL	19.40	106.46	71.81	205.30	311.76	0.25
FCR	24.80	149.64	55.24	156.03	305.67	0.42
FCU	44.20	113.99	70.12	163.61	277.60	0.60
FDS	42.70	201.44	59.69	378.34	579.78	0.65
ECRL	27.57	121.59	78.70	267.12	388.71	0.33
ECRB	24.30	100.64	69.20	235.20	335.84	0.33
ECU	20.50	179.47	45.93	103.44	282.91	0.41
ED	34.90	203.58	74.58	328.27	531.85	0.44
EDM	13.83	214.03	89.44	218.78	432.81	0.15

M = muscle mass; L_b = muscle belly length; L_f = sarcomere adjusted fibre length; TL = total tendon length; MTU = muscle-tendon unit; PCSA = sarcomere adjusted physiological cross-sectional area.

A2. Absolute soft-tissue variables for P2.

Muscle	M (g)	L_b (mm)	L_f (mm)	TL (mm)	MTU (mm)	PCSA (cm^2)
LD	1132.83	274.31	76.08	103.15	377.46	14.04
D	986.73	112.47	86.24	75.45	187.92	10.74
Sb	501.20	125.20	56.50	85.54	210.74	8.24
Sp	157.10	95.91	56.21	42.60	138.51	2.63
If	404.73	167.78	58.97	56.95	224.73	6.39
Tmin	74.53	78.39	62.80	40.59	118.98	1.12
Tmaj	311.10	166.78	63.28	74.11	240.89	4.61
Cb	142.13	99.91	72.03	107.58	207.49	1.86
BB	410.70	128.68	87.12	147.93	276.61	4.44
TB	1051.50	112.92	96.60	148.86	261.78	10.14
An	14.10	38.64	25.23	30.50	69.14	0.52
B	615.20	139.06	78.49	99.44	238.50	7.37
De	94.13	152.47	63.13	89.46	241.93	1.41
Br	548.27	261.04	69.99	171.81	432.85	7.36
Sup	125.60	61.06	29.49	72.33	133.39	3.98
PT	125.97	107.78	50.11	108.72	216.50	2.36
PL	69.47	141.14	79.81	219.51	360.65	0.81
FCR	150.97	151.97	62.42	160.76	312.73	2.28
FCU	143.60	199.69	76.02	201.93	401.62	1.78
FDS	383.37	215.46	62.97	406.53	621.99	5.55
ECRL	64.70	146.00	81.69	394.63	540.63	0.75
ECRB	151.30	106.71	70.80	280.72	387.43	1.99
ECU	112.23	262.53	48.70	118.12	380.65	2.13
ED	174.70	247.31	77.59	384.91	632.22	2.12
EDM	75.07	310.33	93.79	261.23	571.56	0.75

M = muscle mass; L_b = muscle belly length; L_f = sarcomere adjusted fibre length; TL = total tendon length; MTU = muscle-tendon unit; PCSA = sarcomere adjusted physiological cross-sectional area.

A3. Absolute soft-tissue variables for P3.

Muscle	M (g)	L_b (mm)	L_f (mm)	TL (mm)	MTU (mm)	PCSA (cm^2)
D	682.50	94.87	69.37	71.43	166.30	9.22
Sb	353.12	117.82	50.47	66.12	183.94	6.49
Sp	119.82	76.00	53.82	40.56	116.56	2.09
If	278.17	140.60	69.74	53.12	193.71	3.75
Tmin	48.97	70.41	54.54	34.59	105.00	0.85
Tmaj	222.85	140.19	62.59	51.37	191.56	3.35
Cb	103.68	128.53	35.60	99.97	228.50	2.72
BB	281.40	167.10	64.5	142.44	309.54	4.11
TB	697.29	221.31	70.8	144.38	365.69	9.19
An	7.35	35.70	23.085	25.99	61.69	0.30
B	374.20	203.96	53.60	82.54	286.50	6.54
De	63.47	112.55	61.77	84.89	197.44	0.97
Br	326.85	203.96	81.7	157.39	361.35	3.77
Sup	68.00	49.50	25.98	52.51	102.00	2.46
PT	68.19	78.49	47.91	93.51	172.00	1.34
PL	38.74	118.10	75.21	206.71	324.81	0.48
FCR	82.19	145.11	58.23	155.70	300.80	1.33
FCU	88.20	151.14	72.47	177.07	328.21	1.15
FDS	157.34	202.75	60.73	386.74	589.49	2.37
ECRL	40.44	128.10	79.60	325.18	453.27	0.48
ECRB	82.10	97.98	69.40	252.26	350.24	1.10
ECU	60.67	215.30	46.72	105.08	320.38	1.21
ED	99.10	219.75	75.49	350.89	570.64	1.24
EDM	38.75	256.48	91.02	234.31	490.79	0.40

M = muscle mass; L_b = muscle belly length; L_f = sarcomere adjusted fibre length; TL = total tendon length; MTU = muscle-tendon unit; PCSA = sarcomere adjusted physiological cross-sectional area.

A4. Absolute soft-tissue variables for M1.

Muscle	M (g)	L_b (mm)	L_f (mm)	TL (mm)	MTU (mm)	PCSA (cm^2)
D	13.50	69.07	54.23	65.84	0.24	134.91
Sb	17.40	78.08	23.08	66.61	0.70	144.69
Sp	10.40	84.33	30.55	24.48	0.32	108.81
If	11.20	86.44	39.12	40.40	0.27	126.84
Tmin	1.30	33.34	12.57	19.21	0.10	52.55
Tmaj	6.90	67.24	44.81	49.00	0.15	116.24
Cb	0.90	414.41	19.97	52.43	0.04	466.84
Cbm	0.60	22.39	15.78	15.47	0.04	37.86
BB	19.30	14.78	44.40	72.43	0.41	87.21
TB	36.70	129.17	44.78	104.70	0.77	233.87
B	6.73	110.07	39.75	46.97	0.16	157.04
Br	9.03	118.92	56.12	67.19	0.15	186.11
Sup	2.30	55.55	14.22	57.68	0.15	113.23
PT	3.60	71.51	42.29	59.66	0.08	131.17
PL	1.90	84.85	49.00	130.58	0.04	215.43
FCR	4.10	93.37	22.64	95.52	0.17	188.89
FCU	3.40	139.66	54.76	129.56	0.06	269.22
FDS	6.80	92.43	31.44	122.85	0.20	215.28
ECRL	2.70	79.87	44.60	133.19	0.06	213.06
ECRB	3.50	105.49	49.60	137.29	0.07	242.78
ECU	3.40	139.66	54.76	129.56	0.06	269.22
ED	3.90	110.20	30.91	170.87	0.12	281.07
EDM	1.40	93.11	31.33	143.80	0.04	236.91

M = muscle mass; L_b = muscle belly length; L_f = sarcomere adjusted fibre length; TL = total tendon length; MTU = muscle-tendon unit; PCSA = sarcomere adjusted physiological cross-sectional area.

A5. Absolute soft-tissue variables for M2.

Muscle	M (g)	L_b (mm)	L_f (mm)	TL (mm)	MTU (mm)	PCSA (cm^2)
LD	56.50	153.64	40.16	48.57	1.32	202.21
D	33.70	82.65	45.15	37.95	0.70	120.60
Pmaj	36.80	99.77	38.54	40.46	0.90	140.23
Pabd	19.57	85.82	31.93	28.47	0.58	114.29
Sb	23.10	87.19	20.08	38.77	1.04	125.96
Sp	13.50	75.07	21.98	23.68	0.56	98.75
If	17.20	103.17	16.72	27.51	0.93	130.68
Tmin	18.70	45.97	10.58	28.18	1.59	74.15
Tmaj	21.00	80.22	40.93	52.18	0.47	132.40
Cb	1.90	44.39	17.65	58.51	0.10	102.90
Cbm	0.50	26.77	13.41	20.92	0.03	47.69
BB	37.10	122.38	51.93	73.22	0.67	195.60
TB	85.23	127.69	36.78	93.64	2.12	221.33
An	0.50	18.98	9.41	16.59	0.05	35.57
B	10.30	79.03	23.55	34.93	0.40	113.96
De	10.10	76.55	32.08	73.52	0.29	150.07
Br	8.50	124.47	32.68	58.53	0.24	183.00
Sup	2.40	52.03	11.90	47.61	0.18	99.64
PT	7.70	62.88	16.40	56.41	0.40	119.29
PL	3.90	109.61	15.10	122.88	0.24	232.49
FCR	6.40	99.93	21.14	100.00	0.28	199.93
FCU	12.80	114.78	24.92	121.26	0.47	236.04
FDS	12.00	118.03	30.93	144.70	0.36	262.73
ECRL	4.80	83.28	38.76	130.54	0.12	213.82
ECRB	5.40	93.95	32.83	122.07	0.15	216.02
ECU	5.00	148.71	22.36	106.47	0.21	255.18
ED	4.90	127.52	31.14	109.24	0.15	236.76
EDM	1.50	120.47	32.27	111.68	0.04	232.15

M = muscle mass; L_b = muscle belly length; L_f = sarcomere adjusted fibre length; TL = total tendon length; MTU = muscle-tendon unit; PCSA = sarcomere adjusted physiological cross-sectional area.

Appendix B

B1. Absolute hard-tissue variables for P1.

Enthesis	Length (cm)	Width (cm)	Area (mm^2)	Mprox (cm)	Mdist (cm)	Midpoint (cm)	Mspread (cm)
LD	4.46	0.621	2.331	3.74	8.12	5.93	4.38
Pmaj	6.111	0.501	4.165	5.972	11.919	8.946	5.947
D	9.656	2.051	10.988	8.923	19.77	14.347	10.847
Sb	2.719	1.312	2.978	1.638	4.786	3.212	3.148
Sp	1.712	1.596	2.203	0.531	0.889	0.710	0.358
If	2.55	3.212	5.62	2.032	4.66	3.346	2.628
Tmaj	7.373	1.117	6.716	6.757	13.784	10.271	7.027
Tmin	3.065	0.741	2.653	1.998	4.762	3.380	2.764
Cb	8.242	1.158	6.85	6.151	14.556	10.354	8.405
B	13.188	2.745	45.03	4.545	17.91	11.228	13.365
TBlat	11.165	0.813	7.964	7.808	22.502	15.155	14.694
TBmed	20.347	2.731	41.942	3.832	24.319	14.076	20.487
PT	1.818	0.606	1.166	2.606	4.344	3.475	1.738
CFO	2.223	1.024	2.769	1.198	2.764	1.981	1.566
Br	8.784	0.519	4.523	3	12.232	7.616	9.232
ECRL	1.583	0.765	0.675	1.684	3.501	2.593	1.817
CEO	2.212	1.172	1.852	0.457	2.688	1.573	2.231
An	1.405	0.865	0.891	1.268	2.862	2.065	1.594

CFO = common flexor origin; CEO = common extensor origin

B2. Absolute hard-tissue variables for P2.

Enthesis	Length (cm)	Width (cm)	Area (mm^2)	Mprox (cm)	Mdist (cm)	Midpoint (cm)	Mspread (cm)
LD	6.531	0.915	4.626	2.857	11	6.929	8.143
Pmaj	6.572	0.943	5.509	7.086	14.857	10.972	7.771
D	8.391	3.873	22.103	11.387	20.39	15.889	9.003
Sb	3.421	1.528	4.374	1.179	5.037	3.108	3.858
Sp	5.123	1.883	6.792	0.497	1.375	0.936	0.878
If	3.196	3.479	8.215	2.817	6.253	4.535	3.436
Tmaj	5.658	0.657	5.353	6.229	11.657	8.943	5.428
Tmin	4.456	1.197	4.505	1.927	5.393	3.660	3.466
Cb	5.936	1.586	8.224	10.411	17.026	13.719	6.615
B	16.085	4.329	50.482	5.852	22.631	14.242	16.779
TBlat	13.516	0.811	6.665	9.034	22.288	15.661	13.254
TBmed	21.483	3.768	68.422	7.377	27.747	17.562	20.370
PT	3.148	1.156	4.254	3.757	6.422	5.090	2.665
CFO	4.744	2.105	8.611	1.197	5.886	3.542	4.689
Br	6.86	1.076	4.849	9.1	16.291	12.696	7.191
ECRL	4.962	0.775	3.191	4	8.452	6.226	4.452
CEO	4.11	1.321	5.026	0.536	4.963	2.750	4.427
An	2.298	0.878	1.809	1.339	3.581	2.460	2.242

CFO = common flexor origin; CEO = common extensor origin

B3. Absolute hard-tissue variables for P3.

Enthesis	Length (cm)	Width (cm)	Area (mm^2)	Mprox (cm)	Mdist (cm)	Midpoint (cm)	Mspread (cm)
LD	5.813	1.467	4.886	3.967	8.667	6.317	4.334
Pmaj	9.301	0.8	8.14	6.634	16.833	11.734	8.417
D	10.484	2.614	20.152	6.33	20.22	13.275	10.110
Sb	3.215	2.222	4.395	2.084	5.445	3.765	2.723
Sp	2.167	4.167	8.121	0.62	1.836	1.228	0.918
If	2.363	2.186	4.511	1.558	4.465	3.012	2.233
Tmaj	6.971	1.038	5.644	6.333	13.767	10.050	6.884
Tmin	2.04	1.5	2.252	3.744	6.383	5.064	3.192
Cb	6.097	1.138	5.023	9.56	16.04	12.800	8.020
B	16.051	3.858	51.711	5.358	22.679	14.019	11.340
TBlat	11.581	0.774	8.525	7.742	19.097	13.420	9.549
TBmed	19.125	3.742	52.735	5.774	20.487	13.131	10.244
PT	2.026	0.439	1.024	3.318	5.232	4.275	2.616
CFO	3.079	2.08	5.913	0.802	3.839	2.321	1.920
Br	7.797	0.596	3.962	5.272	11.536	8.404	5.768
ECRL	2.459	0.561	1.245	2.797	4.531	3.664	2.266
CEO	2.157	1.849	2.962	0.934	3.578	2.256	1.789
An	1.72	1.283	2.261	0.632	3.414	2.023	1.707

CFO = common flexor origin; CEO = common extensor origin

B4. Absolute hard-tissue variables for M1.

Enthesis	Length (cm)	Width (cm)	Area (mm^2)	Mprox (cm)	Mdist (cm)	Midpoint (cm)	Mspread (cm)
LD	2.236	0.729	1.163	2.241	4.204	3.223	1.963
Pmaj	3.567	0.459	1.372	2.517	6.213	4.365	3.696
D	3.914	1.366	4.187	3.012	8.51	5.761	5.498
Sb	0.781	0.566	0.472	0.154	0.986	0.570	0.832
Sp	0.901	0.334	0.328	0.093	0.352	0.223	0.259
If	0.833	0.871	0.817	0.167	1.112	0.640	0.945
Tmaj	2.671	0.331	0.855	1.848	4.689	3.269	2.841
Tmin	0.564	0.414	0.158	0.818	1.528	1.173	0.710
Cb (pro)	0.74	0.418	0.23	0.534	1.348	0.941	0.814
Cb (med)	2.403	0.219	0.495	1.976	4.721	3.349	2.745
B	5.411	1.159	5.651	3.241	8.424	5.833	5.183
TBlat	4.71	0.385	0.965	3.697	8.76	6.229	5.063
TBmed	5.393	1.304	5.828	1.315	7.228	4.272	5.913
PT	0.793	0.211	0.197	1.127	1.94	1.534	0.813
CFO	1.347	0.728	0.845	0.35	1.817	1.084	1.467
Br	3.059	0.31	0.858	1.654	4.901	3.278	3.247
ECRL	0.375	0.507	0.155	1.511	1.854	1.683	0.343
CEO	0.779	0.622	0.664	0.424	1.4	0.912	0.976
An	0.419	0.229	0.102	0.352	0.954	0.653	0.602

CFO = common flexor origin; CEO = common extensor origin

B5. Absolute hard-tissue variables for M2.

Enthesis	Length (cm)	Width (cm)	Area (mm^2)	Mprox (cm)	Mdist (cm)	Midpoint (cm)	Mspread (cm)
LD	2.622	0.446	1.252	2.361	5.244	3.803	2.883
Pmaj	3.249	0.451	0.787	3.64	5.46	4.550	1.820
D	6.731	1.216	6.203	4.436	11.781	8.109	7.345
Sb	0.394	1.015	0.352	0.189	0.408	0.299	0.219
Sp	0.775	0.474	0.43	0.149	1.157	0.653	1.008
If	0.516	0.67	0.584	0.175	0.808	0.492	0.633
Tmaj	3.545	0.27	1.007	2.175	6.029	4.102	3.854
Tmin	0.802	0.329	0.416	0.905	1.846	1.376	0.941
Cb (pro)	0.748	0.238	0.1	0.606	1.279	0.943	0.673
Cb (med)	1.704	0.149	0.479	4.173	6.45	5.312	2.277
B	7.153	1.095	7.223	1.898	9.61	5.754	7.712
TBlat	5.711	0.436	2.278	3.407	9.354	6.381	5.947
TBmed	0.863	0.402	0.237	0.292	1.079	0.686	0.787
PT	1.309	0.24	0.35	1.47	2.749	2.110	1.279
CFO	1.482	1.167	1.252	0.207	1.73	0.969	1.523
Br	3.524	0.288	0.784	1.72	5.611	3.666	3.891
ECRL	0.358	0.26	0.098	1.417	1.978	1.698	0.561
CEO	6.791	1.162	7.953	1.346	9.07	5.208	7.724
An	1.559	1.042	1.209	0.352	2.019	1.186	1.667

CFO = common flexor origin; CEO = common extensor origin

Appendix C

C1. Absolute biomechanical variables for the cross sections at the midshaft in all primates.

Variable	P1	P2	P3	M1	M2
Body mass (kg)	56.4	140	92.5	8.4	11
Humeral length (mm)	373.8	412.2	401.8	146.2	159.3
TA (mm^2)	509.07	828.13	689.87	112.37	106.58
CA (mm^2)	299.63	562.15	478.02	69.01	72.66
MA (mm^2)	209.44	265.98	211.86	43.37	33.91
Ix (mm^4)	17620.45	60023.75	38741.15	996.48	972.23
Iy (mm^4)	17689.10	40580.71	31944.32	759.87	683.25
Imax (mm^4)	19501.77	60196.30	39254.16	1078.91	974.91
Imin (mm^4)	15807.78	40408.16	31431.31	677.44	680.57
Imax/Imin	1.23	100604.46	1.25	1.59	1.43
J (mm^4)	35309.55	1.49	70685.47	1756.35	1655.48
Theta (°)	44.47	-84.642	-75.16	-63.06	-84.52
Zx (mm^3)	1276.32	3105.77	2245.28	152.75	151.81
Zy (mm^3)	1196.48	2493.36	1947.69	133.00	126.55
Zp (mm^3)	2470.07	5651.62	4200.52	287.05	280.51
Zy/Zx	0.94	0.80	0.87	0.87	0.83

C2. Absolute biomechanical variables for the cross sections at the latissimus dorsi attachment.

Variable	P1	P2	P3	M1	M2
Proximal					
TA (cm^2)	1355.96	2315.55	2056.61	145.09	140.26
CA (cm^2)	356.28	535.85	548.58	65.44	55.95
MA (cm^2)	999.68	1779.70	1508.03	79.66	84.31
Ix (cm^4)	62552.48	160582.48	176389.01	1492.23	1264.51
Iy (cm^4)	76745.63	168985.18	143965.88	966.81	806.19
Imax (cm^4)	80544.59	169624.07	180707.71	1562.40	1292.56
Imin (cm^4)	58753.52	159943.59	139647.17	896.63	778.15
Imax/Imin	1.37	329567.66	1.29	1.74	1.66
J (cm^4)	139298.11	1.06	320354.88	2459.04	2070.70
Theta (°)	24.68	14.886	-71.08	-71.05	-76.50
Zx (cm^3)	2429.08	4938.23	5745.12	176.99	157.37
Zy (cm^3)	2985.06	5604.39	5109.77	138.43	123.35
Zp (cm^3)	5413.69	10517.47	10882.16	319.03	284.22
Zy/Zx	1.23	1.13	0.89	0.78	0.78
Midpoint					
TA (cm^2)	611.83	799.25	817.18	130.76	107.97
CA (cm^2)	213.84	606.84	479.81	61.51	54.24
MA (cm^2)	397.99	192.41	337.38	69.24	53.73
Ix (cm^4)	16921.03	46105.33	40621.14	1361.45	939.41
Iy (cm^4)	17748.53	52356.25	50193.64	781.22	543.88
Imax (cm^4)	18040.80	56168.70	50479.11	1373.00	944.24
Imin (cm^4)	16628.76	42292.87	40335.67	769.67	539.05
Imax/Imin	1.08	98461.58	1.25	1.78	1.75
J (cm^4)	34669.56	1.33	90814.78	2142.67	1483.29
Theta (°)	27.06	-31.612	-9.66	-82.05	83.74
Zx (cm^3)	1178.27	2602.34	2417.38	159.11	135.84
Zy (cm^3)	1203.41	2986.04	2897.45	115.20	93.90

	Zp (cm^3)	2382.02	5586.38	5322.13	279.40	233.45
	Zy/Zx	1.02	1.15	1.20	0.72	0.69
Distal						
	TA (cm^2)	502.65	1008.04	705.65	135.16	114.07
	CA (cm^2)	231.14	742.49	445.17	69.60	59.73
	MA (cm^2)	271.50	265.55	260.47	65.56	54.34
	Ix (cm^4)	15826.15	79125.47	39479.24	1551.57	1059.35
	Iy (cm^4)	12679.33	76960.60	31176.96	925.02	659.99
	Imax (cm^4)	15897.06	100159.46	41586.65	1570.92	1074.16
	Imin (cm^4)	12608.42	55926.62	29069.54	905.68	645.18
	Imax/Imin	1.26	156086.08	1.43	1.73	1.66
	J (cm^4)	28505.48	1.79	70656.20	2476.59	1719.34
	Theta (°)	-81.56	-46.403	-65.78	-80.18	79.29
	Zx (cm^3)	1150.77	4156.40	2366.53	177.51	154.72
	Zy (cm^3)	985.93	4036.40	2144.92	126.51	111.49
	Zp (cm^3)	2142.22	8192.70	4526.69	308.56	269.35
	Zy/Zx	0.86	0.97	0.91	0.71	0.72

C3. Absolute biomechanical variables for the cross sections at the pectoralis attachment.

Variable	P1	P2	P3	M1	M2
Proximal					
TA (cm^2)	604.12	800.11	784.83	136.88	108.37
CA (cm^2)	217.49	618.62	467.94	67.88	61.07
MA (cm^2)	386.64	181.49	316.89	69.01	47.29
Ix (cm^4)	17158.89	47079.80	39797.93	1500.03	1016.02
Iy (cm^4)	17201.68	52719.14	44182.58	876.39	584.69
Imax (cm^4)	17256.50	57602.41	45277.37	1543.46	1020.13
Imin (cm^4)	17104.07	42196.53	38703.14	832.96	580.58
Imax/Imin	1.01	99798.94	1.17	1.85	1.76
J (cm^4)	34360.57	1.37	83980.50	2376.42	1600.71
Theta (°)	-36.85	-34.264	-24.08	-75.69	84.45
Zx (cm^3)	1207.97	2621.17	2395.11	185.37	140.68
Zy (cm^3)	1184.25	2887.78	2687.38	129.81	98.52
Zp (cm^3)	2391.96	5511.12	5080.94	320.20	243.33
Zy/Zx	0.98	1.10	1.12	0.70	0.70
Midpoint					
TA (cm^2)	503.12	1004.74	722.23	135.99	109.53
CA (cm^2)	245.48	742.49	541.92	69.96	58.04
MA (cm^2)	257.64	262.25	180.31	66.03	51.49
Ix (cm^4)	16013.84	77769.73	44166.35	1578.33	994.65
Iy (cm^4)	13866.93	77205.56	35295.52	916.14	595.62
Imax (cm^4)	16063.74	99888.98	44621.93	1589.69	1001.89
Imin (cm^4)	13817.03	55086.31	34839.94	904.78	588.38
Imax/Imin	1.16	154975.29	1.28	1.76	1.70
J (cm^4)	29880.77	1.81	79461.87	2494.47	1590.27
Theta (°)	-81.43	-45.361	-77.54	-82.60	82.40
Zx (cm^3)	1178.70	4069.64	2441.92	178.57	140.47
Zy (cm^3)	1075.34	4100.97	2358.54	122.08	104.00

	Zp (cm^3)	2256.74	8170.38	4808.34	305.27	248.32
	Zy/Zx	0.91	1.01	0.97	0.68	0.74
Distal						
	TA (cm^2)	539.22	958.90	760.60	129.51	115.76
	CA (cm^2)	314.97	697.51	516.88	72.69	62.66
	MA (cm^2)	224.25	261.39	243.72	56.81	53.10
	Ix (cm^4)	15764.96	71280.71	48438.00	1325.00	1099.37
	Iy (cm^4)	24253.47	63850.75	44053.86	940.52	699.54
	Imax (cm^4)	24734.27	74342.03	60498.64	1412.49	1113.07
	Imin (cm^4)	15284.16	60789.43	31993.21	853.04	685.84
	Imax/Imin	1.62	135131.46	1.89	1.66	1.62
	J (cm^4)	40018.44	1.22	92491.86	2265.52	1798.91
	Theta (°)	13.04	61.623	-49.42	-66.71	79.69
	Zx (cm^3)	1150.12	3546.59	2583.00	166.21	156.47
	Zy (cm^3)	1547.79	3507.61	2411.17	139.04	119.06
	Zp (cm^3)	2724.46	7056.12	4996.41	307.48	278.86
	Zy/Zx	1.35	0.99	0.93	0.84	0.76

C4. Absolute biomechanical variables for the cross sections at the deltoideus attachment.

Variable	P1	P2	P3	M1	M2
Proximal					
TA (cm^2)	503.12	1021.69	967.58	109.34	108.76
CA (cm^2)	258.73	746.22	488.75	75.67	62.13
MA (cm^2)	244.39	275.47	478.83	33.67	46.63
Ix (cm^4)	16690.12	81503.70	55149.90	924.26	1056.65
Iy (cm^4)	14244.59	77867.68	66227.52	823.50	605.97
Imax (cm^4)	16692.13	102872.34	70993.05	1029.05	1071.22
Imin (cm^4)	14242.57	56499.04	50384.36	718.71	591.40
Imax/Imin	1.17	159371.38	1.41	1.43	1.81
J (cm^4)	30934.70	1.82	121377.42	1747.76	1662.62
Theta (°)	-88.36	-47.249	28.74	-54.47	79.97
Zx (cm^3)	1228.54	4191.15	2805.37	150.04	148.76
Zy (cm^3)	1092.96	4111.72	3485.11	138.80	107.10
Zp (cm^3)	2324.31	8303.92	6278.95	289.05	260.58
Zy/Zx	0.89	0.98	1.24	0.93	0.72
Midpoint					
TA (cm^2)	522.12	922.83	735.89	135.93	103.40
CA (cm^2)	298.88	655.12	516.71	68.89	68.07
MA (cm^2)	223.23	267.71	219.17	67.04	35.33
Ix (cm^4)	16177.81	71474.70	37256.64	1413.60	887.30
Iy (cm^4)	20190.65	54772.81	43150.78	967.37	640.62
Imax (cm^4)	21889.72	74203.38	47415.53	1476.68	896.58
Imin (cm^4)	14478.74	52044.13	32991.90	904.29	631.34
Imax/Imin	1.51	126247.51	1.44	1.63	1.42
J (cm^4)	36368.46	1.43	80407.43	2380.96	1527.92
Theta (°)	28.61	69.457	-32.94	-70.61	-79.22
Zx (cm^3)	1233.42	3557.76	2102.64	166.43	141.48
Zy (cm^3)	1337.58	2991.66	2538.23	137.40	119.82

	Zp (cm^3)	2578.30	6575.68	4631.86	306.54	263.03
	Zy/Zx	1.08	0.84	1.21	0.83	0.85
Distal						
	TA (cm^2)	500.48	831.87	667.11	109.34	96.46
	CA (cm^2)	309.90	557.98	485.50	75.67	69.18
	MA (cm^2)	190.58	273.89	181.61	33.67	27.28
	Ix (cm^4)	16534.87	61529.80	31752.20	924.26	565.30
	Iy (cm^4)	18340.20	39991.93	35007.18	823.50	904.90
	Imax (cm^4)	18606.75	61581.08	35973.33	1029.05	938.14
	Imin (cm^4)	16268.32	39940.65	30786.04	718.71	532.06
	Imax/Imin	1.14	101521.73	1.17	1.43	1.76
	J (cm^4)	34875.07	1.54	66759.37	1747.76	1470.20
	Theta (°)	19.73	-87.210	25.57	-54.47	-16.63
	Zx (cm^3)	1210.53	3144.86	2113.91	150.04	103.19
	Zy (cm^3)	1265.09	2507.80	1966.55	138.80	121.06
	Zp (cm^3)	2477.24	5717.57	4067.96	289.05	227.01
	Zy/Zx	1.05	0.80	0.93	0.93	1.17

C5. Absolute biomechanical variables for the cross sections at the teres major attachment.

Variable	P1	P2	P3	M1	M2
Proximal					
TA (cm^2)	546.93	842.36	784.83	172.28	159.72
CA (cm^2)	211.06	586.00	467.94	72.04	60.20
MA (cm^2)	335.86	256.36	316.89	100.24	99.52
Ix (cm^4)	15878.13	44727.67	39797.93	2016.22	1567.18
Iy (cm^4)	14005.83	61348.29	44182.58	1386.64	996.26
Imax (cm^4)	16327.89	62184.42	45277.37	2149.17	1581.34
Imin (cm^4)	13556.07	43891.54	38703.14	1253.70	982.09
Imax/Imin	1.20	106075.96	1.17	1.71	1.61
J (cm^4)	29883.96	1.42	83980.50	3402.86	2563.44
Theta (°)	-66.25	-12.345	-24.08	-67.34	-81.16
Zx (cm^3)	1130.74	2586.50	2395.11	203.89	185.09
Zy (cm^3)	1058.64	3093.85	2687.38	176.89	151.34
Zp (cm^3)	2191.53	5715.02	5080.94	383.91	340.65
Zy/Zx	0.94	1.20	1.12	0.87	0.82
Midpoint					
TA (cm^2)	518.33	888.05	722.23	137.83	108.21
CA (cm^2)	277.39	688.03	541.92	68.95	59.23
MA (cm^2)	240.95	200.03	180.31	68.89	48.98
Ix (cm^4)	16291.50	60374.83	44166.35	1512.95	1027.45
Iy (cm^4)	17680.01	61977.53	35295.52	977.65	572.84
Imax (cm^4)	17923.96	73679.36	44621.93	1526.31	1038.70
Imin (cm^4)	16047.55	48673.00	34839.94	964.28	561.59
Imax/Imin	1.12	122352.36	1.28	1.58	1.85
J (cm^4)	33971.51	1.51	79461.87	2490.59	1600.29
Theta (°)	21.13	-43.163	-77.54	-81.13	81.17
Zx (cm^3)	1167.23	3400.11	2441.92	178.05	148.63
Zy (cm^3)	1253.25	3501.42	2358.54	131.35	98.16

	Zp (cm^3)	2420.93	6901.35	4808.34	312.49	251.05
	Zy/Zx	1.07	1.03	0.97	0.74	0.66
Distal						
	TA (cm^2)	524.28	1027.30	760.60	137.83	118.32
	CA (cm^2)	295.03	762.17	516.88	68.95	67.28
	MA (cm^2)	229.25	265.12	243.72	68.89	51.04
	Ix (cm^4)	15527.17	84173.88	48438.00	1512.95	1118.31
	Iy (cm^4)	20866.65	77888.49	44053.86	977.65	779.14
	Imax (cm^4)	21968.00	104200.77	60498.64	1526.31	1118.33
	Imin (cm^4)	14425.81	57861.60	31993.21	964.28	779.12
	Imax/Imin	1.52	162062.37	1.89	1.58	1.44
	J (cm^4)	36393.81	1.80	92491.86	2490.59	1897.45
	Theta (°)	22.47	-48.898	-49.42	-81.13	-89.57
	Zx (cm^3)	1214.07	4299.61	2583.00	178.05	162.39
	Zy (cm^3)	1335.27	4112.64	2411.17	131.35	131.99
	Zp (cm^3)	2561.44	8415.35	4996.41	312.49	296.72
	Zy/Zx	1.10	0.96	0.93	0.74	0.81

C6. Absolute biomechanical variables for the cross sections at the coracobrachialis attachment.

Variable	P1	P2	P3	M1	M2
Proximal					
TA (cm^2)	595.81	975.57	689.39	155.80	108.42
CA (cm^2)	222.42	729.70	483.22	60.80	58.20
MA (cm^2)	373.38	245.87	206.17	95.00	50.22
Ix (cm^4)	17760.05	72875.10	42006.56	1493.70	985.64
Iy (cm^4)	16534.08	74037.82	29394.16	1048.25	578.44
Imax (cm^4)	17846.30	93599.55	42668.45	1580.79	996.87
Imin (cm^4)	16447.83	53313.36	28732.27	961.15	567.22
Imax/Imin	1.09	146912.92	1.49	1.64	1.76
J (cm^4)	34294.13	1.76	71400.72	2541.94	1564.09
Theta (°)	-75.62	-44.173	-77.41	-67.98	80.70
Zx (cm^3)	1250.68	3957.04	2260.75	166.24	140.13
Zy (cm^3)	1122.45	3882.20	2108.26	141.28	96.83
Zp (cm^3)	2370.79	7837.93	4390.76	309.90	240.49
Zy/Zx	0.90	0.98	0.93	0.85	0.69
Midpoint					
TA (cm^2)	518.40	1002.87	737.84	130.99	115.07
CA (cm^2)	282.19	711.74	554.27	71.03	64.59
MA (cm^2)	236.21	291.13	183.57	59.96	50.49
Ix (cm^4)	16171.46	71899.42	42533.80	1511.76	1118.55
Iy (cm^4)	18284.47	73390.54	39547.58	868.84	709.84
Imax (cm^4)	18438.11	75366.37	45146.14	1519.79	1137.79
Imin (cm^4)	16017.82	69923.59	36935.24	860.82	690.60
Imax/Imin	1.15	145289.96	1.22	1.77	1.65
J (cm^4)	34455.93	1.08	82081.38	2380.60	1828.39
Theta (°)	14.59	-37.050	-55.66	-83.66	78.03
Zx (cm^3)	1168.58	3591.39	2449.09	181.94	158.71
Zy (cm^3)	1274.72	3835.79	2494.30	130.31	119.52

	Zp (cm^3)	2445.21	7421.63	4941.33	317.91	281.58
	Zy/Zx	1.09	1.07	1.02	0.72	0.75
Distal						
	TA (cm^2)	521.71	890.78	774.26	139.98	117.66
	CA (cm^2)	283.00	627.96	561.10	71.15	70.08
	MA (cm^2)	238.71	262.82	213.16	68.83	47.58
	Ix (cm^4)	15842.35	73864.81	46469.92	1576.96	1101.81
	Iy (cm^4)	19285.70	45741.00	50962.25	1011.83	787.37
	Imax (cm^4)	21187.81	75027.88	62715.70	1592.42	1101.82
	Imin (cm^4)	13940.25	44577.93	34716.47	996.37	787.36
	Imax/Imin	1.52	119605.81	1.81	1.60	1.40
	J (cm^4)	35128.06	1.68	97432.17	2588.79	1889.18
	Theta (°)	30.82	78.730	-40.38	-80.73	-89.73
	Zx (cm^3)	1194.45	3659.22	2523.26	181.13	164.96
	Zy (cm^3)	1301.16	2635.35	2662.22	136.56	136.51
	Zp (cm^3)	2501.54	6371.72	5188.16	321.27	303.55
	Zy/Zx	1.09	0.72	1.06	0.75	0.83

C7. Absolute biomechanical variables for the cross sections at the triceps brachii (lateral head) attachment.

Variable	P1	P2	P3	M1	M2
Proximal					
TA (cm^2)	507.18	890.06	735.40	132.48	109.45
CA (cm^2)	207.48	684.43	463.71	62.94	56.51
MA (cm^2)	299.69	205.63	271.69	69.54	52.94
Ix (cm^4)	14756.38	60291.87	39879.67	1404.07	940.37
Iy (cm^4)	11810.71	61611.06	35747.88	830.51	571.01
Imax (cm^4)	14898.51	73711.18	43331.43	1417.70	943.02
Imin (cm^4)	11668.57	48191.74	32296.12	816.88	568.36
Imax/Imin	1.28	121902.93	1.34	1.74	1.66
J (cm^4)	26567.08	1.53	75627.55	2234.58	1511.38
Theta (°)	-77.89	-43.518	-55.99	-81.34	85.18
Zx (cm^3)	1056.41	3431.76	2414.09	164.10	130.03
Zy (cm^3)	925.32	3493.01	2427.68	115.42	96.20
Zp (cm^3)	1987.62	6924.89	4841.00	283.72	229.56
Zy/Zx	0.88	1.02	1.01	0.70	0.74
Midpoint					
TA (cm^2)	521.17	930.44	734.59	129.51	118.03
CA (cm^2)	279.82	671.21	570.04	72.75	69.63
MA (cm^2)	241.35	259.23	164.54	56.75	48.40
Ix (cm^4)	16132.29	70938.81	41459.77	1343.02	1122.54
Iy (cm^4)	18729.99	57449.48	41447.94	930.33	783.17
Imax (cm^4)	20821.31	74001.10	46742.55	1437.46	1122.69
Imin (cm^4)	14040.97	54387.20	36165.16	835.89	783.02
Imax/Imin	1.48	128388.29	1.29	1.72	1.43
J (cm^4)	34862.28	1.36	82907.71	2273.35	1905.71
Theta (°)	33.74	66.726	-45.03	-66.66	-88.78
Zx (cm^3)	1220.97	3578.26	2357.45	173.34	164.06
Zy (cm^3)	1252.00	3170.56	2516.85	139.12	137.41

	Zp (cm^3)	2474.89	6767.14	4869.06	314.97	303.90
	Zy/Zx	1.03	0.89	1.07	0.80	0.84
Distal						
	TA (cm^2)	482.43	803.70	726.78	108.51	94.64
	CA (cm^2)	272.72	570.19	524.52	74.66	65.70
	MA (cm^2)	209.71	233.51	202.26	33.85	28.94
	Ix (cm^4)	13689.37	53599.52	48671.99	903.01	714.02
	Iy (cm^4)	16994.36	41949.78	36288.84	815.26	600.27
	Imax (cm^4)	17041.89	54679.71	52185.92	1014.05	773.72
	Imin (cm^4)	13641.83	40869.59	32774.91	704.21	540.57
	Imax/Imin	1.25	95549.30	1.59	1.44	1.43
	J (cm^4)	30683.73	1.34	84960.82	1718.26	1314.29
	Theta (°)	-6.79	-73.759	-64.82	-53.23	-59.60
	Zx (cm^3)	1096.60	3000.71	2394.39	148.70	119.19
	Zy (cm^3)	1176.82	2556.28	2071.15	135.74	113.02
	Zp (cm^3)	2279.24	5575.81	4489.51	284.52	232.58
	Zy/Zx	1.07	0.85	0.87	0.91	0.95

C8. Absolute biomechanical variables for the cross sections at the triceps brachii (medial head) attachment.

Variable	P1	P2	P3	M1	M2
Proximal					
TA (cm^2)	932.35	812.61	907.10	188.52	406.11
CA (cm^2)	284.28	599.65	464.20	69.19	98.25
MA (cm^2)	648.07	212.96	442.90	119.33	307.86
Ix (cm^4)	36068.88	49208.09	46333.19	2167.68	6215.56
Iy (cm^4)	38334.16	52022.56	59310.30	1512.07	5156.82
Imax (cm^4)	38673.79	59050.65	59591.84	2215.93	6458.11
Imin (cm^4)	35729.25	42180.00	46051.65	1463.81	4914.27
Imax/Imin	1.08	101230.65	1.29	1.51	1.31
J (cm^4)	74403.04	1.40	105643.48	3679.75	11372.39
Theta (°)	19.85	-40.198	8.29	-75.33	-66.65
Zx (cm^3)	1871.44	2711.41	2615.21	209.67	476.16
Zy (cm^3)	1873.57	2867.19	3260.81	181.08	458.90
Zp (cm^3)	3745.08	5578.58	5884.51	393.79	936.35
Zy/Zx	1.00	1.06	1.25	0.86	0.96
Midpoint					
TA (cm^2)	524.21	890.64	732.64	134.98	344.69
CA (cm^2)	308.28	621.35	557.85	70.37	105.57
MA (cm^2)	215.93	269.29	174.79	64.60	239.12
Ix (cm^4)	16236.30	76944.73	41230.71	1586.02	5984.11
Iy (cm^4)	21051.26	43797.91	40592.58	914.82	4300.65
Imax (cm^4)	22594.50	78002.19	45559.16	1599.27	6053.77
Imin (cm^4)	14693.06	42740.45	36264.14	901.57	4230.98
Imax/Imin	1.54	120742.64	1.26	1.77	1.43
J (cm^4)	37287.56	1.83	81823.29	2500.83	10284.76
Theta (°)	26.23	80.028	-46.97	-82.08	78.73
Zx (cm^3)	1242.46	3752.72	2372.18	179.16	466.91
Zy (cm^3)	1382.62	2618.20	2510.19	121.91	404.02

	Zp (cm^3)	2635.77	6485.98	4877.40	305.79	876.75
	Zy/Zx	1.11	0.70	1.06	0.68	0.87
Distal						
	TA (cm^2)	468.44	788.90	681.09	116.24	194.76
	CA (cm^2)	314.09	618.33	478.99	74.84	67.25
	MA (cm^2)	154.34	170.57	202.10	41.40	127.51
	Ix (cm^4)	13365.13	46643.94	36626.56	1123.12	2225.05
	Iy (cm^4)	18697.51	50889.45	32430.79	825.72	1367.95
	Imax (cm^4)	18898.82	56274.22	36823.59	1229.18	2231.01
	Imin (cm^4)	13163.82	41259.17	32233.76	719.66	1361.98
	Imax/Imin	1.44	97533.39	1.14	1.71	1.64
	J (cm^4)	32062.64	1.36	69057.35	1948.84	3593.00
	Theta (°)	-10.80	-36.788	-78.04	-62.85	85.25
	Zx (cm^3)	1130.10	2688.63	2242.23	162.40	232.86
	Zy (cm^3)	1279.43	2759.89	1921.37	134.44	169.05
	Zp (cm^3)	2425.27	5450.70	4158.34	298.49	407.20
	Zy/Zx	1.13	1.03	0.86	0.83	0.73

C9. Absolute biomechanical variables for the cross sections at the brachialis attachment.

Variable	P1	P2	P3	M1	M2
Proximal					
TA (cm^2)		908.03	967.58	130.58	183.17
CA (cm^2)		568.04	488.75	63.89	60.26
MA (cm^2)		339.99	478.83	66.69	122.92
Ix (cm^4)		46437.60	55149.90	1406.00	1863.98
Iy (cm^4)		71424.81	66227.52	780.35	1194.25
Imax (cm^4)		72213.67	70993.05	1410.73	1873.57
Imin (cm^4)		45648.74	50384.36	775.62	1184.67
Imax/Imin		117862.41	1.41	1.82	1.58
J (cm^4)		1.58	121377.42	2186.35	3058.24
Theta (°)		-9.923	28.74	-85.05	-83.23
Zx (cm^3)		2666.92	2805.37	167.44	210.39
Zy (cm^3)		3299.32	3485.11	114.18	160.51
Zp (cm^3)		6034.83	6278.95	287.09	375.24
Zy/Zx		1.24	1.24	0.68	0.76
Midpoint					
TA (cm^2)		982.32	735.89	135.10	117.87
CA (cm^2)		694.20	516.71	74.36	65.62
MA (cm^2)		288.11	219.17	60.74	52.26
Ix (cm^4)		71351.41	37256.64	1469.82	1139.28
Iy (cm^4)		68078.01	43150.78	1006.72	755.83
Imax (cm^4)		72312.37	47415.53	1563.88	1146.51
Imin (cm^4)		67117.04	32991.90	912.66	748.60
Imax/Imin		139429.42	1.44	1.71	1.53
J (cm^4)		1.08	80407.43	2476.54	1895.11
Theta (°)		64.528	-32.94	-67.66	82.25
Zx (cm^3)		3537.27	2102.64	179.62	159.79
Zy (cm^3)		3596.10	2538.23	142.96	125.57

	Zp (cm^3)	7131.50	4631.86	325.32	288.25
	Zy/Zx	1.02	1.21	0.80	0.79
Distal					
	TA (cm^2)	798.24	667.11	110.65	93.58
	CA (cm^2)	577.52	485.50	75.07	64.06
	MA (cm^2)	220.72	181.61	35.57	29.52
	Ix (cm^4)	52561.97	31752.20	946.35	693.99
	Iy (cm^4)	42458.87	35007.18	826.52	585.60
	Imax (cm^4)	53932.17	35973.33	1051.53	747.56
	Imin (cm^4)	41088.68	30786.04	721.33	532.02
	Imax/Imin	95020.85	1.17	1.46	1.41
	J (cm^4)	1.31	66759.37	1772.86	1279.58
	Theta (°)	-70.936	25.57	-55.64	-60.10
	Zx (cm^3)	2949.67	2113.91	154.36	117.12
	Zy (cm^3)	2506.79	1966.55	139.65	110.20
	Zp (cm^3)	5467.69	4067.96	294.27	227.70
	Zy/Zx	0.85	0.93	0.90	0.94